

# Characterising and evaluation of the seal capacity based on core and cutting analysis of the Nini-4 and Nini-4a wells

Project Greensand – WP4 final report

Niels H. Schovsbo, Henrik I. Petersen, Rikke Weibel,  
Hanne D. Holmslykke & Niels Springer

# **Characterising and evaluation of the seal capacity based on core and cutting analysis of the Nini-4 and Nini-4a wells**

Project Greensand – WP4 final report

Niels H. Schovsbo, Henrik I. Petersen, Rikke Weibel,  
Hanne D. Holmslykke & Niels Springer

Released 01.10.2022

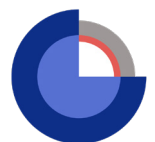


## Table of Contents

<b>Summary</b> .....	3
<b>Introduction</b> .....	6
<b>Stratigraphy and sampling</b> .....	7
<b>Cleaning procedures</b> .....	12
<b>Batch experiments</b> .....	13
<b>Particle size distribution</b> .....	14
<b>Mineralogy and petrography</b> .....	16
<b>Porosity and Bulk Density</b> .....	25
<b>Permeability</b> .....	27
<b>Vitrinite Reflectance</b> .....	30
<b>Organic petrographic composition</b> .....	31
<b>Organic carbon and total sulphur contents and Rock-Eval pyrolysis</b> .....	33
<b>Elemental composition from Hand-Held XRF</b> .....	34
<b>Elemental Composition from ICP-MS</b> .....	36
<b>Specific Surface Area (BET)</b> .....	39
<b>Mercury Injection Capillary Pressure (MICP)</b> .....	41
<b>Mudgas logs</b> .....	49
<b>References</b> .....	58
<b>Appendix A - BET analysis</b> .....	61
<b>Appendix B – MICP analysis</b> .....	62
<b>Appendix C – XRD analysis</b> .....	63
<b>Appendix D – Results in Execl sheet</b> .....	64

## SUMMARY

The primary seal in the Nini West Field is about 340 m thick and composed of shales that belong to the Eocene to Miocene Horda Fm and the lower to mid Lark Fm (Figure 1). The Horda Fm is characterised by greenish grey to greyish green fissile mudstone. Subordinate limestone benches and thin layers of black mudstones occur at some levels in the formation. The lower Lark Fm is dominated by dark, greenish grey, non-fissile mudstones with subordinate intervals of brownish grey mudstones. The secondary seal is about 550 m thick and belong to the mid to upper Lark Fm (Figure 1). This shale is composed by pale to dark brownish grey mudstones with subordinate intervals of greenish grey mudstones. The combined seal sequence is thus almost 900 m thick in the Nini West area. The above lying strata i.e. the remaining c. 800 m belongs to the Nolde Sand and the Nordland Group and is considered overburden.

The lower primary seal and the basal/lateral seal has been examined in the Nini 4/4a well following an extensive analysis program to study the composition (mineralogy and elements), grain size, porosity, permeability, and surface area and pore structure from Hg injection capillary pressure data (MICP). In addition to this a 3D geomechanical study and a report on seal reactivity at reservoir conditions to CO<sub>2</sub> enriched brine will form the basis for the Project Greensand reporting on the seal capacity.

The base and lateral seal is composed by the Sele and Lista Fms. This formation consists of illite, quartz and minor amounts of K-feldspar, plagioclase, pyrite and varying amounts of zeolite minerals such as heulandite. The top seal complex is composed by the Horda and Lark Fms. In Horda heulandite is abundant in the lower part and decreases upwards. The clay minerals are mainly of illitic and smectitic composition. The smectitic component consists of randomly stratified mixed-layer smectite/illite, according to their second order peak at 8.76Å when glycolated.

The total clay volume of the seal has been evaluated from well logs calibrated with XRD measurements. In the Horda Fm the clay content is generally above 60% with peaks of 80% in parts of the formation, which also are the most smectitic. In the Lark Fm the clay content decreases to about 40% in the top L1 unit wherefrom is gradually increases to more than 50% from the mid Lark Fm and upwards (Figure 1). The claystone of the seal is dominated by clay size particles. The clay size fraction represents up about 60% of the rock while the sand size fraction constitutes less than 5% and typically only 1% of the rock. From thin section analysis coarse grained particles include diagenetic formed minerals such as heulandite that may precipitates in the sand size as replacements of diatoms or as silt size crystals within the matrix.

The organic maceral content is low, and the individual macerals occur as isolated particles in the mineral matrix, hence not forming a coherent network of organic matter that could affect seal integrity. The observation of a single particle of solid bitumen indicate migration of hydrocarbons into the lowermost part of the caprock (Horda Fm, basal Lark L1) as also demonstrated by the mudgas composition. Thus, the vast majority of the seal complex does not contain migrated hydrocarbons.

Porosities in the seal is determined by direct measurements on both cuttings and core samples. The data is used to calibrate porosity calculations from the density wire-line log based on a grain density

model. The evaluation show that seal has a porosity around 16-20% in the primary and secondary seal intervals (Figure 1). Low porosities are calculated in high density beds likely representing carbonate stringers that occur abundantly in the lower Lark Fm and in the Horda Fm. XRD data indicate that siderite has a local peak in concentration here suggesting that this mineral is the cementing phase. Porosities of more than 30% is modelled in the sandy beds within the Lark L2 unit that separate the primary and secondary seals from each other (c.f. Schovsbo 2020).

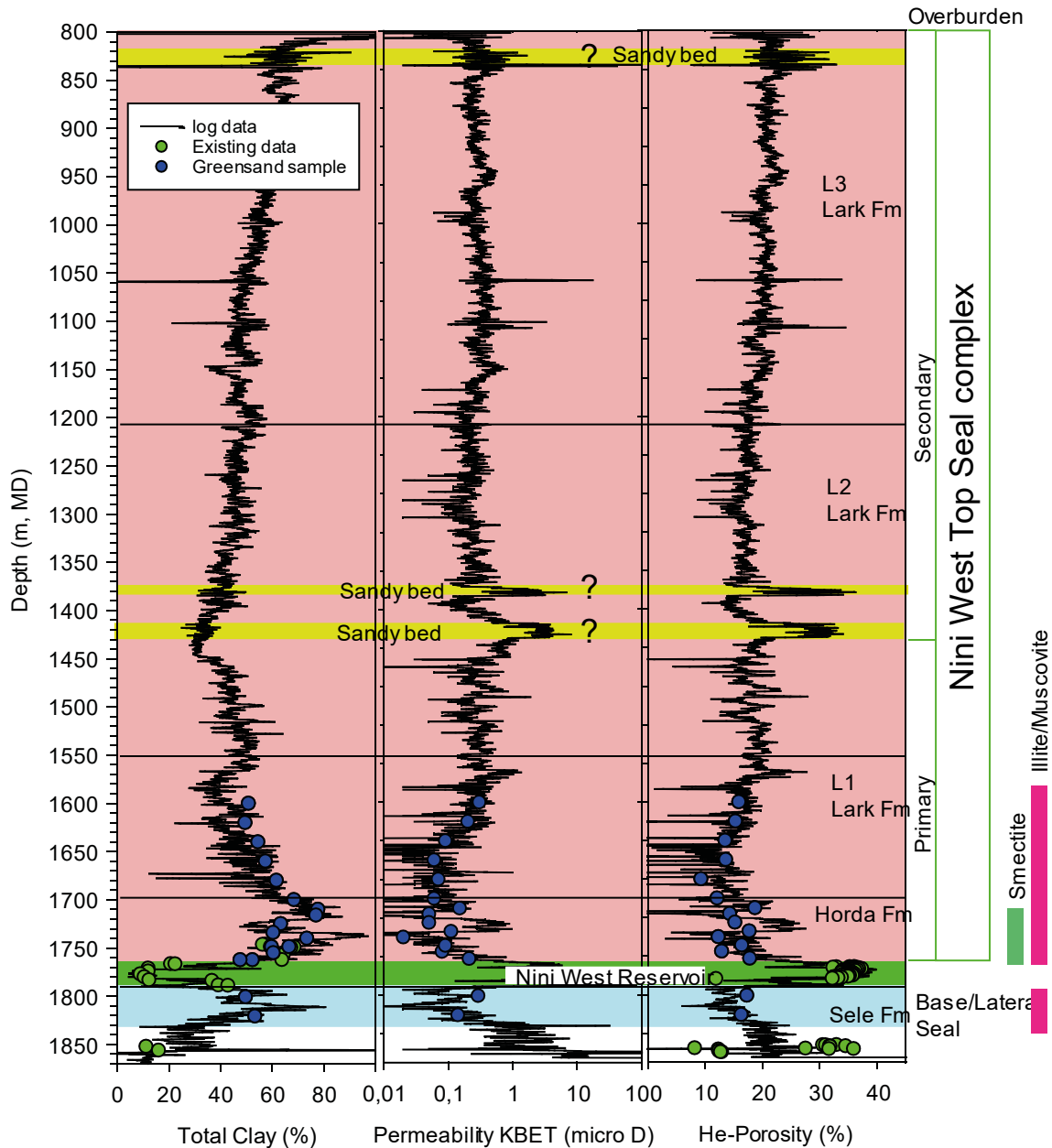


**Figure 1** Summary of the petrophysical evaluation of the Nini West Seal Complex and the base and lateral seal in the Nini-4 well. The log-based evaluation has been calibrated to measured data and described in the technical sections. Bars to the right indicate dominant clay type. For definitions of the seal complexes see Schovsbo (2020). ? marks high permeability zones interpreted with the Seal permeability model.

**Summary of the petrophysical interpretation of the permeability and porosity within the seals.**  $K_{BET}$  is modelled from the surface area, porosity, and grain density. P10, P50, P90 reflect different percentiles of the data assuming a log-normal distribution.

Seal	$K_{BET}$ Mean	$K_{BET}$ P10	$K_{BET}$ P50	$K_{BET}$ P90	Porosity Mean	Porosity P10	Porosity P50	Porosity P90
	microD	microD	microD	microD	%	%	%	%
<b>Secondary</b>	0.35	0.12	0.28	0.64	19.5	15.5	19.2	23.8
<b>Primary</b>	0.39	0.03	0.16	0.88	17.0	10.0	16.0	25.4
<b>Base/lateral</b>	0.43	0.03	0.18	0.97	15.8	11.9	15.5	20.1

The permeability is measured from MICP data as the theoretical permeability ( $K_w$ ) and is modelled from analysis of specific surface areas based on the Kozeny equation from both samples and wireline logs. The seal samples have permeabilities in the micro to nano Darcy range (Figure 1).

Most of the mudstone analysed (85%) have narrow unimodal pore throat size distributions and most (65%) have pore throat sorting (PTS) index  $\leq 1.5$  that characterise a very well sorted sediment. Some samples (40%) have extremely small throat sizes,  $r_{50}$  and the mean hydraulic radius (MHR) of 6-8 nm, that characterise a very fine grained and tight sediment. Very few samples have pore throats  $> 100$  nm. Pore throat size is the major controlling property on permeability and capillary pressure and thereby the important displacement pressure in the  $CO_2$  – brine – mudstone system, ie. the pressure where dense  $CO_2$  is expected to invade the Nini West caprock.

The seal capacity has been estimated and expressed as the maximum vertical column  $H_{max1}$  of dense  $CO_2$  that the caprock can withhold before displacement of the wetting brine phase in the caprock, on the condition that the caprock remains strongly water-wet (ie. contact angle  $\Theta = 0^\circ$ , so  $\cos \Theta = 1$  in the Washburn equation). This capacity is here estimated to be between a high case of 2074 m assuming seal from tightest rock type measured and complete water-wet seal to 604 m assuming a sealing rock type represented as an average of all measurements (excluding 3 samples) and a semi water wet seal. This suggest that regardless of the selected measurements, and assuming a  $CO_2$  max column  $< 100$  m in the Nini West reservoir then there is a comfortable caprock safety column overhead for  $CO_2$  sequestration in the reservoir even for the most pessimistic scenario.

The general very low gas concentrations and the gas composition in the seal complex demonstrate that the caprock has an efficient sealing capability that area-wise seems to extend beyond the Nini West Field. This is supported by: 1. Only very limited vertical migration of thermogenic gas into the lower part of the primary seal (Horda Fm and Lark L1); 2. No migration of thermogenic gas into the upper part of the primary seal and the secondary seal; 3. Many hundreds of meters of caprock is overlying the vertical thermogenic gas migration front; 4. The gas recorded in most of the seal complex and the overburden is very likely non-moveable *in situ* generated biogenic gas.

## INTRODUCTION

The purpose of the EUDP funded Project Greensand is to examine if the Paleocene sand in the depleted Danish North Sea oil- and gas fields can be utilized for safe long-term storage of CO<sub>2</sub> (Carbon Storage). The project tests the Nini West reservoir and seal from experiments. The seal is tested on samples from below the reservoir and from the overlying mudstones, to demonstrate the viability of the caprock properties and thus to contribute to the overall evaluation of the storage site.

The mudstone that seals the Nini West oil field are proven caprocks in the Danish North Sea and elsewhere in the North Sea. The most important property controlling seal efficiency of a mudrock is the pore throat size because it controls permeability and capillary entry pressure (Katsube and Williamson, 1994; Bruno et al. 2014). In addition, the mineralogy of the seal is investigated as the minerals may react with CO<sub>2</sub> and potentially alter the properties of the seal. As an example in a CO<sub>2</sub> sequestration context, calcareous shales may not unconditionally be an ideal seal due to mineral reactions taking place between CO<sub>2</sub> dissolved in the aqueous pore fluid and reactive minerals like carbonates (i.e. on the EU Weyburn Monitoring Project see Riding and Rochelle, 2005). Further Krushin (1997) observed that organic shales offered a lower seal quality due to matrix shrinking during subsidence and following hydrocarbon generation, which gave rise to larger entry pressure pore throats.

Here we report on the work package 4 (WP 4). The purpose of this WP was to address the seal capacity on core and cuttings material by analysing the transmissivity, mineralogy, permeability, pore size distribution and geomechanical properties. An accompanying report (Holmslykke et al. 2021) address the reactivity of the seal from experimental data. In addition to this a 3D geomechanical study commissioned to Baker reports on the mechanical properties. The seal complex and general geology for the Nini West storage complex has been outlined in the Greensand report WP4 TRL 3 by Schovsbo (2020) and by the Greensand consortium report to DNV for fulfilment of the Statement of Feasibility. All reports form the basis for the final Greensand project reporting on the seal capacity.

## STRATIGRAPHY AND SAMPLING

A description of the geological setting, the lithostratigraphic units, and the well correlation within the Nini West Seal Complex is presented in Schovsbo (2020). The stratigraphy in the area is based on the detailed and comprehensive log stratigraphy that exists for the section in the Siri Canyon (Figures 2–3, Schiøler et al., 2007). In this study a detailed lithostratigraphy has been established for the Nini-4/-4A wells (Figure 4).

The seal in the Nini West area was divided into a primary and a secondary seal by Schovsbo (2020) (Figure 4). The primary seal in the Nini West Field is in the Nini-4 well 340 m thick and is composed of shales that belong to the Eocene to Miocene Horda Fm and the lower to mid Lark Fm. The Horda Fm is characterised by greenish grey to greyish green fissile mudstone. Subordinate limestone beds and thin layers of black mudstones occur at some levels in the formation. The lower Lark Fm is dominated by dark, greenish grey, non-fissile mudstones with subordinate intervals of brownish grey mudstones. The secondary seal is in the Nini-4 well is 550 m thick and belongs to the mid to upper Lark Fm. This shale is composed of pale to dark brownish grey mudstones with subordinate intervals of greenish grey mudstones. The combined seal sequence is thus almost 900 m thick in the Nini West area. The above lying strata, i.e. the remaining c. 800 m, belongs to the Nolde Sand and the Nordland Group and is considered as overburden (Figure 4).

A total of 20 samples were picked from the primary seal, the base seal, and the lateral seal (Sele Fm) in the Nini-4 and Nini 4a wells (Figure 5, Table 1). The samples were primarily picked from Nini-4 (16 samples) and aimed at characterising the primary seal complex and the base/lateral seal. The samples in Nini-4a was picked to include more of the lithological variation of the cored section. For characterising the composition of the remaining seal i.e. the upper part of the primary seal and the secondary seal calibrated well logs were used combined with cuttings descriptions as documented by Schovsbo (2020).

The sampling was guided by existing data on mineralogy picked from the Nini-4 well and reported together with the core analysis report. Existing data was reviewed and summarised by Schovsbo (2020).

### Concluding remarks

Both the primary seal complex and the base/lateral seal were sampled and characterised. For characterising the composition of the remaining seal i.e. the upper part of primary seal and the secondary seal calibrated well logs were used.

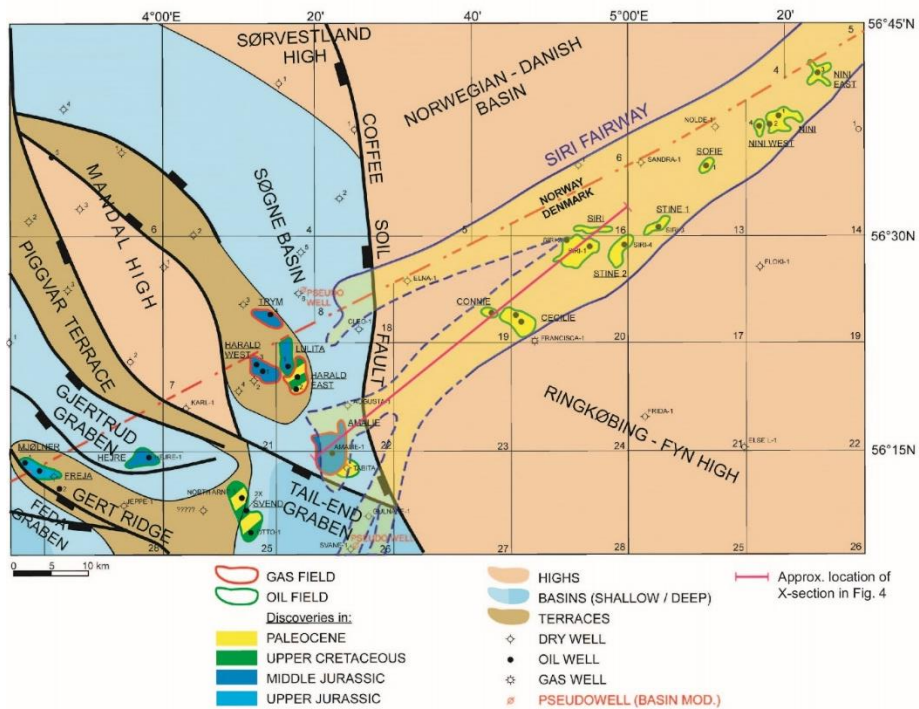


**Figure 2** Siri Canyon with location of the Nini West field and Nini-4 well position. From Ohm et al. (2006).

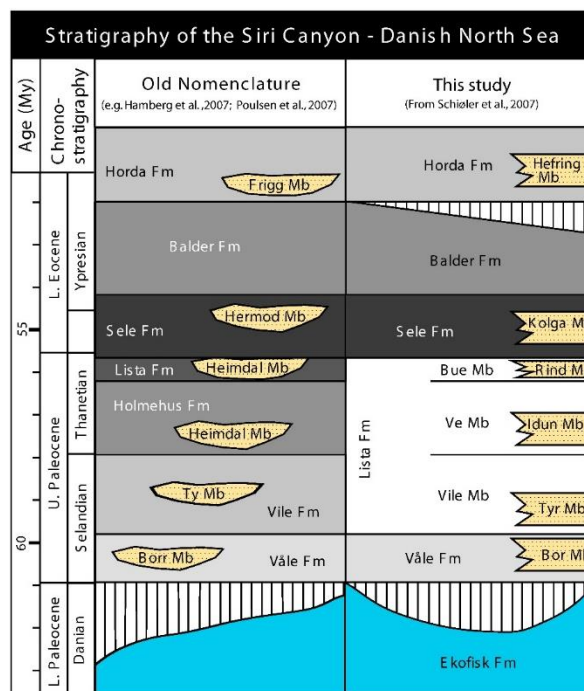


**Figure 3** Stratigraphy of the reservoir and lowermost seal. The Nini West reservoir is represented by Kolga sand remobilised into the Balder Fm.

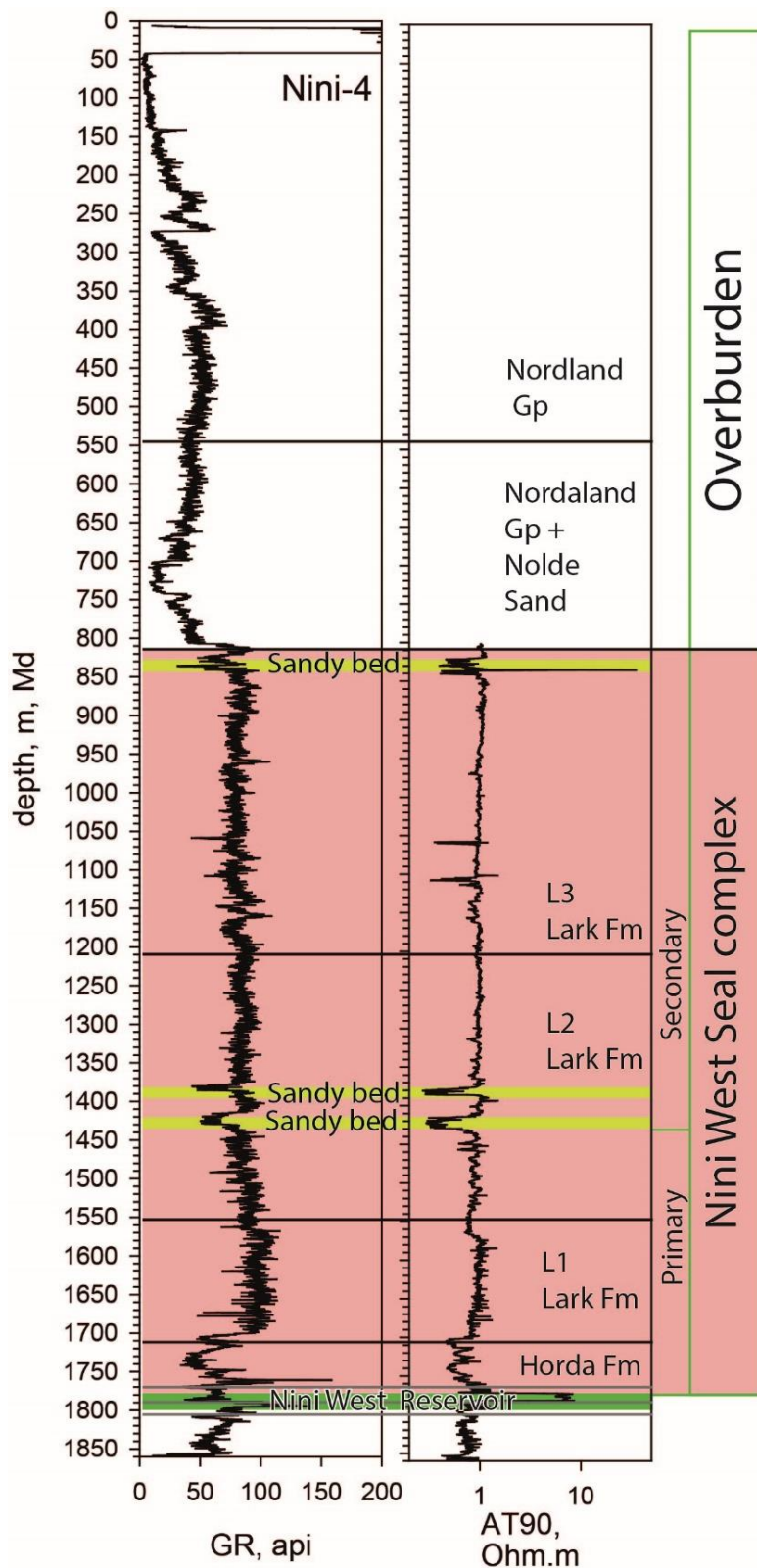


**Figure 4** Seal and overburden units in the Nini-4 well. Stratigraphy is after Schiøler et al (2007). Illustration is from Schovsbo (2020). The base seal shale below the Nini West reservoir is composed by the Sele and Lista Fms (c.f. Figure 3).

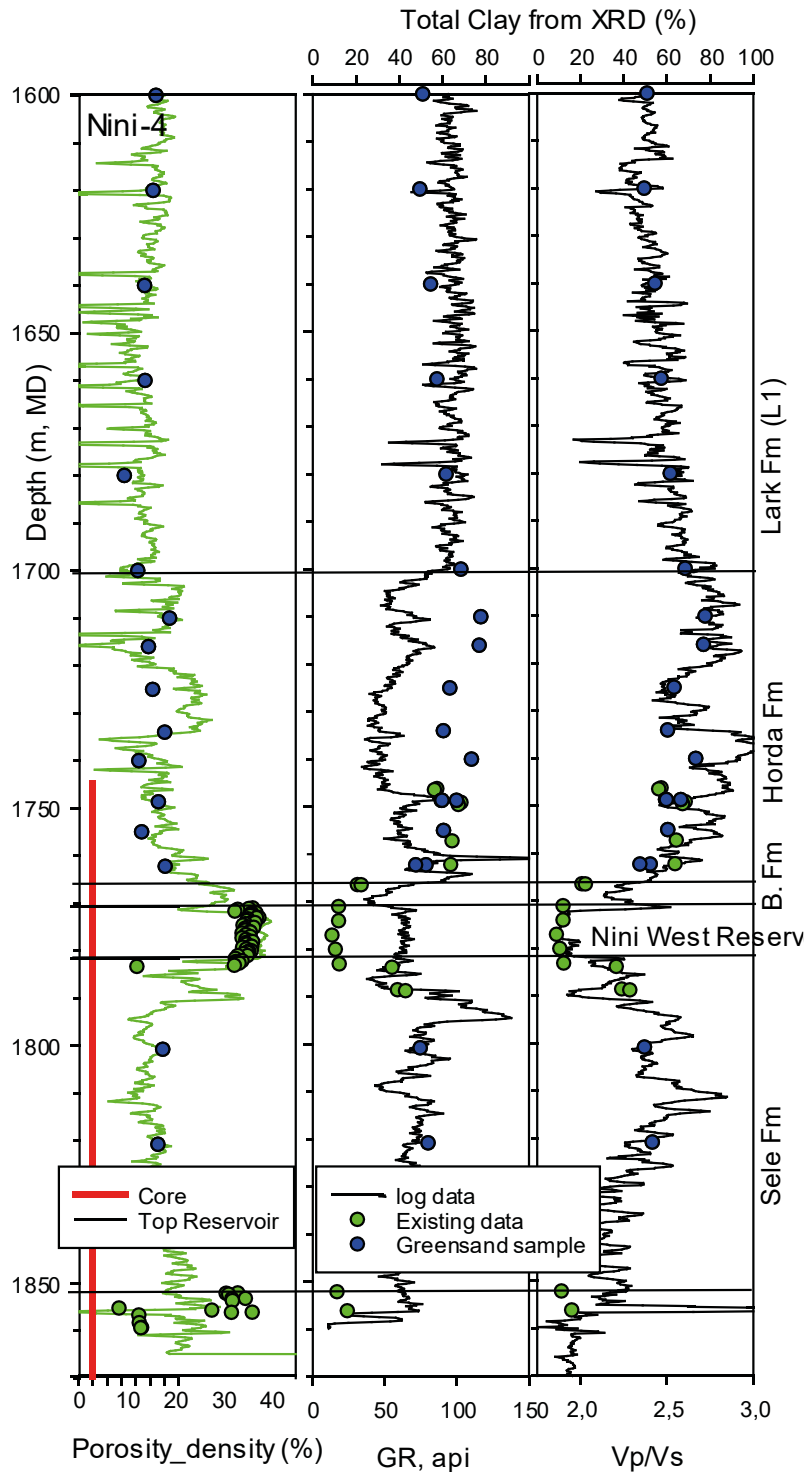


**Figure 5** Sample positions of 16 samples picked in the Nini-4 well together with well-logs with selected data (Porosity, Total clay volume (from XRD) and wireline logs; NPHI, interpreted PHI from density, GR and the Vp/Vs ratio). The Nini-4 well was drilled as a vertical well. Note that total clay content is shown on x-axis with label above.

**Table 1** Sample list with lithostratigraphy and seal units of the Nini-4 and -4A samples.

Internal number	Material	Well	Depth top (m, md)	Depth bund (m, md)	Formation	Seal
1	cuttings	Nini-4	1590	1600	Lark	Primary Seal
2	cuttings	Nini-4	1610	1620	Lark	Primary Seal
3	cuttings	Nini-4	1630	1640	Lark	Primary Seal
4	cuttings	Nini-4	1650	1660	Lark	Primary Seal
5	cuttings	Nini-4	1670	1680	Lark	Primary Seal
6	cuttings	Nini-4	1690	1700	Lark -Horda	Primary Seal
7	cuttings	Nini-4	1707	1710	Horda	Primary Seal
8	cuttings	Nini-4	1713	1716	Horda	Primary Seal
9	cuttings	Nini-4	1722	1725	Horda	Primary Seal
10	cuttings	Nini-4	1731	1734	Horda	Primary Seal
11	cuttings	Nini-4	1737	1740	Horda	Primary Seal
12	cuttings	Nini-4	1749	1755	Horda	Primary Seal
13	core	Nini-4		1762,27	Horda	Primary Seal
14	core	Nini-4		1820,79	Sele	Base/Lateral Seal
15	core	Nini-4		1748,65	Horda	Primary Seal
16	core	Nini-4a		1910,37	Horda	Primary Seal
17	core	Nini-4a		1915,46	Horda	Primary Seal
18	core	Nini-4		1800,76	Sele	Base/Lateral Seal
19	core	Nini-4a		1902,72	Horda	Primary Seal
20	core	Nini-4a		1955,56	Horda	Primary Seal

## CLEANING PROCEDURES

The 20 samples collected for analysis from the Nini-4 and -4A wells represent both core and cuttings samples. Each sample represent approximately 60-gram material and all samples were cleaned with dichloromethane to remove mud system contamination and then extracted in a soxhlet apparatus with dichloromethane and methanol solution (Table 2).

**Table 2** Sample list showing sampling depth (m MD), formation, sample type, and preparation procedure before analysis.

Internal number	Material	Well	Depth top (m, md)	Depth bund (m, md)	Formation	Material	Sample material	-Preparation, Cleaning drying, crushing if possible
1	cuttings	Nini-4	1590	1600	Lark	wet cuttings	1-4 mm size fraction used.	Cleaned in methanol+ dichloromethane
2	cuttings	Nini-4	1610	1620	Lark	wet cuttings	1-4 mm size fraction used.	Cleaned in methanol+ dichloromethane
3	cuttings	Nini-4	1630	1640	Lark	wet cuttings	1-4 mm size fraction used.	Cleaned in methanol+ dichloromethane
4	cuttings	Nini-4	1650	1660	Lark	wet cuttings	1-4 mm size fraction used.	Cleaned in methanol+ dichloromethane
5	cuttings	Nini-4	1670	1680	Lark	wet cuttings	1-4 mm size fraction used.	Cleaned in methanol+ dichloromethane
6	cuttings	Nini-4	1690	1700	Lark - Horda	wet cuttings	1-4 mm size fraction used.	Cleaned in methanol+ dichloromethane
7	cuttings	Nini-4	1707	1710	Horda	wet cuttings	1-4 mm size fraction used.	Cleaned in methanol+ dichloromethane
8	cuttings	Nini-4	1713	1716	Horda	wet cuttings	1-4 mm size fraction used.	Cleaned in methanol+ dichloromethane
9	cuttings	Nini-4	1722	1725	Horda	wet cuttings	1-4 mm size fraction used.	Cleaned in methanol+ dichloromethane
10	cuttings	Nini-4	1731	1734	Horda	wet cuttings	1-4 mm size fraction used.	Cleaned in methanol+ dichloromethane
11	cuttings	Nini-4	1737	1740	Horda	wet cuttings	1-4 mm size fraction used.	Cleaned in methanol+ dichloromethane
12	cuttings	Nini-4	1749	1755	Horda	wet cuttings	1-4 mm size fraction used.	Cleaned in methanol+ dichloromethane
13	core	Nini-4		1762,27	Horda	core	two 1 1/2 plugs same level	Cleaned in methanol+ dichloromethane
14	core	Nini-4		1820,79	Sele	core	two 1 1/2 plugs same level	Cleaned in methanol+ dichloromethane
15	core	Nini-4		1748,65	Horda	core	two 1 1/2 plugs same level	Cleaned in methanol+ dichloromethane
16	core	Nini-4a		1910,37	Horda	core	two 1 1/2 plugs same level	Cleaned in methanol+ dichloromethane
17	core	Nini-4a		1915,46	Horda	core	two 1 1/2 plugs same level	Cleaned in methanol+ dichloromethane
18	core	Nini-4		1800,76	Sele	core	two 1 1/2 plugs same level	Cleaned in methanol+ dichloromethane
19	core	Nini-4a		1902,72	Horda	core	two 1 1/2 plugs same level	Cleaned in methanol+ dichloromethane
20	core	Nini-4a		1955,56	Horda	core	two 1 1/2 plugs same level	Cleaned in methanol+ dichloromethane

## BATCH EXPERIMENTS

To examine the reactivity of the seal towards CO<sub>2</sub> samples #13 and #15 from the Nini-4 well were prepared for reactivity testing at GEUS.

Results from this experiment are reported by Holmslykke et al. (2021). The main conclusion on the mineralogical changes after exposure of samples to CO<sub>2</sub> saturated brines for extended time was that the mineral reactions are limited and thus that the seal rock is chemical stable. The data show that only a slight increase in the illite content and comparable decrease in smectite from XRD spectra analysis was observed after the CO<sub>2</sub> experiment. However, transformation of smectite-layers into illite-layers could not be verified by direct measurements of the mineralogical composition of the clay fraction and was not supported by water chemical analysis or thermodynamic modelling. Heulandite-filled secondary porosity after diatom frustules varied in appearance after CO<sub>2</sub> exposure. Some minerals show clear dissolution voids whereas other seems to be unaffected. Opal spheres was not observed and might have been dissolved during the experiments.

## PARTICLE SIZE DISTRIBUTION

The particle size distribution was determined by GEUS (laboratory numbers 20530–20548) following the standard described in ISO 17892-4:2016.

As the mudstones are unconsolidated approximately 30 gram of uncrushed sample material was carefully dissolved in water. For grain size determinations the hydrometer sedimentation method was used. Size fractions were determined by sieving whereby a sample was separated by test sieves into particle size classes. This procedure is aligned with the sedimentation process of soil particles setting through a liquid, where the difference in settling rate enables the particle size classes to be separated.

The analysis was successfully completed for 19 samples as sample #10 had too little material (Table 3). All but sample #20 have a dominant particle size  $<63 \mu\text{m}$  and of these most samples have more than 50% clay particles.

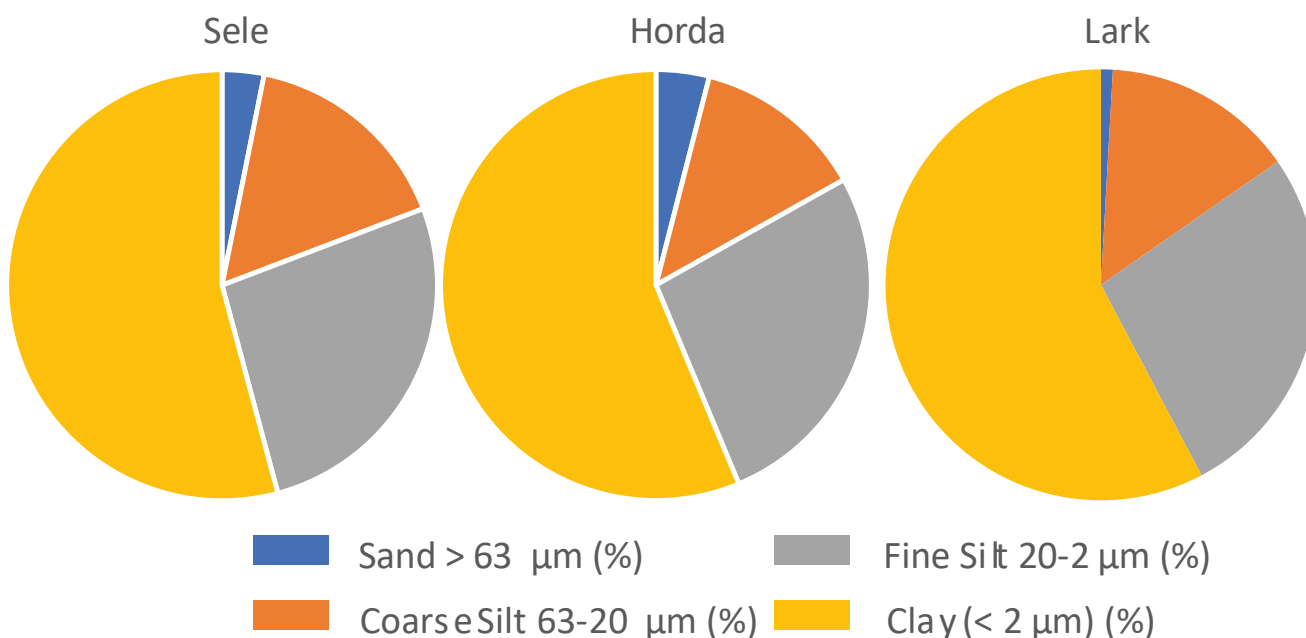


**Figure 6** Grain size distribution of the seal samples divided into stratigraphic units. Results are presented in Table 3.

The particle size distribution for the Sele, Horda and Lark Fms is quite alike (Table 3 and Figure 6). All have less than 5% sand fraction particles and are totally dominated by clay size particles. Within the silt size fraction, the fine silt size dominates (Figure 6).

**Table 3** Results of particle size distribution analysis. n.d.: Not determined.

Well	Depth top (m, md)	Depth bund (m, md)	Formation	Internal number	Sand > 63 $\mu\text{m}$ (%)	Coarse Silt 63-20 $\mu\text{m}$ (%)	Fine Silt 20-2 $\mu\text{m}$ (%)	Clay (< 2 $\mu\text{m}$ ) (%)
Nini-4	1590	1600	Lark	1	1	23	27	50
Nini-4	1610	1620	Lark	2	1	17	28	53
Nini-4	1630	1640	Lark	3	1	9	27	63
Nini-4	1650	1660	Lark	4	1	12	27	60
Nini-4	1670	1680	Lark	5	1	10	27	63
Nini-4	1690	1700	Lark -Horda	6	1	16	27	57
Nini-4	1707	1710	Horda	7	2	6	33	59
Nini-4	1713	1716	Horda	8	2	12	20	67
Nini-4	1722	1725	Horda	9	2	14	37	47
Nini-4	1731	1734	Horda	10	n.d.			
Nini-4	1737	1740	Horda	11	3	11	33	52
Nini-4	1749	1755	Horda	12	3	18	31	48
Nini-4		1762,27	Horda	13	8	10	33	50
Nini-4		1820,79	Sele	14	0	13	29	58
Nini-4		1748,65	Horda	15	5	16	20	59
Nini-4a		1910,37	Horda	16	13	17	24	46
Nini-4a		1915,46	Horda	17	4	17	26	53
Nini-4		1800,76	Sele	18	7	24	31	38
Nini-4a		1902,72	Horda	19	1	15	25	59
Nini-4a		1955,56	Horda	20	85	n.d.		

From thin section analysis (Figure 9, 10) it was noted that coarse grained particles include diagenetic formed minerals such as heulandite that may precipitates in the sand size as replacements of diatoms or as silt size crystals within the matrix. The large fraction of clay sized particles is in good agreement with the domination of clay minerals and the mudstone rock type.

### Concluding remarks

The investigated samples are composed of mudstone dominated by clay size particles. The clay size fraction represents up about 60% of the rock while the sand size fraction constitutes less than 5% and typically only 1% of the rock. From thin section analysis coarse grained particles include diagenetic formed minerals such as heulandite that may precipitates in the sand size as replacements of diatoms or as silt size crystals within the matrix. The large fraction of clay sized particles is in good agreement with the domination of clay minerals and the mudstone rock type.

## MINERALOGY AND PETROGRAPHY

Mineralogical compositions of the mudstones were obtained by X-ray diffraction (XRD) of bulk rock and clay fraction samples at DTU. Samples for bulk rock analysis were crushed in a wolfram-carbide mortar. The powder was pressed into a disk prior to bulk rock analysis. Air dry samples were prepared by suspending 0.03 g of the clay fraction into 1.5 mL distilled water and spread evenly over a glass plate and dried 24 hours. Subsequently, the samples were saturated with ethylene glycol for two days at 60°C before analysis. The samples were first heated to 350°C in an oven for 2 hours and left to cool overnight before analysis. Second heat treatment was at 550°C. Both randomly oriented bulk samples and oriented clay fraction samples were analyzed by a Panalytical-X-Pert Pro. Semi-quantification was performed by multiplying peak height with correction factors similar to the method by Hillier (2003). Two bulk rock samples were scanned on a Bruker-AXS diffractometer D8 Advance with primary beam Ge111 monochromatic CuK $\alpha$  radiation and a LynxEye silicon-strip detector at University of Copenhagen. Quantification of major mineral phases was done by Rietveld analysis of X-ray diffractograms of bulk-rock samples. The results were used to adjust the correction factor of heulandite.

The mudstone samples were impregnated in blue epoxy for easy identification of porosity and prepared as polished thin sections. The thin sections were investigated in transmitted and reflected light microscopy. Supplementary studies of the mudstones were performed on carbon-coated thin sections using a Zeiss Sigma 300 VP operating at 10–15 kV equipped with double Bruker energy dispersive X-ray spectrometers (EDS) with 30 mm<sup>2</sup> active areas.

The composition of the caprock mudstones in the Nini-4 and Nini-4A wells is presented in Figures 7 and 8. Samples from the Sele, Horda and Lark Fms in the Nini-4 well were analyzed, whereas in the Nini-4A well only samples from the Horda Fm were analyzed.

The Sele Fm consists of illite, quartz and minor amounts of K-feldspar, plagioclase, pyrite and varying amounts of heulandite. The clay minerals are mainly illite in the Sele Fm. Heulandite is abundant in the lower part of the overlying Horda Fm and decreases upwards. Clay minerals comprise the majority (> 55–60%) of the Horda Fm, whereas heulandite and quartz are present in smaller amounts. Less abundant minerals comprise plagioclase, siderite and pyrite. The clay minerals are mainly of illitic and smectitic composition. The smectitic component consists of randomly stratified mixed-layer smectite/illite, according to their second order peak at 8.76Å when glycolated. The illitic component is a mixture of discrete illite and ordered interstratified mixed-layer illite/smectite. The uppermost part of the Horda Fm (immediately beneath the Lark Fm) has a relatively high content of cristobalite, and kaolinite is introduced as part of the clay minerals. Opal CT consist of a mix between cristobalite and tridymite, so the cristobalite is likely hosted in this phase. The clay mineral composition of the Lark Fm shows an upward change from a combination of smectite, illite and kaolinite to a more illitic composition and increasing amounts of kaolinite and rare chlorite.

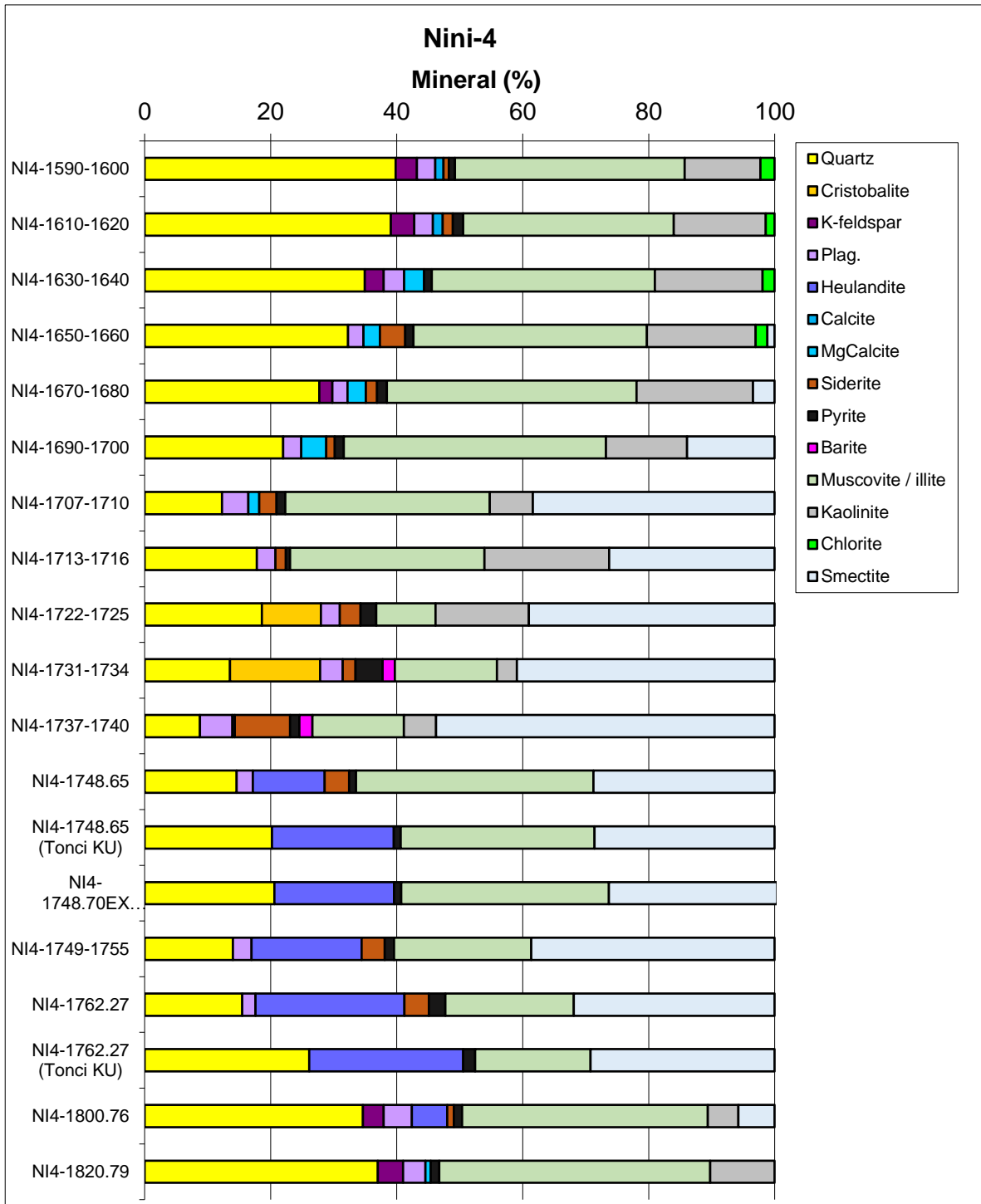


**Figure 7** Mineralogical composition, based on bulk rock XRD, of the caprock sediments overlying the glauconitic sandstones in the Nini-4 well.

The samples from the Nini-4A well are mineralogically similar to the central part of the Horda Fm in the Nini-4 well. Only small with variation in the smectitic/illitic clay and siderite/pyrite contents are seen.

Major petrographically differences can be observed between the Sele and Horda Fms, since the Sele Fm contains common silt-sized glauconite clasts, whereas the Horda Fm contains sand-sized areas filled with heulandite crystals that is a zeolite mineral (Figure 9). Glauconite is not recognized in the clay mineralogical analysis due to its presence in small amounts and a likely composition of mixed-layer smectite/illite similar to the glauconitic clasts in the sandstones from the Våle and Lista Fms. Heulandite occurs as filling of secondary porosity probably after dissolved diatom frustules, which can have sizes up to 200 µm. The heulandite-filled diatoms are almost perfectly round, and the clay matrix has been deformed around them in the investigated parts of the Horda Fm from the Nini-4 well (Figures 9A–C and 7D). Heulandite forms interlocking crystals in typically microquartz and Fe-rich clays matrix (Figure 10B–D). Occasionally, heulandite encloses opal spheres (Figure 10). The lowermost sample from the Horda Fm in the Nini-4A well has a remarkably darker colour, possibly due to more disperse organic matter, and the heulandite-filled secondary porosity after diatom frustules is occasionally deformed (Figure 9E). Calcite-cemented lamina with a high concentration of calcareous bioclasts is present in this sample. Pyrite occurs as framboids mainly associated with organic matter or together with heulandite in secondary porosity after diatoms (Figure 10F).

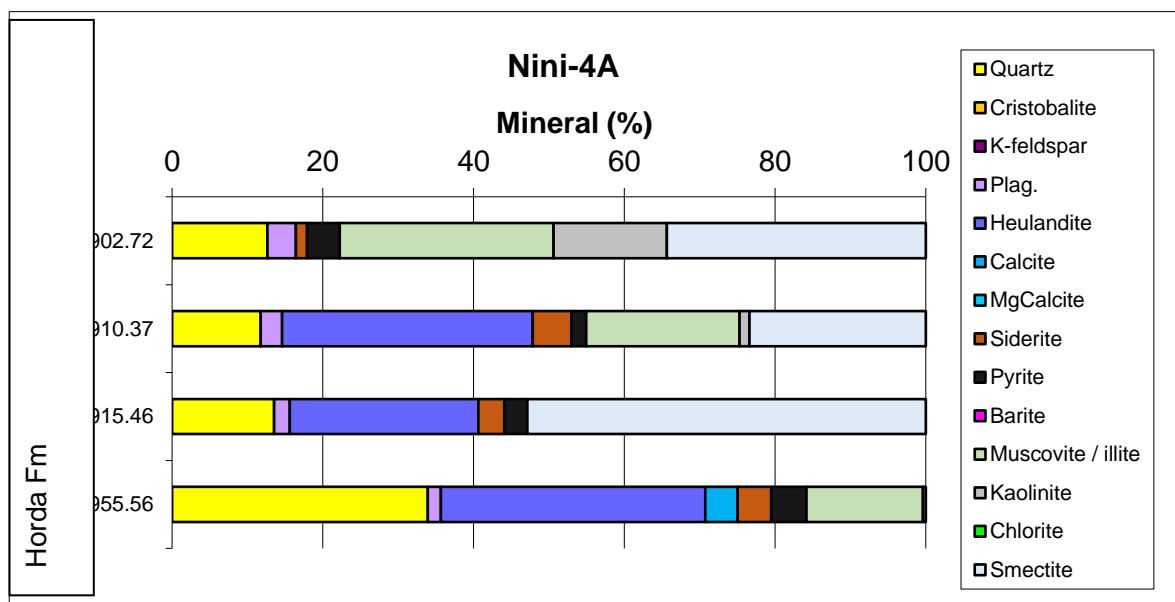


**Figure 8** Mineralogical composition, based on bulk rock XRD, of the caprock sediments overlying the glauconitic sandstones in the Nini-4A well.

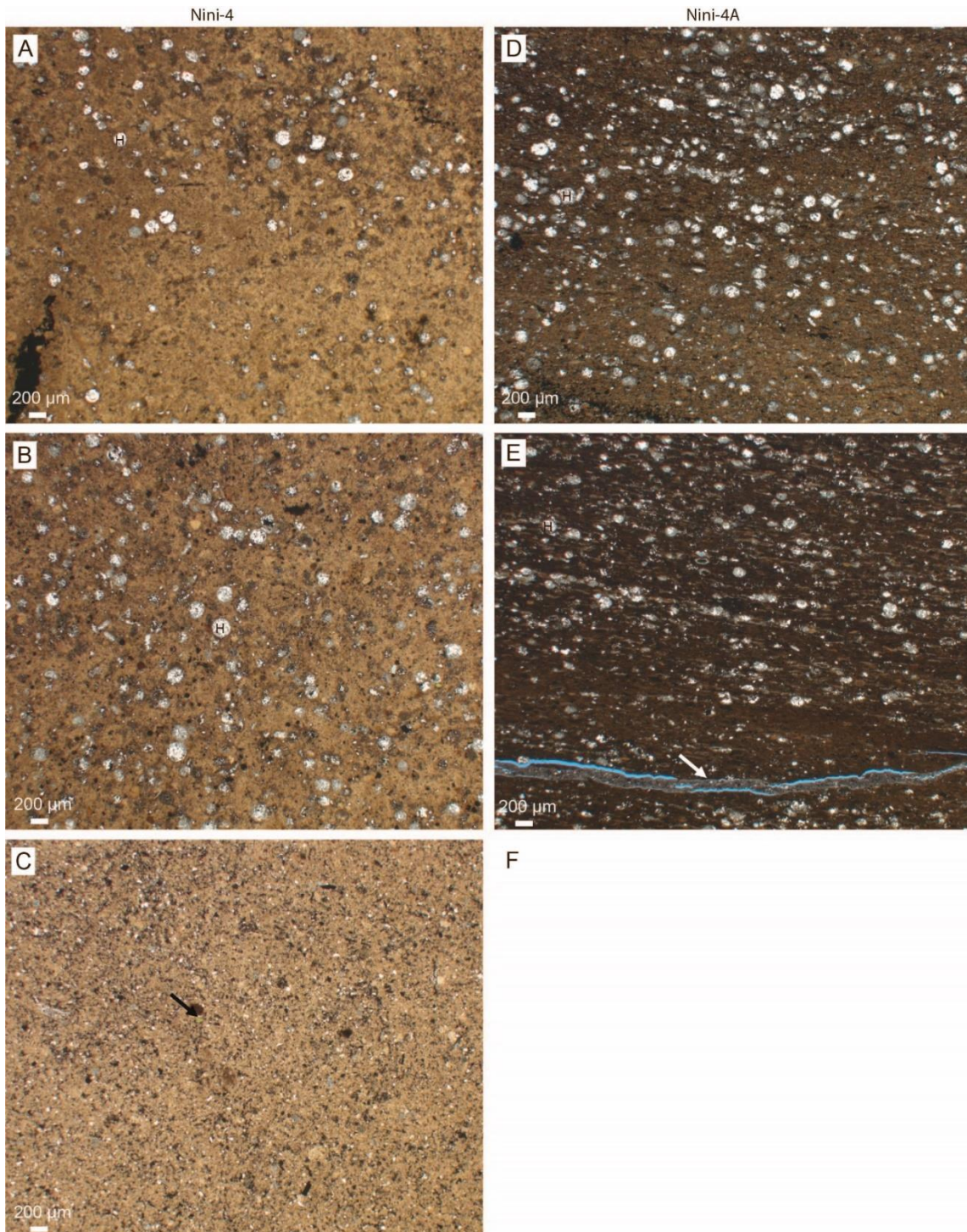


**Figure 9** Overview of thin sections from the Sele and Horda Fms. A. Horda Fm, Nini-4, 1748.65 m. B. Horda Fm, Nini-4, 1762.27 m. C. Glauconite clasts (arrow) is common in the Sele Fm, Nini-4, 1820.79 m. D. Horda Fm, Nini-4A, 1910.37. E. Calcitic bioclasts lamina (arrow) occur in this part of the Horda Fm, Nini-4A, 1915.46 m.

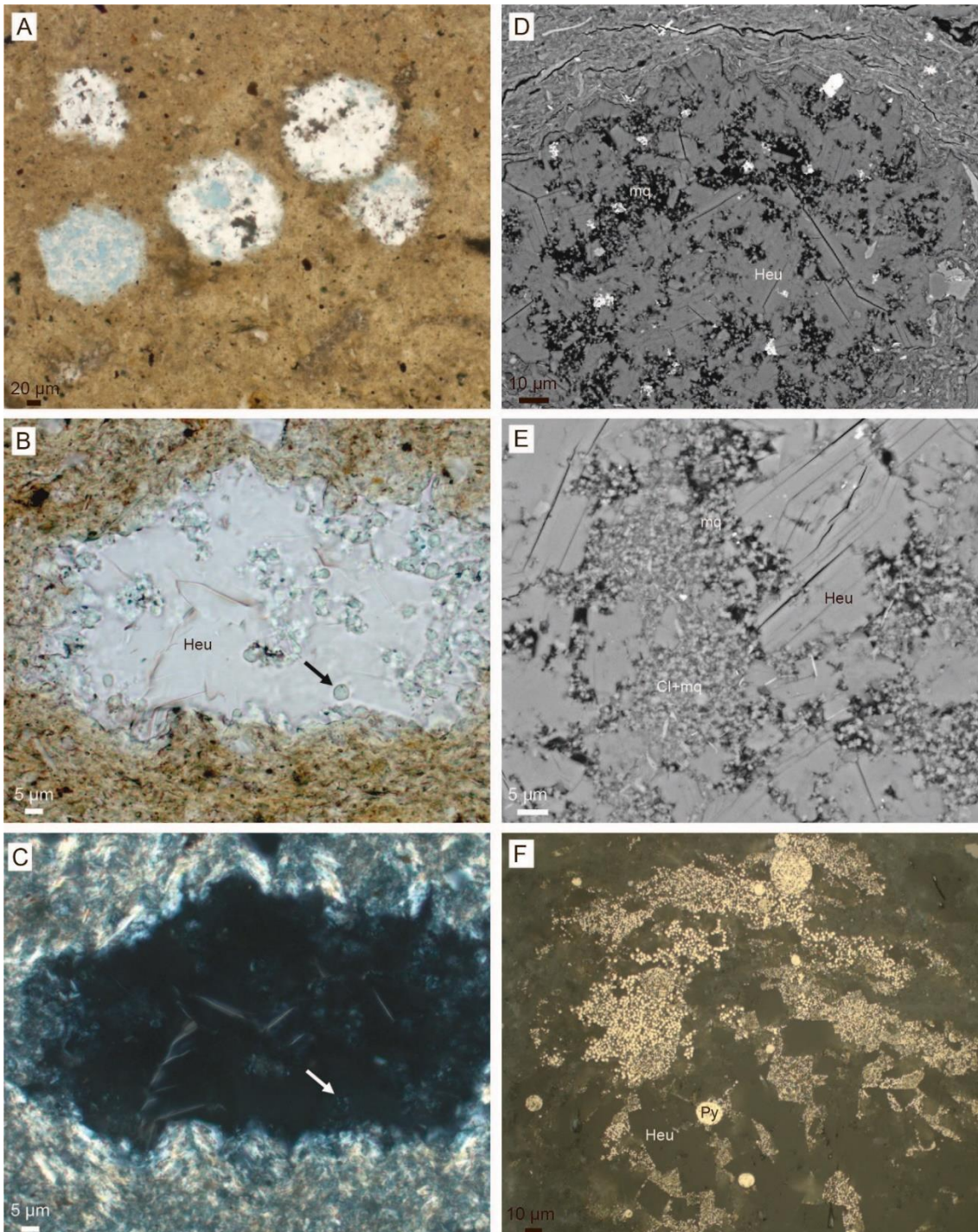


**Figure 10** Details from the Horda Fm, Nini-4, 1748.65 m. A. Different degrees of heulandite filling of former diatoms. B. Heulandite (Heu) enclosing opal spheres (arrow). C. Similar to B with crossed nicols. D. Lamina deformed around the heulandite-filled secondary porosity after diatom frustule. Backscatter electron micrograph. E. Microquartz (mq) and Fe-rich smectitic clays (Cl) enclosed in heulandite-filled porosity after diatom frustule, Backscatter electron micrograph. F. Frambooids of pyrite (Py) in centre of heulandite-filled secondary porosity after diatom frustule. Reflected light.

### Grain size and total clay content

There is an overall good relationship between grain size determination and total clay content determined by bulk XRD analysis (Figure 11). The ratio between the two determinations are 0.88 suggesting that most clay minerals are in the clay size fraction. Other clay size particles likely include opal/quartz and heulandite.

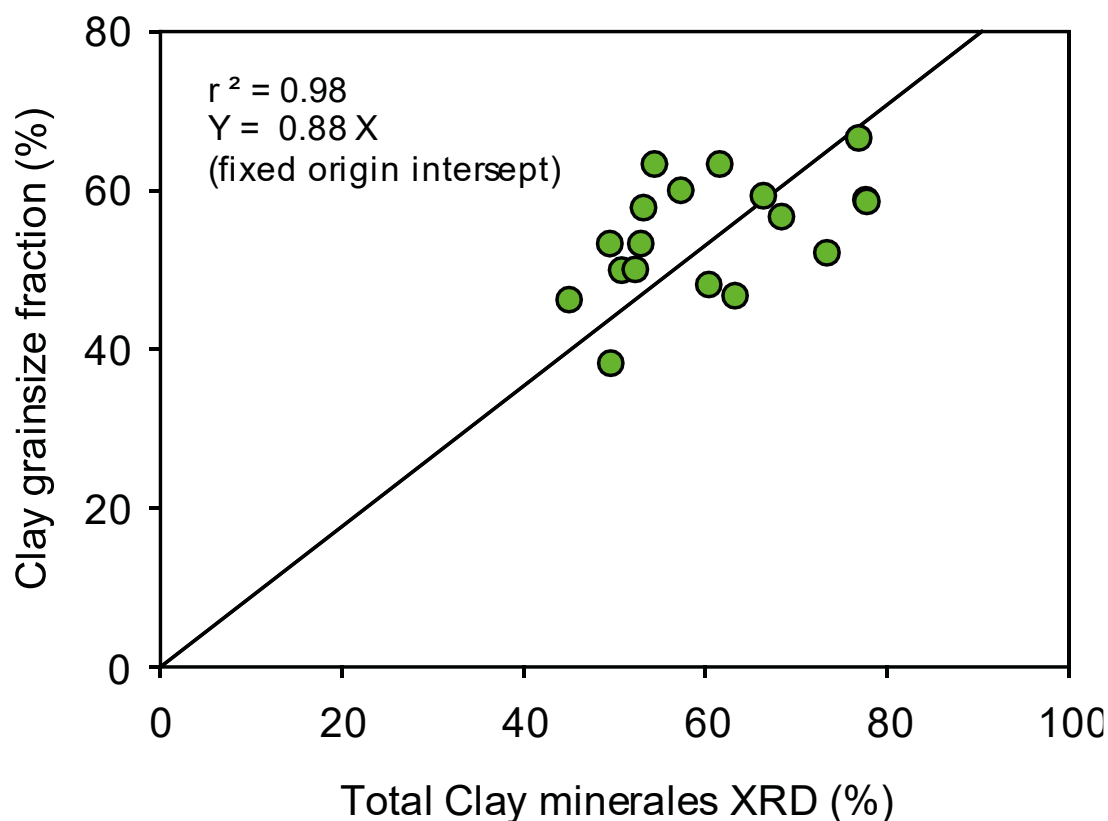


**Figure 11** Comparison between grain size determinations (Table 3) and bulk clay content determined by XRD.

### Petrophysical evaluation of the clay content

Wire-line logs have been used to evaluate the non-sampled part of the seal as these are sensitive to the mineralogical composition of the rock, notably the clay mineral content and composition. The classical tool for clay volume determinations is the gamma ray log that measure the radiation from K, Th and U. These elements occur in clays but also in other minerals such as K-feldspars and in addition U may also be hosted in organic material. Likewise, the gamma ray response of clay minerals depends on the specific composition. Highest K content and thus radioactive response is in muscovite/illite and lowest is in kaolinite and smectite.

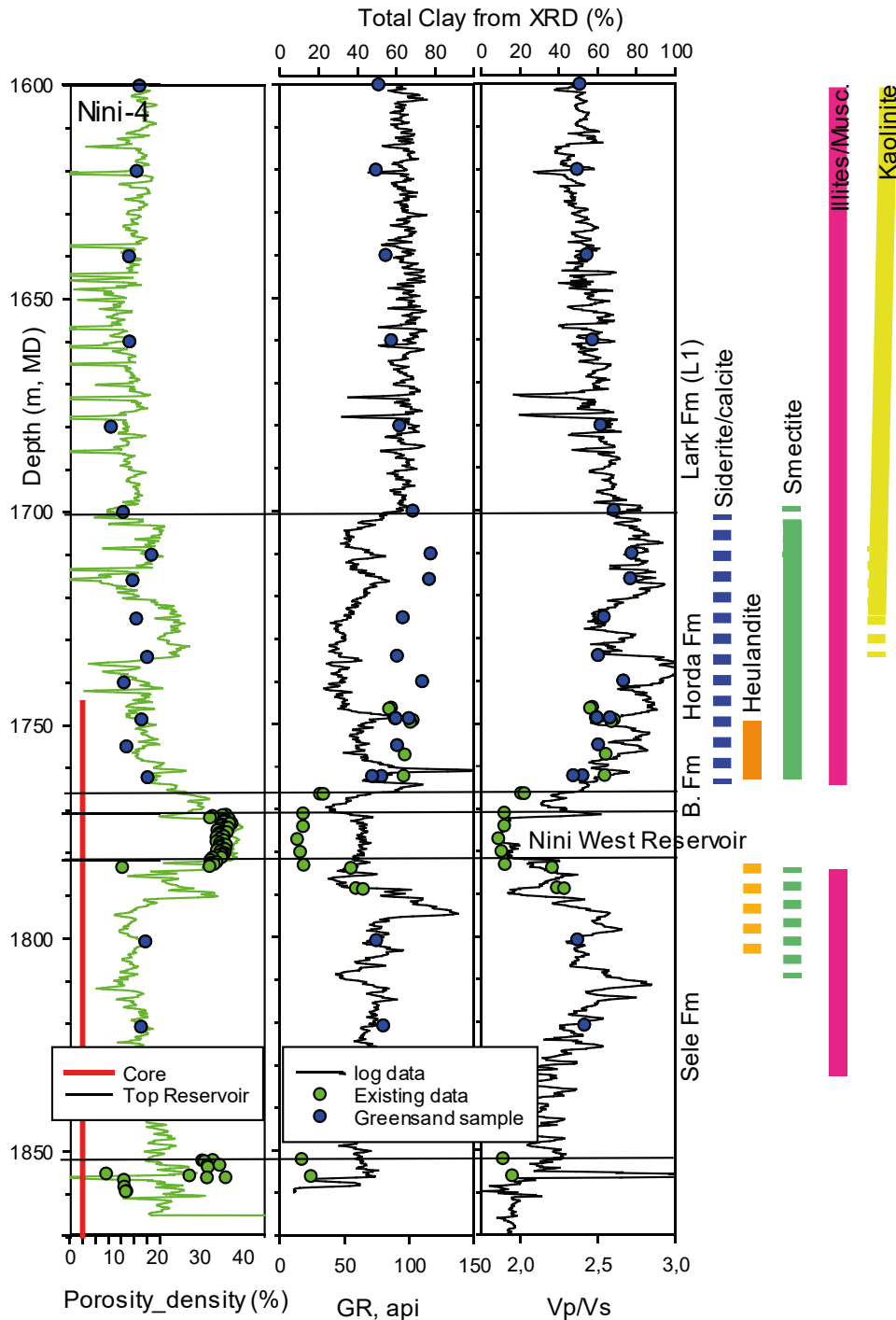


**Figure 12** Nini-4, porosity and total clay content from samples and wire-line logs (PHI interpreted from density log, gamma ray (GR) and the Vp/Vs ratio). Abbreviation: GR: Gamma Ray log; B: Balder; Musc.: Muscovite. Heulandite is a zeolite mineral. Smectite, illite and muscovite are clay minerals. Full line indicates dominant mineral proportion; broken line subsidiary mineral proportion. For full mineralogical analysis see Figure 7 and Appendix C.

In the Nini-4 well, the total clay content measured by XRD in the Horda Fm compares poor to the down-hole gamma ray log variation likely reflecting the variable clay mineral assemblage and the “hot” organic rich zones (Figure 12). Relative low gamma ray responses are seen in the smectite rich intervals likely reflecting its low K content. The clay volume determined from XRD compares on the other hand well to the VP/VS ratio that also is known to be lithological sensitive. Clean reservoir sand usually has a low VP/VS ratio and clay rich parts have a high ratio. However, the VP/VS ratio also depends on occurrence of fractures and on the fluid type and thus care should be taken when interpreting the results. In the Nini-4 only low amounts of gas to none is present in the seal (see later sections and in Figure 23) and no fracture zones are known and thus the VP/VS ratio dominantly reflect lithological changes and is here used as a proxy for clay mineral variation (Figure 12).

From plotting the down-hole variation of the total clay content with the VP/Vs ratio a simple rescaling of the VP/VS to match the total clay content has been found:

$$\text{Total clay content (\%)} = (\text{VP/VS} - 1.8) / 0.013$$

The constants 1.8 and 0.013 have been read from the Nini-4 VP/VS log representing high and low total clay content determined from XRD. The model has been calibrated to fit both the base/lateral seal (Sele Fm) and the Horda and Lark top seal formations. As the total clay content determined from XRD also correlated with the fraction in clay size of the samples (Figure 11) a correlation to this property thus also is possible to establish.

The petrophysical evaluation of the clay content show very good agreement with the measured data (Figure 12) which gives good confidence that the method can be used also in the upper Lark sections that has not been analysed. However, the model places most emphasis on the Horda Formation and the basal seal section. If more analysis from the Lark formation will be available, then it is likely that parameters will be selected for each formation due their different clay mineralogical composition. A value of 1.7 instead of 1.8 in the formula above for the Lark Fm will thus provide a better match with the measured total clay content, however, this value will calculate to high clay content in the Horda Formation.

Peak clay content is seen in Horda Fm where levels >70% have been measured and modelled. These peak levels correspond to intervals with high smectite abundance, and it appears that this clay type dilutes the normal background sedimentation.

In general, the clay content decreases slightly throughout the lower Lark Fm. In the mid Lark Fm the clay content stabilises, from where it increases up through the mid to upper Lark Fm (Figure 1).

## **Concluding remarks**

The mineralogical data is much in-line with existing data from the Nini-4 wells picked from the cored Sele and Horda Fms (Humphrey & Lucas 2003). The base and lateral seal is composed by the Sele

Fm. This formation consists of illite, quartz and minor amounts of K-feldspar, plagioclase, pyrite and varying amounts of heulandite. The top seal complex is composed by the Horda and Lark Fms. In the Horda Fm heulandite is abundant in the lower part and decreases upwards. The clay minerals are mainly of illitic and smectitic composition. The smectitic component consists of randomly stratified mixed-layer smectite/illite, according to their second order peak at 8.76Å when glycolated.

Total clay volume can be evaluated from well logs. In the Horda Fm the clay content is generally above 60% with peaks of 80% in parts of the Horda Fm. In the Lark Fm the Clay content decreases to about 40% in the top L1 unit wherefrom is gradually increases to more than 50% from the mid Lark Fm and upwards (Figure 1).

If more analysis from the Lark formation will be available, then it is likely that the petrophysical parameters will be selected for each formation due their different clay mineralogical composition. A value of 1.7 instead of 1.8 in eth formula above for the Lark Fm will thus provide a better match with the measured total clay content, however, this value will calculate to high clay content in the Horda Formation.

## POROSITY AND BULK DENSITY

Porosity and bulk density determinations were carried out at GEUS (Table 4). All samples were dried at 60°C for two days. The core samples consist of an approximately 1 cm long core plug. Density measurements were done by normalising the weight of the sample relative to the bulk volume measured by submersion of the sample in a Hg bath using Archimedes' principle. The porosity was determined on the same samples by subtraction of the measured grain volume from the measured bulk volume. The He technique, employing Boyle's Law, was used for grain volume determination, applying a double-chambered helium porosimeter with digital readout. For each measurement stable He volumes were reached in less than 15 minutes to ensure complete filling of the pore volume. For more detailed descriptions of methods, instrumentation, and principles of calculation, see recommended practices for core analysis (American Petroleum Institute, 1998).

The porosity of the core samples varies from 12.81–21.17%, but with most porosities being >18% (Table 4). Grain densities range from 2.45–2.66 g/cm<sup>3</sup>.

For cuttings samples He porosities were determined as part of the MICP data acquisition. The porosities following this method range between 14-19% and are thus within the range of porosities determined on core sample (Table 4).

### Petrophysical evaluation of porosity from bulk density

Porosity (PHI) was evaluated in the Nini-4 well from the formation density log (Figure 12). The porosity was calculated as:

$$\text{PHI (\%)} = (\sigma_{\text{grain}} - \sigma_{\text{bulk}}) / (\sigma_{\text{grain}} - \sigma_{\text{fluid}})$$

and

$$\sigma_{\text{grain}} = (1 - V_{\text{clay}}) \cdot 2.7 \text{ g/cm}^3 + (V_{\text{clay}}) \cdot 2.3 \text{ g/cm}^3$$

where  $\sigma_{\text{grain}}$  is the grain density calculated from the volume of clay ( $V_{\text{clay}}$ ) assuming a grain density of 2.7 g/cm<sup>3</sup> for clean reservoir and a grain density for pure clay of 2.3 g/cm<sup>3</sup>,  $\sigma_{\text{bulk}}$  is the bulk formation density from the density log and  $\sigma_{\text{fluid}}$  is the fluid density assumed to be 1.05 g/cm<sup>3</sup> reflecting a medium saline brine in the Nini area (c.f. Schovsbo et al. 2016; Olsen et al. 2020). We note that the grain density endmember for clay is low compared to reported clay densities reported by Deer et al. (1966). The model assumption compares, however, well to Totten et al. (2002) and implies that a smectite to smectite-rich mixed layer clay dominates. Further analysis based on a larger data set should evaluate this further.

The wireline evaluation show that the caprock has a porosity around 16–20% in the primary and secondary seal intervals (Figures 1 and 12). Low porosities are calculated in high density beds likely representing carbonate stringers that occur abundantly in the lower Lark Fm (c.f. Schiøler et al. 2007). An interval characterised by low porosity occur in the Horda Fm around 1740 m. This interval likely

reflects a more cemented zone of the seal as the XRD data indicate that siderite has a local peak in concentration here, suggesting this mineral is the cementing phase. Porosities of more than 30% is modelled in the sandy beds within the Lark L2 unit (Figure 1). These beds separate the primary and secondary seals from each other. The beds are also identified in the cuttings from these intervals they have a high sand grain content. Schovsbo (2020) suggested that the beds are porous as they have low formation resistivity interpreted to reflect the presence of conductive saline fluids.

**Table 4** Results of porosity, grain density and permeability measurements.

Material	Well	Depth top (m, md)	Depth bund (m, md)	Formation	Internal number	Measured Porosity (%)	He porosity MICP (%)	Grain Density (g/cm3)	Measured Air Permeability (mD)
cuttings	Nini-4	1590	1600	Lark	1		15,9		
cuttings	Nini-4	1610	1620	Lark	2		15,3		
cuttings	Nini-4	1630	1640	Lark	3		14,2		
cuttings	Nini-4	1650	1660	Lark	4		13,7		
cuttings	Nini-4	1670	1680	Lark	5		12,1		
cuttings	Nini-4	1690	1700	Lark -Horda	6		15,3		
cuttings	Nini-4	1707	1710	Horda	7		18,7		
cuttings	Nini-4	1713	1716	Horda	8		14,3		
cuttings	Nini-4	1722	1725	Horda	9		15,2		
cuttings	Nini-4	1731	1734	Horda	10		17,7		
cuttings	Nini-4	1737	1740	Horda	11		12,3		
cuttings	Nini-4	1749	1755	Horda	12		13,6		
core	Nini-4		1762,27	Horda	13	18,2	17,8	2,55	< 0,0001
core	Nini-4		1820,79	Sele	14	18,7	16,3	2,64	
core	Nini-4		1748,65	Horda	15	18,6	16,4	2,56	< 0,0001
core	Nini-4a		1910,37	Horda	16	16,3	15,6	2,48	
core	Nini-4a		1915,46	Horda	17	19,2	15,5	2,56	
core	Nini-4		1800,76	Sele	18	21,2	17,8	2,66	
core	Nini-4a		1902,72	Horda	19	20,6	12,3	2,64	
core	Nini-4a		1955,56	Horda	20	12,8	16,6	2,45	< 0,0001
core	Nini-4		1762,27	Horda	13a	17,87		2,54	
core	Nini-4		1762,27	Horda	13b	18,62		2,57	

## Concluding remarks

Porosities in the seal is determined by direct measurements on both cuttings and core samples. The data is used to calibrate porosity calculations from the density wire-line log based on a grain density model. The evaluation show that seal has a porosity around 16–20% in the primary and secondary seal intervals. Low porosities are calculated in high density beds likely representing carbonate stringers that occur abundantly in the lower Lark Fm and in the Horda Fm. XRD data indicate that siderite has a local peak in concentration, suggesting this mineral is the cementing phase. Porosities of more than 30% is modelled in the sandy beds within the Lark L2 unit that separate the primary and secondary seals from each other (c.f. Schovsbo 2020).

## PERMEABILITY

N<sub>2</sub>-permeability was measured at GEUS' core laboratory in a core holder with sleeve pressure of 27 bara (400 Psi). Gas pressure was 0.5 bar. Flow was measured on flow meter as ml. per minute.

Modelled permeability was estimated from capillary tube models, which use easily measured physical properties such as porosity, grain density and specific surface area data (Kozeny, 1927).

$$K_{BET} = c \frac{\varphi^3}{(1 - \varphi)^2 S_s^2}$$

where  $K_{BET}$  is the permeability,  $\varphi$  is porosity,  $S_s$  is specific surface (grain-surface area per grain volume). See data in Tables 4 and 5. The  $c$  factor is the Kozeny constant that will have a value between 0.22–0.24 depending on porosity (Mortensen et al., 1998).

Measured air permeability is below detection limit of the method applied, i.e. less than 0.0001 mD (Table 4). Modelled permeabilities from specific surface analysis (BET) range between 0.09–1.9  $\mu$ D with general values around 0.13  $\mu$ D (Table 5).

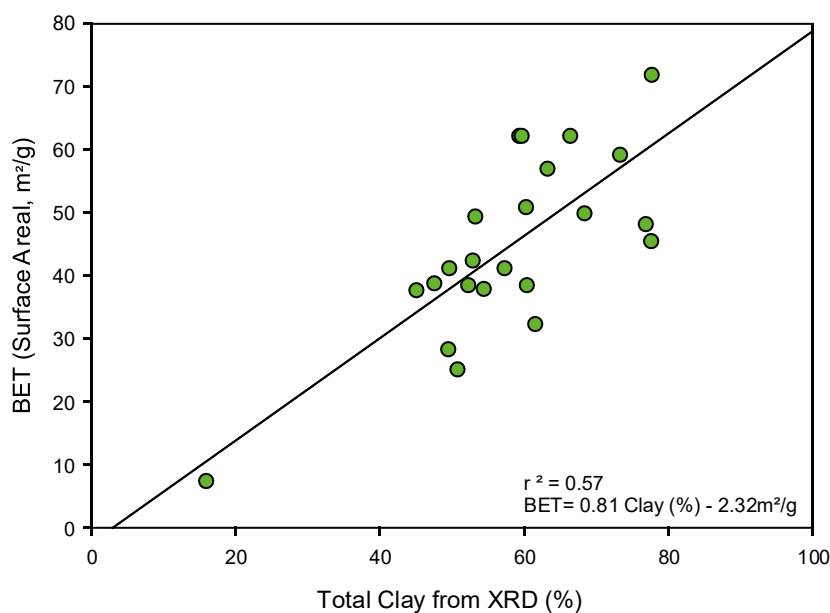


**Figure 13** Relationship between Total Clay determined from XRD and BET measurements. Note that samples with more than one XRD determination are plotted several times. The linear relationship  $BET (m^2/g) = 0.81 \cdot Clay(\%) - 2.32 m^2/g$  ( $r^2 = 0.57$ ) has been used in the petrophysical interpretation of the permeability.

Compared to the XRD determined composition there is a linearly correlation between BET and total clay content (Figure 13). Since the surface area – both internal and external – varies per clay type the correlation is not perfect. Samples with very high clay content tend to plot above the regression line. These samples are also more smectite rich that is known to have a high surface area. However, at

current the relationship can be used when the permeability is evaluated based on wire-line logs although improvement can be made if models to discriminate the individual clays types is included.

**Table 5** Specific surface analysis (BET) and modelled permeabilities ( $K_{BET}$ ).

Laboratory number	Internal number	Material	Well	Depth top (m, md)	Depth bund (m, md)	Surface Areal, m <sup>2</sup> /g	$K_{BET}$ ( $\mu$ D)
45970	1	cuttings	Nini-4	1590	1600	25,1	0,30
45971	2	cuttings	Nini-4	1610	1620	28,3	0,20
45972	3	cuttings	Nini-4	1630	1640	37,9	0,09
45973	4	cuttings	Nini-4	1650	1660	41,2	0,06
45974	5	cuttings	Nini-4	1670	1680	32,3	0,07
45975	6	cuttings	Nini-4	1690	1700	49,9	0,06
45976	7	cuttings	Nini-4	1707	1710	45,5	0,15
45977	8	cuttings	Nini-4	1713	1716	48,2	0,05
45978	9	cuttings	Nini-4	1722	1725	57,0	0,05
45979	10	cuttings	Nini-4	1731	1734	50,9	0,11
45980	11	cuttings	Nini-4	1737	1740	59,2	0,02
45981	12	cuttings	Nini-4	1749	1755	38,5	0,08
45983	13	core	Nini-4		1762,27	38,8	0,21
45985	14	core	Nini-4		1820,79	49,4	0,14
45982	15	core	Nini-4		1748,65	62,2	0,09
45987	16	core	Nini-4a		1910,37	37,7	0,16
45988	17	core	Nini-4a		1915,46	42,4	0,21
45984	18	core	Nini-4		1800,76	41,2	0,29
45986	19	core	Nini-4a		1902,72	71,9	0,09
45989	20	core	Nini-4a		1955,56	7,4	1,93

### Petrophysical evaluation of the permeability

The permeability is modelled based on the Kozeny equation and with wireline derived inputs of porosity, grain density and the surface area determined from the  $V_{clay}$  – surface areas relationship in Figure 13. The modelled permeabilities are presented in Figure 1 and is valid within the shale rich sections only as no calibration data for the reservoir section has been included. We thus estimate that only modelled  $K_{BET}$  between 0.01 - 100  $\mu$ D should be evaluated as it is assumed that the current model has is upper limits around 100  $\mu$ D.

### Porosity and Permeability relationships

The porosity-permeability relationship for the Greensand seal samples, existing reservoir samples from the Nini-4 well and the wireline-based porosity-permeability model for the seal is presented in Figure 14. The porosity of the reservoir is above 30% and permeabilities are up to 2D. Poorer quality

reservoir samples have porosities up to 15% and permeabilities in the milli Darcy range. For the reservoir section the porosity-permeability relationship can be described by a power function ( $y = ax^b$ ) with the power of 4.93 and constant of  $3.04 \cdot 10^{-2}$  or  $3.04 \cdot 10^{-3}$  depending on the reservoir quality (Figure 14).

The seal samples plot with porosities up to 19% and permeabilities in the micro to nano Darcy range (Figure 14). The wire-line modelled results plot within the same range as the samples but also defines porosity-permeability ranges that are not reflected in the sample data. For both samples and the wire-line log interpretation in the seal section a power function with same power as in the reservoir but with a constant of  $1.5 \cdot 10^{-8}$  can be fitted to the data as representative of the general relationship.

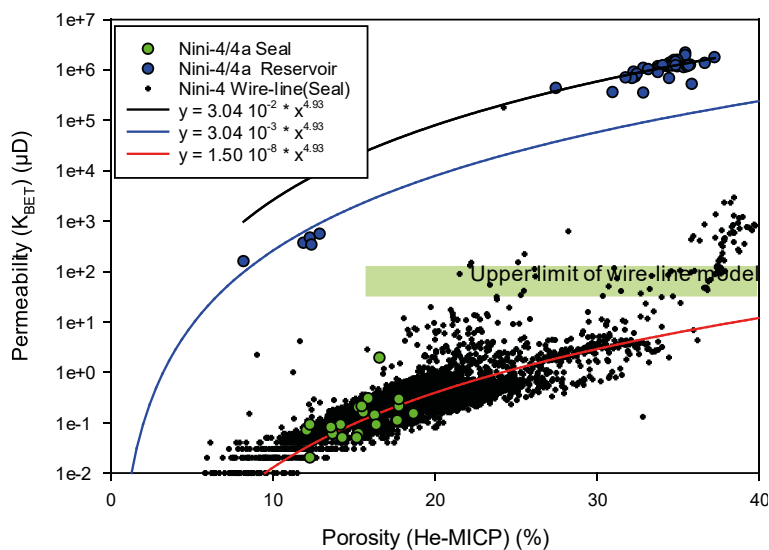


**Figure 14** Porosity and permeability relationships for reservoir sand and seal in the Nini-4 well. The power functions ( $y = ax^b$ ) show general trends in the data. The functions all have a power of 4.93 but differ in a. In the reservoir the two functions have a of  $3.04 \cdot 10^{-2}$  and  $3.04 \cdot 10^{-3}$  and in the seal the a is  $1.5 \cdot 10^{-8}$ .

### Concluding remarks

The permeability is modelled based on the Kozeny equation from both samples and wireline logs. The seal samples plot with porosities up to 22% and permeabilities in the micro to nano Darcy range. The wire-line modelled results plot within the same range as the samples but also defines porosity-permeability ranges that are not reflected in the samples. For both the samples and wire-line logs a power function ( $y = ax^b$ ) with a power of 4.93 and a constant of  $1.5 \cdot 10^{-8}$  can be fitted to the data as representative of the general relationship.

## VITRINITE REFLECTANCE

Vitrinite reflectance (VR) measurements were carried out at GEUS on four samples from the caprock (Laboratory internal reference project 461042101).

The VR measurements followed standard procedures (ASTM, 2014). The analyst was accredited and certified by the International Committee for Coal and Organic Petrology (ICCP). The measurements were conducted using a Leitz Orthoplan reflected light microscope equipped with a 50x objective and the Diskus Fossil System (Hilgers Technisches Buero). The VR readings were taken at 546 nm (monochromatic light). Before measurement the microscope was calibrated against a YAG 0.903% $R_o$  standard with integrated optical zero standard.

The VR measurements were taken in the depth range 1600 m MD (Lark L1) to 1762.27 m MD (Horda Fm), and yielded VR values from 0.37% $R_o$  to 0.46% $R_o$  (Table 6).

### Concluding remarks

The VR values show that the caprock is thermally immature with respect to hydrocarbon generation. There is no risk for *in situ* generated hydrocarbons in the caprock that could compromise seal integrity.

**Table 6** Vitrinite reflectance and Leco/Rock Eval data.

Formation	Internal number	TOC (wt%)	TC (wt%)	TIC (wt%)	TS (wt%)	Tmax (°C)	S1 (mgHC/g rock)	S2 (mg HC/ g rock)	HI (mgHC/g TOC)	PI	PC	Total Ro (%)	Std. dev.	Total N	Ro (%)	Std. dev.	N
Lark	1	2.66	2.67	0.01	1.27	417	0.13	1.50	56	0.08	0.14	0.37	0.04	70	0.36	0.04	69
Lark	2	2.44	2.57	0.13	1.58	426	0.10	2.39	98	0.04	0.21						
Lark	3	1.58	1.77	0.18	0.86	430	0.07	1.55	98	0.04	0.13						
Lark	4	1.45	1.63	0.18	1.16	427	0.07	1.13	78	0.06	0.10						
Lark	5	1.69	1.79	0.09	1.71	416	0.09	0.82	48	0.10	0.08						
Lark -Horda	6	1.11	1.32	0.21	1.05	420	0.07	0.73	66	0.09	0.07	0.37	0.05	50	0.37	0.05	50
Horda	7	0.47	0.74	0.27	0.93	409	0.06	0.45	95	0.12	0.04						
Horda	8	0.44	0.50	0.06	0.42	344	0.05	0.37	85	0.12	0.03						
Horda	9	0.53	0.86	0.32	1.04	345	0.06	0.74	139	0.08	0.07						
Horda	10	0.52	0.66	0.14	1.44	419	0.07	0.79	152	0.08	0.07						
Horda	11	0.39	1.12	0.72	0.70	346	0.04	0.37	94	0.10	0.03						
Horda	12	1.53	1.51	0.00	1.92	419	0.10	1.05	69	0.09	0.10	0.38	0.04	55	0.38	0.04	55
Horda	13	0.70	0.75	0.04	1.87	427	0.08	0.69	98	0.10	0.06	0.46	0.05	55	0.46	0.05	55
Sele	14	0.40	0.37	0.00	0.26	432	0.04	0.12	30	0.25	0.01						
Horda	15	0.37	0.39	0.02	1.06	428	0.06	0.25	68	0.19	0.03						
Horda	16	1.05	1.05	0.00	1.62	433	0.06	1.08	103	0.05	0.09						
Horda	17	0.76	0.82	0.06	2.21	429	0.05	0.69	91	0.07	0.06						
Sele	18	0.46	0.41	0.00	0.38	430	0.04	0.16	35	0.20	0.02						
Horda	19	0.57	0.58	0.00	1.08	427	0.05	0.29	51	0.15	0.03						
Horda	20	1.36	1.36	0.00	2.56	414	0.18	2.00	147	0.08	0.18						

## ORGANIC PETROGRAPHIC COMPOSITION

A single sample from the Horda Fm (1748.65 m MD; internal number 15) was investigated qualitatively by incident light microscopy in white and fluorescence-inducing blue light at GEUS (Figures 15 and 16).

The content of organic matter (macerals) is low which is supported by a TOC content of 0.37 wt.% (see below). The caprock displays a weak microlamination that is accentuated by the presence of yellow fluorescing elongated, compressed alginite macerals. Alginite may be of the marine *Tasmanites* and *Leiosphaerida* types. Few tiny huminite (atrinite) and inertodetrinite particles have been observed, sometimes highlighting the microlamination. Large concentrations of syngenetic framboidal pyrite can occur and often these are concentrated as bands parallel to the microlamination. A dark particle with a dark orange fluorescence colour is likely solid bitumen.

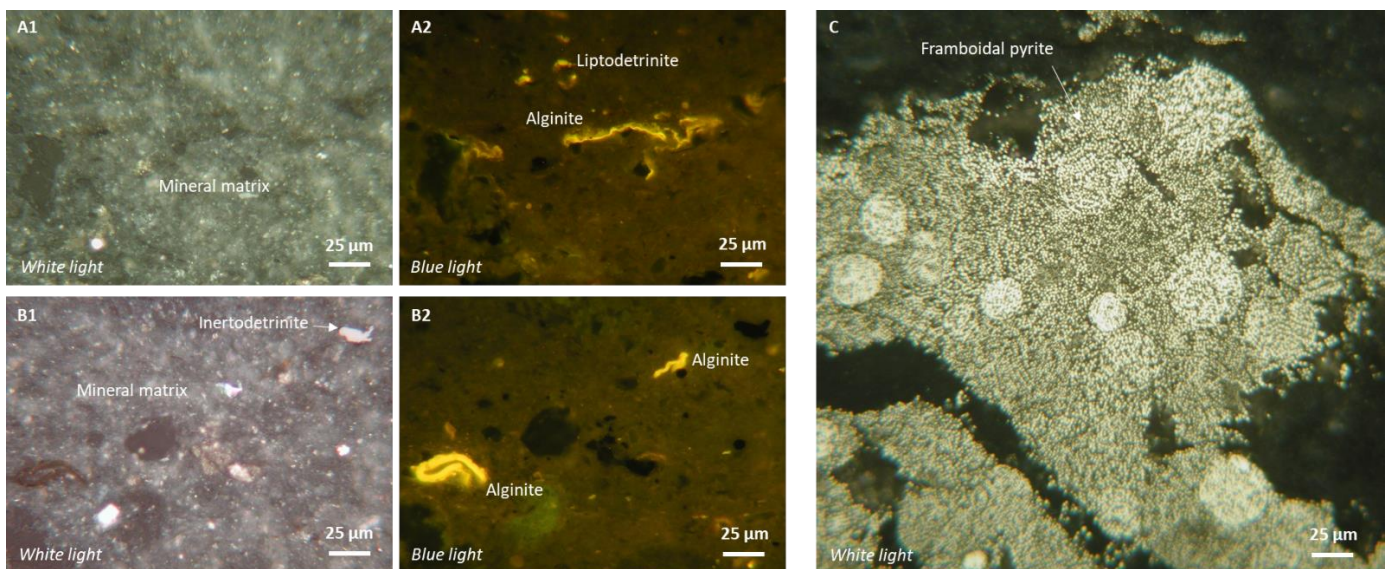


**Figure 15** Reflected light microphotographs of macerals and pyrite in the caprock sample from the Horda Fm (1748.65 m MD; internal number 15). A1, B1, C: reflected white light; A2, B2: fluorescence-inducing blue light.

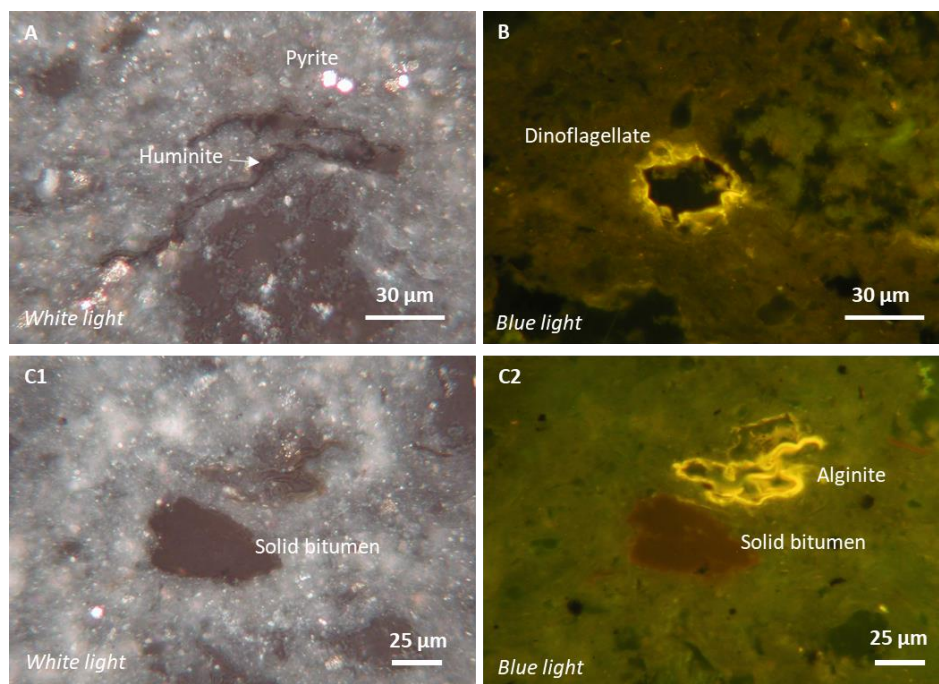


**Figure 16** Reflected light microphotographs of macerals and pyrite in the caprock sample from the Horda Fm (1748.65 m MD; internal number 15). A, C1: reflected white light; B, C2: fluorescence-inducing blue light.

### Concluding remarks

The maceral content is low, and the individual macerals occur as isolated particles in the mineral matrix, hence not forming a coherent network of organic matter that could affect seal integrity. A single particle of solid bitumen may be indicative of migration of hydrocarbons into the lowermost part of the caprock (Horda Fm, basal Lark L1) as also demonstrated by the mudgas composition (see below). Thus, the vast majority of the seal complex does not contain high concentrations of organic matter or migrated hydrocarbons.

## ORGANIC CARBON AND TOTAL SULPHUR CONTENTS AND ROCK-EVAL PYROLYSIS

The analyses were conducted at GEUS. Total Carbon (TC, wt.%), Total Organic Carbon (TOC, wt.%) and Total Sulphur (TS, wt.%) contents were determined by combustion in a LECO CS-200 induction furnace after elimination of carbonate-bonded carbon by prolonged HCl treatment. In-house and international standards were measured during analysis and the analytical reproducibility is 0.1% for all. Rock-Eval type pyrolysis was carried out using a HAWK instrument (Wildcat Instruments, USA). Calibration was done using the IFP-160000 standard with one blank and one in-house (Marl Slate) control standards being run for every 10 samples to ensure instrument stability. The S<sub>2</sub> peak represents the remaining generation potential in the sample that is liberated during pyrolysis. Based on the Rock-Eval pyrolysis the Hydrogen Index (HI) was calculated from the S<sub>2</sub> yield by normalising to the TOC content ( $(S_2/TOC) \cdot 100$ ). T<sub>max</sub> represents the temperature at which the maximum rate of hydrocarbon generation (S<sub>2</sub>) occurs. The S<sub>1</sub> peak, representing free hydrocarbons in the sample, was not considered here due to the samples were extracted before pyrolysis. For reference see e.g. Bordenave et al. (1993).

The TOC content of the Horda Fm shales ranges from 0.37–1.53 wt.% but most values are <0.8 wt.% (Table 6). The TOC content is slightly higher in the Lark L1, ranging from 1.11–2.56 wt.%. The content increases towards the top of the analysed interval. TOC and TC contents are almost identical testifying to non-calcareous shale. The HI values reach a maximum of 152 mg HC/g TOC but typically they lie between 50 and 100 mg HC/g TOC (Table 6), suggesting that the organic matter dominantly is terrigenous, perhaps mixed with refractory organic carbon, and with only minor amounts of algae-derived kerogen. This agrees with the organic petrography (maceral composition; see above). The T<sub>max</sub> ranges from 344–432 °C, reflecting the low thermal maturity of the primary seal. Values <400 °C are unreliable, likely caused by low TOC content.

### Concluding remarks

A recent study has indicated that organic-rich shales with a TOC content of up to 7.9 wt.% have the potential to be suitable caprocks (Guiltinan et al., 2017). The primary seal of Nini West, and particularly the lowermost Horda Fm shales, is organic-lean, and the organic matter in the rock matrix is mainly composed of less reactive kerogen. This suggests that the low TOC content will not have an adverse effect on seal integrity.

## ELEMENTAL COMPOSITION FROM HAND-HELD XRF

The elemental composition was measured at GEUS (internal laboratory series 1028–1066) (Table 7). The measurements were done using a hand-held Niton™ Xl3t Gold+ XRF device (HH-XRF). The device is equipped with an Ag anode that measures at 6–50 kV and up to 200  $\mu$ A and provides semi-quantitative element concentrations. The measuring area is about 5 mm in diameter, and the measuring time was 2 minutes per measuring point, applying the “test all geo filter” that measured dually on low and high filters. Measurements were performed on 1 cm thick powder pellets made of crushed material. Measurements were made on both in-house and certified powder samples to ensure data quality and reliability. For reference on method and calibration see Schovsbo et al. (2018).

The HH-XRF provide element concentrations for: Mo, Zr, Sr, U, Rb, Th, Pb, As, Zn, Cu, Ni, Fe, Mn, Cr, V, Ti, Ca, K, S, Ba, Cs, Nb, Bi, Al, P, Si and Cl and the elemental composition of the seal samples are presented in Table 7. In the accompanying excel sheet (Appendix D) all element concentrations, associated error limits and level of detection limits are provided.

Element concentrations were also measured using the ICP-MS techniques. ICP-MS determined element ranges are presented in Table 8. For critical elements such as Al, K and Ca the two measured varies significantly (Tables 7 and 8). Average Al from HH-XRF is thus 42260 ppm whereas it is 89956 ppm from ICP-MS. The K content is 14483 ppm by HH-XRF whereas it is 21469 ppm from ICP-MS.

The ICP-MS technique is generally regarded as analytical better and is here referred to for citing element abundance, but the HH-XRF was tested as a mean to provide a fast measure on the elemental composition.

### Concluding remarks

The HH-XRF was tested as a mean to provide a fast measure (2 minutes pr. analysis) of the elemental composition as compared to the traditional ICP-MS techniques that on the other hand is generally regarded as analytical better. The HH-XRF results deviated from the ICP-MS data and should not be used directly without corrections to standards. However, HH-XRF is very useful for studying the relative variation of elemental compositions as it provides a fast and inexpensive measure of composition.

**Table 7** Elemental composition and range of the 20 caprock rock samples measured from the Nini-4 and 4A wells by HH-XRF. Full data set is provided in excel spreadsheet (Appendix D). LOD – Level of detection. Compare to Table 8 for ICP-MS determined elements.

Element	Average	Median	Minimum	Maksimum
HH XRF	ppm	ppm	ppm	ppm
Al	42560	41316	20997	56167
As	18	20	6	34
Ba	3342	3699	230	6705
Bi	< LOD			
Ca	5772	5151	2965	11547
Cl	1833	1946	1095	2776
Cr	168	177	102	215
Cs	21	19	10	38
Cu	66	67	43	99
Fe	48112	46526	31719	68573
K	14483	13078	8390	22143
Mn	984	529	207	6108
Mo	< LOD			
Nb	12	11	6	18
Ni	76	74	30	126
P	677	664	324	1478
Pb	18	18	10	30
Rb	83	77	47	128
S	12523	11733	4154	40198
Si	220085	207728	194552	294933
Sr	572	472	248	1168
Th	10	9	6	16
Ti	5094	5207	2543	6276
U	< LOD			
V	209	207	109	274
Zn	134	125	72	288
Zr	158	141	83	239

## ELEMENTAL COMPOSITION FROM ICP-MS

The ICP-MS analyses were carried out on an Elan 6100 ICP-MS instrument at GEUS (internal laboratory reference 20-033 and 20-046). Crushed samples were dissolved in HF and HNO<sub>3</sub> acid for two days at 130°C and element concentrations were determined using the Perkin Elmer TotalQuant software that provides semi-quantitative concentrations for 66 elements (Table 8). A second calibration was made using internal standard under the method SPOR. The laboratory pointed out that the samples after acid digestion had a petroleum odour. This may affect the analytical quality slightly, however the discrepancy is evaluated to be minor and insignificant.

An overview of the elemental composition, average, median and minimum and maximum for the analysed samples is presented in Table 8. For full data-set see associated excel file (Appendix D).

The analysis provides both major, minor and trace element concentrations (Table 8). The seal samples have a low content of redox elements such as U (average 2.8 ppm), Mo (average 3 ppm) and V (average 224 ppm) that are typically enriched under stagnant and reducing bottom waters. No statistically significant relationship between uranium and TOC could be established as there only appear to be a minor tendency for TOC rich samples to also be uranium rich (Figure 17A). This agrees with the terrestrial nature of the organic matter that has a less pronounced tendency to lead to a uranium enrichment. The total clay content correlates as expected with the aluminium content; however, the relationship is weak likely due to the presence of other aluminium bearing phases such as feldspar and heulandite in the samples (Figure 17B).

To test the observation that the gamma ray is of lesser use to identify the clay content (c.f. Figure 12) the clean gamma ray response was calculated from measured K and Th content using the formula from Ellis & Singer (2007):

$$\text{Clean Gamma ray (CGR) (API)} = 16 \cdot \text{K (\%)} + 8 \cdot \text{Th (ppm)}$$

The relationship between CGR and smectite and illite is shown in Figure 17C. The comparison shows that there is a weak correlation between the amount of illite and the clean gamma ray whereas there is no correlation between the smectite content and clean gamma ray response. The results are as expected since illite contains the most radioactive K and Th, whereas the K content in smectite depends on the illite interlays and can be quite variable although less than pure illite. The results are also as expected from comparison between total clay content and the gamma ray log (Figure 12).

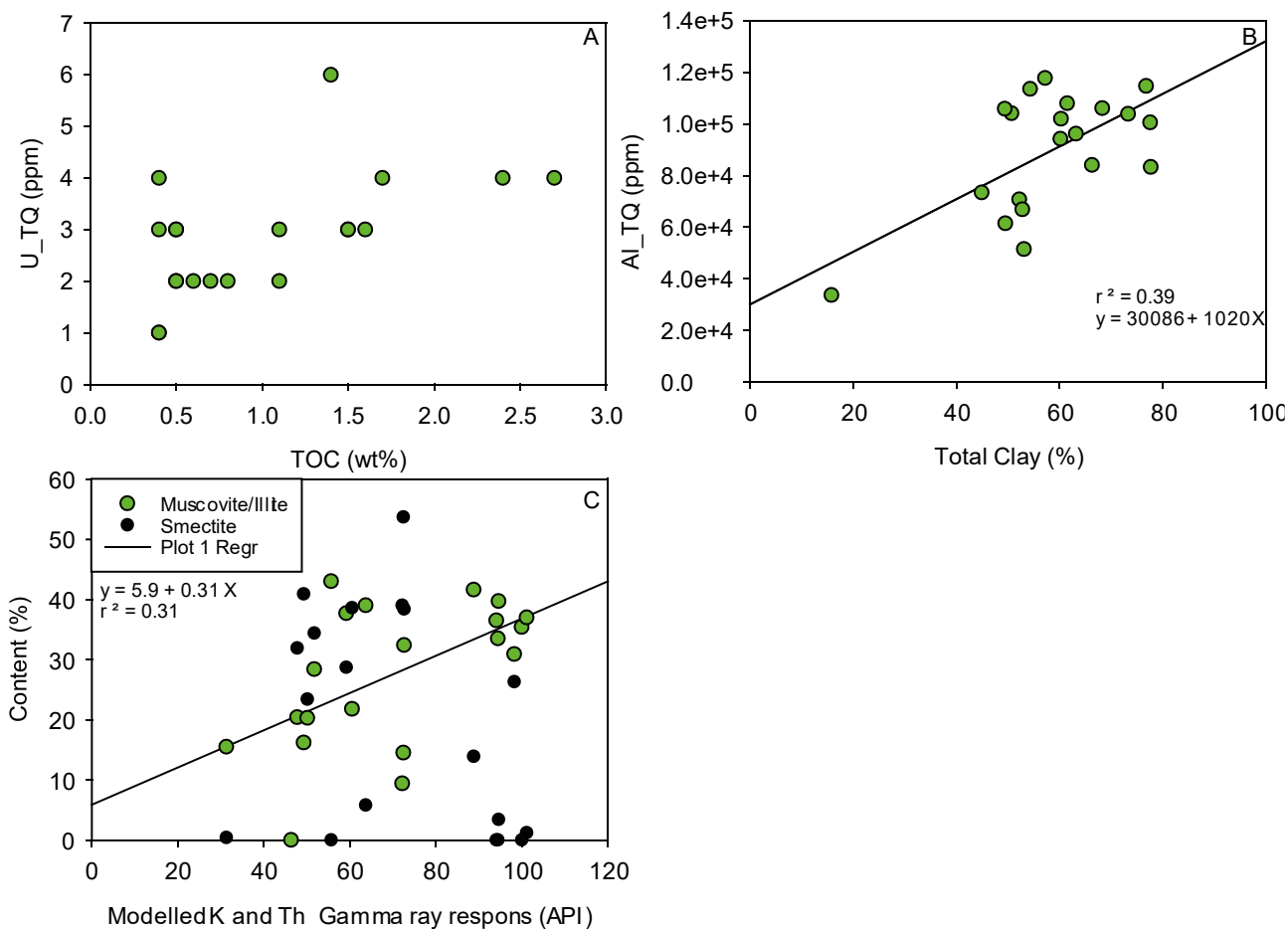


**Figure 17** A) Uranium (ppm) versus TOC (wt.%), B) Aluminium (ppm) versus total clay content (%) from XRD and C) Clay content (%) of smectite and Muscovite/Illite to modelled clean (K and Th) gamma ray. API response is calculated from ICP-MS (TQ) determined elements following  $API = 16 \cdot K (\%) + 8 \cdot Th (ppm)$ .

### Concluding remarks

The elemental composition of 52 elements has been determined for the seal. The elements include both major, minor and trace components. Comparison to other data types has been made for a few selected cases. The uranium content does not correlate to TOC content. This reflects the overall terrestrial nature of the organic carbon. “Hot” uranium rich zones in the seal with abundant marine labile organic carbon do, however occur. The relationship between major elements such as Al, K and trace elements such as Th with clay content is rather complex due to the compositional variability of the clay minerals and due to presence of other aluminium and radioactive minerals than clay in the seal. Comparison between modelled API values and the clay content confirm that the gamma ray logs cannot be used directly to model the total clay content.

**Table 8** Elemental composition and range of the 20 caprock rock samples measured from the Nini-4 and -4A wells by ICP-MS TotalQuant method. Full dataset is provided in the attached excel sheet (Appendix D). TQ: TotalQuant.

Element	Average ppm	Median ppm	Minimum ppm	Maksimum ppm
Al_TQ	89657	98450	33712	117857
As_TQ	22	20	4	52
Ba_TQ	3707	3575	357	8890
Be_TQ	3,34	3,44	1,77	4,78
Bi_TQ	0,30	0,14	0,00	1,55
Ca_TQ	6513	5590	2993	20767
Cd_TQ	0,22	0,21	0,08	0,52
Ce_TQ	87	93	43	109
Co_TQ	32	29	15	63
Cr_TQ	120	123	46	155
Cs_TQ	5,13	4,93	2,50	7,37
Cu_TQ	63	59	36	111
Dy_TQ	4,87	5,15	2,64	6,03
Er_TQ	2,38	2,54	1,26	3,03
Eu_TQ	2,01	2,08	1,03	2,65
Fe_TQ	51198	52280	29449	66367
Ga_TQ	22	23	9	28
Gd_TQ	6,58	6,84	3,46	7,97
Hf_TQ	2,77	2,77	1,26	3,52
Ho_TQ	0,90	0,96	0,48	1,10
K_TQ	21491	21960	8753	30919
La_TQ	33	31	18	42
Li_TQ	91	79	47	159
Lu_TQ	0,32	0,34	0,17	0,39
Mg_TQ	13434	13333	3829	17221
Mn_TQ	690	418	229	3485
Mo_TQ	3,25	1,67	0,48	33,25
Na_TQ	11128	11123	7357	16690
Nb_TQ	16	16	8	20
Nd_TQ	35	36	19	44
Ni_TQ	87	88	26	158
P_TQ	586	511	261	1443
Pb_TQ	22	24	10	31
Pr_TQ	9,08	8,94	4,87	11,54
Rb_TQ	99	101	43	140
Sb_TQ	1,17	0,97	0,38	2,97
Sc_TQ	16	16	7	22
Se_TQ	3,19	2,96	1,46	7,07
Sm_TQ	7,34	7,79	3,75	9,06
Sn_TQ	2,11	2,00	1,28	2,77
Sr_TQ	576	511	258	1167
Ta_TQ	0,92	0,88	0,45	1,21
Tb_TQ	0,95	1,00	0,50	1,16
Th_TQ	8,96	8,24	4,31	12,92
Ti_TQ	5624	5944	2874	6463
Tm_TQ	0,34	0,36	0,18	0,43
U_TQ	2,86	2,75	1,40	5,77
V_TQ	224	236	112	303
Y_TQ	22	23	13	28
Yb_TQ	2,33	2,27	1,15	4,07
Zn_TQ	145	147	23	220
Zr_TQ	158	159	75	201

## SPECIFIC SURFACE AREA (BET)

The specific surface area was measured at DTU using the Brunauer–Emmett–Teller (BET) method. The surface area results are summarised in Table 5. Details for each sample is presented in Appendix A. The specific surface measurements range from 7.4–71 m<sup>2</sup>/g with the general value around 45 m<sup>2</sup>/g. The lowest surface area is measured in sample #20 that also represents the most coarse-grained sample (c.f. Table 3).

*Received laboratory report from Tobias Orlander (DTU):*

---

The twenty samples were analyzed using a Quantachrome autosorb iQ.

To determine the internal surface area by the Brunauer-Emmett-Teller (BET) method, the quantity of nitrogen gas adsorbed into or desorbed from the sample at equilibrium vapour pressure was measured (Petrophysical lab at DTU). Data were obtained by adding or removing a known quantity of nitrogen gas into or out of a sample cell containing 0.5 to 1 g of degassed sample material maintained at a constant temperature.

The BET monolayer surface area calculation requires a so-called BET cross-plot  $1/[W(P_0/P)-1]$  vs.  $P/P_0$ , but restricted to the linear region of the adsorption isotherm. The standard BET procedure requires a minimum of three points in the relative pressure range. Determination of the monolayer surface area from the BET theory (Brunauer et al., 1938) use the BET equation:

$$\frac{1}{W((P_0/P)-1)} = \frac{1}{W_m C} + \frac{C-1}{W_m C} \left( \frac{P}{P_0} \right)$$

where,  $W$  is the weight of the total nitrogen gas adsorbed at a relative pressure,  $P/P_0$ , and  $W_m$  is the weight of adsorbate constituting a monolayer of surface coverage. The BET  $C$ -term is related to the energy of adsorption in the first adsorbed layer. The weight of a monolayer of adsorbate  $W_m$  and  $C$  can be obtained from the slope ( $s$ ) and intercept ( $i$ ) in the linear  $1/[W(P_0/P)-1]$  vs.  $P/P_0$  plot, where:

$$s = \frac{C-1}{W_m C}, \quad i = \frac{1}{W_m C}, \quad W_m = \frac{1}{s+i}$$

The slope ( $s$ ) and intercept ( $i$ ) are listed in the sample file (Appendix A). With knowledge of the molecular cross-sectional area  $A_{cs}$  of the adsorbate nitrogen molecule (for a hexagonal close-packed nitrogen monolayer at 77 K, the cross-sectional area ( $A_{cs}$ ) for nitrogen is 16.2 Å<sup>2</sup>). The total surface area  $S_t$  of the sample material can be expressed as:

$$S_t = \frac{W_m N A_{cs}}{M}$$

where,  $N$  is Avogadro's number and  $M$  is the molar mass (molecular weight) of the adsorbate (nitrogen). The surface area ( $S_t$ ) is listed in Table 5 and for each sample in Appendix A.

In order to find the linear range of the BET plot for microporous materials in a way that reduces any subjectivity in assessment of the monolayer capacity, Rouquerol et al. (2007) suggested a formal procedure based on the criteria that (1) the quantity of  $C$  must be positive (i.e. any negative value is an indication that data are outside the valid range of the BET equation) and (2) the application of the BET equation is limited to the relative pressure range where the term  $n(1 - P/P_0)$  continuously increases with  $P/P_0$  ( $n$  is the adsorbed amount). This procedure is suggested in the ISO 9277:2010 standard.

### **Concluding remarks**

The specific surface area of the seal samples is high in agreement with the clay mineral composition and fine-grained nature of the rock. The measurement of specific surface is used as key input in modelling the permeabilities.

## MERCURY INJECTION CAPILLARY PRESSURE (MICP)

Cleaned and dried sample material was used for MICP analysis. About 4.0–4.7 g cuttings, apart from sample lab. no. 7 where only 1.2 g was available, and 3.2–5.7 g plug trim material was used.

The MICP analyses were carried out at Core Technical Services (CTS), Aberdeen, on a Micromeritics Instrument Corp. AutoPore IV 9500 porosimeter. Air-mercury, drainage capillary pressure tests were run from vacuum to 60,000 psia (400 MPa) pressure. Approximately 80 pressure steps (60-100) were recorded for each sample during an injection test; equilibrium was assumed after each pressure increment when the rate of mercury intrusion drops below 0.001  $\mu\text{L/g-sec}$ . Besides a capillary pressure curve, mercury injection tests also offer information on the pore throat size distribution and sorting, entry/displacement pressures and theoretical permeability, and thereby important data for an evaluation of the caprock sealing capacity (Table 9). Relevant diagrams of the 20 samples analysed are included in Appendix B. An explanation to results in Table 9 is given below:

*Mercury injection porosity* is determined from the following equation:

$$\text{Hg-porosity [\%]} = (\text{Hg pore volume})/(\text{Hg bulk volume}) \cdot 100\%$$

Results are given in the AutoPore raw data file. The mercury porosity is often lower than the helium porosity, particularly for micro porous lithologies, because mercury, at maximum injection pressure of 60,000 psia, will not enter the pore volume concealed in pores with throat radius below  $\sim 2$  nm.

*Permeability*. Also known as the theoretical or Swanson permeability  $K_w$  is a model brine permeability determined from the following equation:

$$K_w = 431 \left( \frac{S_b}{P_c} \right)_A^{2.109} \quad [\text{mD}] \text{ @ } 1000 \text{ psi effective stress (eq.1)}$$

The expression  $(S_b/P_c)_A$  is Swanson's parameter where  $S_b$  denotes the mercury saturation [% relative to bulk volume] and  $P_c$  is the injection (or capillary) pressure [psia]. The parameter is found as the maximum value of the relation  $(S_b/P_c)$  calculated for all pressure steps during a mercury injection run. Swanson's equation (Swanson, 1981) rests on previous work by Purcell (1949) and Thomeer, and Swanson demonstrated that the relationship between overburden brine permeability and reciprocal mercury capillary pressure for both cuttings and plug trim samples was significant for a large number of sandstones and carbonates. The equation preferred for our study is valid for sandstones and shaly sands down to and even below 1  $\mu\text{D}$  (Swanson, 1981 eq. 1). However, shaly sandstones with expandable clays may have lower permeability than predicted from the equation.

*Hg  $P_{cd}$* . Air-Mercury displacement pressure is determined from the intersection by the tangent to the capillary transition zone (plateau) with the "Drainage Cycle Injection Pressure" axis at the "Equivalent Saturation" = 1.0 in the "Entry Pressure" diagram included with the AutoPore raw data

file. The pressure reading is reported in [psia] and normally identifies an injection pressure where 10–20 [%PV] has been saturated by invading mercury.

*A/B  $P_{cd}$ .* Air-Brine displacement pressure is calculated from the above air-mercury entry pressure by a conversion involving the relation between the effective surface tension figures for air-brine and air-mercury as given in the AutoPore raw data file. The conversion constant is 0.196 and the result is further recalculated from [psia] to [MPa].

*scCO<sub>2</sub>  $P_{cd}$ .* Dense (super critical) CO<sub>2</sub>-brine displacement pressure for the Nini West reservoir-caprock system. The dense CO<sub>2</sub> displacement pressure is calculated from the air-mercury displacement pressure by a conversion involving the relation between the effective surface tension (IFT)<sub>e</sub> figures for scCO<sub>2</sub>-brine and air-mercury as given below in Table 10. The conversion constant is 0.095 and the result is further recalculated from [psia] to [MPa].

*Column height  $H_{max}$ .* The seal capacity  $H_{max}$ , expressed as the maximum height of a buoyant non-wetting fluid column of dense CO<sub>2</sub> the seal will resist, can be calculated from the following equation where  $P_{cd}$  is the scCO<sub>2</sub> displacement pressure:

$$H_{max} = \frac{P_{cd}}{g(\rho_w - \rho_{nw})} \text{ [m]}$$

$g$  is the acceleration of gravity, and  $\rho$  is the density of brine ( $\rho_w$ ) and scCO<sub>2</sub> ( $\rho_{nw}$ ) as given in Table 10.

*Pore throat data.* The median pore throat radius  $r_{50}$  identifies the radius where 50% of the effective sample pore volume have been invaded by mercury; the result is given in nano meter [nm]. The minimum pore throat radius  $r$  which can be invaded by mercury at a certain pressure is calculated from the Washburn equation (Washburn, 1921):

$$r = \left( \frac{2\sigma \times \cos\theta}{P_c} \right),$$

where  $\sigma$  and  $\theta$  is the surface tension and contact angle between air and mercury, and  $P_c$  is the injection (or capillary) pressure. The quantity  $(\sigma \times \cos\theta)$  is also known as the effective surface tension (IFT)<sub>e</sub>. The pore throat sorting (PTS) index characterises the degree of ordering of the pore network from the following expression (Jennings, 1987):

$$PTS = \sqrt{\frac{(\text{Third-quartilepressure})}{(\text{First-quartilepressure})}}.$$

The first and third quartile pressures are read directly from the mercury injection capillary pressure curve at the 25% and 75% Hg-saturations.  $PTS \approx 1$  characterises the perfect homogeneous pore network (one pore size),  $PTS \leq 1.5$  is a uni-modal very well sorted network.

*MHR.* The Mean Hydraulic Radius  $r_h$  is the average pore throat radius of the sample in [ $\mu\text{m}$ ].

**Table 9** Petrophysical and seal capacity data obtained from mercury injection data measured at cuttings and plug trims from the Nini-4/4a wells. 'Labcon' and 'Rescon': laboratory and reservoir P, T conditions. \*indicate samples with a bi-modal pore-throat size distribution. Abbreviations:  $P_{cd}$ : Displacement pressure.

Sample ID	Type	Porosity		Perm.	Hg $P_{cd}$	A/B $P_{cd}$	scCO <sub>2</sub> $P_{cd}$	$H_{max}$	Pore throat data		MHR
		by He [%]	by Hg [%]	$k_w$ [ $\mu$ D]	Labcon [psia]	Labcon [MPa]	Rescon [MPa]	(waterwet) [m]	radius $r_{50}$ [nm]	PTS index	radius $r_h$ [ $\mu$ m]
1	cuttings	15.9	15.9	0.360	1800	2.4	1.2	365	16	1.9	0.037
2		15.3	15.3	0.253	2200	3.0	1.4	446	16	1.7	0.032
3		14.2	13.5	0.131	4000	5.4	2.6	811	12	1.4	0.010
4		13.7	13.6	0.118	4200	5.7	2.8	852	12	1.5	0.009
5		12.1	9.3	0.038	5000	6.8	3.3	1014	10	1.5	0.009
6		15.3	12.1	0.035	7000	9.5	4.6	1420	7	1.5	0.006
7		18.7	18.7	0.060	10000	13.5	6.6	2028	8	1.4	0.005
8		14.3	14.3	0.042	8000	10.8	5.2	1623	7	1.5	0.006
9		15.2	15.2	0.055	9000	12.2	5.9	1825	7	1.4	0.005
10		17.7	17.7	12.4	100/2500	0.14/3.4	0.07/1.64	21.7/507 *	14	4.5	0.230
11		12.3	12.3	0.029	9000	12.2	5.9	1825	6	1.5	0.005
12		13.6	12.9	0.140	1000/4300	1.4/5.8	0.66/2.83	204/876 *	10	2.0	0.023
13	Plug trims	17.8	17.8	0.157	5000	6.8	3.3	1014	10	1.5	0.012
14		16.3	16.3	0.060	9000	12.2	5.9	1825	7	1.4	0.005
15		16.4	16.4	0.080	6500	8.8	4.3	1318	8	1.4	0.006
16		15.6	15.6	0.183	3000	4.1	2.0	608	13	1.6	0.011
17		15.5	15.3	0.141	5000	6.8	3.3	1014	11	1.4	0.009
18		17.8	17.3	1.37	400/2000	0.54/2.7	0.27/1.31	84/406 *	17	2.3	0.078
19		12.3	11.9	0.021	10500	14.2	6.9	2130	5.5	1.4	0.004
20		16.6	11.6	0.707	1100	1.5	0.7	223	33	1.9	0.034

**Table 10.** Fluid and seal capacity data at reservoir conditions for the Nini West storage site (Liu et al., 2016; NIST Webbook, 2020; Olsen et al., 2020; present study). Column height  $H_{max1}$  assumes the caprock is water wet,  $H_{max2}$  is corrected for a change in contact angle of 60°. Abbreviations:  $(IFT)_e$ : effective surface tension.

Depth [m]	Temp. [°C]	Brine TDS [mg/L]	Pore P [MPa]	$\rho_w$ (brine) [kg/m <sup>3</sup> ]	$\rho_{nw}$ (scCO <sub>2</sub> ) [kg/m <sup>3</sup> ]	$(IFT)_e$		$P_{cd}$ [MPa]	$H_{max1}$ [m]	$H_{max2}$ [m]
						air-Hg [mN/m]	scCO <sub>2</sub> -brine			
1700	60	93000	20.0	1053	723.7	367.7	35	3.9	1207	604
								6.7	2074	1037

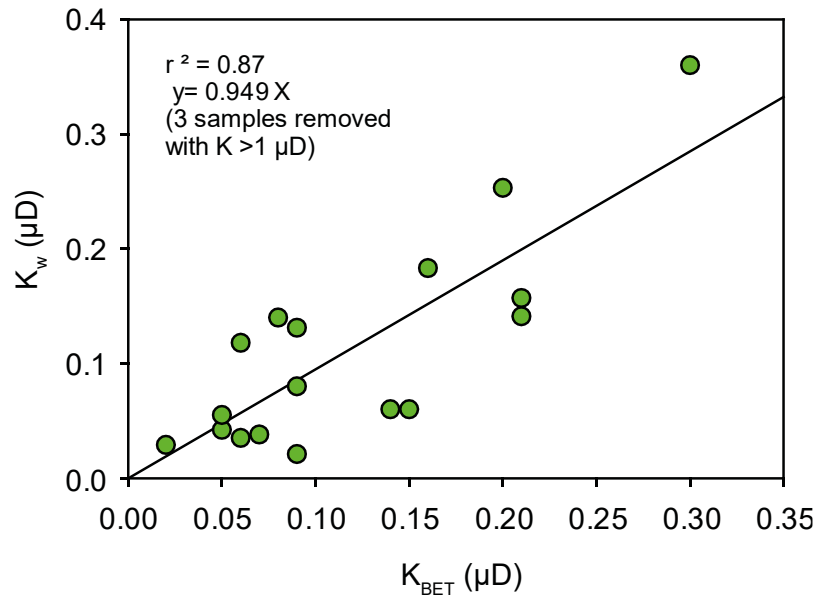


**Figure 18** Relationship between permeability modelled from specific surface determinations ( $K_{BET}$ ) using the Kozeny equation and the theoretical or Swanson permeability ( $K_w$ ). 3 samples with high modelled K due to bimodal pore structure has been removed from the plot.

The relationship between modelled permeabilities from specific surface areas using the Kozeny equation and the theoretical or Swanson permeability is shown in Figure 18. This shows that there is a statistically significant correlation between the two measurements if three samples with high permeability are removed. The correlation confirms the validity of the two approaches. The fact that the correlation is not 1:1 suggests that assumptions regarding some of the constants involved in the equations should be reassessed at a later stage.

### Concluding remarks

The sampling programme for Nini-4/4a included both washed cuttings and core plug samples that are normally preferred over cuttings due to the well-known problems in extensive sample handling of ditch samples, cavings and difficulty of measuring the true bulk volume of cuttings. It is therefore of interest to detect any differences between the two sample types in the further interpretation of the sealing potential from the MICP analyses. In the porosity-permeability scatter diagram of Figure 19 no statistically significant difference between the sample types can be detected, an observation that seems to validate the careful sampling procedure for cuttings introduced in the work by Mbia et al. (2013).

Mainly two geological formations are present among the samples, the Lark and Horda Fms, and in search for differences in the petrophysical properties porosity-permeability scatter diagrams were produced (Figure 19). No significant difference was found, mainly due to the considerable scatter (variability) among the samples. Thus, in the following interpretation of the MICP data (see Table 9) all samples will be treated as belonging to one sealing caprock. Attention should be given to the very low brine permeabilities, Tables 5 and 9, spanning a range of more than one order of magnitude from 0.02 – 0.4  $\mu\text{D}$  except for 3 screened samples having bi-modal pore size distributions. This is equivalent to a low risk score ( $< 10^{-18} \text{ m}^2$ ) in Bruno et al. (2014; their Table 2) of risk factors in caprock analysis. Swanson (1981, p. 2502) commented that his permeability equation for sandstones and shaly sands down to approximately 1  $\mu\text{D}$  may not be valid if expandable clays are present. The mudstones analysed in this study contain variable amounts of smectite from low to high in samples 5-19 (Figures 7 and 8). It seems reasonable to conclude that the model brine permeabilities  $k_w$  listed in Table 9 are likely to represent a maximum estimate of the *in-situ* reservoir conditions permeability of the Nini caprock mudstones.

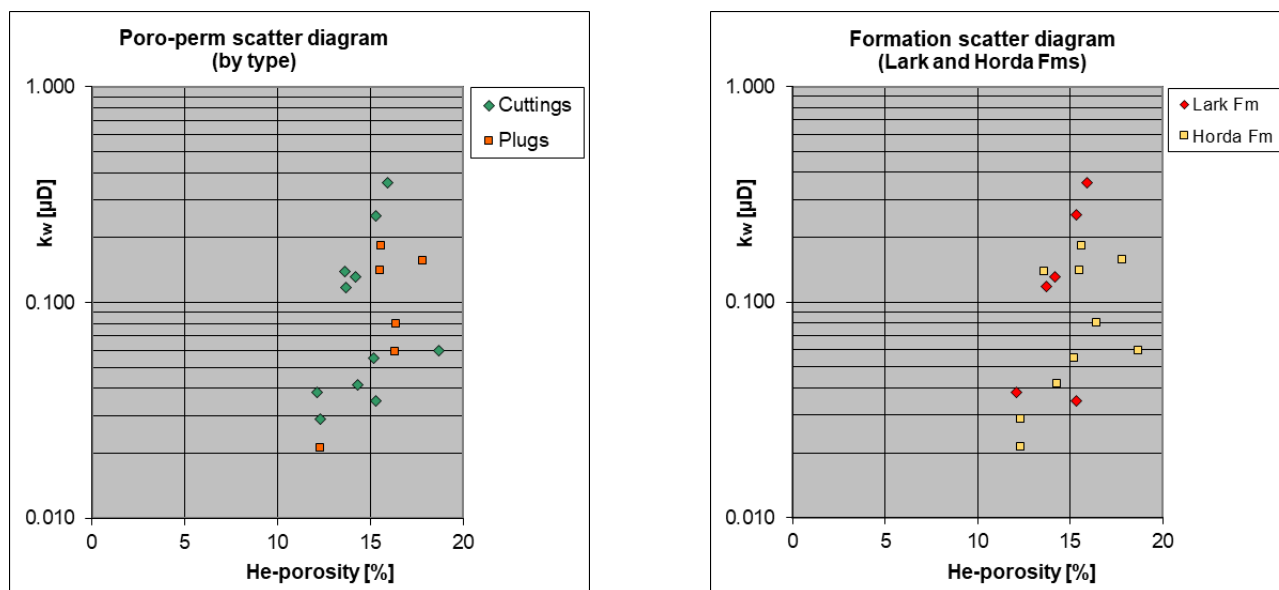


**Figure 19** No significant difference between cuttings and plugs (left) or between the two primary seal formations (right) can be detected. Three samples having bi-modal pore throat size distributions and/or brine permeability above 1  $\mu\text{D}$ , and therefore less relevant for the evaluation of the vertical sealing capacity, were excluded from the diagrams.

From inspection of the MICP diagrams, the majority of the mudstones (85%) have narrow unimodal pore throat size distributions (Figure 20) and most (65%) have PTS index  $\leq 1.5$  (Table 9) that characterises a very well sorted sediment. Some samples (40%) have extremely small throat sizes,  $r_{50}$  and MHR of 6-8 nm, that characterises a very fine grained and tight sediment (Table 9). Very few samples have pore throats  $> 100$  nm. Pore throat size is the major controlling property on permeability and capillary pressure and thereby the important displacement pressure in the CO<sub>2</sub> – brine – mudstone system, ie. the pressure where dense CO<sub>2</sub> is expected to invade the Nini West caprock. Some examples of the capillary pressure curves measured for the Nini mudstones are shown in Figure 21.

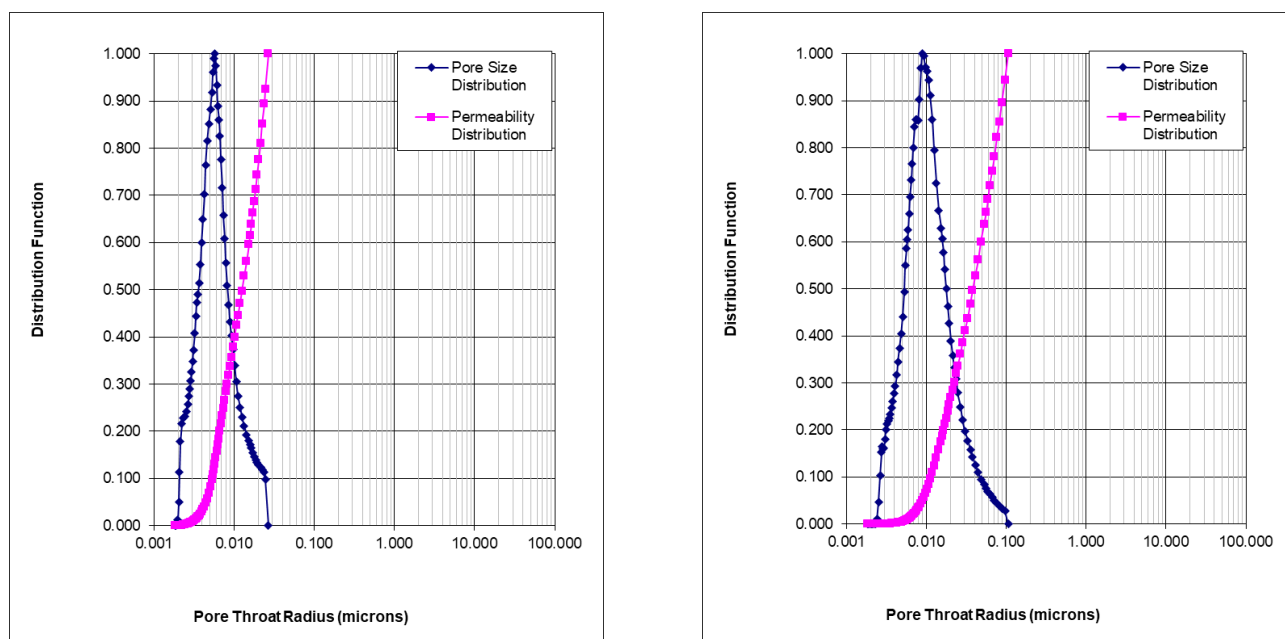


**Figure 20** Pore size distribution diagrams, cuttings sample 7 (left) and core plug sample 13 (right). Observe the narrow, unimodal distributions that are common to most cuttings and core plug samples of the caprock mudstones above the Nini West reservoir.

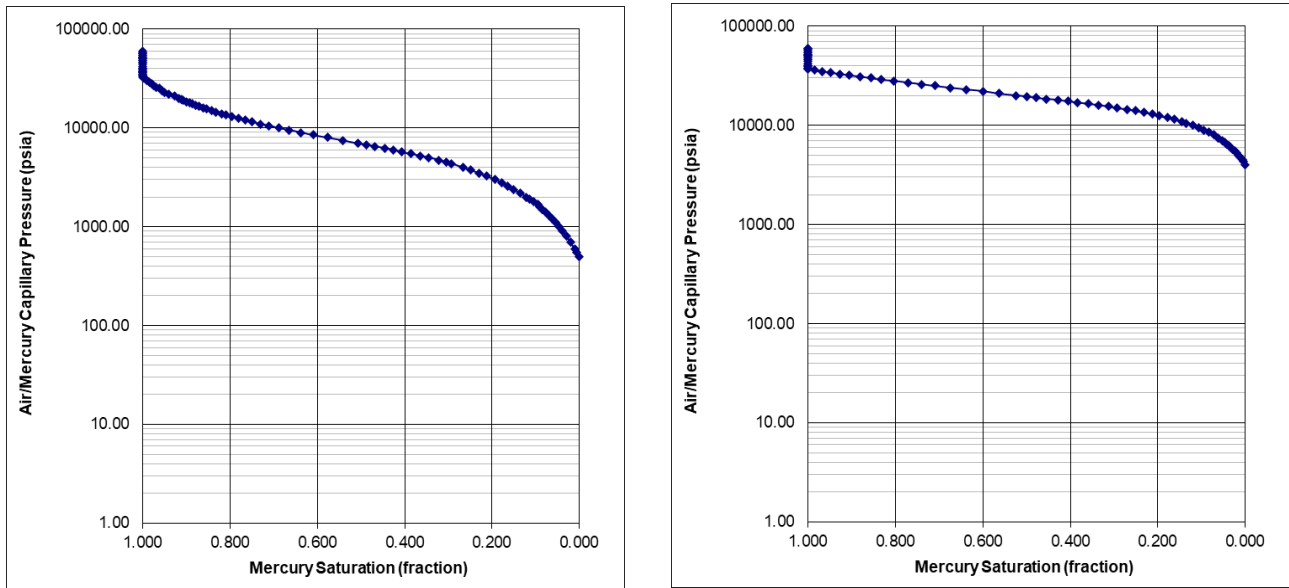


**Figure 21** Air-mercury capillary pressure curves for cuttings sample 2 of the Lark Fm (left) and plug sample 19 of the Horda Fm (right). Observe the relatively 'flat' transition zone characteristic of a well sorted pore network. Sample 19 is in a class of its own having displacement pressure  $P_{cd}$  just above 10,000 psia ( $\sim 70$  MPa) and mean hydraulic radius of 4 nm, Table 9.

The petrophysical parameters at reservoir conditions used in the calculation of the seal capacity is shown in Table 10. The capacity is expressed as the maximum vertical column  $H_{max1}$  of dense  $CO_2$  the caprock can withhold before displacement of the wetting brine phase in the caprock, on the condition that the caprock remains strongly water-wet (ie. contact angle  $\Theta = 0^\circ$ , so  $\cos \Theta = 1$  in the Washburn equation). However, the condition of wettability at reservoir conditions for shales has been questioned, and there are very conflicting results on the subject. A review can be found in Jafari & Jung (2016), and we will here use a conservative (pessimistic) estimate of  $60^\circ$  for the contact angle (ie. contact angle  $\Theta = 60^\circ$ , so  $\cos \Theta = 0.5$  in the Washburn equation), which means that the caprock in a less water-wet scenario will hold back only half the column height  $H_{max2}$  (Table 10). Besides the two wettability scenarios, the table gives two different estimates for the dense  $CO_2$  displacement pressure  $P_{cd}$ . Sampling from the Nini wells covers a vertical interval of  $\sim 350$  m of the Eocene mudstones, and the upper value of 3.9 MPa is the arithmetic mean of all samples except the 3 samples with bi-modal pore size distribution. It is generally accepted the capillary sealing capacity is defined by the tightest formation, so the lower value of 6.7 MPa in Table 10 is the mean of cuttings sample 7 and plug sample 19, the two samples having the highest displacement pressure.

Regardless of the selected figure in Table 10, and with a CO<sub>2</sub> max column < 100 m in the Nini West reservoir, there is a comfortable caprock safety column overhead for CO<sub>2</sub> sequestration in the reservoir even for the most pessimistic scenario.

## MUDGAS LOGS

Digital % Total Gas (TG) and C<sub>1</sub>–C<sub>5</sub> (ppm) mudgas data were available for the two Nini West wells (Nini-2, Nini-4) and the Nini-3, Nena-1 and Sofie-1 wells, while only paper copy data were available for the Nolde-1 well (Dansk Operatørselskab i-s, 1997). The mudgas captured in the circulating mud was liberated by the degasser (“gas trap”) and pulled into the gas analysis manifold. A gas chromatogram (GC) and FID coupled to the flowline was used for qualitative and quantitative monitoring of the C<sub>1</sub>–C<sub>5</sub> gases in the drilling mud returns. Gas isotope data were not available for interpretation of gas origin.

The Nini West Seal Complex in the Nini-2 and Nini-4 wells has low and constant TG contents which in the lowermost part of the caprock are composed of C<sub>1</sub> and only very minor C<sub>2</sub> quantities (Horda Fm and basal Lark L1); no higher hydrocarbon gases were measured (Figures 22 and 23). The constant very low C<sub>2</sub> concentration recorded through the seal complex of Nini-2 well is likely an artefact caused by erroneous measurements (perhaps due to gas detection issues due to the very low C<sub>2</sub> concentrations). The Nolde Sand in the overburden in the Nini-2 well contains significantly more gas composed of C<sub>1</sub> and C<sub>2</sub> compared to the seal complex (Figure 22).

In contrast to the dry gas in the seal complex, contain the Tyr Sand reservoir in the Nini-2 well and the Frigg Sand in the Horda Fm in the Nini-4 well wetter gas composed of C<sub>1</sub>–C<sub>4</sub> (Figures 22 and 23). The Frigg Sand reservoir is associated with a major TG peak at the base of the seal complex (base Horda Fm).

The gas distribution and composition in the Nini-3 well northeast of the Nini West Field is quite similar, but with a more pronounced presence of C<sub>2</sub> gas in the Lark L1 (Figure 24). The TG content is high in the upper part of Lark L1 but drops to a very low quantity in the base of Lark L2 (Figure 24). An incorrect constant low C<sub>2</sub> content was recorded in Lark L2 and L3. Wetter gas composed of C<sub>1</sub>–C<sub>4</sub> was measured in the reservoir sand below the seal complex.

The Nena-1 well south of the Nini West Field shows a slightly fluctuating but low TG content mainly composed of C<sub>1</sub> but also scattered occurrences of low amounts of C<sub>2</sub> (Figure 25). The proportion of TG is higher in the overburden, including the basal and upper part of the Frida Member sand. No higher hydrocarbon gases were recorded in the well.

A very low quantity of TG was measured in the Horda Fm and overlying shales (Nini West Seal Complex equivalent) in the Sofie-1 well southwest of the Nini West Field (Figure 26). The gas is composed of C<sub>1</sub> and scattered occurrences of low concentrations of C<sub>2</sub>. The presence of nC<sub>5</sub> between c. 1201–1260 m MD without the presence of C<sub>3</sub> and C<sub>4</sub> is likely an artefact. Low concentrations of wetter gas composed of C<sub>1</sub>–C<sub>3</sub> were measured in the upper Frigg Sand reservoir below the base of the seal (base Horda Fm) (Figure 26).

No digital mudgas data were available for the Nolde-1 well situated west of the Nini West Field, but mudgas logs from the final well report reveal overall low TG quantities measured from top Balder Fm to top Hordaland Group (seal complex equivalent) (Figure 27). The gas is mainly composed of

low concentrations of C<sub>1</sub> and some C<sub>2</sub> up to about 90 m (c. 1390–1400 m) above base seal at 1490 m depth. Minor amounts of C<sub>3</sub> gas were measured in the basal about 20 m of the seal. A gas peak recorded at 759 m in Oligocene carbonaceous sand is entirely composed of C<sub>1</sub>.

### **Concluding remarks**

The general very low gas concentrations and the gas composition in the seal complex demonstrate that the caprock has an efficient sealing capability that area-wise seems to extend beyond the Nini West Field (Figure 28). This is supported by: 1. Only very limited vertical migration of thermogenic gas into the lower part of the primary seal (Horda Fm and Lark L1); 2. No migration of thermogenic gas into the upper part of the primary seal and the secondary seal; 3. Many hundreds of meters of caprock is overlying the vertical thermogenic gas migration front; 4. The gas recorded in most of the seal complex and the overburden is very likely non-moveable *in situ* generated biogenic gas.

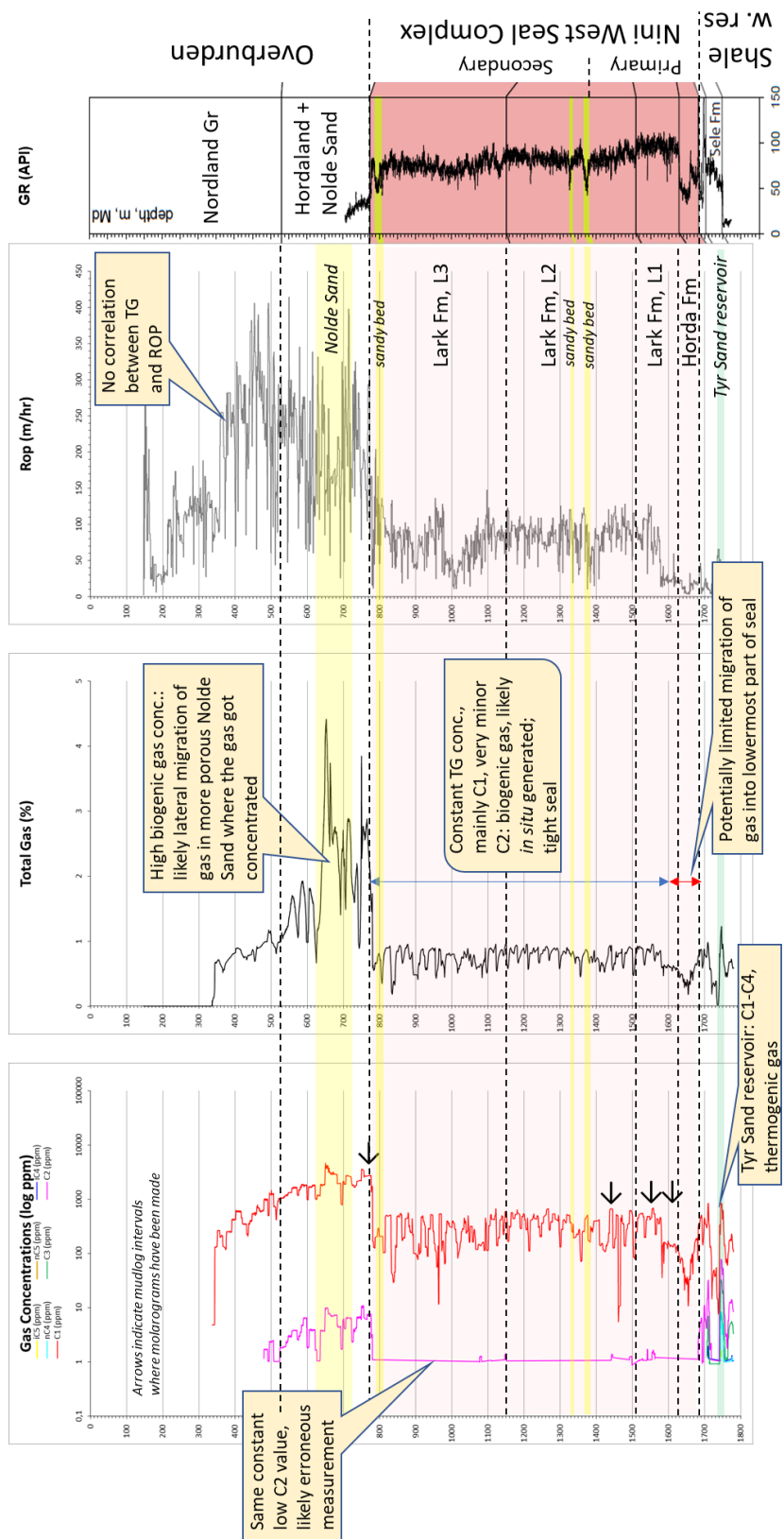


Figure 22 Mudgas, Total Gas, ROP and GR logs of the Nini-2 well.

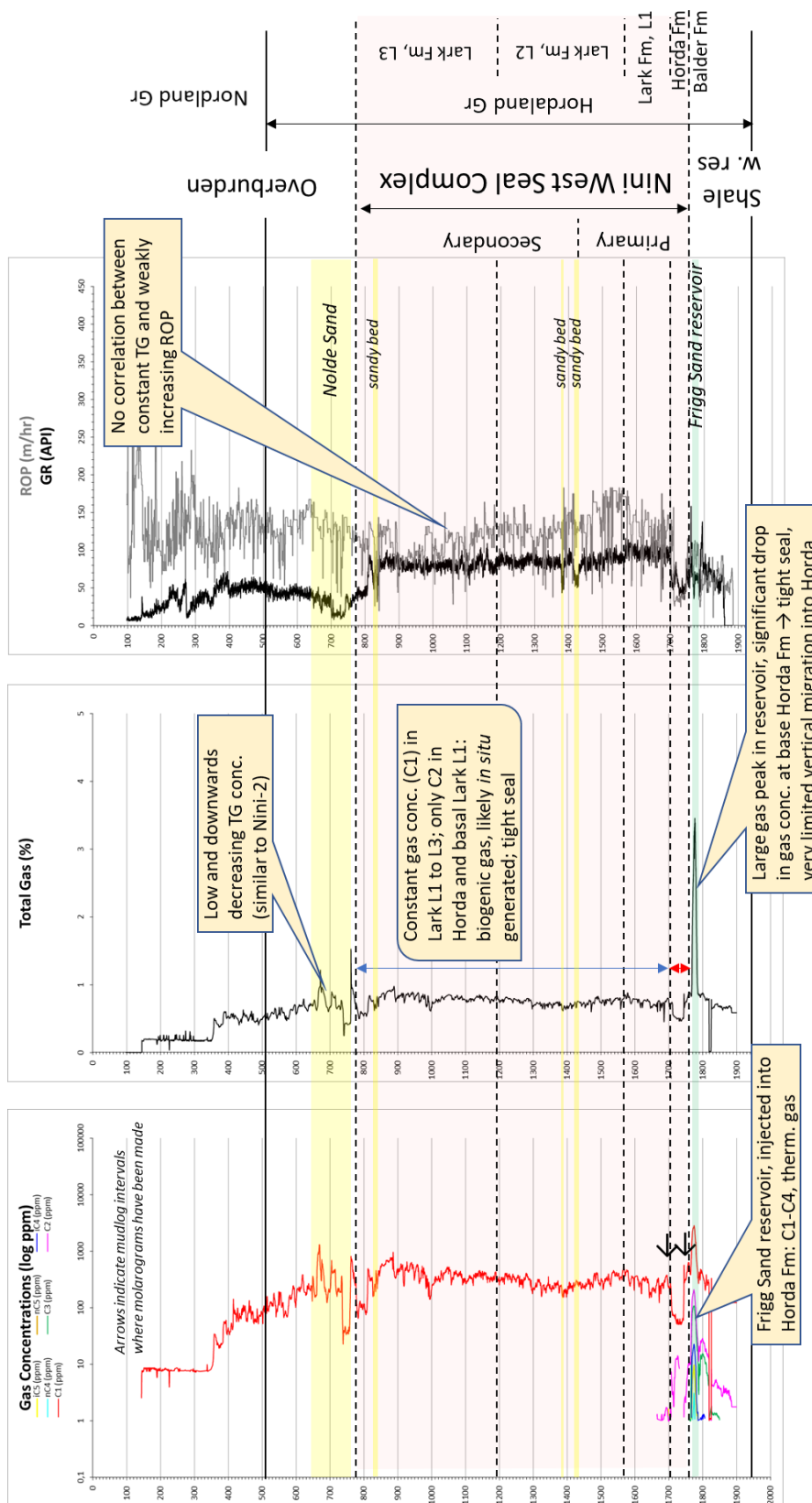


Figure 23 Mudgas, Total Gas, ROP and GR logs of the Nini-4 well.

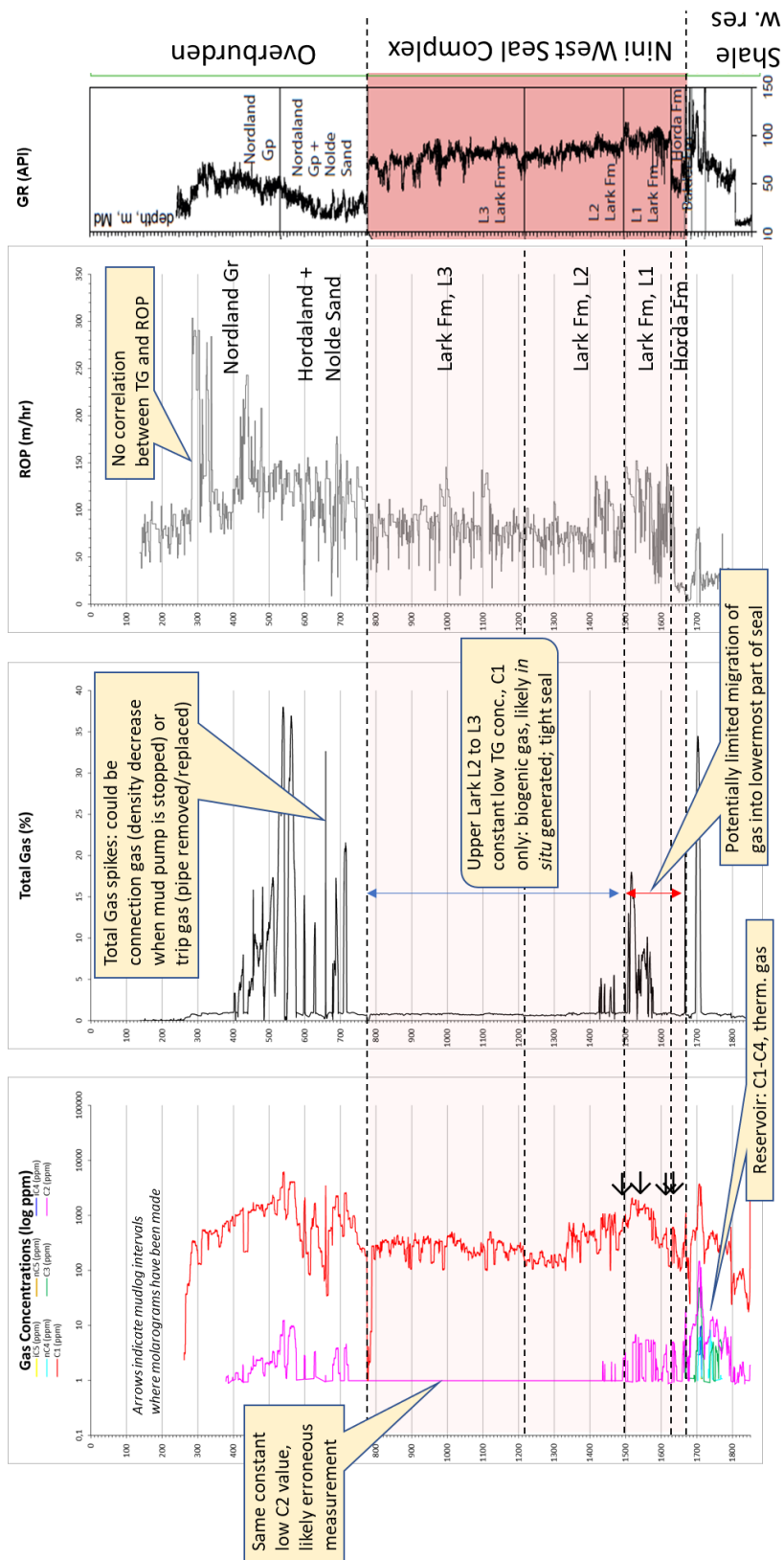


Figure 24 Mudgas, Total Gas, ROP and GR logs of the Nini-3 well.

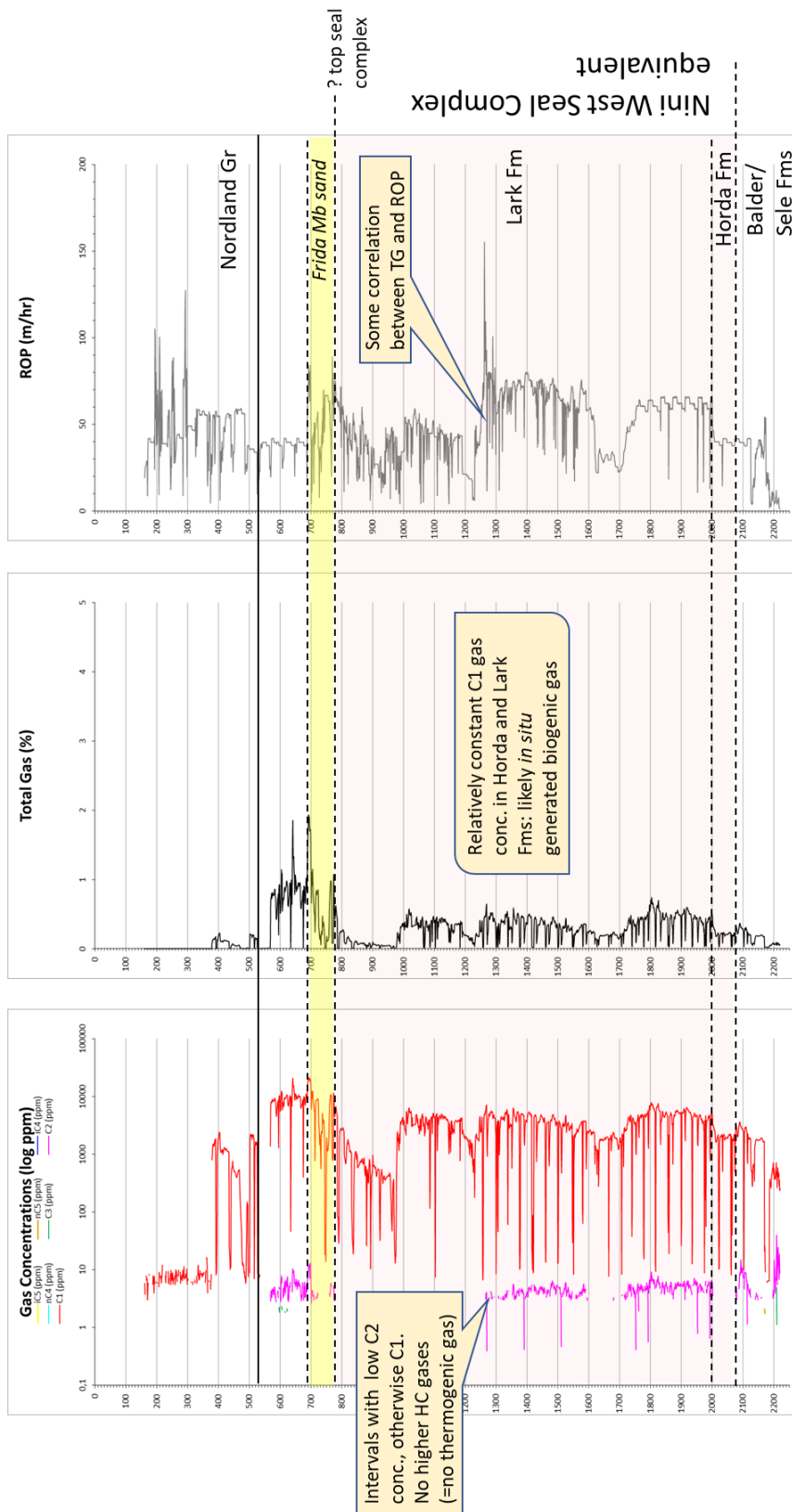


Figure 25 Mudgas, Total Gas and ROP logs of the Nena-1 well.

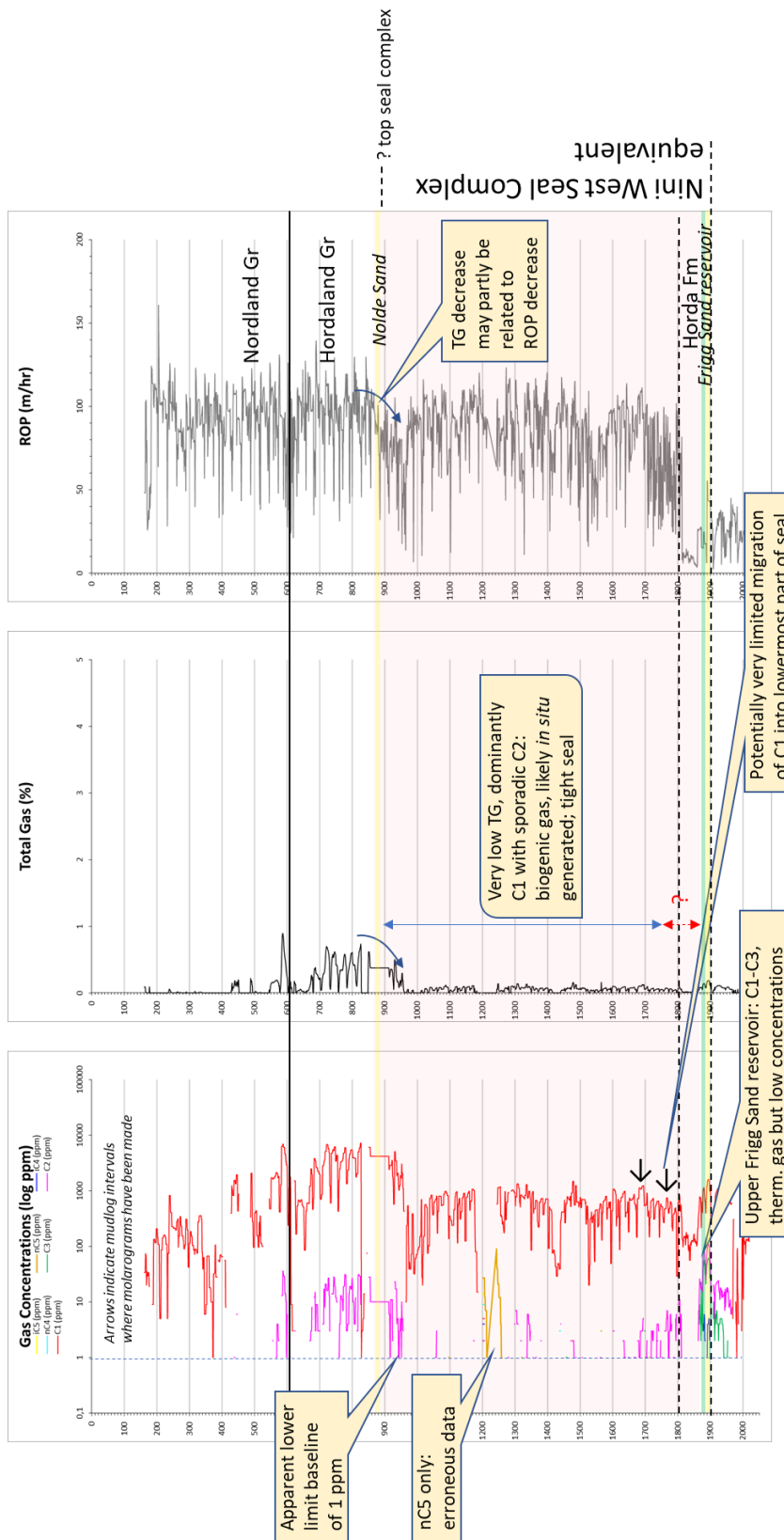
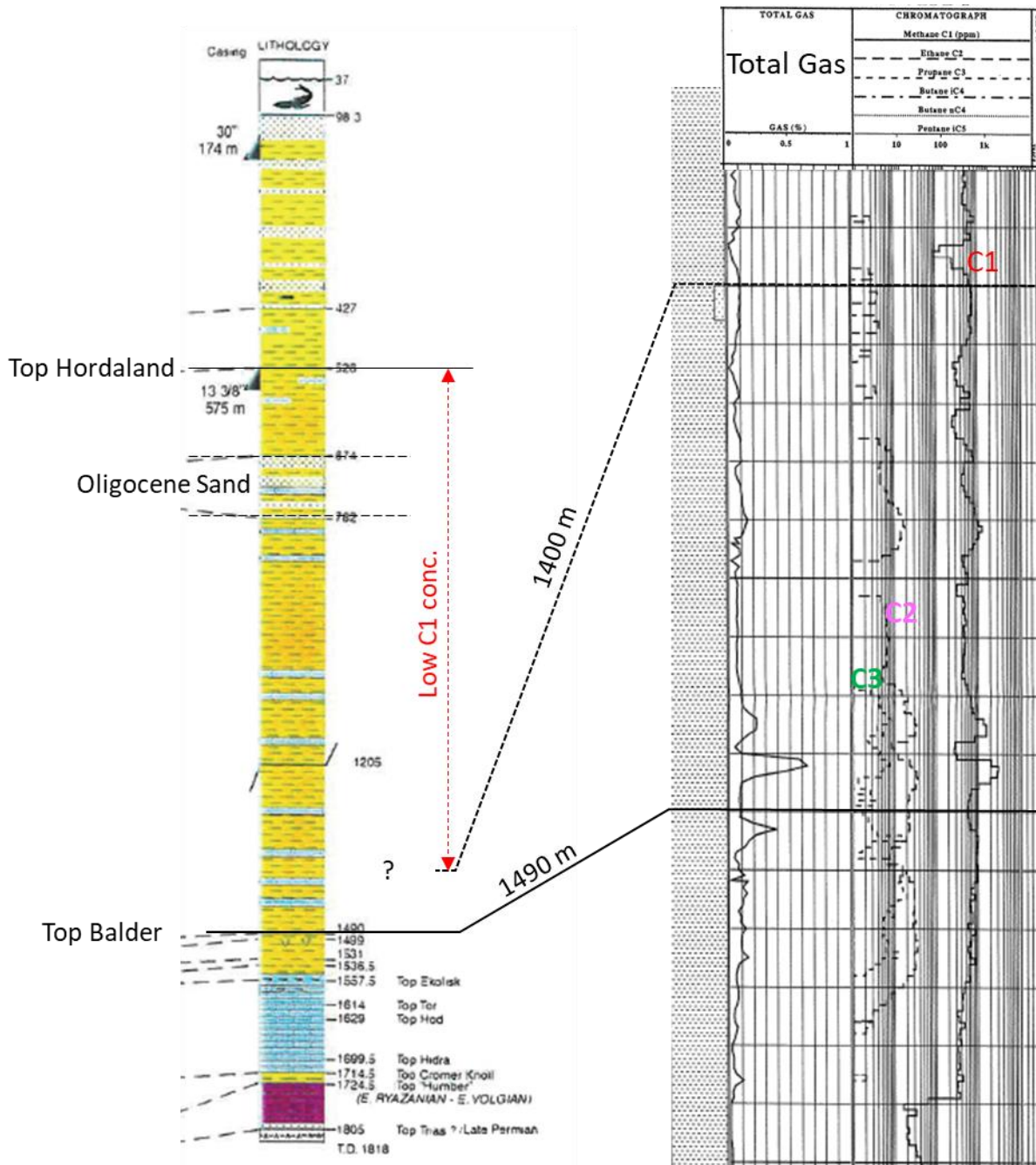
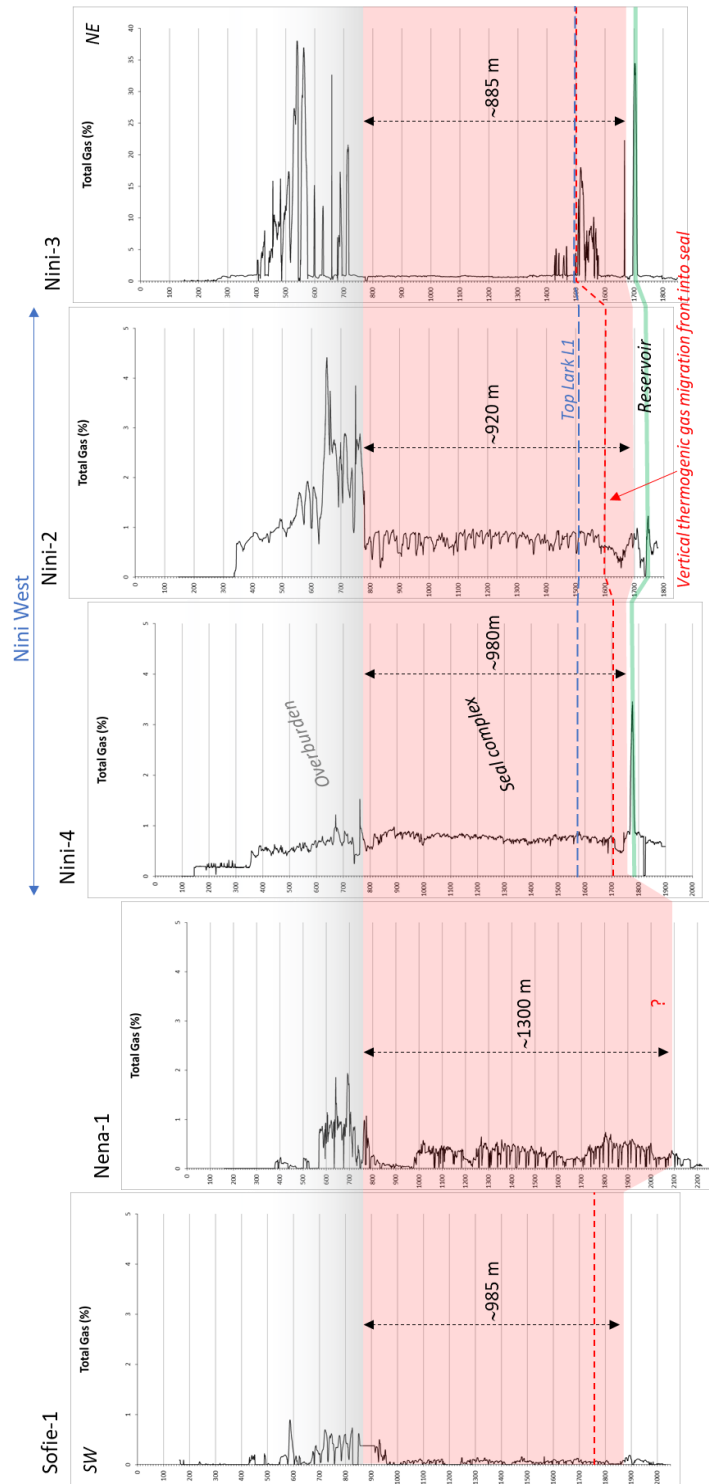


Figure 26 Mudgas, Total Gas and ROP logs of the Sofie-1 well.



**Figure 27** Mudgas and Total Gas logs of the Nolde-1 well. Gas log interval from the Nolde-1 final well report (Dansk Operatørselskab i-s, 1997).



**Figure 28** Semi-regional SW-NE correlation of the seal complex showing that vertical migration of thermogenic gas only has been recorded into the lower part of the primary seal (top Lark L1) indicating high sealing capability of the caprock.

## ACKNOWLEDGMENT

The EUDP funded “Project Greensand” is acknowledge for financial support. The Project Greensand consists of a consortium of GEUS, INEOS, Maersk Drilling and Wintershall DEA. The technical teams at GEUS and DTU (contact person Tobias Orlander) are thanked for analytical assistance.

## REFERENCES

- American Petroleum Institute, 1998. Recommended practices for core analysis. Recommended practice 40, second edition. American Petroleum Institute, Washington, 236 pp.
- ASTM, 2014. D7708 Standard test method for microscopical determination of the reflectance of vitrinite dispersed in sedimentary rocks. ASTM International, West Conshohocken, PA, [www.astm.org](http://www.astm.org)
- Bordenave, M.L., Espitalié, J., Leplat, P., Oudin, J.L., Vandenbrouke, M., 1993. Chapter II.2. Screening techniques for source rock evaluation. In : Bordenave, M.L. (Ed), Applied petroleum geochemistry. Éditions Technip, Paris, 219–278.
- Brunauer, S., Emmett, P. H., Teller, E., 1938. Adsorption of gases in multimolecular layers. Journal of the American Chemical Society 60, 309–319.
- Bruno, M., et al., 2014. Development of improved caprock integrity analysis and riskassessment techniques. Energy Procedia 63, 4708-4744.
- Dansk Operatørselskab I-S, 1997. Final well report, well 5605/-1 Nolde-1. Exploration license 4/95, 149 pp.
- Deer, D.A., Howie, R.A., and Zussman, J., 1966. An Introduction to the Rock Forming Minerals, Longman Scientific & Technical, Essex, England
- Ellis, D.V. & Singer, J.M. 2007: Well logging for earth scientists. 2nd edition. Springer, Dordrecht, the Netherlands, 687 pp.
- Guiltinan, E.J., Cardenas, M.B., Bennett, P.C., Zhang, T., Espinoza, D.N., 2017. The effect of organic matter and thermal maturity on the wettability of supercritical CO<sub>2</sub> on organic shales. International Journal of Greenhouse Gas Control 65, 15–22.
- Hillier, S., 2003. Quantitative analysis of clay and other minerals in sandstones by X-ray powder diffraction (XRPD). In: Worden, R.H. and Morad, S. (Eds), Clay mineral cements in sandstones. International Association of Sedimentologists Special Publication 34, 213–251.
- Holmslykke et al 2021: WP2 batch final report on Greensand project.

- Humphrey, N. & Lucas, P.M. 2003: Wells Nini-4 and Nini-4A, Offshore Denmark, Petrographic Study of lower Tertiary Sediments. Report No. 8658/Id. Robertson Research International, 49 p with three appendices.
- ISO 17892-4, 2016. Geotechnical investigation and testing - Laboratory testing of soil - Part 4: Determination of particle size distribution, 31 pp.
- ISO 9277, 2010. Determination of the specific surface area of solids by gas adsorption – BET method, 24 pp.
- Jennings, J.B., 1987. Capillary pressure techniques: Application to exploration and development geology. AAPG Bulletin 71, 1196–1209.
- Katsube, T.J., Williamson, M.A., 1994. Effects of diagenesis on shale nano-pore structure and implications for sealing capacity. Clay Minerals 29, 451-461
- Kozeny, J. 1927. Ueber kapillare Leitung des Wassers im Boden. Sitzungsberichte der Kaiserlichen Akademie der Wissenschaften, Wien, 136, 271–306.
- Krushin, J.T., 1997. Seal capacity of nonsmectite clays. In: Surdam R.C. (Editor), Seal, traps and the petroleum system. AAPG Memoirs 67, 31-47.
- Liu, Y., Li, H.A., Okuno, R., 2016. Measurements and modeling of interfacial tension for CO<sub>2</sub>/CH<sub>4</sub>/brine systems under reservoir conditions. Industrial & Engineering Chemistry Research 55, 12358–12375.
- Mbia, E., Fabricious, I.L., Collins, O.O., 2013: Equivalent pore radius and velocity of elastic waves in shale. Skjold Flank-1 Well, Danish North Sea. Journal of Petroleum Science and Engineering 109, 280–290. <https://doi.org/10.1016/j.petrol.2013.08.026>
- Mortensen, J., Engstrøm, F., Lind, I., 1998. The relation among porosity, permeability, and specific surface of chalk from the Gorm field, Danish North Sea. SPE Reservoir Evaluation and Engineering 1, 245–251.
- NIST Chemistry Webbook, 2020. National Institute of Standards and Technology, US Department of Commerce. [Thermophysical Properties of Fluid Systems \(nist.gov\)](https://www.nist.gov).
- Ohm, S.E., Karlsen, D.A., Roberts, A., Johannesen, E. & Høiland, O. 2006: The Paleocene sandy Siri Fairway: An efficient “pipeline” draining the prolific Central Graben? Journal Petroleum Geology 29, 53–82.
- Olsen, D., Mohammadkhani, S., Weibel, R., Schovsbo, N.H., 2020. Preliminary results of CO<sub>2</sub>-flooding experiment Exp-1. Greensand Project Phase 1 WP2. GEUS Report 2020/54, 19 pp.

- Purcell, W.R., 1949. Capillary pressures - Their measurement using mercury and the calculation of permeability therefrom. *Petroleum Transactions, AIME* 186, 39–48.
- Riding, J.B., & Rochelle, C.A., 2005. The IEA Weyburn CO<sub>2</sub> monitoring and storage project. Final report of the European Team. British Geological Survey Research Report RR/05/03. <http://nora.nerc.ac.uk/id/eprint/3682/1/RR05003.pdf>
- Rouquerol, J., Llewellyn, P., Rouquerol, F., 2007. Is the BET equation applicable to microporous adsorbents?: Characterization of Porous Solids VII. P.
- Schiøler, P., Andsbjerg, J., Clausen, O.R., Dam, G., Dybkjær, K., Hamberg, L., Heilmann-Clausen, C., Johannesen, E.P., Kristensen, L.E., Prince, I., Rasmussen, J.A., 2007. Lithostratigraphy of the Palaeogene–Lower Neogene succession of the Danish North Sea. *Geological Survey of Denmark and Greenland Bulletin* 12, 77 pp.
- Schovsbo, N.H., Hedegaard, K., Holmslykke, H.D., Kjølner, C., Kristensen, L., Thomsen, E., Esbensen, K.H., 2016. Formation water and produced water types in Danish oil and gas fields: Implications for enhanced oil recovery by “smart” water. *Geological Survey of Denmark and Greenland Bulletin* 35, 43–46.
- Schovsbo, N.H., 2020. Evaluation and risking of the seal capacity for CO<sub>2</sub> storage in the Nini West Oil Field, Denmark. Project Greensand WP4 TRL3. Danmarks og Grønlands Geologiske Undersøgelse Rapport 2020/26, 61 pp.
- Schovsbo, N.H., Nielsen A.T., Harstad, A.O., Bruton, D.L., 2018. Stratigraphy and geochemical composition of the Cambrian Alum Shale Formation in the Porsgrunn core, Skien-Langesund district, southern Norway. *Bulletin of the Geological Society of Denmark* 66, 1–20.
- Swanson, B.F., 1981. A simple correlation between permeabilities and mercury capillary pressures. *Journal of Petroleum Technology*, 2498–2504.
- Totten, M.W., Hanan, M.A., Knight, D., Borges, J., 2002. Characteristics of mixed-layer smectite/illite density separates during burial diagenesis. *Mineralogical Society of America* 87. <https://doi.org/10.2138/am-2002-11-1207>
- Washburn, E.W., 1921. Note on a method of determining the distribution of pore sizes in a porous material. *Proceedings of the National Academy of Science* 7, 115–116.

## APPENDIX A - BET ANALYSIS

Quantachrome® ASiQwin™- Automated Gas Sorption Data

Acquisition and Reduction

© 1994-2016, Quantachrome Instruments

version 5.0

Analysis Report

Operator: DIJUVA Date:2020/11/05 Operator: DIJUVA Date:2020/11/05

Sample ID: Nini-4a 1955.56 om Filename: 201105-02.qps

Sample Desc: Comment: \_6 Point BET

Sample Weight: 0.8839 g Instrument: Autosorb iQ Station 1

Approx. Outgas Time:3.1 hrs Final Outgas Temp.:60 °C Extended info: Available

Analysis gas: Nitrogen Non-ideality: 6.58e-05 1/Torr CellType: 9mm

Analysis Time: 0:16 hr:min Bath temp.: 77.35 K

Analysis Mode: Standard VoidVol Remeasure:off

VoidVol. Mode: He Measure Cold Zone V: 5.38854 cc Warm Zone V: 7.43636 cc

Data Reduction Parameters

Thermal Transpiration: onEff. mol. diameter (D): 3.54 ÅEff. cell stem diam. (d): 4.0000 mm

Adsorbate modelNitrogen Temperature 77.350K

Molec. Wt.: 28.013 Cross Section: 16.200 Å<sup>2</sup> Liquid Density: 0.806 g/cc

Relative Pressure P/Po	Volume @ STP cc/g	1 / [ W((Po/P) - 1) ] 1/g
5.12307e-02	1.4465	2.9868e+01
1.00427e-01	1.6648	5.3653e+01
1.50989e-01	1.8469	7.7046e+01
2.01163e-01	2.0164	9.9921e+01
2.51102e-01	2.1852	1.2277e+02
3.01162e-01	2.3591	1.4616e+02

BET summary

Slope = 463.315 1/g

Intercept = 6.687e+00 1/g

Correlation coefficient, r = 0.999961

C constant= 70.290

Surface Area = 7.410 m<sup>2</sup>/g

Quantachrome® ASiQwin™- Automated Gas Sorption Data

Acquisition and Reduction

© 1994-2016, Quantachrome Instruments

version 5.0

Analysis Report  
 Operator: DIJUVA Date:2020/09/25 Operator: DIJUVA Date:2020/11/03  
 Sample ID: Nini-4a 1915.46 Filename: 200925-01.qps  
 Sample Desc: Comment: \_6 Point BET  
 Sample Weight: 0.3554 g Instrument: Autosorb iQ Station 1  
 Approx. Outgas Time:3.1 hrs Final Outgas Temp.:60 °C Extended info: Available  
 Analysis gas: Nitrogen Non-ideality: 6.58e-05 1/Torr CellType: 9mm  
 Analysis Time: 0:18 hr:min Bath temp.: 77.35 K  
 Analysis Mode: Standard VoidVol Remeasure:off  
 VoidVol. Mode: He Measure Cold Zone V: 5.71822 cc Warm Zone V: 7.41878 cc

Data Reduction Parameters

Thermal Transpiration: onEff. mol. diameter (D): 3.54 ÅEff. cell stem diam. (d): 4.0000 mm

Adsorbate modelNitrogen Temperature 77.350K  
 Molec. Wt.: 28.013 Cross Section: 16.200 Å<sup>2</sup> Liquid Density: 0.806 g/cc

Relative Pressure P/Po	Volume @ STP cc/g	1 / [ W((Po/P) - 1) ] 1/g
4.81127e-02	9.3131	4.3424e+00
9.64780e-02	10.3339	8.2676e+00
1.47803e-01	11.1689	1.2425e+01
1.98630e-01	11.9075	1.6655e+01

BET summary

Slope = 81.722 1/g  
 Intercept = 3.905e-01 1/g  
 Correlation coefficient, r = 0.999980  
 C constant = 210.261

Surface Area = 42.412 m<sup>2</sup>/g

Quantachrome® ASiQwin™- Automated Gas Sorption Data

Acquisition and Reduction

© 1994-2016, Quantachrome Instruments

version 5.0

Analysis Report  
 Operator: DIJUVA Date:2020/09/29 Operator: DIJUVA Date:2020/11/03  
 Sample ID: Nini-4a 1910.37 Filename: 200929-02.qps  
 Sample Desc: Comment: \_6 Point BET  
 Sample Weight: 0.7392 g Instrument: Autosorb iQ Station 1  
 Approx. Outgas Time:3.1 hrs Final Outgas Temp.:60 °C Extended info: Available  
 Analysis gas: Nitrogen Non-ideality: 6.58e-05 1/Torr CellType: 9mm  
 Analysis Time: 0:25 hr:min Bath temp.: 77.35 K  
 Analysis Mode: Standard VoidVol Remeasure:off  
 VoidVol. Mode: He Measure Cold Zone V: 4.92241 cc Warm Zone V: 8.05149 cc

Data Reduction Parameters

Thermal Transpiration: onEff. mol. diameter (D): 3.54 ÅEff. cell stem diam. (d): 4.0000 mm

Adsorbate modelNitrogen Temperature 77.350K  
 Molec. Wt.: 28.013 Cross Section: 16.200 Å<sup>2</sup> Liquid Density: 0.806 g/cc

Relative Pressure P/Po	Volume @ STP cc/g	1 / [ W((Po/P) - 1) ] 1/g
5.35612e-02	8.1429	5.5607e+00
9.94516e-02	9.0242	9.7914e+00
1.50321e-01	9.8143	1.4423e+01
2.01261e-01	10.5324	1.9142e+01

BET summary

Slope = 91.856 1/g  
 Intercept = 6.417e-01 1/g  
 Correlation coefficient, r = 0.999995  
 C constant = 144.143

Surface Area = 37.650 m<sup>2</sup>/g

Quantachrome® ASiQwin™- Automated Gas Sorption Data

Acquisition and Reduction

© 1994-2016, Quantachrome Instruments

version 5.0

Analysis Report

Operator: DIJUVA Date:2020/11/05 Operator: DIJUVA Date:2020/11/05

Sample ID: Nini-4 1902.72 om Filename: 201105-01.qps

Sample Desc: Comment: \_6 Point BET

Sample Weight: 1.0379 g Instrument: Autosorb iQ Station 1

Approx. Outgas Time:3.1 hrs Final Outgas Temp.:60 °C Extended info: Available

Analysis gas: Nitrogen Non-ideality: 6.58e-05 1/Torr CellType: 9mm

Analysis Time: 0:40 hr:min Bath temp.: 77.35 K

Analysis Mode: Standard VoidVol Remeasure:off

VoidVol. Mode: He Measure Cold Zone V: 5.41874 cc Warm Zone V: 7.4521 cc

Data Reduction Parameters

Thermal Transpiration: onEff. mol. diameter (D): 3.54 ÅEff. cell stem diam. (d): 4.0000 mm

Adsorbate modelNitrogen Temperature 77.350K

Molec. Wt.: 28.013 Cross Section: 16.200 Å<sup>2</sup> Liquid Density: 0.806 g/cc

Relative Pressure P/Po	Volume @ STP cc/g	1 / [ W((Po/P) - 1) ] 1/g
4.76800e-02	16.0150	2.5014e+00
1.00545e-01	17.7836	5.0293e+00
1.49631e-01	18.9822	7.4168e+00

BET summary

Slope = 48.209 1/g

Intercept = 1.961e-01 1/g

Correlation coefficient, r = 0.999988

C constant= 246.882

Surface Area = 71.945 m<sup>2</sup>/g

Quantachrome® ASiQwin™- Automated Gas Sorption Data

Acquisition and Reduction

© 1994-2016, Quantachrome Instruments

version 5.0

Analysis Report  
 Operator: DIJUVA Date:2020/09/28 Operator: DIJUVA Date:2020/11/03  
 Sample ID: Nini-4 1820.79 Filename: 200928-03.qps  
 Sample Desc: Comment: \_6 Point BET  
 Sample Weight: 0.597 g Instrument: Autosorb iQ Station 1  
 Approx. Outgas Time:3.1 hrs Final Outgas Temp.:60 °C Extended info: Available  
 Analysis gas: Nitrogen Non-ideality: 6.58e-05 1/Torr CellType: 9mm  
 Analysis Time: 0:26 hr:min Bath temp.: 77.35 K  
 Analysis Mode: Standard VoidVol Remeasure:off  
 VoidVol. Mode: He Measure Cold Zone V: 4.93326 cc Warm Zone V: 8.27447 cc

Data Reduction Parameters

Thermal Transpiration: onEff. mol. diameter (D): 3.54 ÅEff. cell stem diam. (d): 4.0000 mm

Adsorbate modelNitrogen Temperature 77.350K  
 Molec. Wt.: 28.013 Cross Section: 16.200 Å<sup>2</sup> Liquid Density: 0.806 g/cc

Relative Pressure P/Po	Volume @ STP cc/g	1 / [ W((Po/P) - 1) ] 1/g
5.15608e-02	10.3719	4.1937e+00
9.90119e-02	11.6422	7.5524e+00
1.50374e-01	12.7584	1.1099e+01
2.00765e-01	13.7688	1.4597e+01
2.50658e-01	14.7355	1.8163e+01

BET summary

Slope = 69.971 1/g  
 Intercept = 5.922e-01 1/g  
 Correlation coefficient, r = 0.999983  
 C constant= 119.149

Surface Area = 49.353 m<sup>2</sup>/g

Quantachrome® ASiQwin™- Automated Gas Sorption Data

Acquisition and Reduction

© 1994-2016, Quantachrome Instruments

version 5.0

Analysis Report  
 Operator: DIJUVA Date:2020/09/29 Operator: DIJUVA Date:2020/11/03  
 Sample ID: Nini-4 1800.76 Filename: 200929-01.qps  
 Sample Desc: Comment: \_6 Point BET  
 Sample Weight: 0.4947 g Instrument: Autosorb iQ Station 1  
 Approx. Outgas Time:3.1 hrs Final Outgas Temp.:60 °C Extended info: Available  
 Analysis gas: Nitrogen Non-ideality: 6.58e-05 1/Torr CellType: 9mm  
 Analysis Time: 0:20 hr:min Bath temp.: 77.35 K  
 Analysis Mode: Standard VoidVol Remeasure:off  
 VoidVol. Mode: He Measure Cold Zone V: 5.55644 cc Warm Zone V: 7.57994 cc

Data Reduction Parameters

Thermal Transpiration: onEff. mol. diameter (D): 3.54 ÅEff. cell stem diam. (d): 4.0000 mm

Adsorbate modelNitrogen Temperature 77.350K  
 Molec. Wt.: 28.013 Cross Section: 16.200 Å<sup>2</sup> Liquid Density: 0.806 g/cc

Relative Pressure P/Po	Volume @ STP cc/g	1 / [ W((Po/P) - 1) ] 1/g
4.96308e-02	8.9506	4.6683e+00
1.01420e-01	10.0236	9.0093e+00
1.46503e-01	10.7528	1.2772e+01
1.96208e-01	11.4921	1.6995e+01

BET summary

Slope = 84.041 1/g  
 Intercept = 4.872e-01 1/g  
 Correlation coefficient, r = 0.999993  
 C constant = 173.507

Surface Area = 41.199 m<sup>2</sup>/g

Quantachrome® ASiQwin™- Automated Gas Sorption Data

Acquisition and Reduction

© 1994-2016, Quantachrome Instruments

version 5.0

Analysis Report  
 Operator: DIJUVA Date:2020/09/25 Operator: DIJUVA Date:2020/11/03  
 Sample ID: Nini-4 1762.27 Filename: 200925-02.qps  
 Sample Desc: Comment: \_6 Point BET  
 Sample Weight: 0.3749 g Instrument: Autosorb iQ Station 1  
 Approx. Outgas Time:3.1 hrs Final Outgas Temp.:60 °C Extended info: Available  
 Analysis gas: Nitrogen Non-ideality: 6.58e-05 1/Torr CellType: 9mm  
 Analysis Time: 0:18 hr:min Bath temp.: 77.35 K  
 Analysis Mode: Standard VoidVol Remeasure:off  
 VoidVol. Mode: He Measure Cold Zone V: 5.70323 cc Warm Zone V: 7.45392 cc

Data Reduction Parameters

Thermal Transpiration: onEff. mol. diameter (D): 3.54 ÅEff. cell stem diam. (d): 4.0000 mm

Adsorbate modelNitrogen Temperature 77.350K  
 Molec. Wt.: 28.013 Cross Section: 16.200 Å<sup>2</sup> Liquid Density: 0.806 g/cc

Relative Pressure P/Po	Volume @ STP cc/g	1 / [ W((Po/P) - 1) ] 1/g
5.14033e-02	8.5384	5.0779e+00
9.71577e-02	9.4180	9.1423e+00
1.48024e-01	10.1818	1.3653e+01
1.98658e-01	10.8658	1.8255e+01

BET summary

Slope = 89.408 1/g  
 Intercept = 4.624e-01 1/g  
 Correlation coefficient, r = 0.999983  
 C constant= 194.362

Surface Area = 38.751 m<sup>2</sup>/g

Quantachrome® ASiQwin™- Automated Gas Sorption Data

Acquisition and Reduction

© 1994-2016, Quantachrome Instruments

version 5.0

Analysis Report  
 Operator: DIJUVA Date:2020/09/24 Operator: DIJUVA Date:2020/11/03  
 Sample ID: Nini-4 1749-1755 Filename: 200924-01.qps  
 Sample Desc: Comment: \_6 Point BET  
 Sample Weight: 0.4641 g Instrument: Autosorb iQ Station 1  
 Approx. Outgas Time:3.1 hrs Final Outgas Temp.:60 °C Extended info: Available  
 Analysis gas: Nitrogen Non-ideality: 6.58e-05 1/Torr CellType: 9mm  
 Analysis Time: 0:22 hr:min Bath temp.: 77.35 K  
 Analysis Mode: Standard VoidVol Remeasure:off  
 VoidVol. Mode: He Measure Cold Zone V: 4.86679 cc Warm Zone V: 8.40599 cc

Data Reduction Parameters

Thermal Transpiration: onEff. mol. diameter (D): 3.54 ÅEff. cell stem diam. (d): 4.0000 mm

Adsorbate modelNitrogen Temperature 77.350K  
 Molec. Wt.: 28.013 Cross Section: 16.200 Å<sup>2</sup> Liquid Density: 0.806 g/cc

Relative Pressure P/Po	Volume @ STP cc/g	1 / [ W((Po/P) - 1) ] 1/g
4.69908e-02	7.3935	5.3360e+00
1.01214e-01	8.6636	1.0400e+01
1.52720e-01	9.6553	1.4937e+01
1.96371e-01	10.4303	1.8745e+01
2.52895e-01	11.4055	2.3746e+01
2.96361e-01	12.1517	2.7732e+01

BET summary

Slope = 89.281 1/g  
 Intercept = 1.243e+00 1/g  
 Correlation coefficient, r = 0.999948  
 C constant = 72.816

Surface Area = 38.471 m<sup>2</sup>/g

Quantachrome® ASiQwin™- Automated Gas Sorption Data

Acquisition and Reduction

© 1994-2016, Quantachrome Instruments

version 5.0

Analysis Report  
 Operator: DIJUVA Date:2020/09/28 Operator: DIJUVA Date:2020/11/03  
 Sample ID: Nini-4 1748.65 Filename: 200928-01.qps  
 Sample Desc: Comment: \_6 Point BET  
 Sample Weight: 0.3809 g Instrument: Autosorb iQ Station 1  
 Approx. Outgas Time:3.1 hrs Final Outgas Temp.:60 °C Extended info: Available  
 Analysis gas: Nitrogen Non-ideality: 6.58e-05 1/Torr CellType: 9mm  
 Analysis Time: 0:23 hr:min Bath temp.: 77.35 K  
 Analysis Mode: Standard VoidVol Remeasure:off  
 VoidVol. Mode: He Measure Cold Zone V: 4.91134 cc Warm Zone V: 8.33266 cc

Data Reduction Parameters

Thermal Transpiration: onEff. mol. diameter (D): 3.54 ÅEff. cell stem diam. (d): 4.0000 mm

Adsorbate modelNitrogen Temperature 77.350K  
 Molec. Wt.: 28.013 Cross Section: 16.200 Å<sup>2</sup> Liquid Density: 0.806 g/cc

Relative Pressure P/Po	Volume @ STP cc/g	1 / [ W((Po/P) - 1) ] 1/g
4.86150e-02	13.0728	3.1275e+00
9.96610e-02	14.7939	5.9867e+00
1.51711e-01	16.1760	8.8461e+00
2.02680e-01	17.3924	1.1694e+01

BET summary

Slope = 55.536 1/g  
 Intercept = 4.346e-01 1/g  
 Correlation coefficient, r = 0.999993  
 C constant = 128.780

Surface Area = 62.221 m<sup>2</sup>/g

Quantachrome® ASiQwin™- Automated Gas Sorption Data

Acquisition and Reduction

© 1994-2016, Quantachrome Instruments

version 5.0

Analysis Report  
 Operator: DIJUVA Date:2020/09/23 Operator: DIJUVA Date:2020/11/03  
 Sample ID: Nini-4 1737-1740 Filename: 200923-01.qps  
 Sample Desc: Comment: \_6 Point BET  
 Sample Weight: 0.7456 g Instrument: Autosorb iQ Station 1  
 Approx. Outgas Time:3.1 hrs Final Outgas Temp.:60 °C Extended info: Available  
 Analysis gas: Nitrogen Non-ideality: 6.58e-05 1/Torr CellType: 9mm  
 Analysis Time: 0:30 hr:min Bath temp.: 77.35 K  
 Analysis Mode: Standard VoidVol Remeasure:off  
 VoidVol. Mode: He Measure Cold Zone V: 5.63637 cc Warm Zone V: 7.48277 cc

Data Reduction Parameters

Thermal Transpiration: onEff. mol. diameter (D): 3.54 ÅEff. cell stem diam. (d): 4.0000 mm

Adsorbate modelNitrogen Temperature 77.350K  
 Molec. Wt.: 28.013 Cross Section: 16.200 Å<sup>2</sup> Liquid Density: 0.806 g/cc

Relative Pressure P/Po	Volume @ STP cc/g	1 / [ W((Po/P) - 1) ] 1/g
4.89520e-02	13.0368	3.1590e+00
9.99869e-02	14.5520	6.1083e+00
1.47090e-01	15.6025	8.8437e+00
1.97647e-01	16.5897	1.1881e+01

BET summary

Slope = 58.600 1/g  
 Intercept = 2.656e-01 1/g  
 Correlation coefficient, r = 0.999956  
 C constant = 221.673

Surface Area = 59.161 m<sup>2</sup>/g

Quantachrome® ASiQwin™- Automated Gas Sorption Data

Acquisition and Reduction

© 1994-2016, Quantachrome Instruments

version 5.0

Analysis Report  
 Operator: DIJUVA Date:2020/09/21 Operator: DIJUVA Date:2020/11/03  
 Sample ID: Nini-4 1731-1734 Filename: 200921-03.qps  
 Sample Desc: Comment: \_6 Point BET  
 Sample Weight: 0.762 g Instrument: Autosorb iQ Station 1  
 Approx. Outgas Time:3.1 hrs Final Outgas Temp.:60 °C Extended info: Available  
 Analysis gas: Nitrogen Non-ideality: 6.58e-05 1/Torr CellType: 9mm  
 Analysis Time: 0:29 hr:min Bath temp.: 77.35 K  
 Analysis Mode: Standard VoidVol Remeasure:off  
 VoidVol. Mode: He Measure Cold Zone V: 4.69076 cc Warm Zone V: 8.32564 cc

Data Reduction Parameters

Thermal Transpiration: onEff. mol. diameter (D): 3.54 ÅEff. cell stem diam. (d): 4.0000 mm

Adsorbate modelNitrogen Temperature 77.350K  
 Molec. Wt.: 28.013 Cross Section: 16.200 Å<sup>2</sup> Liquid Density: 0.806 g/cc

Relative Pressure P/Po	Volume @ STP cc/g	1 / [ W((Po/P) - 1) ] 1/g
4.87393e-02	10.5508	3.8855e+00
1.01160e-01	12.0420	7.4779e+00
1.47723e-01	13.0933	1.0592e+01
1.98083e-01	14.1383	1.3979e+01
2.48116e-01	15.1462	1.7432e+01

BET summary

Slope = 67.778 1/g  
 Intercept = 5.902e-01 1/g  
 Correlation coefficient, r = 0.999986  
 C constant= 115.837

Surface Area = 50.937 m<sup>2</sup>/g

Quantachrome® ASiQwin™- Automated Gas Sorption Data

Acquisition and Reduction

© 1994-2016, Quantachrome Instruments

version 5.0

Analysis Report  
 Operator: DIJUVA Date:2020/09/21 Operator: DIJUVA Date:2020/11/03  
 Sample ID: Nini-4 1722-1725 Filename: 200921-01.qps  
 Sample Desc: Comment: \_6 Point BET  
 Sample Weight: 0.9736 g Instrument: Autosorb iQ Station 1  
 Approx. Outgas Time:3.1 hrs Final Outgas Temp.:60 °C Extended info: Available  
 Analysis gas: Nitrogen Non-ideality: 6.58e-05 1/Torr CellType: 9mm  
 Analysis Time: 0:35 hr:min Bath temp.: 77.35 K  
 Analysis Mode: Standard VoidVol Remeasure:off  
 VoidVol. Mode: He Measure Cold Zone V: 4.38793 cc Warm Zone V: 8.58499 cc

Data Reduction Parameters

Thermal Transpiration: onEff. mol. diameter (D): 3.54 ÅEff. cell stem diam. (d): 4.0000 mm

Adsorbate modelNitrogen Temperature 77.350K  
 Molec. Wt.: 28.013 Cross Section: 16.200 Å<sup>2</sup> Liquid Density: 0.806 g/cc

Relative Pressure P/Po	Volume @ STP cc/g	1 / [ W((Po/P) - 1) ] 1/g
4.73248e-02	11.9552	3.3246e+00
9.67769e-02	13.5254	6.3383e+00
1.49445e-01	14.8266	9.4817e+00
2.00945e-01	15.9858	1.2587e+01
2.51517e-01	17.0841	1.5738e+01

BET summary

Slope = 60.626 1/g  
 Intercept = 4.484e-01 1/g  
 Correlation coefficient, r = 0.999975  
 C constant= 136.202

Surface Area = 57.021 m<sup>2</sup>/g

Quantachrome® ASiQwin™- Automated Gas Sorption Data

Acquisition and Reduction

© 1994-2016, Quantachrome Instruments

version 5.0

Analysis Report

Operator: DIJUVA Date:2020/09/18 Operator: DIJUVA Date:2020/11/03

Sample ID: Nini-4 1713-1716 Filename: 200918-02.qps

Sample Desc: Comment: \_6 Point BET

Sample Weight: 0.7665 g Instrument: Autosorb iQ Station 1

Approx. Outgas Time:3.1 hrs Final Outgas Temp.:60 °C Extended info: Available

Analysis gas: Nitrogen Non-ideality: 6.58e-05 1/Torr CellType: 9mm

Analysis Time: 0:27 hr:min Bath temp.: 77.35 K

Analysis Mode: Standard VoidVol Remeasure:off

VoidVol. Mode: He Measure Cold Zone V: 5.6387 cc Warm Zone V: 7.45533 cc

Data Reduction Parameters

Thermal Transpiration: onEff. mol. diameter (D): 3.54 ÅEff. cell stem diam. (d): 4.0000 mm

Adsorbate modelNitrogen Temperature 77.350K

Molec. Wt.: 28.013 Cross Section: 16.200 Å<sup>2</sup> Liquid Density: 0.806 g/cc

Relative Pressure P/Po	Volume @ STP cc/g	1 / [ W((Po/P) - 1) ] 1/g
4.84846e-02	10.3334	3.9454e+00
1.01771e-01	11.6779	7.7629e+00
1.48588e-01	12.5859	1.1095e+01
1.98710e-01	13.4633	1.4738e+01

BET summary

Slope = 71.777 1/g

Intercept = 4.569e-01 1/g

Correlation coefficient, r = 0.999991

C constant= 158.089

Surface Area = 48.212 m<sup>2</sup>/g

Quantachrome® ASiQwin™- Automated Gas Sorption Data

Acquisition and Reduction

© 1994-2016, Quantachrome Instruments

version 5.0

Analysis Report  
 Operator: DIJUVA Date:2020/09/14 Operator: DIJUVA Date:2020/11/03  
 Sample ID: NINi-4 1707-1710 Filename: 200914-02.qps  
 Sample Desc: Comment: \_6 Point BET  
 Sample Weight: 0.6012 g Instrument: Autosorb iQ Station 1  
 Approx. Outgas Time:3.1 hrs Final Outgas Temp.:60 °C Extended info: Available  
 Analysis gas: Nitrogen Non-ideality: 6.58e-05 1/Torr CellType: 9mm  
 Analysis Time: 0:22 hr:min Bath temp.: 77.35 K  
 Analysis Mode: Standard VoidVol Remeasure:off  
 VoidVol. Mode: He Measure Cold Zone V: 4.42584 cc Warm Zone V: 8.69489 cc

Data Reduction Parameters

Thermal Transpiration: onEff. mol. diameter (D): 3.54 ÅEff. cell stem diam. (d): 4.0000 mm

Adsorbate modelNitrogen Temperature 77.350K  
 Molec. Wt.: 28.013 Cross Section: 16.200 Å<sup>2</sup> Liquid Density: 0.806 g/cc

Relative Pressure P/Po	Volume @ STP cc/g	1 / [ W((Po/P) - 1) ] 1/g
5.27571e-02	8.9559	4.9758e+00
9.88009e-02	10.2253	8.5786e+00
1.50180e-01	11.3871	1.2417e+01
2.00666e-01	12.4366	1.6151e+01
2.50961e-01	13.4490	1.9933e+01

BET summary

Slope = 75.219 1/g  
 Intercept = 1.077e+00 1/g  
 Correlation coefficient, r = 0.999956  
 C constant = 70.811

Surface Area = 45.644 m<sup>2</sup>/g

Quantachrome® ASiQwin™- Automated Gas Sorption Data

Acquisition and Reduction

© 1994-2016, Quantachrome Instruments

version 5.0

Analysis Report  
 Operator: DIJUVA Date:2020/09/24 Operator: DIJUVA Date:2020/11/03  
 Sample ID: Nini-4 1690-1700 Filename: 200924-02.qps  
 Sample Desc: Comment: \_6 Point BET  
 Sample Weight: 0.6231 g Instrument: Autosorb iQ Station 1  
 Approx. Outgas Time:3.1 hrs Final Outgas Temp.:60 °C Extended info: Available  
 Analysis gas: Nitrogen Non-ideality: 6.58e-05 1/Torr CellType: 9mm  
 Analysis Time: 0:25 hr:min Bath temp.: 77.35 K  
 Analysis Mode: Standard VoidVol Remeasure:off  
 VoidVol. Mode: He Measure Cold Zone V: 4.77378 cc Warm Zone V: 8.31218 cc

Data Reduction Parameters

Thermal Transpiration: onEff. mol. diameter (D): 3.54 ÅEff. cell stem diam. (d): 4.0000 mm

Adsorbate modelNitrogen Temperature 77.350K  
 Molec. Wt.: 28.013 Cross Section: 16.200 Å<sup>2</sup> Liquid Density: 0.806 g/cc

Relative Pressure P/Po	Volume @ STP cc/g	1 / [ W((Po/P) - 1) ] 1/g
4.93643e-02	10.1839	4.0798e+00
9.65135e-02	11.5497	7.4003e+00
1.48390e-01	12.7472	1.0937e+01
1.99094e-01	13.8137	1.4399e+01
2.49352e-01	14.8214	1.7932e+01

BET summary

Slope = 69.050 1/g  
 Intercept = 6.928e-01 1/g  
 Correlation coefficient, r = 0.999981  
 C constant= 100.674

Surface Area = 49.934 m<sup>2</sup>/g

Quantachrome® ASiQwin™- Automated Gas Sorption Data

Acquisition and Reduction

© 1994-2016, Quantachrome Instruments

version 5.0

Analysis Report

Operator: DIJUVA Date:2020/09/23 Operator: DIJUVA Date:2020/11/03

Sample ID: Nini-4 1670-1680 Filename: 200923-02.qps

Sample Desc: Comment: \_6 Point BET

Sample Weight: 0.3969 g Instrument: Autosorb iQ Station 1

Approx. Outgas Time:3.1 hrs Final Outgas Temp.:60 °C Extended info: Available

Analysis gas: Nitrogen Non-ideality: 6.58e-05 1/Torr CellType: 9mm

Analysis Time: 0:18 hr:min Bath temp.: 77.35 K

Analysis Mode: Standard VoidVol Remeasure:off

VoidVol. Mode: He Measure Cold Zone V: 5.64176 cc Warm Zone V: 7.5483 cc

Data Reduction Parameters

Thermal Transpiration: onEff. mol. diameter (D): 3.54 ÅEff. cell stem diam. (d): 4.0000 mm

Adsorbate modelNitrogen Temperature 77.350K

Molec. Wt.: 28.013 Cross Section: 16.200 Å<sup>2</sup> Liquid Density: 0.806 g/cc

Relative Pressure P/Po	Volume @ STP cc/g	1 / [ W((Po/P) - 1) ] 1/g
4.68636e-02	6.4976	6.0545e+00
9.61473e-02	7.4419	1.1437e+01
1.47557e-01	8.2295	1.6830e+01
1.98262e-01	8.9413	2.2129e+01
2.48326e-01	9.6245	2.7464e+01
2.98299e-01	10.3116	3.2986e+01

BET summary

Slope = 106.567 1/g

Intercept = 1.092e+00 1/g

Correlation coefficient, r = 0.999962

C constant= 98.565

Surface Area = 32.347 m<sup>2</sup>/g

Quantachrome® ASiQwin™- Automated Gas Sorption Data

Acquisition and Reduction

© 1994-2016, Quantachrome Instruments

version 5.0

Analysis Report  
 Operator: DIJUVA Date:2020/09/22 Operator: DIJUVA Date:2020/11/03  
 Sample ID: Nini-4 1650-1660 Filename: 200922-02.qps  
 Sample Desc: Comment: \_6 Point BET  
 Sample Weight: 0.39 g Instrument: Autosorb iQ Station 1  
 Approx. Outgas Time:3.1 hrs Final Outgas Temp.:60 °C Extended info: Available  
 Analysis gas: Nitrogen Non-ideality: 6.58e-05 1/Torr CellType: 9mm  
 Analysis Time: 0:19 hr:min Bath temp.: 77.35 K  
 Analysis Mode: Standard VoidVol Remeasure:off  
 VoidVol. Mode: He Measure Cold Zone V: 4.72312 cc Warm Zone V: 8.43631 cc

Data Reduction Parameters

Thermal Transpiration: onEff. mol. diameter (D): 3.54 ÅEff. cell stem diam. (d): 4.0000 mm

Adsorbate modelNitrogen Temperature 77.350K  
 Molec. Wt.: 28.013 Cross Section: 16.200 Å<sup>2</sup> Liquid Density: 0.806 g/cc

Relative Pressure P/Po	Volume @ STP cc/g	1 / [ W((Po/P) - 1) ] 1/g
5.21095e-02	7.5727	5.8084e+00
1.02440e-01	8.8819	1.0281e+01
1.53537e-01	9.9940	1.4522e+01
1.96523e-01	10.8739	1.7997e+01
2.53220e-01	12.0213	2.2569e+01
2.96634e-01	12.8901	2.6178e+01

BET summary

Slope = 82.767 1/g  
 Intercept = 1.680e+00 1/g  
 Correlation coefficient, r = 0.999866  
 C constant= 50.267

Surface Area = 41.239 m<sup>2</sup>/g

Quantachrome® ASiQwin™- Automated Gas Sorption Data

Acquisition and Reduction

© 1994-2016, Quantachrome Instruments

version 5.0

Analysis Report  
 Operator: DIJUVA Date:2020/09/21 Operator: DIJUVA Date:2020/11/03  
 Sample ID: Nini-4 1630-1640 Filename: 200921-02.qps  
 Sample Desc: Comment: \_6 Point BET  
 Sample Weight: 0.8181 g Instrument: Autosorb iQ Station 1  
 Approx. Outgas Time:3.1 hrs Final Outgas Temp.:60 °C Extended info: Available  
 Analysis gas: Nitrogen Non-ideality: 6.58e-05 1/Torr CellType: 9mm  
 Analysis Time: 0:24 hr:min Bath temp.: 77.35 K  
 Analysis Mode: Standard VoidVol Remeasure:off  
 VoidVol. Mode: He Measure Cold Zone V: 4.70858 cc Warm Zone V: 8.42744 cc

Data Reduction Parameters

Thermal Transpiration: onEff. mol. diameter (D): 3.54 ÅEff. cell stem diam. (d): 4.0000 mm

Adsorbate modelNitrogen Temperature 77.350K  
 Molec. Wt.: 28.013 Cross Section: 16.200 Å<sup>2</sup> Liquid Density: 0.806 g/cc

Relative Pressure P/Po	Volume @ STP cc/g	1 / [ W((Po/P) - 1) ] 1/g
4.78626e-02	7.3587	5.4657e+00
9.71078e-02	8.4775	1.0151e+01
1.48749e-01	9.4392	1.4812e+01
1.99281e-01	10.3186	1.9298e+01
2.49357e-01	11.1753	2.3784e+01
2.99083e-01	12.0347	2.8369e+01

BET summary

Slope = 90.675 1/g  
 Intercept = 1.241e+00 1/g  
 Correlation coefficient, r = 0.999951  
 C constant = 74.066  
 Surface Area = 37.888 m<sup>2</sup>/g

Quantachrome® ASiQwin™- Automated Gas Sorption Data

Acquisition and Reduction

© 1994-2016, Quantachrome Instruments

version 5.0

Analysis Report  
 Operator: DIJUVA Date:2020/09/18 Operator: DIJUVA Date:2020/11/03  
 Sample ID: NIni-4 1610-1620 Filename: 200918-01.qps  
 Sample Desc: Comment: \_6 Point BET  
 Sample Weight: 0.5689 g Instrument: Autosorb iQ Station 1  
 Approx. Outgas Time:3.1 hrs Final Outgas Temp.:60 °C Extended info: Available  
 Analysis gas: Nitrogen Non-ideality: 6.58e-05 1/Torr CellType: 9mm  
 Analysis Time: 0:20 hr:min Bath temp.: 77.35 K  
 Analysis Mode: Standard VoidVol Remeasure:off  
 VoidVol. Mode: He Measure Cold Zone V: 5.60044 cc Warm Zone V: 7.49066 cc

Data Reduction Parameters

Thermal Transpiration: onEff. mol. diameter (D): 3.54 ÅEff. cell stem diam. (d): 4.0000 mm

Adsorbate modelNitrogen Temperature 77.350K  
 Molec. Wt.: 28.013 Cross Section: 16.200 Å<sup>2</sup> Liquid Density: 0.806 g/cc

Relative Pressure P/Po	Volume @ STP cc/g	1 / [ W((Po/P) - 1) ] 1/g
5.09222e-02	5.7734	7.4358e+00
1.02697e-01	6.6156	1.3842e+01
1.47045e-01	7.1985	1.9162e+01
1.96685e-01	7.8073	2.5092e+01
2.46860e-01	8.4040	3.1206e+01
2.96734e-01	9.0068	3.7482e+01

BET summary

Slope = 121.713 1/g  
 Intercept = 1.254e+00 1/g  
 Correlation coefficient, r = 0.999968  
 C constant = 98.063

Surface Area = 28.321 m<sup>2</sup>/g

Quantachrome® ASiQwin™- Automated Gas Sorption Data

Acquisition and Reduction

© 1994-2016, Quantachrome Instruments

version 5.0

Analysis Report  
 Operator: DIJUVA Date:2020/09/16 Operator: DIJUVA Date:2020/11/03  
 Sample ID: NIni-4 1590-1600 Filename: 200916-01.qps  
 Sample Desc: Comment: \_6 Point BET  
 Sample Weight: 0.3824 g Instrument: Autosorb iQ Station 1  
 Approx. Outgas Time:3.1 hrs Final Outgas Temp.:60 °C Extended info: Available  
 Analysis gas: Nitrogen Non-ideality: 6.58e-05 1/Torr CellType: 9mm  
 Analysis Time: 0:18 hr:min Bath temp.: 77.35 K  
 Analysis Mode: Standard VoidVol Remeasure:off  
 VoidVol. Mode: He Measure Cold Zone V: 4.73274 cc Warm Zone V: 8.45526 cc

Data Reduction Parameters

Thermal Transpiration: onEff. mol. diameter (D): 3.54 ÅEff. cell stem diam. (d): 4.0000 mm

Adsorbate modelNitrogen Temperature 77.350K  
 Molec. Wt.: 28.013 Cross Section: 16.200 Å<sup>2</sup> Liquid Density: 0.806 g/cc

Relative Pressure P/Po	Volume @ STP cc/g	1 / [ W((Po/P) - 1) ] 1/g
5.14955e-02	3.7575	1.1561e+01
9.75201e-02	4.5632	1.8947e+01
1.47818e-01	5.3476	2.5953e+01
1.98307e-01	6.1052	3.2418e+01
2.48571e-01	6.8477	3.8652e+01
2.98023e-01	7.5908	4.4750e+01

BET summary

Slope = 133.270 1/g  
 Intercept = 5.575e+00 1/g  
 Correlation coefficient, r = 0.998800  
 C constant= 24.907

Surface Area = 25.082 m<sup>2</sup>/g

## **APPENDIX B – MICP ANALYSIS**

The capillary pressure and pore network characteristics were measured by the automatic mercury injection technique for 12 cuttings samples (ID 1-12) and 8 plug trim samples (ID 13-20). Sampling details, laboratory constants used during the data reduction and diagrams necessary for the seal capacity evaluation are shown in the data sheets below. A listing of selected MICP data for all samples is given in Table 9. The total set of raw data and diagrams were forwarded to GEUS in an Excel file from Core Technical Services, Aberdeen.

### Mercury Injection Drainage

Client Geus  
Well Nini-4  
Reference 45970

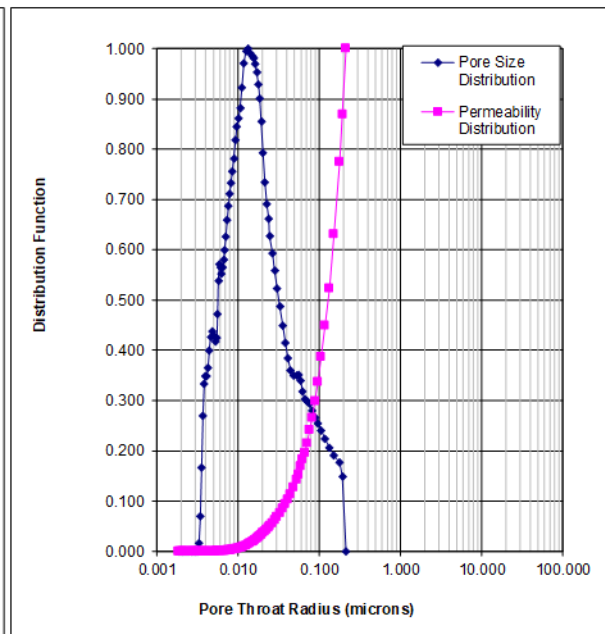
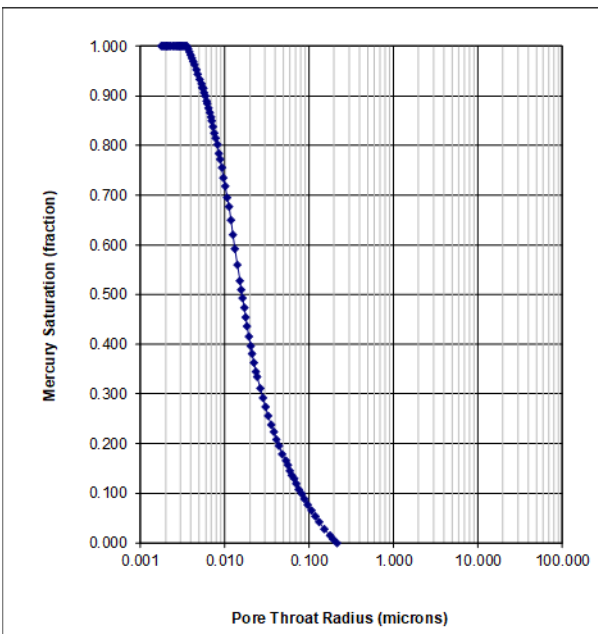
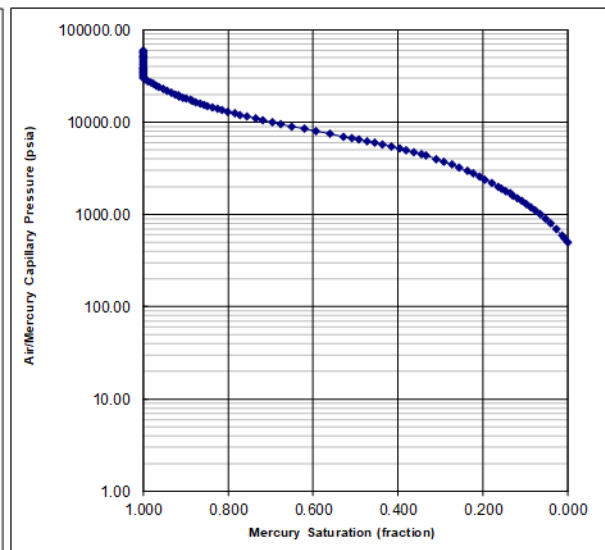
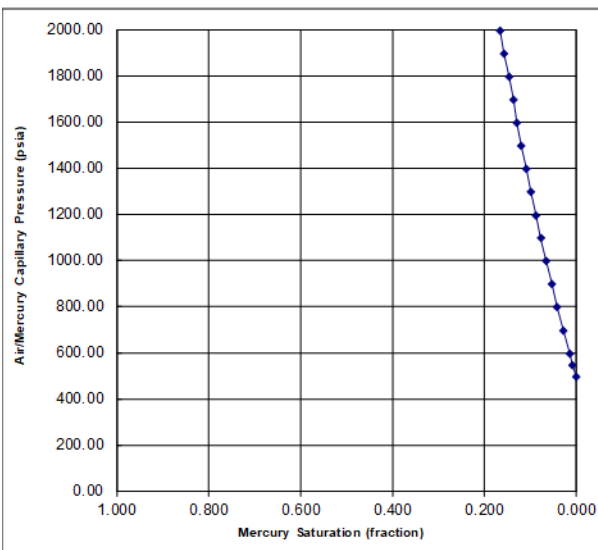
Brine Density Gradient	0.44	psig/foot
Oil Density Gradient	0.33	psig/foot

Sample Identification	1	
Sample Depth	1590.00	m
Plug Permeability (Air)	n/a	mD
Plug Porosity (He)	0.159	fraction

IFT x Cos(contact angle)		
	Lab	Res
Air/Brine	72	50
Air/Oil	24	
Oil/Brine	42	26
Air/Hg	368	

Injection Sample Porosity	0.159	fraction
Injection Sample Pore Vol	0.347	cc
Injection Sample Bulk Vol	2.187	cc
Injection Sample Weight	4.6600	g

Mean Hydraulic Radius	0.037	microns
Swanson's Parameter	0.001	
FZI		



### Mercury Injection Drainage

Client Geus  
Well Nini-4  
Reference 45971

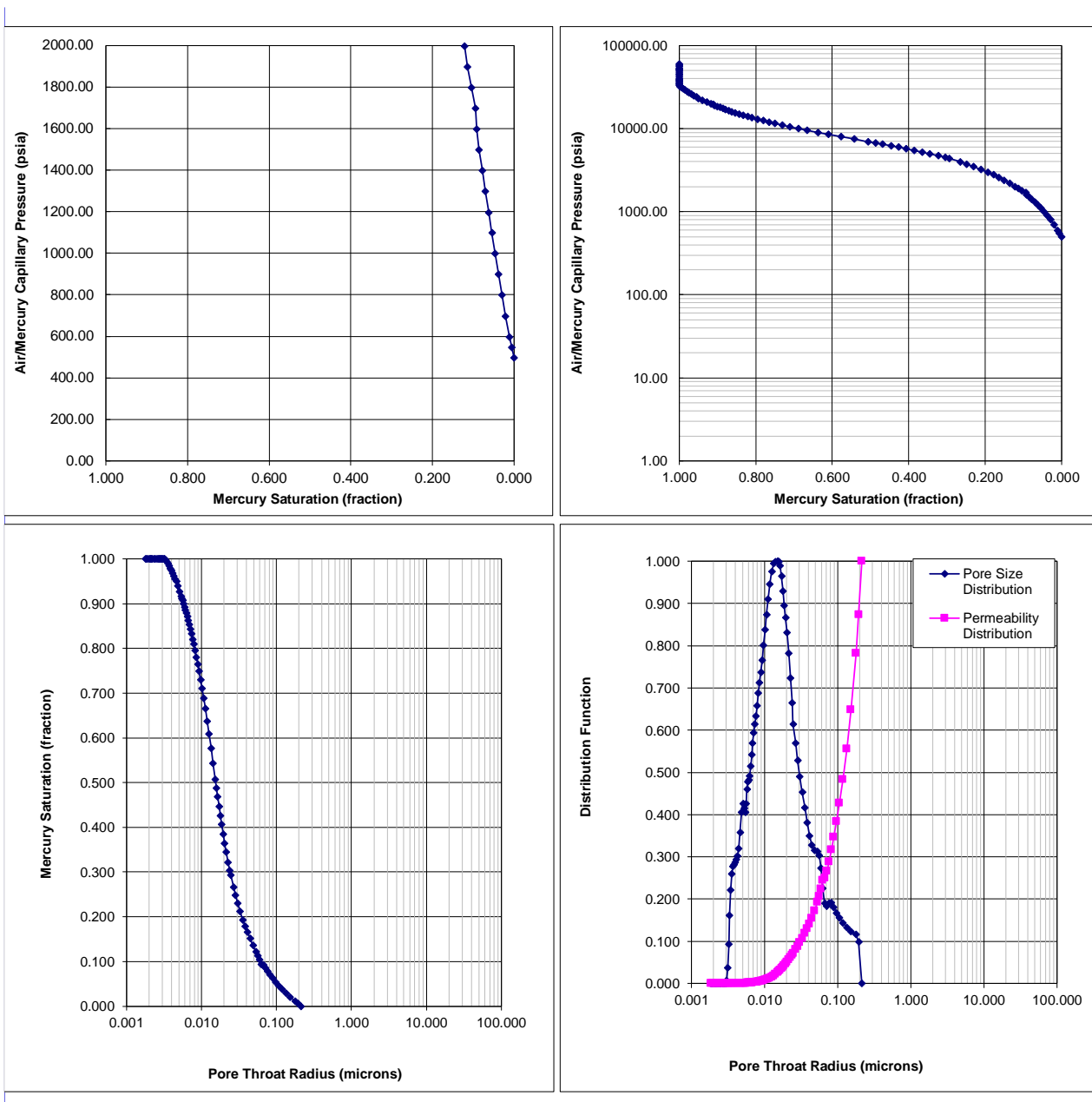
Brine Density Gradient	0.44	psig/foot
Oil Density Gradient	0.33	psig/foot

Sample Identification	2	
Sample Depth	1610.00	m
Plug Permeability (Air)	n/a	mD
Plug Porosity (He)	0.153	fraction

IFT x Cos(contact angle)		
	Lab	Res
Air/Brine	72	50
Air/Oil	24	
Oil/Brine	42	26
Air/Hg	368	

Injection Sample Porosity	0.153	fraction
Injection Sample Pore Vol	0.335	cc
Injection Sample Bulk Vol	2.192	cc
Injection Sample Weight	4.7000	g

Mean Hydraulic Radius	0.032	microns
Swanson's Parameter	0.001	
FZI #VÆRDI!		



### Mercury Injection Drainage

Client Geus  
Well Nini-4  
Reference 45972

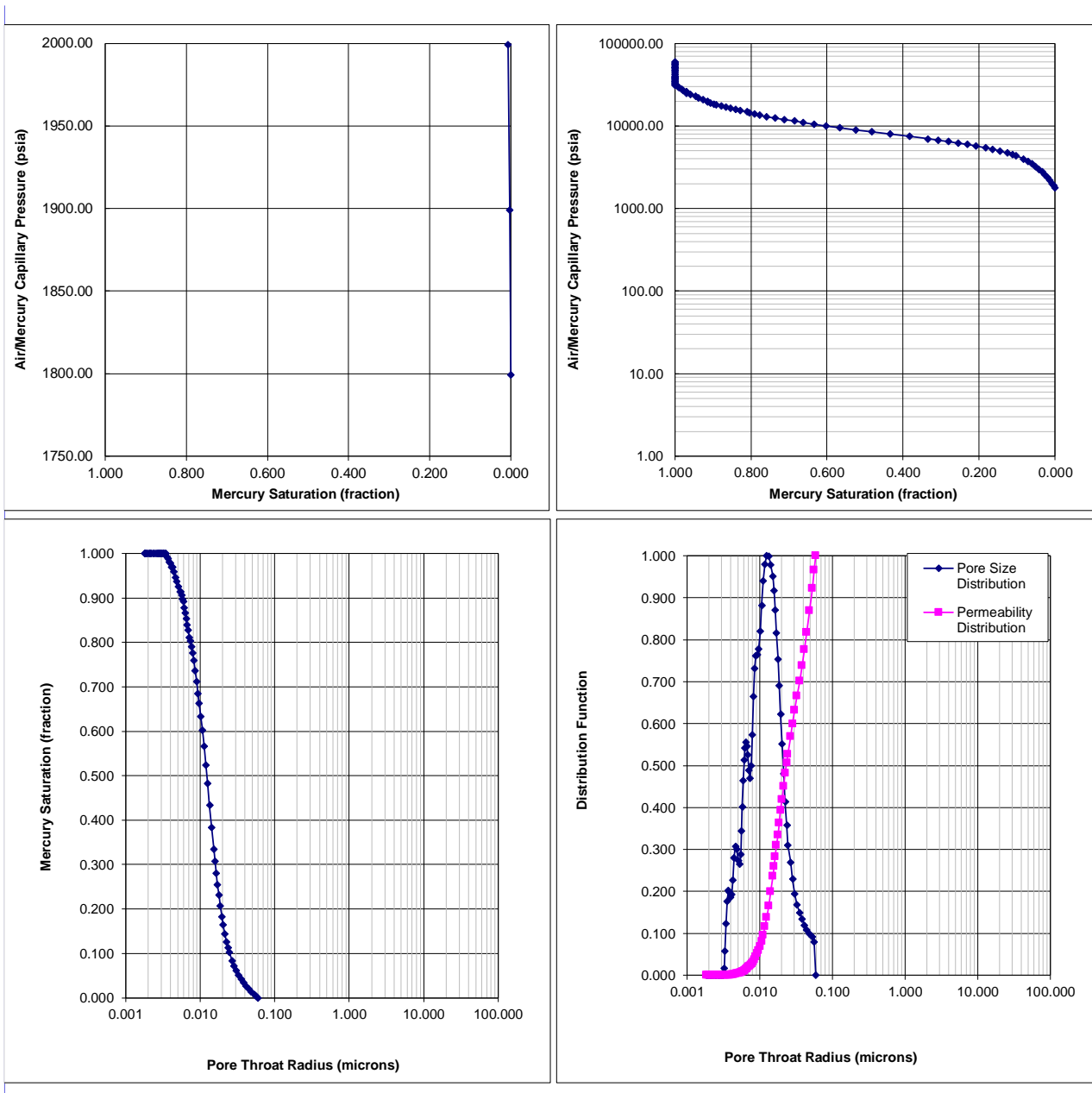
Brine Density Gradient	0.44	psig/foot
Oil Density Gradient	0.33	psig/foot

Sample Identification	3	
Sample Depth	1630.00	m
Plug Permeability (Air)	n/a	mD
Plug Porosity (He)	0.142	fraction

IFT x Cos(contact angle)		
	Lab	Res
Air/Brine	72	50
Air/Oil	24	
Oil/Brine	42	26
Air/Hg	368	

Injection Sample Porosity	0.135	fraction
Injection Sample Pore Vol	0.291	cc
Injection Sample Bulk Vol	2.163	cc
Injection Sample Weight	4.7100	g

Mean Hydraulic Radius	0.010	microns
Swanson's Parameter	0.001	
FZI	#VÆRDI!	



### Mercury Injection

Client Geus  
Well Nini-4  
Reference 45973

Brine Density Gradient	0.44	psig/foot
Oil Density Gradient	0.33	psig/foot

IFT x Cos(contact angle)		
	Lab	Res
Air/Brine	72	50
Air/Oil	24	
Oil/Brine	42	26
Air/Hg	368	

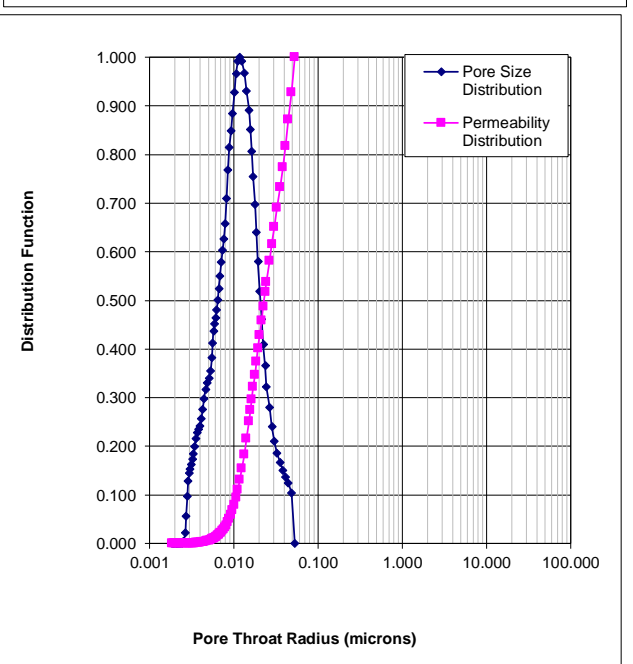
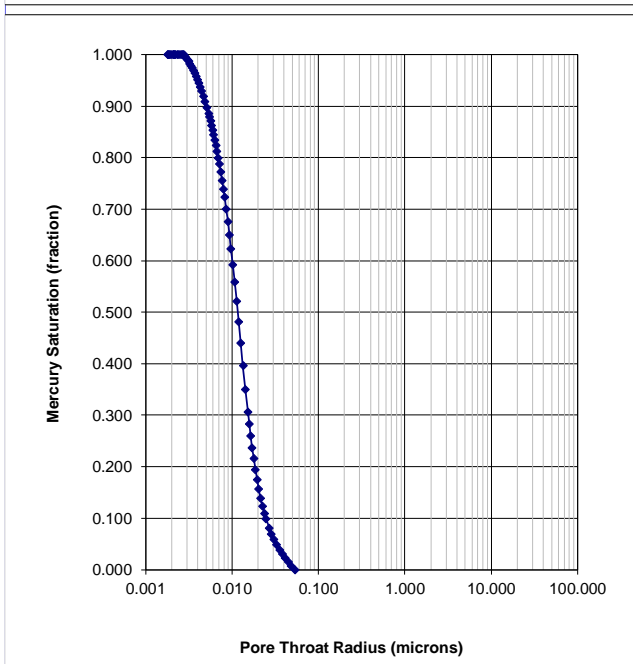
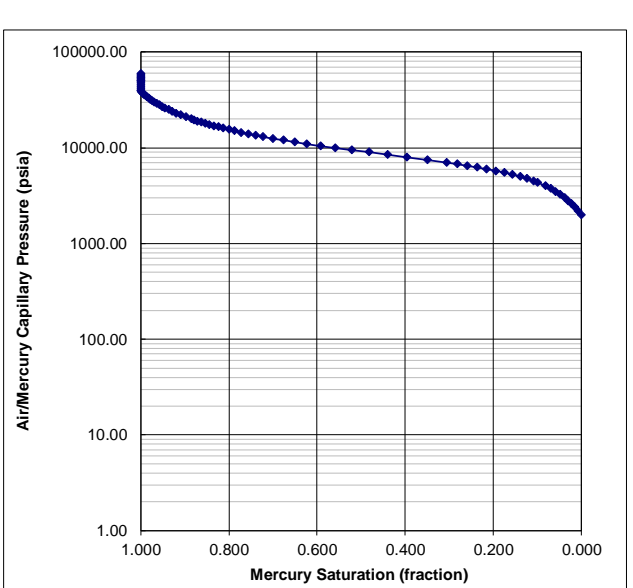
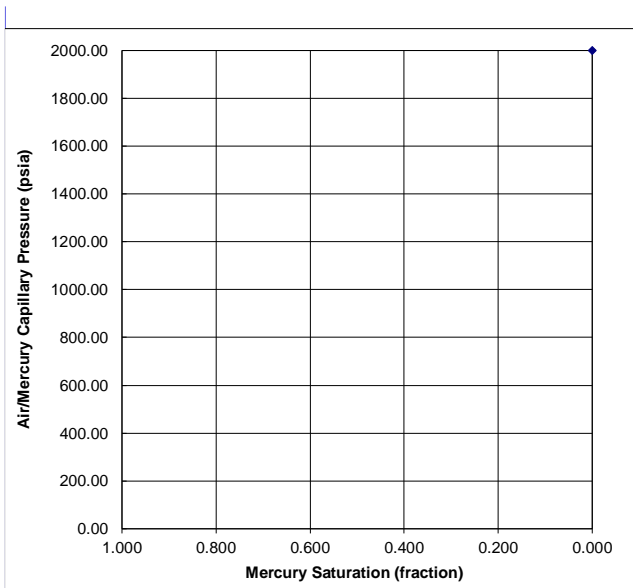
  

Mean Hydraulic Radius	0.009	microns
Swanson's Parameter	0.001	
	FZI	#V/ÆRDI!

Sample Identification	4	
Sample Depth	1650.00	m
Plug Permeability (Air)	n/a	mD
Plug Porosity (He)	0.137	fraction

Injection Sample Porosity	0.136	fraction
Injection Sample Pore Vol	0.288	cc
Injection Sample Bulk Vol	2.112	cc
Injection Sample Weight	4.6900	g



### Mercury Injection

Client Geus  
Well Nini-4  
Reference 45974

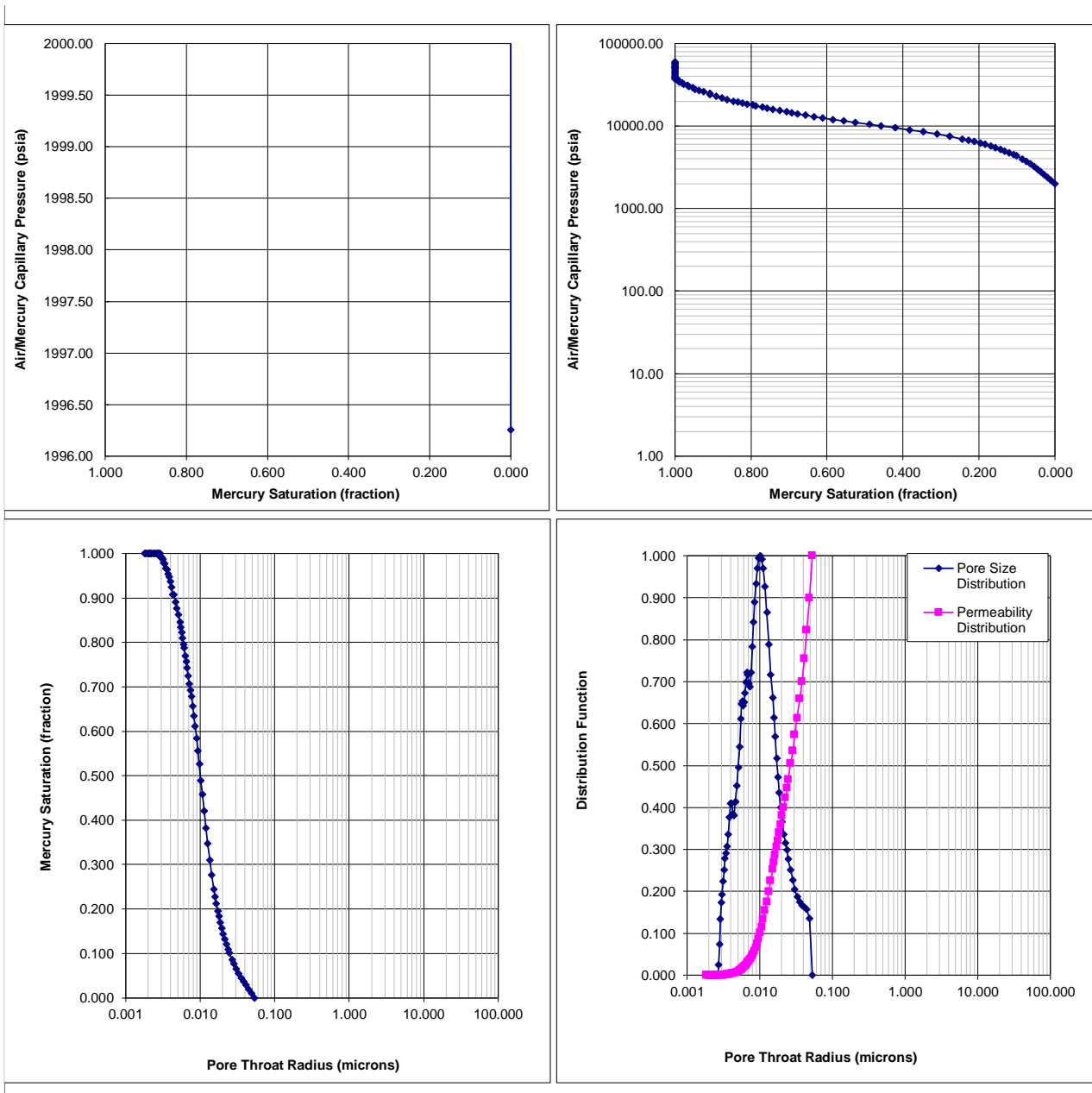
Brine Density Gradient	0.44	psig/foot
Oil Density Gradient	0.33	psig/foot

Sample Identification	5	
Sample Depth	1670.00	m
Plug Permeability (Air)	n/a	mD
Plug Porosity (He)	0.121	fraction

IFT x Cos(contact angle)		
	Lab	Res
Air/Brine	72	50
Air/Oil	24	
Oil/Brine	42	26
Air/Hg	368	

Injection Sample Porosity	0.093	fraction
Injection Sample Pore Vol	0.268	cc
Injection Sample Bulk Vol	2.900	cc
Injection Sample Weight	4.4400	g

Mean Hydraulic Radius	0.009	microns
Swanson's Parameter	0.000	
FZI $\nabla$ #V $\nabla$ ERDI!		



### Mercury Injection

Client Geus  
Well Nini-4  
Reference 45975

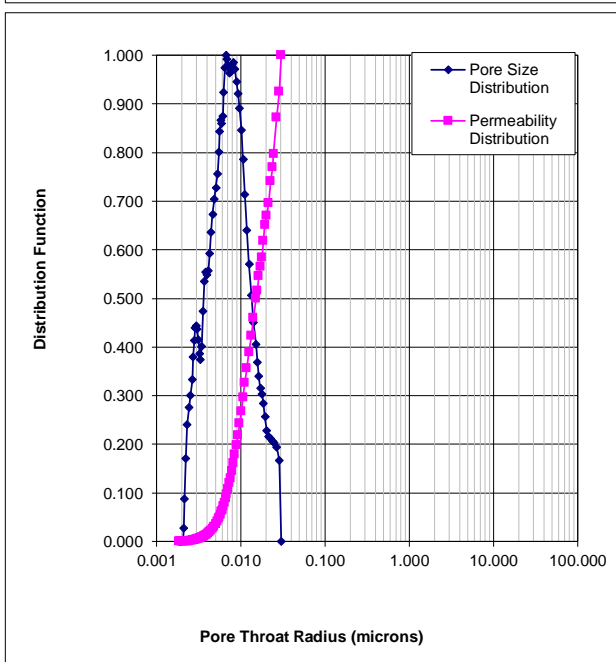
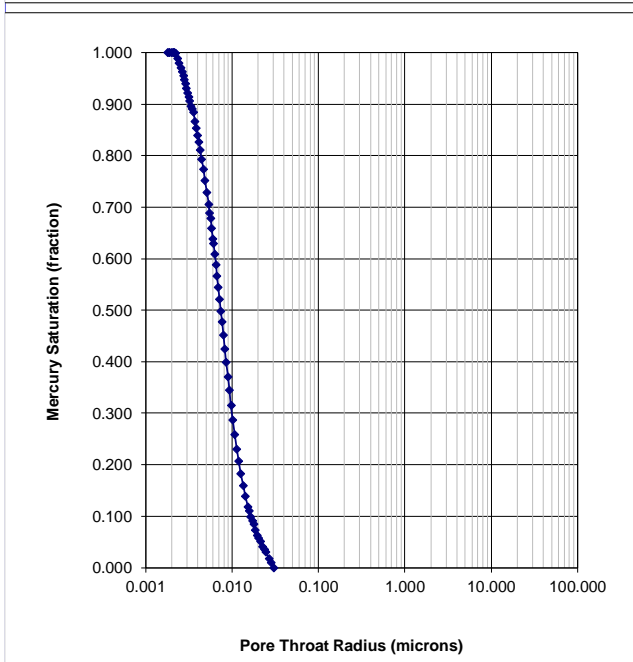
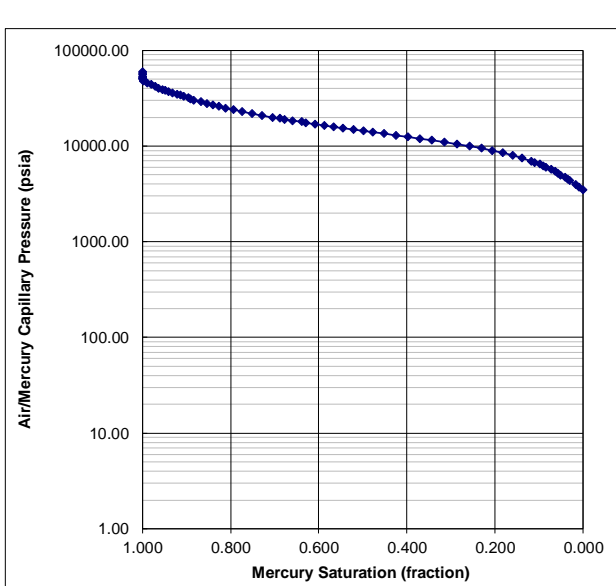
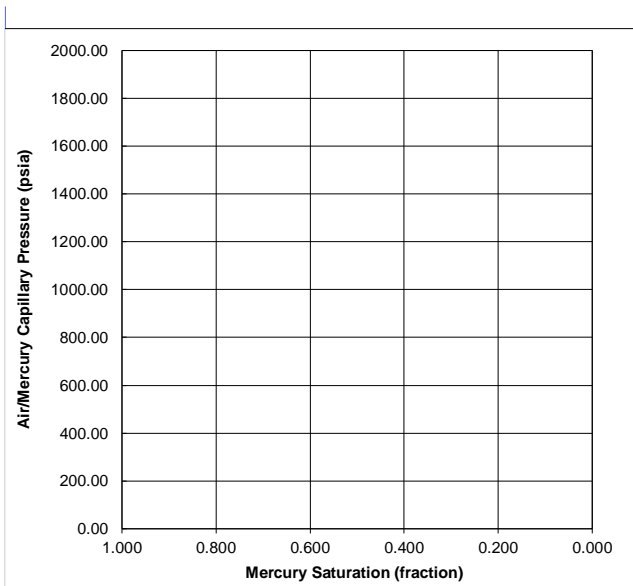
Brine Density Gradient	0.44	psig/foot
Oil Density Gradient	0.33	psig/foot

Sample Identification	6	
Sample Depth	1690.00	m
Plug Permeability (Air)	n/a	mD
Plug Porosity (He)	0.153	fraction

IFT x Cos(contact angle)		
	Lab	Res
Air/Brine	72	50
Air/Oil	24	
Oil/Brine	42	26
Air/Hg	368	

Injection Sample Porosity	0.121	fraction
Injection Sample Pore Vol	0.288	cc
Injection Sample Bulk Vol	2.382	cc
Injection Sample Weight	4.0400	g

Mean Hydraulic Radius	0.006	microns
Swanson's Parameter	0.000	
FZI <input type="checkbox"/> #VÆRDI!		



### Mercury Injection

Client Geus  
Well Nini-4  
Reference 45976

Brine Density Gradient	0.44	psig/foot
Oil Density Gradient	0.33	psig/foot

IFT x Cos(contact angle)		
	Lab	Res
Air/Brine	72	50
Air/Oil	24	
Oil/Brine	42	26
Air/Hg	368	

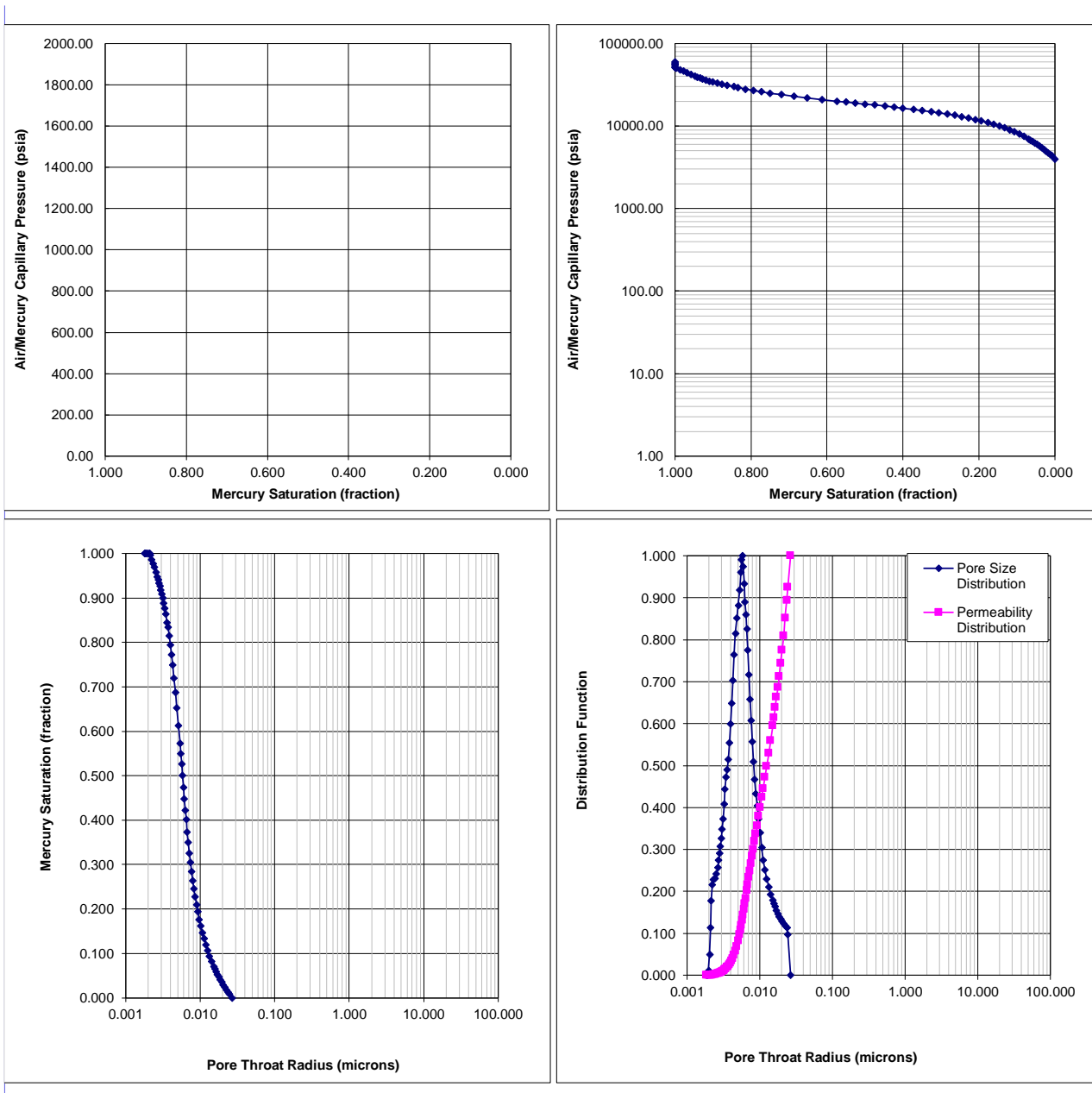
  

Mean Hydraulic Radius	0.005	microns
Swanson's Parameter	0.001	
	FZI	#V/ÆRDI!

Sample Identification	7	
Sample Depth	1707.00	m
Plug Permeability (Air)	n/a	mD
Plug Porosity (He)	0.187	fraction

Injection Sample Porosity	0.187	fraction
Injection Sample Pore Vol	0.110	cc
Injection Sample Bulk Vol	0.591	cc
Injection Sample Weight	1.2200	g



### Mercury Injection

Client Geus  
Well Nini-4  
Reference 45977

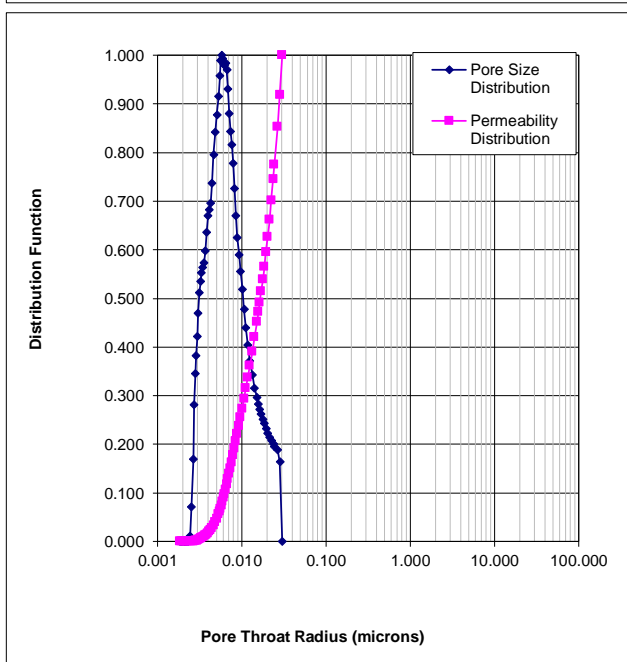
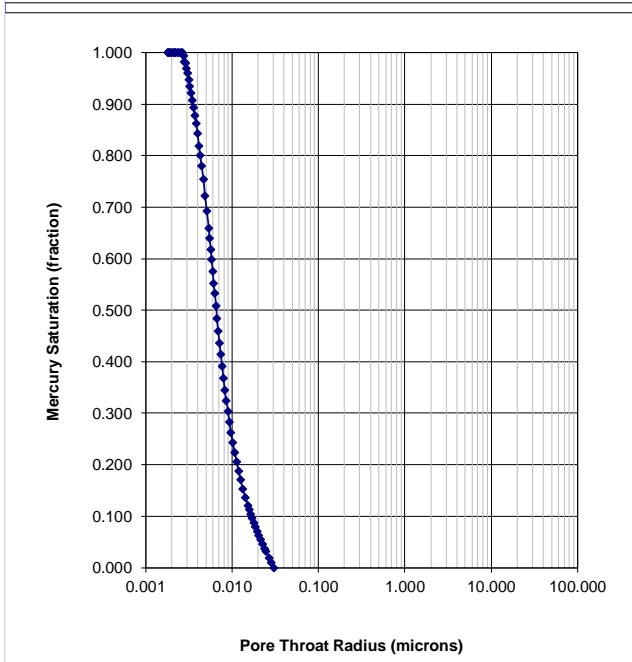
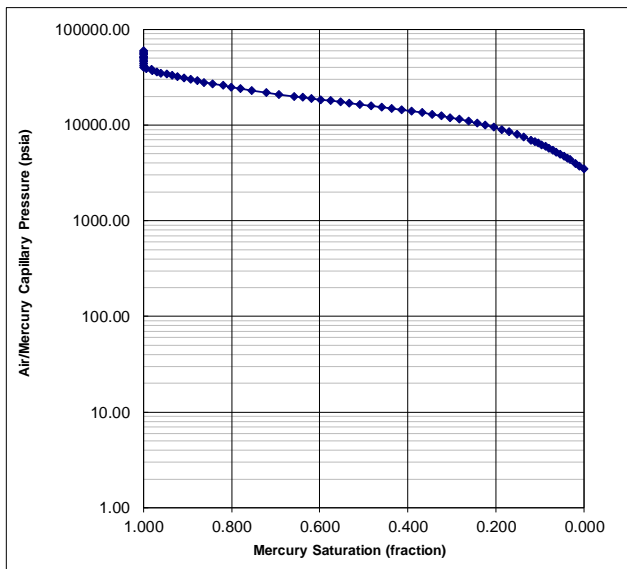
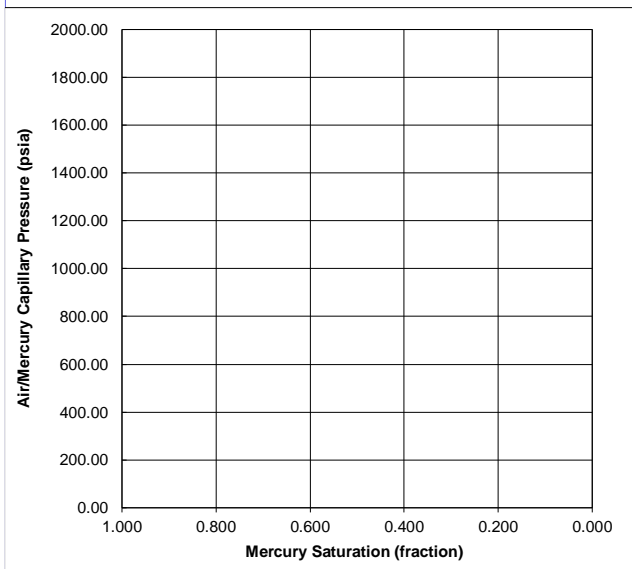
Brine Density Gradient	0.44	psig/foot
Oil Density Gradient	0.33	psig/foot

Sample Identification	8	
Sample Depth	1713.00	m
Plug Permeability (Air)	n/a	mD
Plug Porosity (He)	0.143	fraction

IFT x Cos(contact angle)		
	Lab	Res
Air/Brine	72	50
Air/Oil	24	
Oil/Brine	42	26
Air/Hg	368	

Injection Sample Porosity	0.143	fraction
Injection Sample Pore Vol	0.294	cc
Injection Sample Bulk Vol	2.058	cc
Injection Sample Weight	4.3400	g

Mean Hydraulic Radius	0.006	microns
Swanson's Parameter	0.000	
FZI <input type="checkbox"/> #V/ÆRDI!		



### Mercury Injection

Client Geus  
Well Nini-4  
Reference 45978

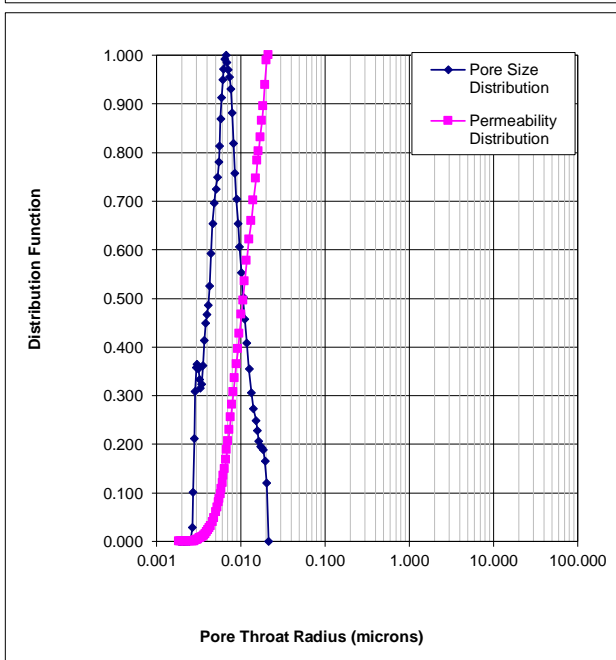
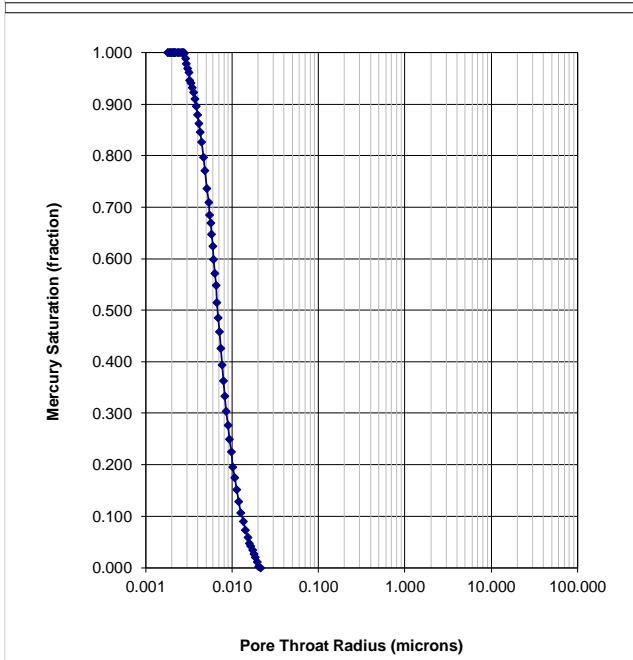
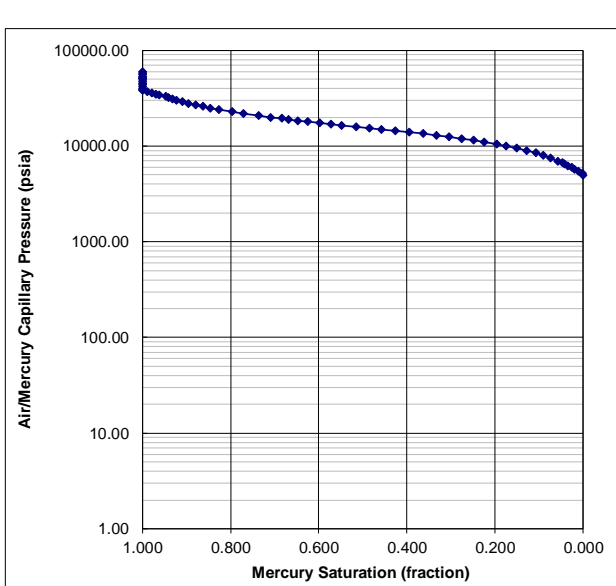
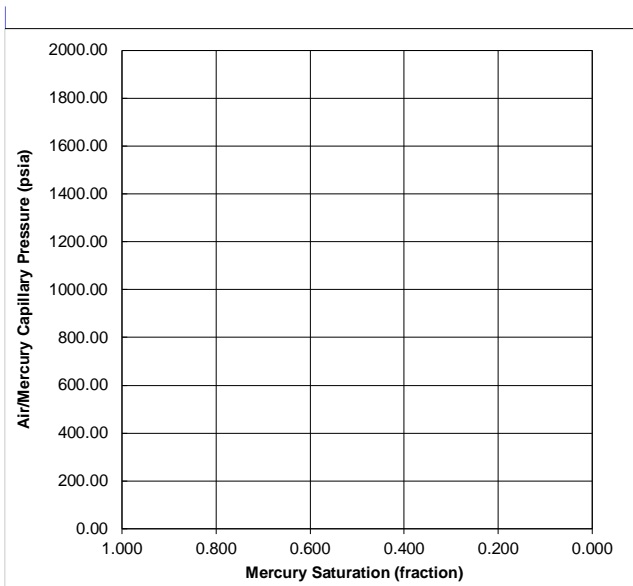
Brine Density Gradient	0.44	psig/foot
Oil Density Gradient	0.33	psig/foot

Sample Identification	9	
Sample Depth	1722.00	m
Plug Permeability (Air)	n/a	mD
Plug Porosity (He)	0.152	fraction

IFT x Cos(contact angle)		
	Lab	Res
Air/Brine	72	50
Air/Oil	24	
Oil/Brine	42	26
Air/Hg	368	

Injection Sample Porosity	0.152	fraction
Injection Sample Pore Vol	0.294	cc
Injection Sample Bulk Vol	1.934	cc
Injection Sample Weight	4.3600	g

Mean Hydraulic Radius	0.005	microns
Swanson's Parameter	0.001	
FZI	#V/ÆRDI!	



### Mercury Injection

Client Geus  
Well Nini-4  
Reference 45979

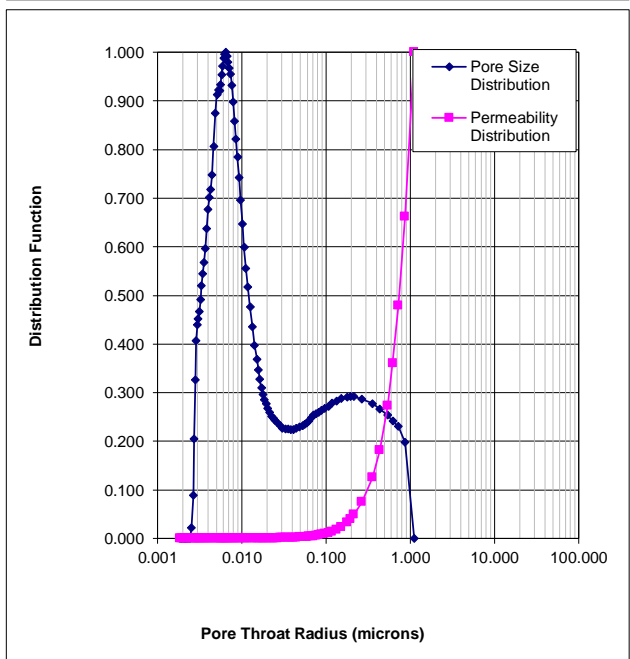
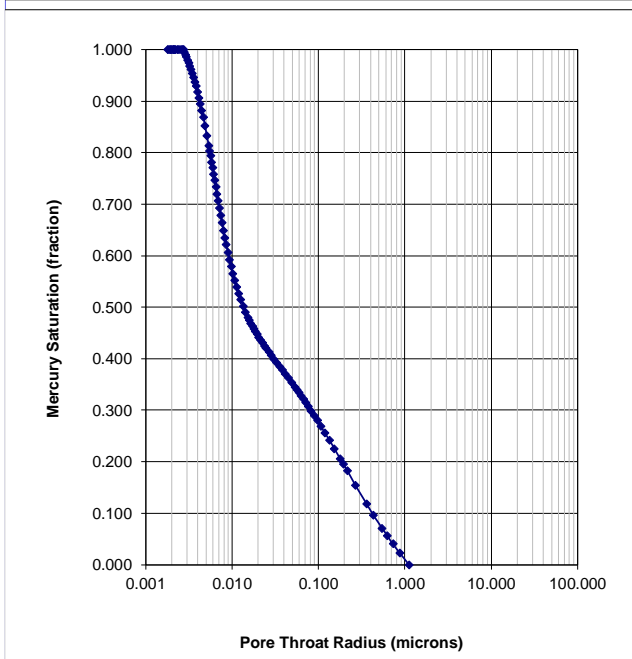
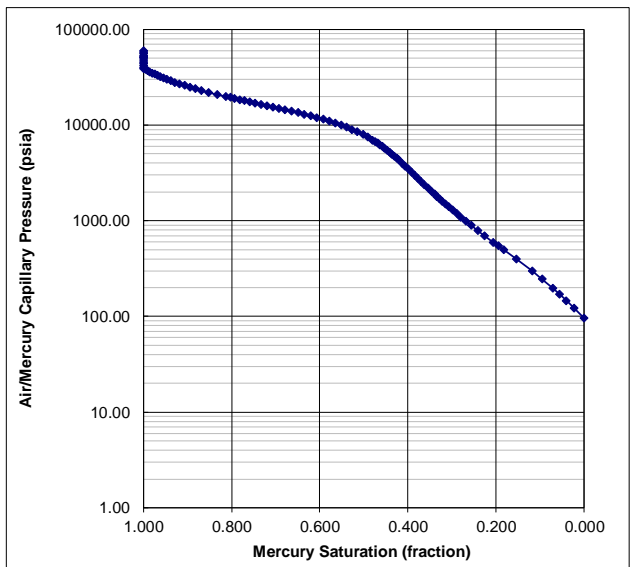
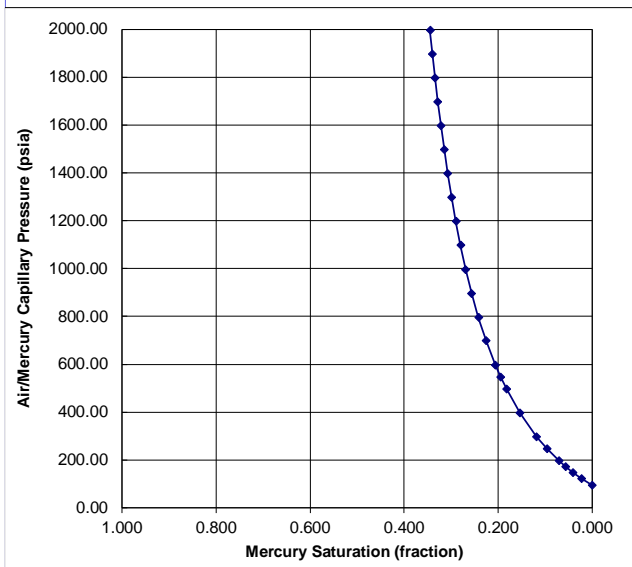
Brine Density Gradient	0.44	psig/foot
Oil Density Gradient	0.33	psig/foot

Sample Identification	10	
Sample Depth	1731.00	m
Plug Permeability (Air)	n/a	mD
Plug Porosity (He)	0.177	fraction

IFT x Cos(contact angle)		
	Lab	Res
Air/Brine	72	50
Air/Oil	24	
Oil/Brine	42	26
Air/Hg	368	

Injection Sample Porosity	0.177	fraction
Injection Sample Pore Vol	0.402	cc
Injection Sample Bulk Vol	2.269	cc
Injection Sample Weight	4.3400	g

Mean Hydraulic Radius	0.230	microns
Swanson's Parameter	0.007	
FZI		



### Mercury Injection

Client Geus  
Well Nini-4  
Reference 45980

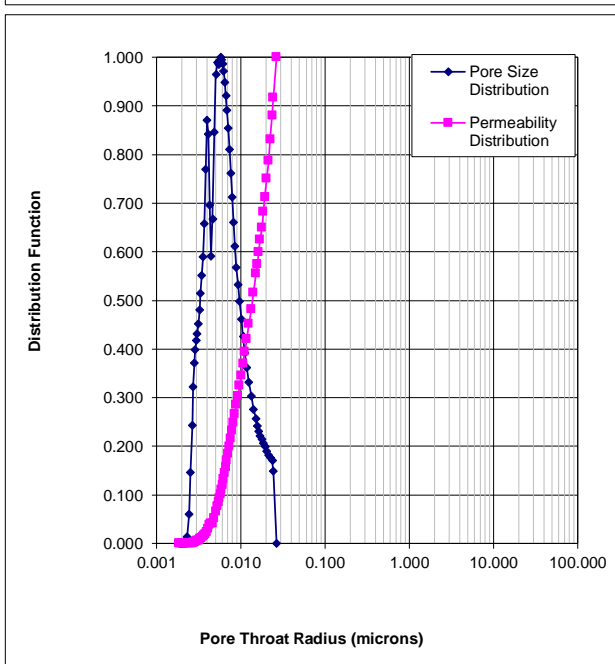
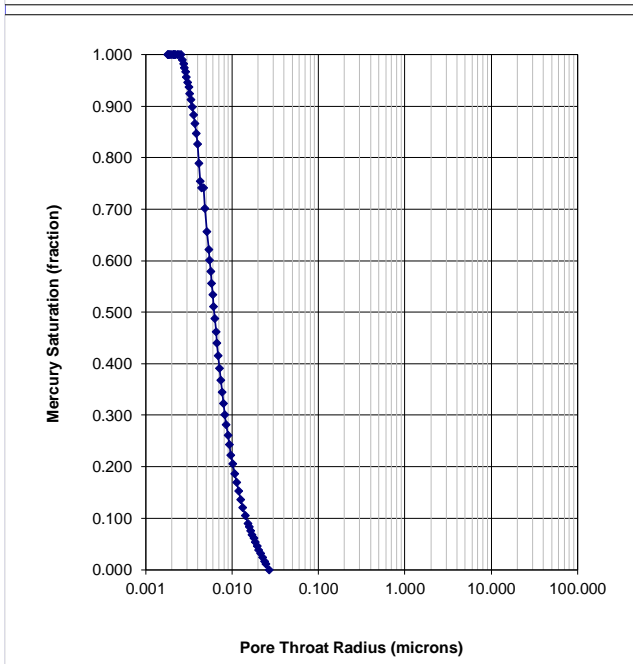
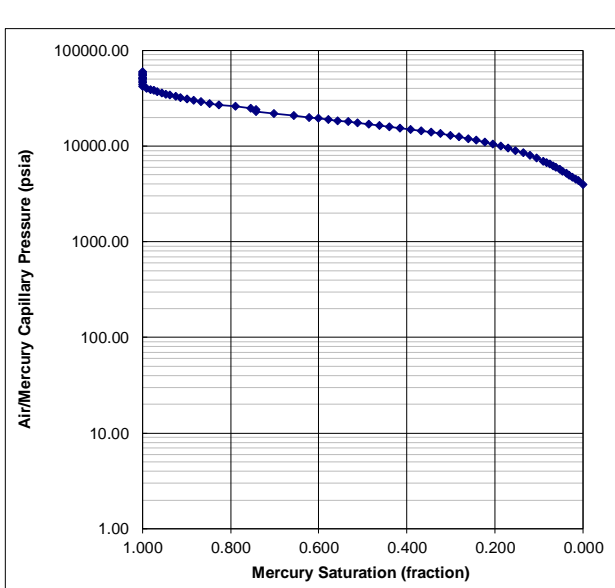
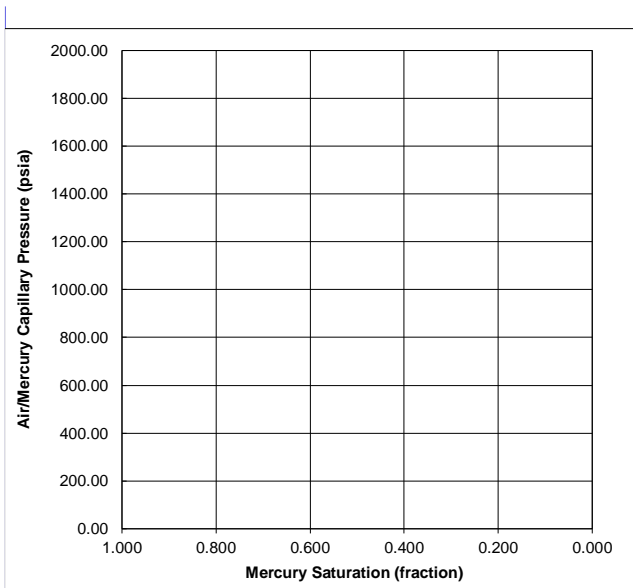
Brine Density Gradient	0.44	psig/foot
Oil Density Gradient	0.33	psig/foot

Sample Identification	11	
Sample Depth	1737.00	m
Plug Permeability (Air)	n/a	mD
Plug Porosity (He)	0.123	fraction

IFT x Cos(contact angle)		
	Lab	Res
Air/Brine	72	50
Air/Oil	24	
Oil/Brine	42	26
Air/Hg	368	

Injection Sample Porosity	0.123	fraction
Injection Sample Pore Vol	0.271	cc
Injection Sample Bulk Vol	2.203	cc
Injection Sample Weight	4.2100	g

Mean Hydraulic Radius	0.005	microns
Swanson's Parameter	0.000	
FZI	#V/ÆRDI!	



### Mercury Injection

Client Geus  
Well Nini-4  
Reference 45981

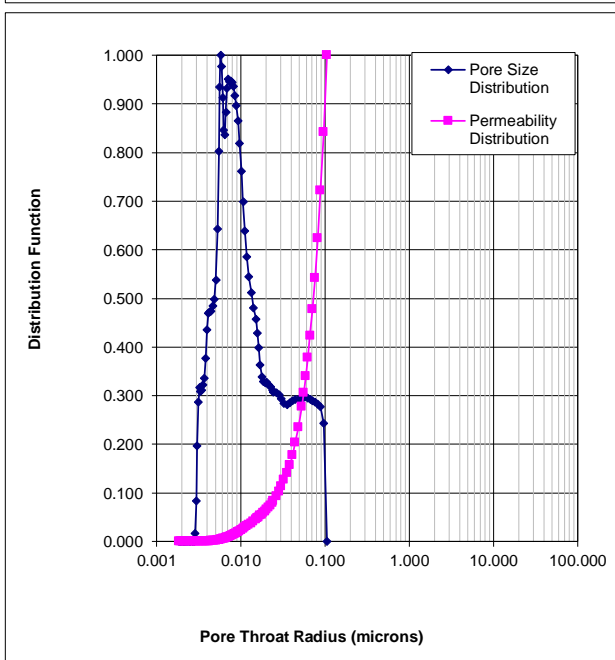
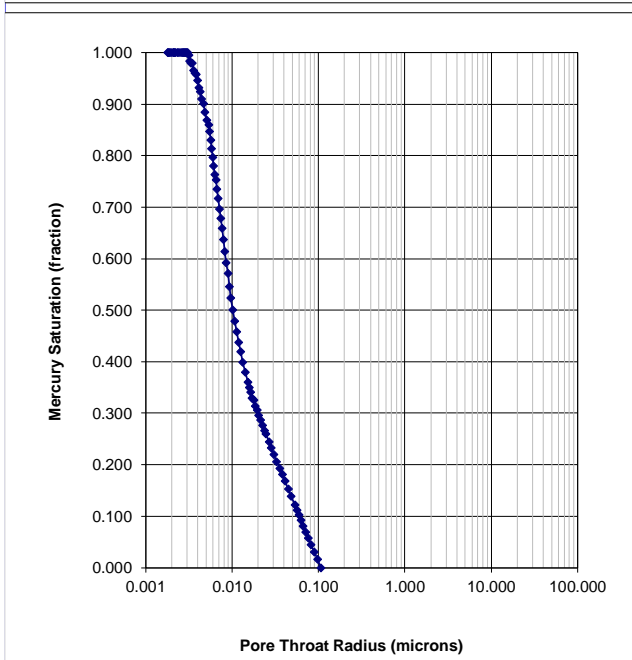
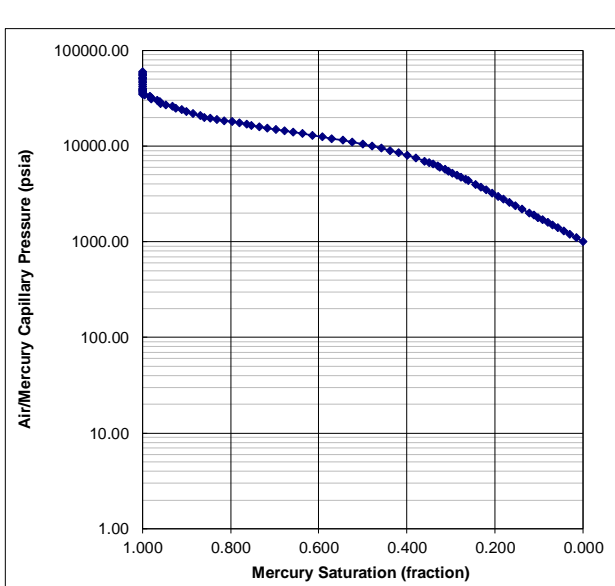
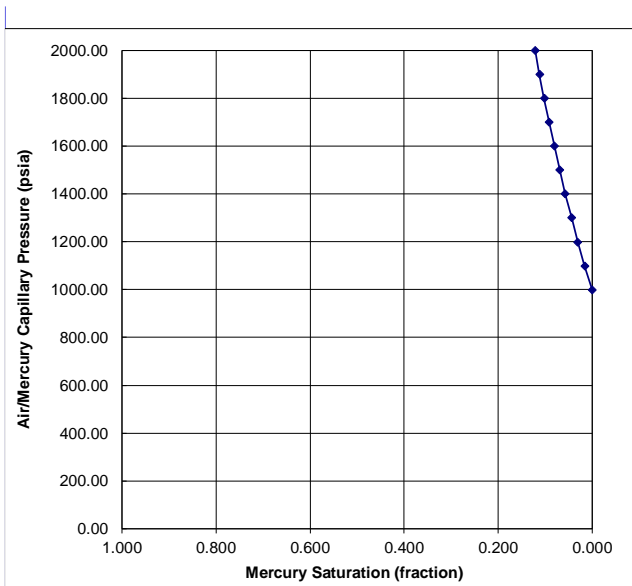
Brine Density Gradient	0.44	psig/foot
Oil Density Gradient	0.33	psig/foot

Sample Identification	12	
Sample Depth	1749.00	m
Plug Permeability (Air)	n/a	mD
Plug Porosity (He)	0.136	fraction

IFT x Cos(contact angle)		
	Lab	Res
Air/Brine	72	50
Air/Oil	24	
Oil/Brine	42	26
Air/Hg	368	

Injection Sample Porosity	0.129	fraction
Injection Sample Pore Vol	0.259	cc
Injection Sample Bulk Vol	2.008	cc
Injection Sample Weight	4.2800	g

Mean Hydraulic Radius	0.023	microns
Swanson's Parameter	0.001	
FZI	#V/ÆRDI!	



### Mercury Injection

Client Geus  
Well Nini-4  
Reference 45983

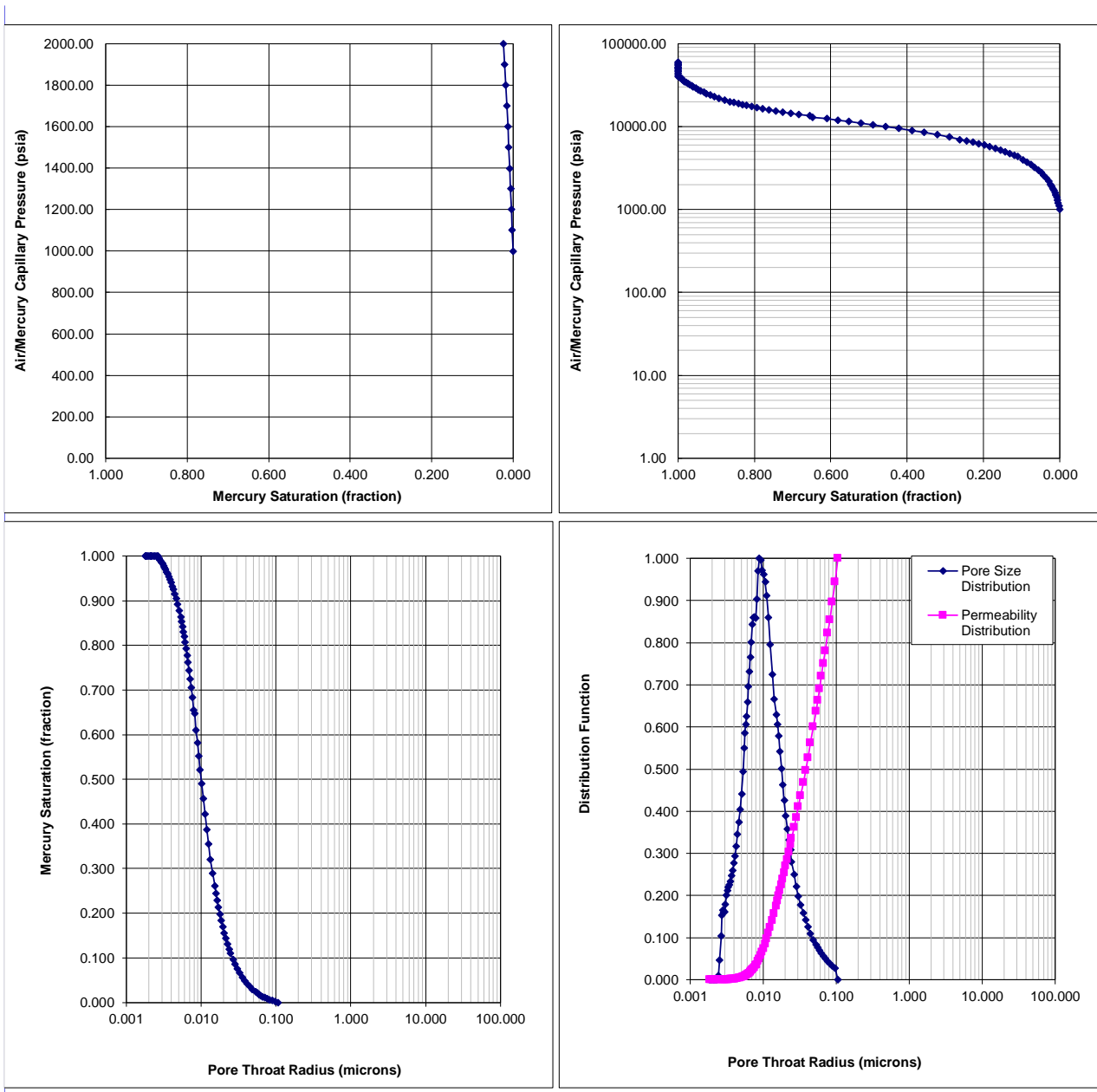
Brine Density Gradient	0.44	psig/foot
Oil Density Gradient	0.33	psig/foot

Sample Identification	13	
Sample Depth	1762.27	m
Plug Permeability (Air)	0.000	mD
Plug Porosity (He)	0.178	fraction

IFT x Cos(contact angle)		
	Lab	Res
Air/Brine	72	50
Air/Oil	24	
Oil/Brine	42	26
Air/Hg	368	

Injection Sample Porosity	0.178	fraction
Injection Sample Pore Vol	0.375	cc
Injection Sample Bulk Vol	2.114	cc
Injection Sample Weight	4.4100	g

Mean Hydraulic Radius	0.012	microns
Swanson's Parameter	0.001	
FZI	0.003	



### Mercury Injection

Client Geus  
Well Nini-4  
Reference 45985

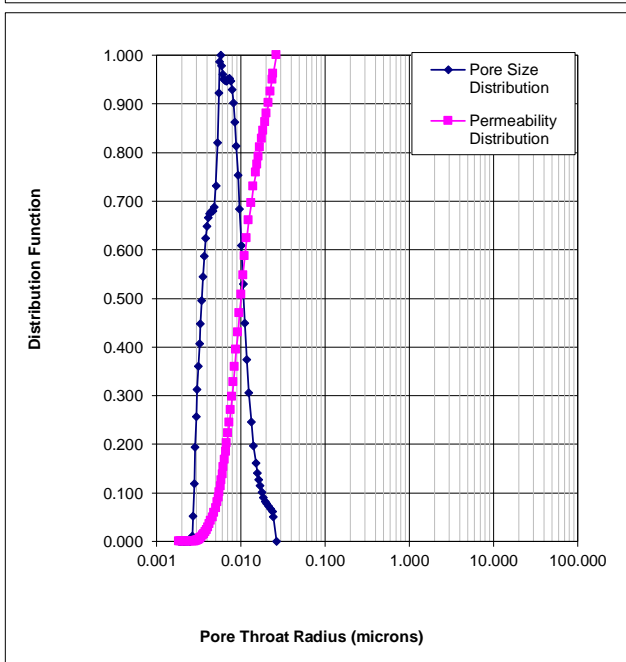
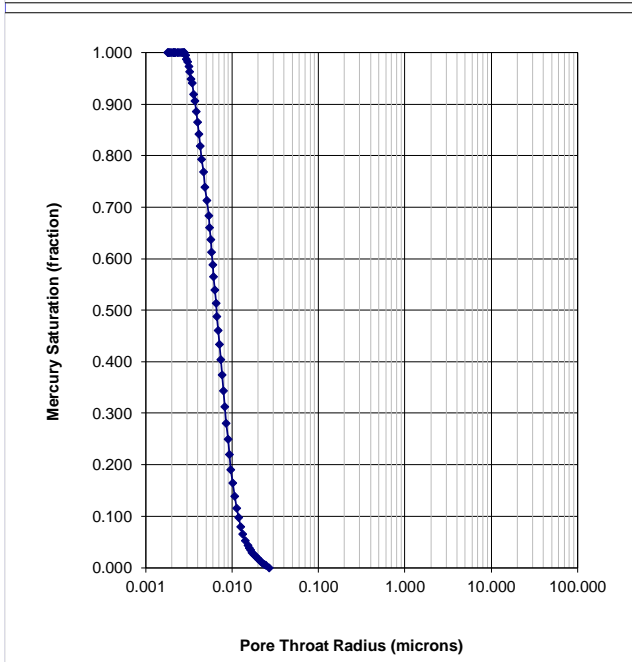
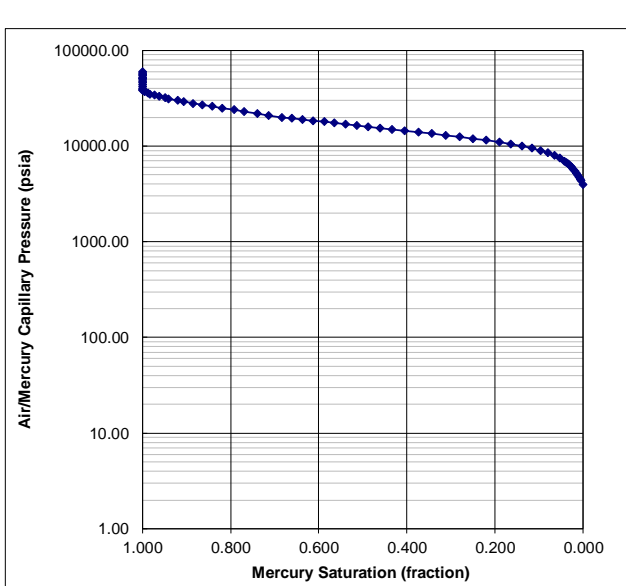
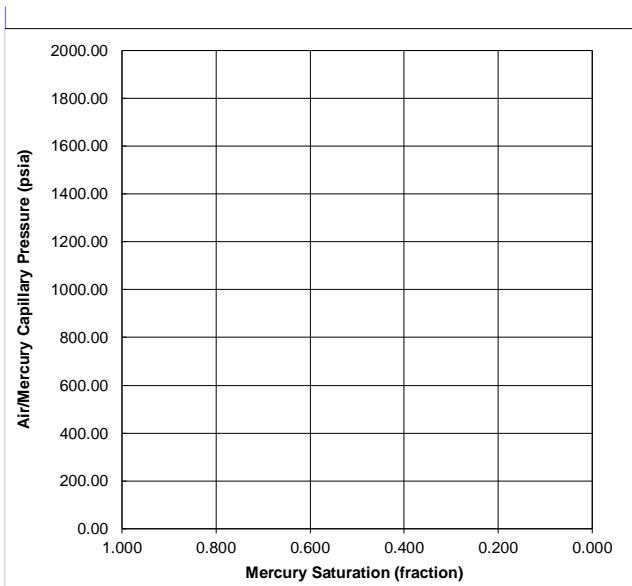
Brine Density Gradient	0.44	psig/foot
Oil Density Gradient	0.33	psig/foot

Sample Identification	14	
Sample Depth	1820.79	m
Plug Permeability (Air)	n/a	mD
Plug Porosity (He)	0.163	fraction

IFT x Cos(contact angle)		
	Lab	Res
Air/Brine	72	50
Air/Oil	24	
Oil/Brine	42	26
Air/Hg	368	

Injection Sample Porosity	0.163	fraction
Injection Sample Pore Vol	0.257	cc
Injection Sample Bulk Vol	1.575	cc
Injection Sample Weight	3.4000	g

Mean Hydraulic Radius	0.005	microns
Swanson's Parameter	0.001	
FZI	#V/ÆRDI!	



### Mercury Injection

Client Geus  
Well Nini-4  
Reference 45982

Brine Density Gradient	0.44	psig/foot
Oil Density Gradient	0.33	psig/foot

IFT x Cos(contact angle)		
	Lab	Res
Air/Brine	72	50
Air/Oil	24	
Oil/Brine	42	26
Air/Hg	368	

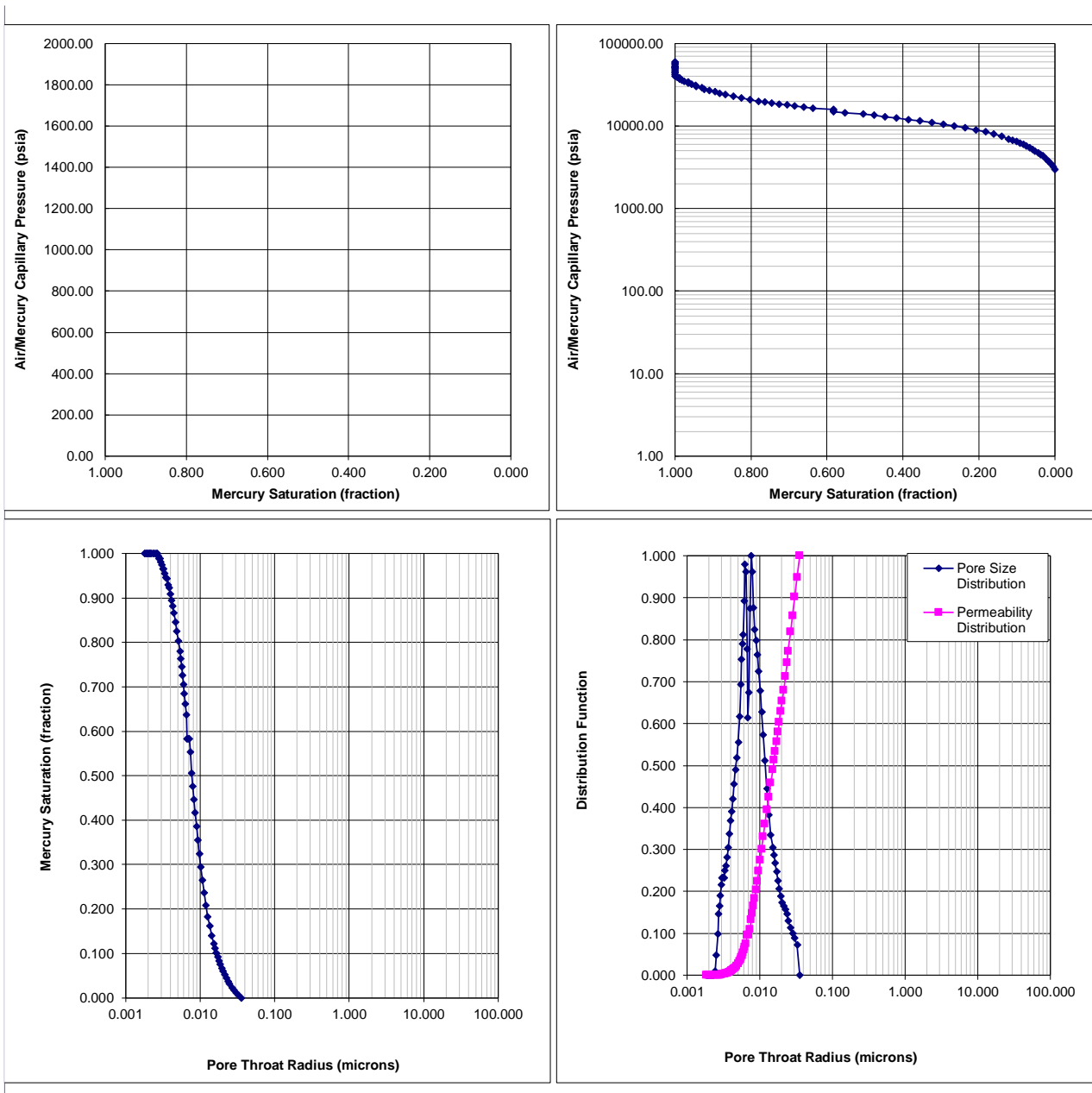
  

Mean Hydraulic Radius	0.006	microns
Swanson's Parameter	0.001	
FZI	0.004	

Sample Identification	15	
Sample Depth	1748.65	m
Plug Permeability (Air)	0.000	mD
Plug Porosity (He)	0.164	fraction

Injection Sample Porosity	0.164	fraction
Injection Sample Pore Vol	0.301	cc
Injection Sample Bulk Vol	1.838	cc
Injection Sample Weight	3.8600	g



### Mercury Injection

Client Geus  
Well Nini-4a  
Reference 45987

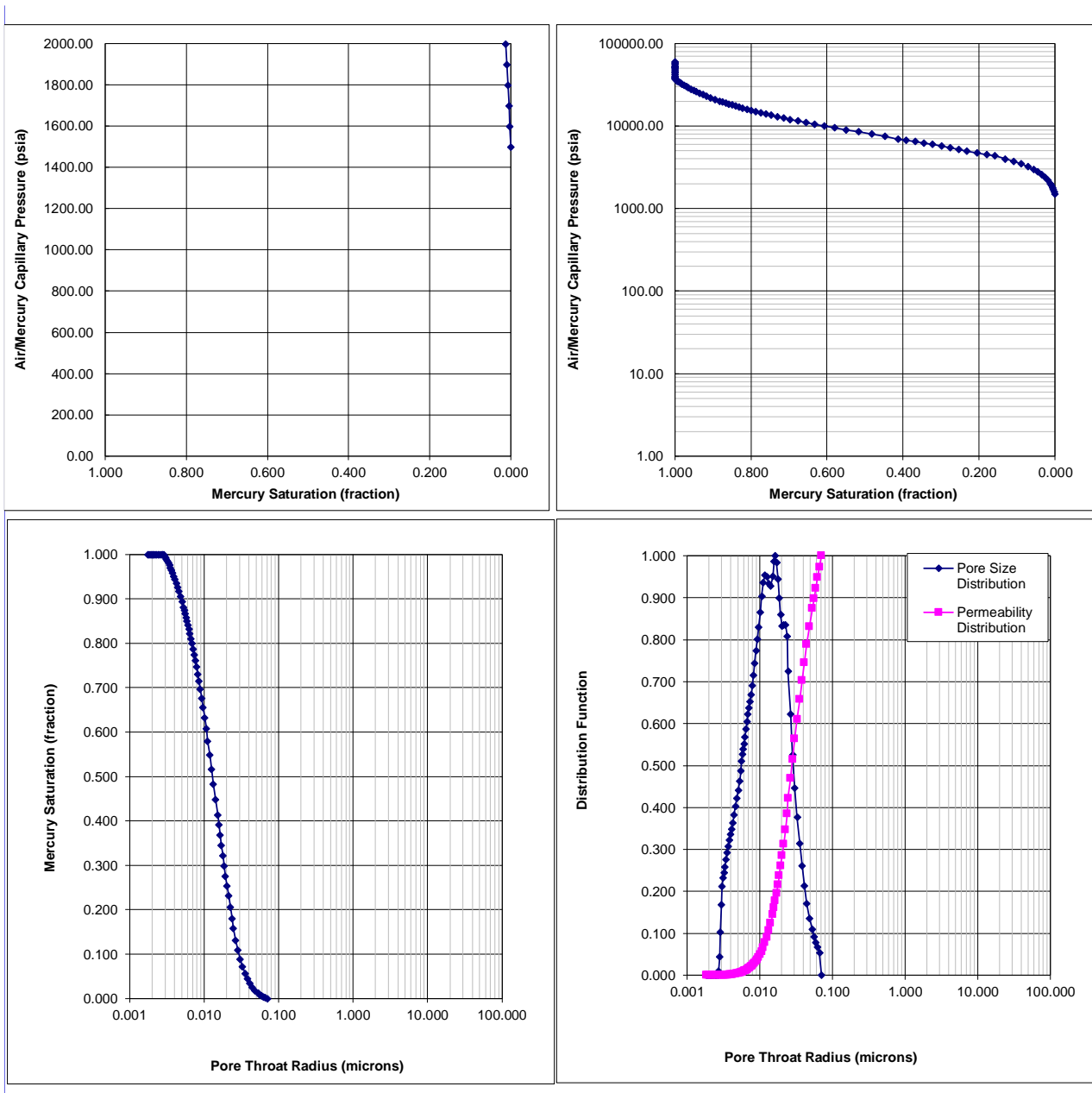
Brine Density Gradient	0.44	psig/foot
Oil Density Gradient	0.33	psig/foot

Sample Identification	16	
Sample Depth	1910.37	m
Plug Permeability (Air)	n/a	mD
Plug Porosity (He)	0.156	fraction

IFT x Cos(contact angle)		
	Lab	Res
Air/Brine	72	50
Air/Oil	24	
Oil/Brine	42	26
Air/Hg	368	

Injection Sample Porosity	0.156	fraction
Injection Sample Pore Vol	0.395	cc
Injection Sample Bulk Vol	2.539	cc
Injection Sample Weight	5.2300	g

Mean Hydraulic Radius	0.011	microns
Swanson's Parameter	0.001	
FZI	#VÆRDI!	



### Mercury Injection

Client Geus  
Well Nini-4a  
Reference 45988

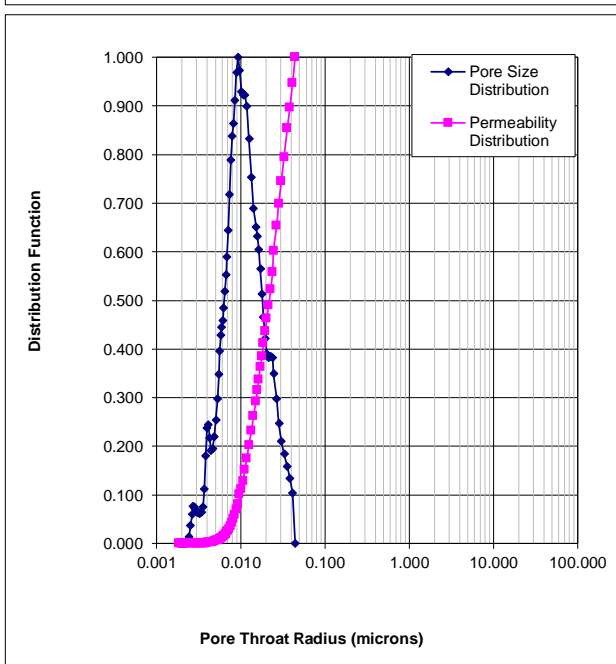
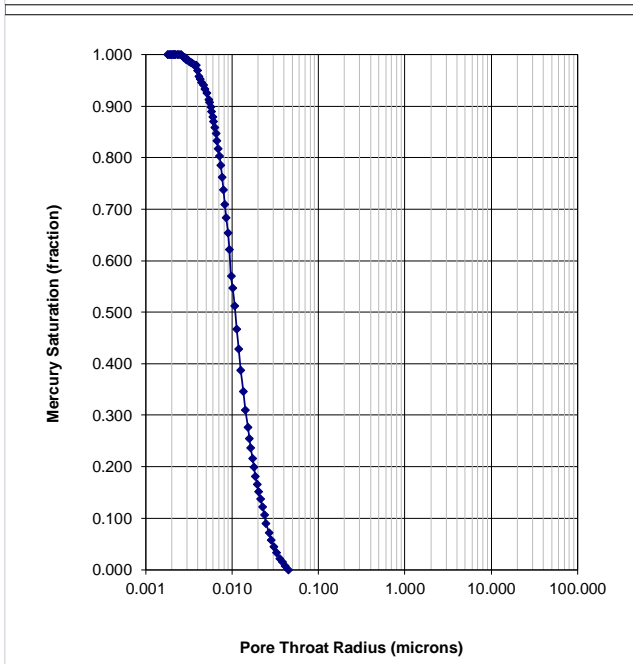
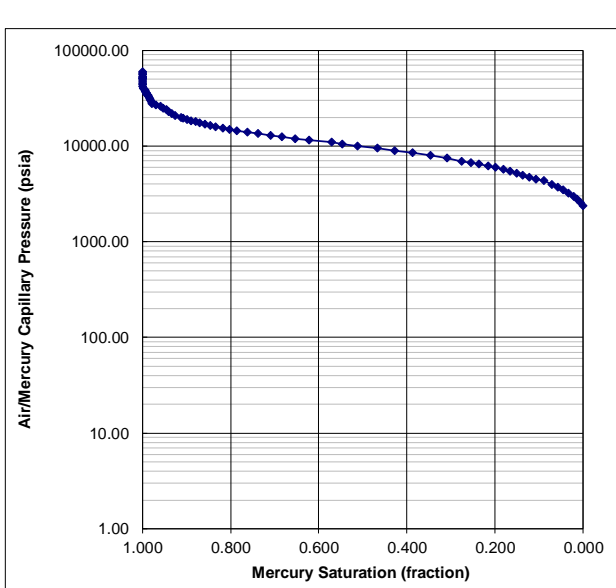
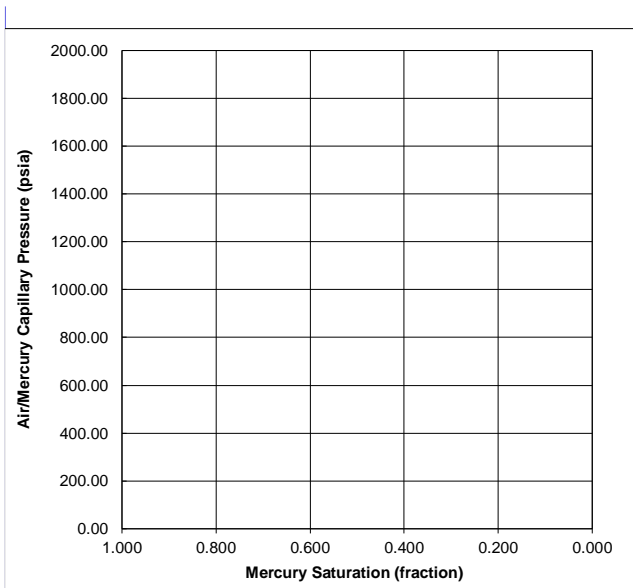
Brine Density Gradient	0.44	psig/foot
Oil Density Gradient	0.33	psig/foot

Sample Identification	17	
Sample Depth	1915.46	m
Plug Permeability (Air)	n/a	mD
Plug Porosity (He)	0.155	fraction

IFT x Cos(contact angle)		
	Lab	Res
Air/Brine	72	50
Air/Oil	24	
Oil/Brine	42	26
Air/Hg	368	

Injection Sample Porosity	0.153	fraction
Injection Sample Pore Vol	0.264	cc
Injection Sample Bulk Vol	1.723	cc
Injection Sample Weight	3.6400	g

Mean Hydraulic Radius	0.009	microns
Swanson's Parameter	0.001	
FZI	#V/ÆRDI!	



### Mercury Injection

Client Geus  
Well Nini-4  
Reference 45984

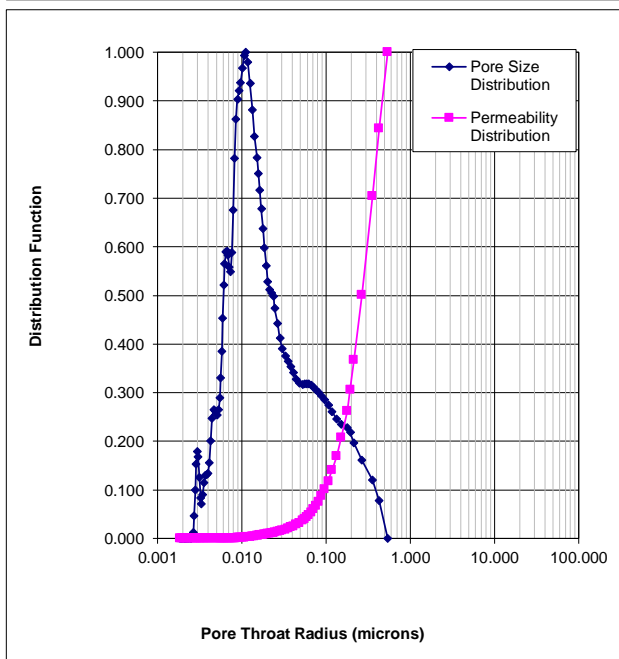
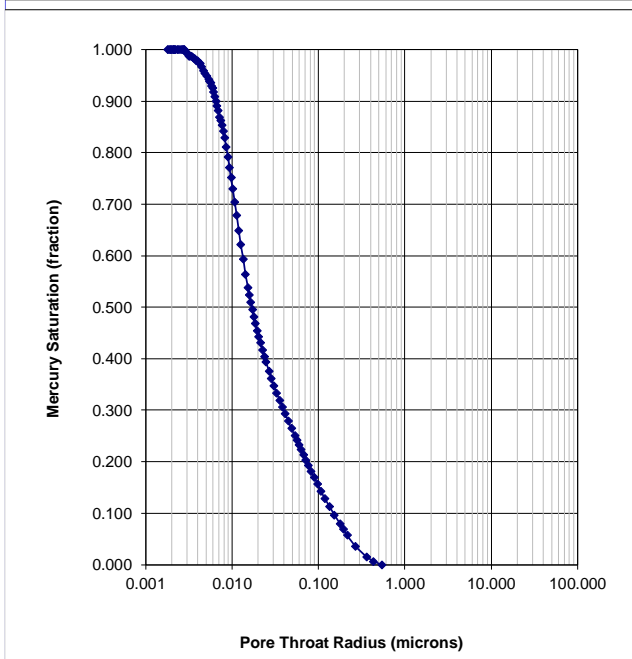
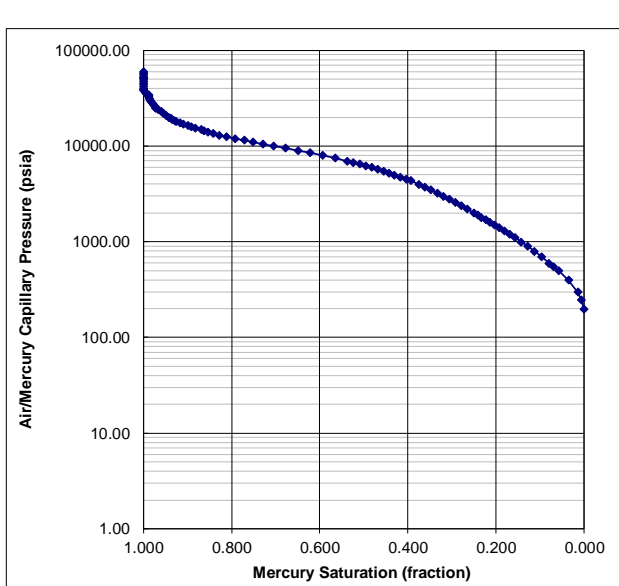
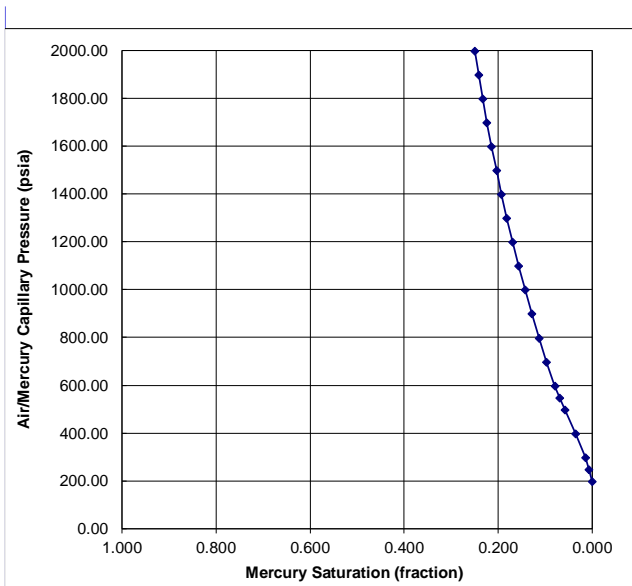
Brine Density Gradient	0.44	psig/foot
Oil Density Gradient	0.33	psig/foot

Sample Identification	18	
Sample Depth	1800.76	m
Plug Permeability (Air)	n/a	mD
Plug Porosity (He)	0.178	fraction

IFT x Cos(contact angle)		
	Lab	Res
Air/Brine	72	50
Air/Oil	24	
Oil/Brine	42	26
Air/Hg	368	

Injection Sample Porosity	0.173	fraction
Injection Sample Pore Vol	0.467	cc
Injection Sample Bulk Vol	2.695	cc
Injection Sample Weight	5.6800	g

Mean Hydraulic Radius	0.078	microns
Swanson's Parameter	0.002	
FZI #VÆRDI!		



### Mercury Injection

Client Geus  
Well Nini-4  
Reference 45986

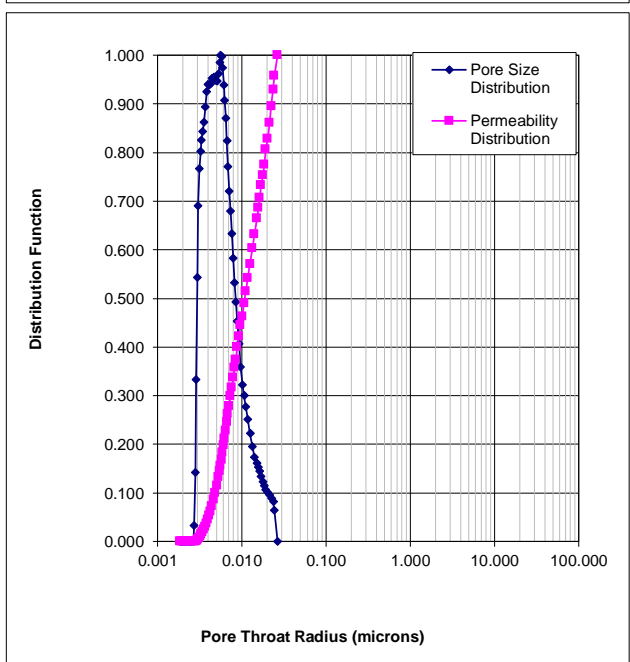
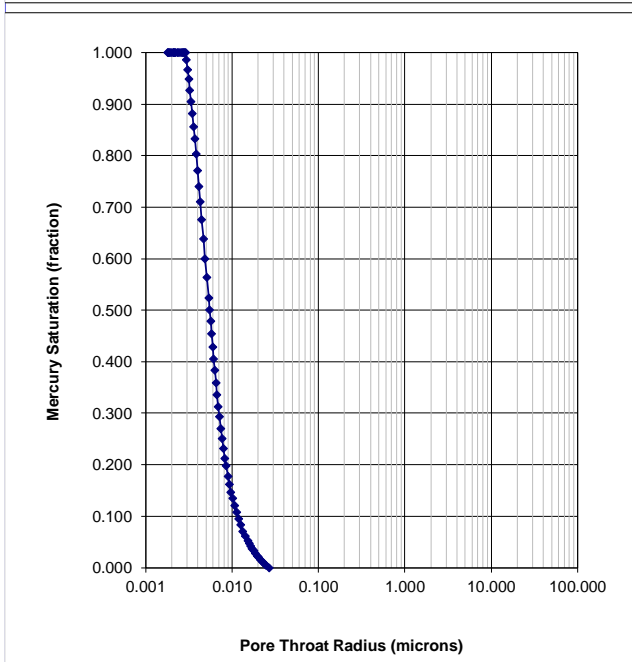
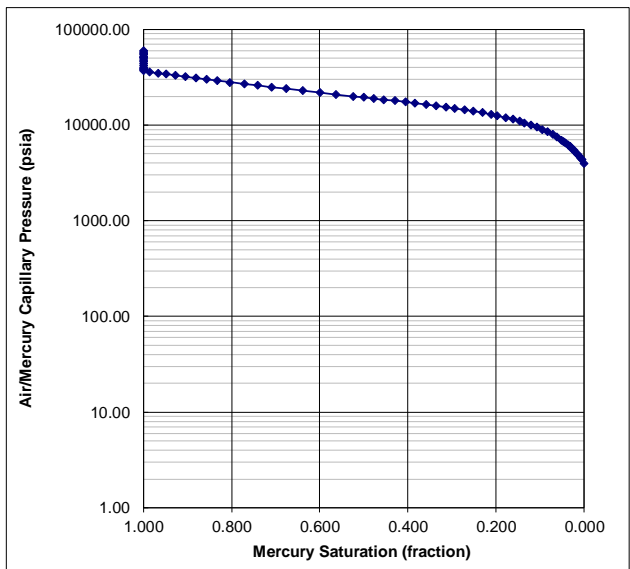
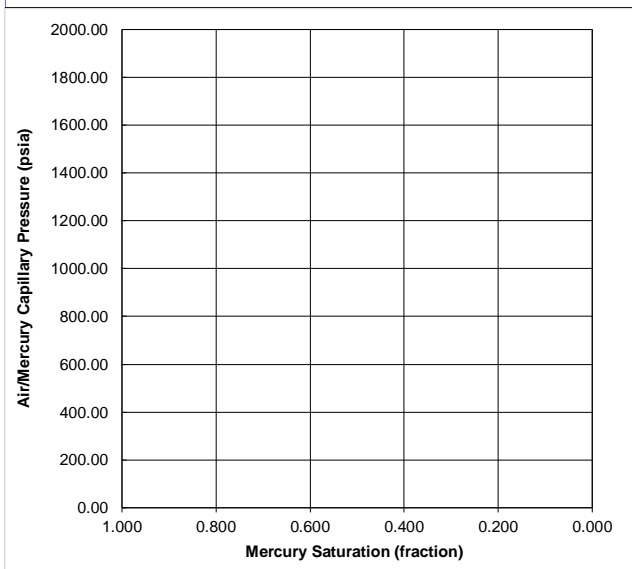
Brine Density Gradient	0.44	psig/foot
Oil Density Gradient	0.33	psig/foot

Sample Identification	19	
Sample Depth	1902.72	m
Plug Permeability (Air)	n/a	mD
Plug Porosity (He)	0.123	fraction

IFT x Cos(contact angle)		
	Lab	Res
Air/Brine	72	50
Air/Oil	24	
Oil/Brine	42	26
Air/Hg	368	

Injection Sample Porosity	0.119	fraction
Injection Sample Pore Vol	0.184	cc
Injection Sample Bulk Vol	1.544	cc
Injection Sample Weight	3.2600	g

Mean Hydraulic Radius	0.004	microns
Swanson's Parameter	0.000	
FZI $\nabla$ #V $\nabla$ ERDI!		



### Mercury Injection

Client Geus  
Well Nini-4a  
Reference 45989

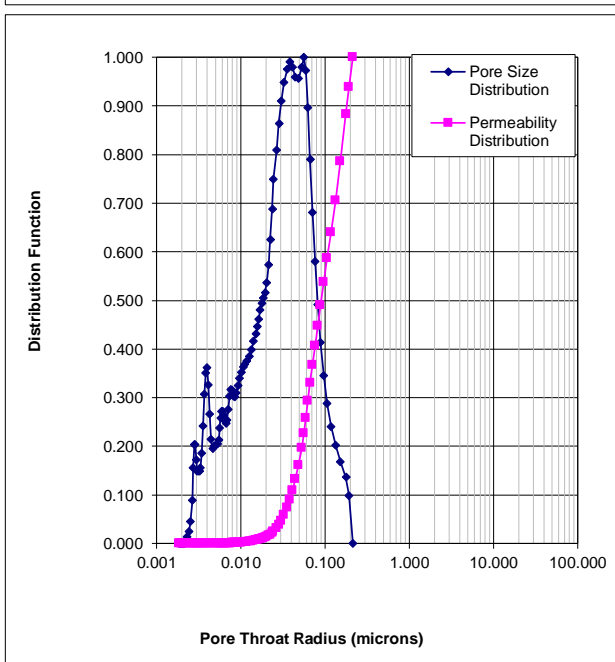
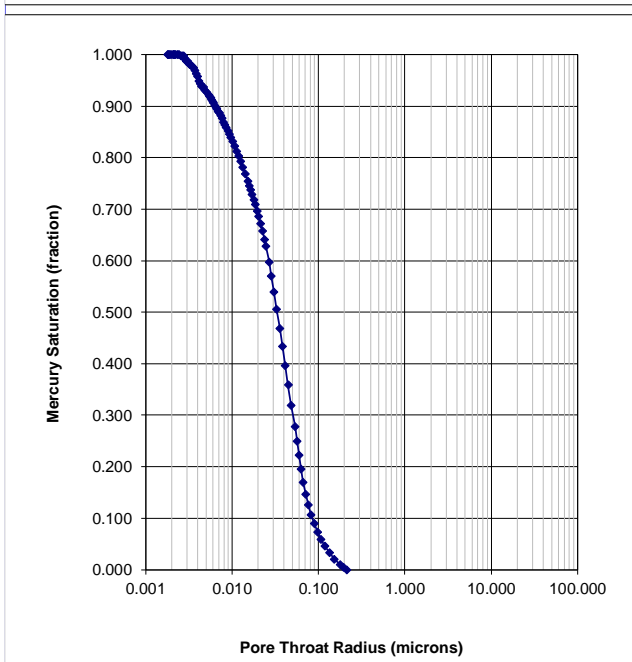
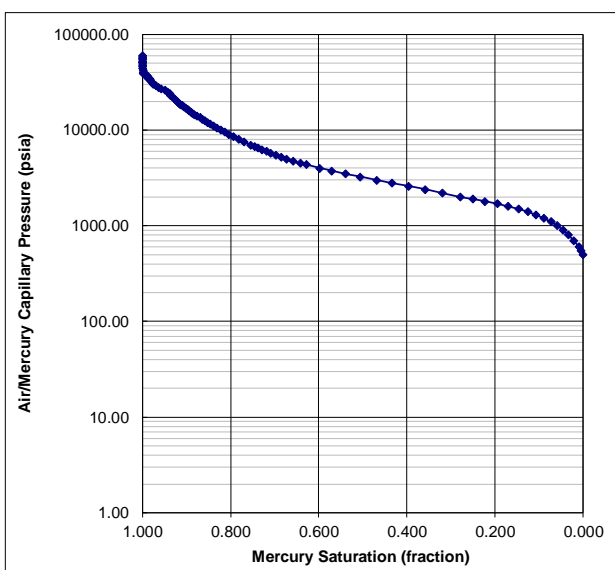
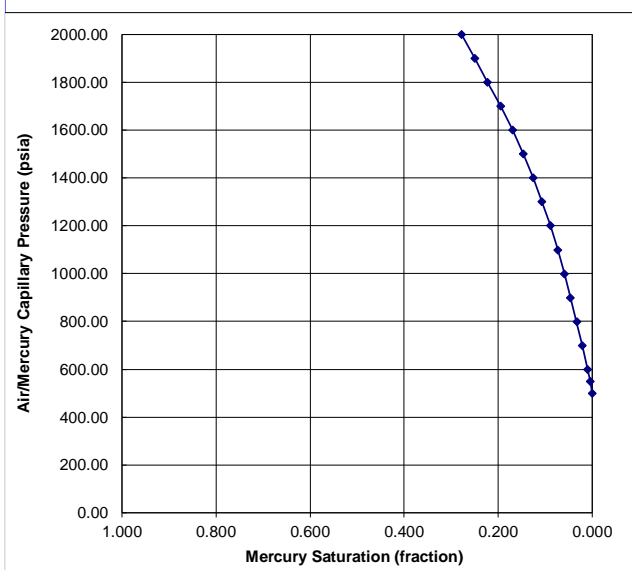
Brine Density Gradient	0.44	psig/foot
Oil Density Gradient	0.33	psig/foot

Sample Identification	20	
Sample Depth	1955.56	m
Plug Permeability (Air)	0.000	mD
Plug Porosity (He)	0.166	fraction

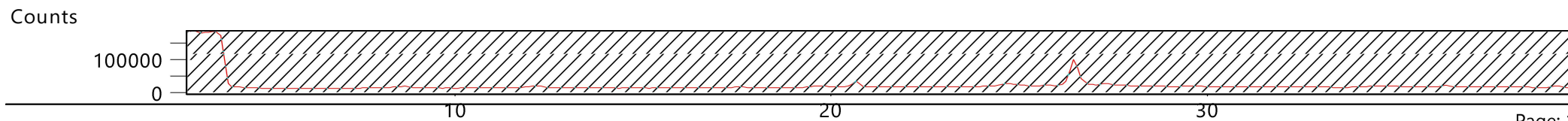
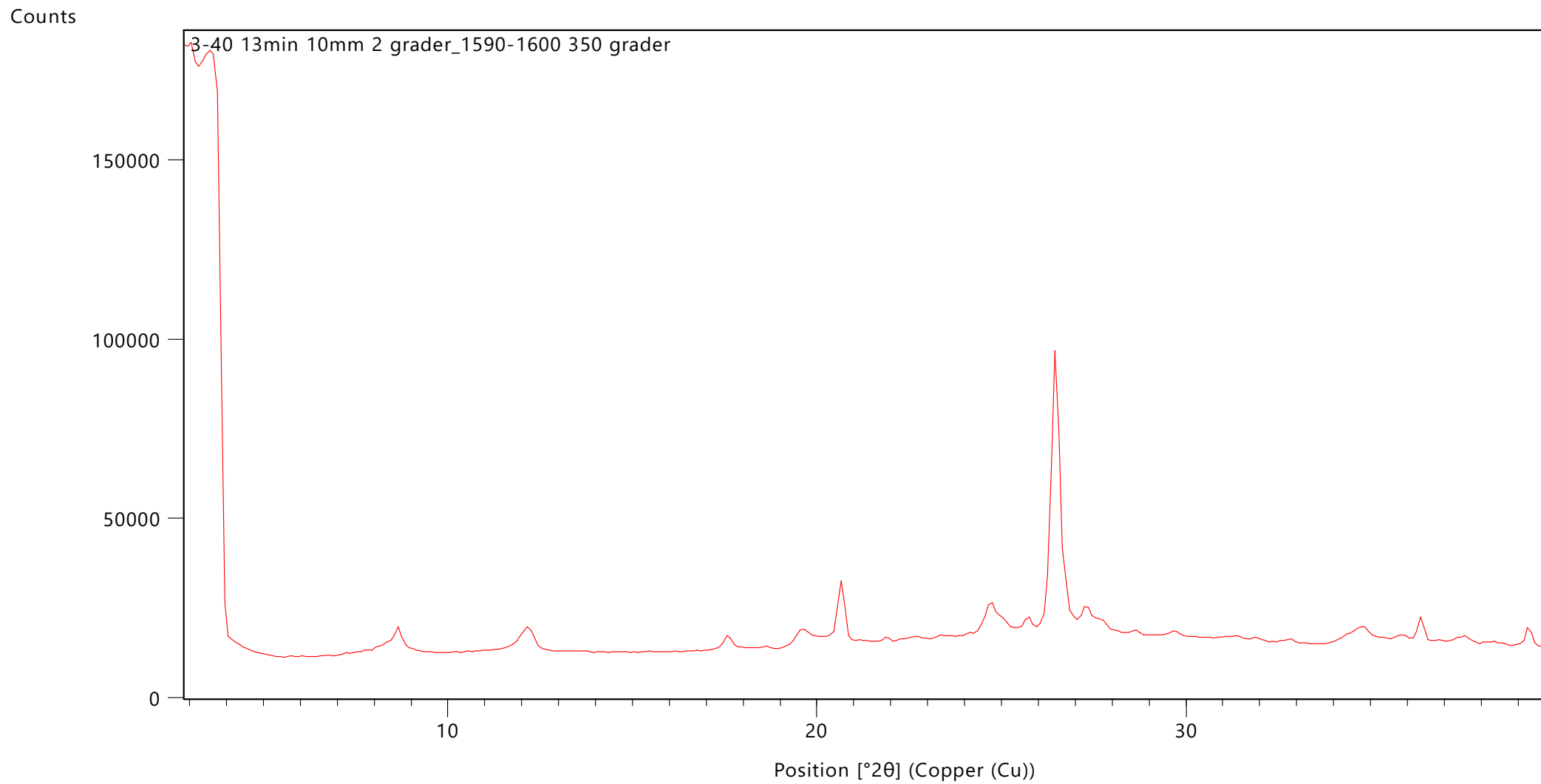
IFT x Cos(contact angle)		
	Lab	Res
Air/Brine	72	50
Air/Oil	24	
Oil/Brine	42	26
Air/Hg	368	

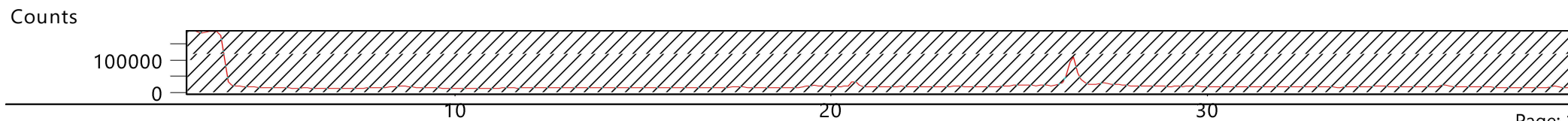
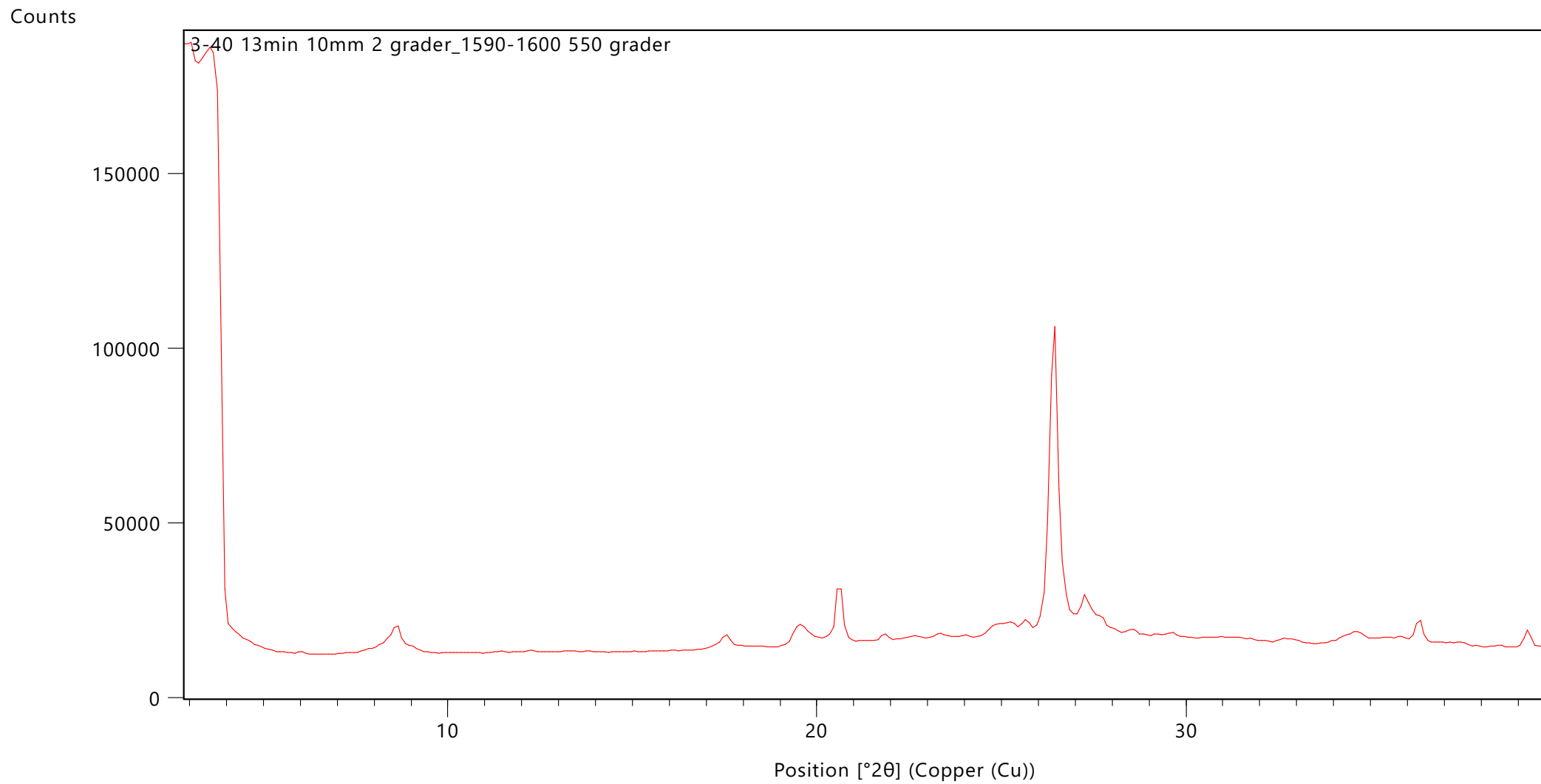
Injection Sample Porosity	0.116	fraction
Injection Sample Pore Vol	0.181	cc
Injection Sample Bulk Vol	1.569	cc
Injection Sample Weight	3.3200	g

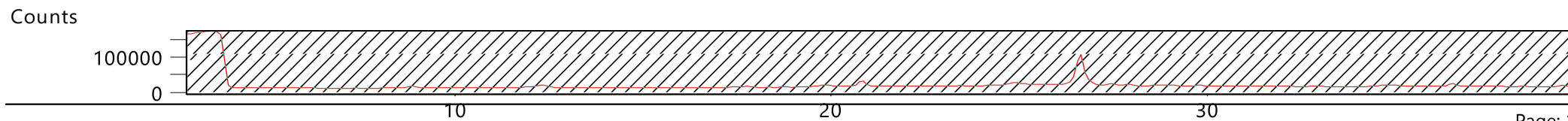
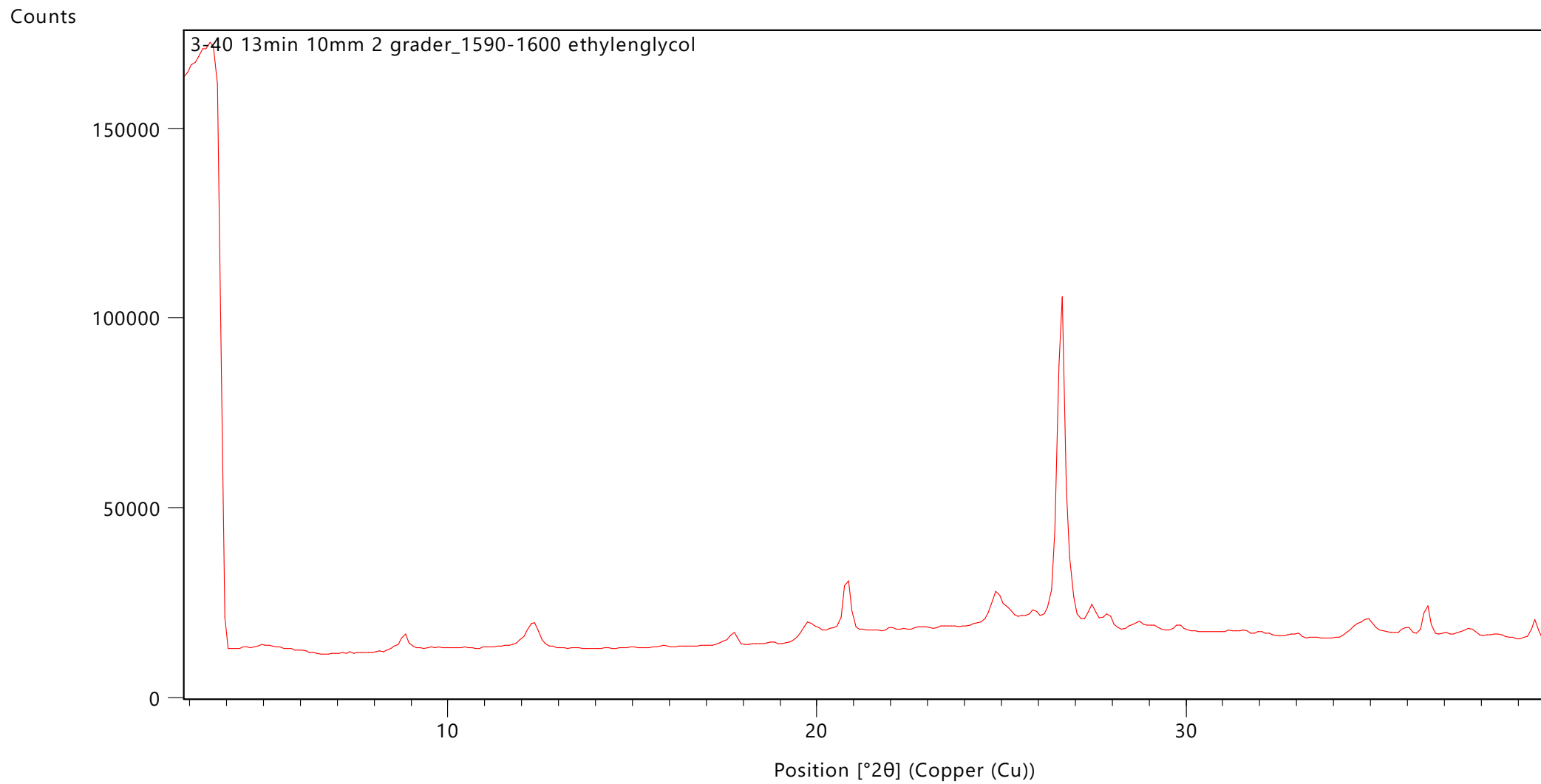
Mean Hydraulic Radius	0.034	microns
Swanson's Parameter	0.002	
FZI	0.007	

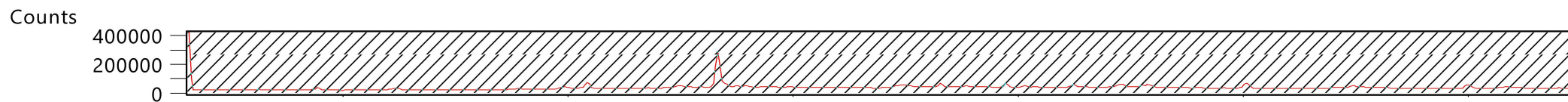
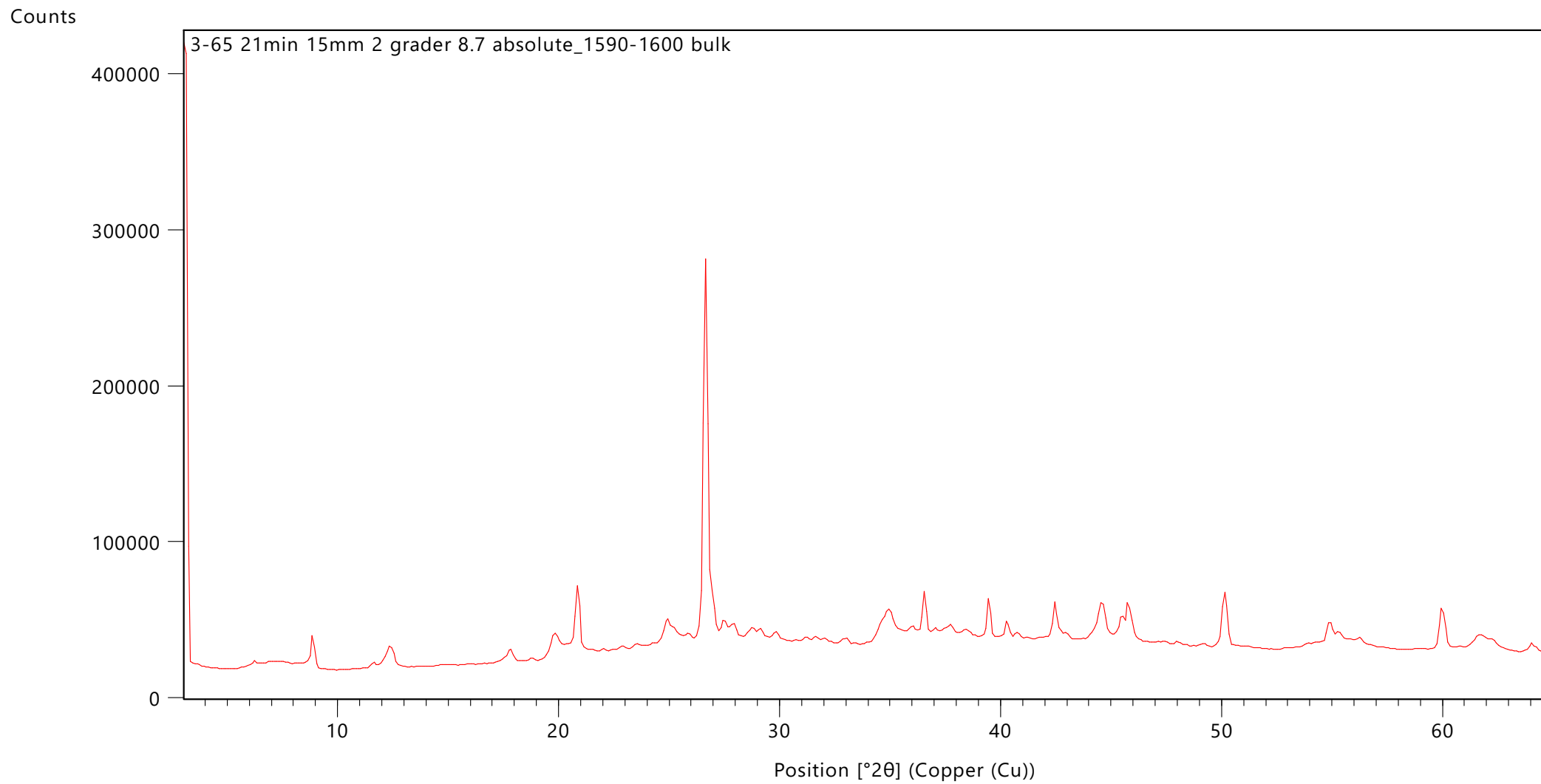


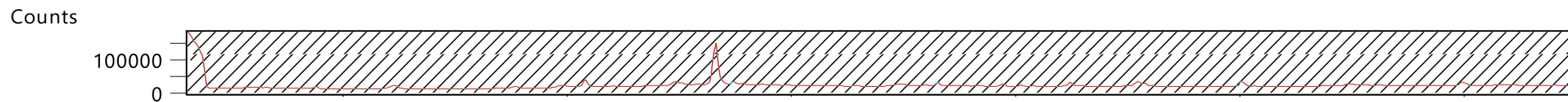
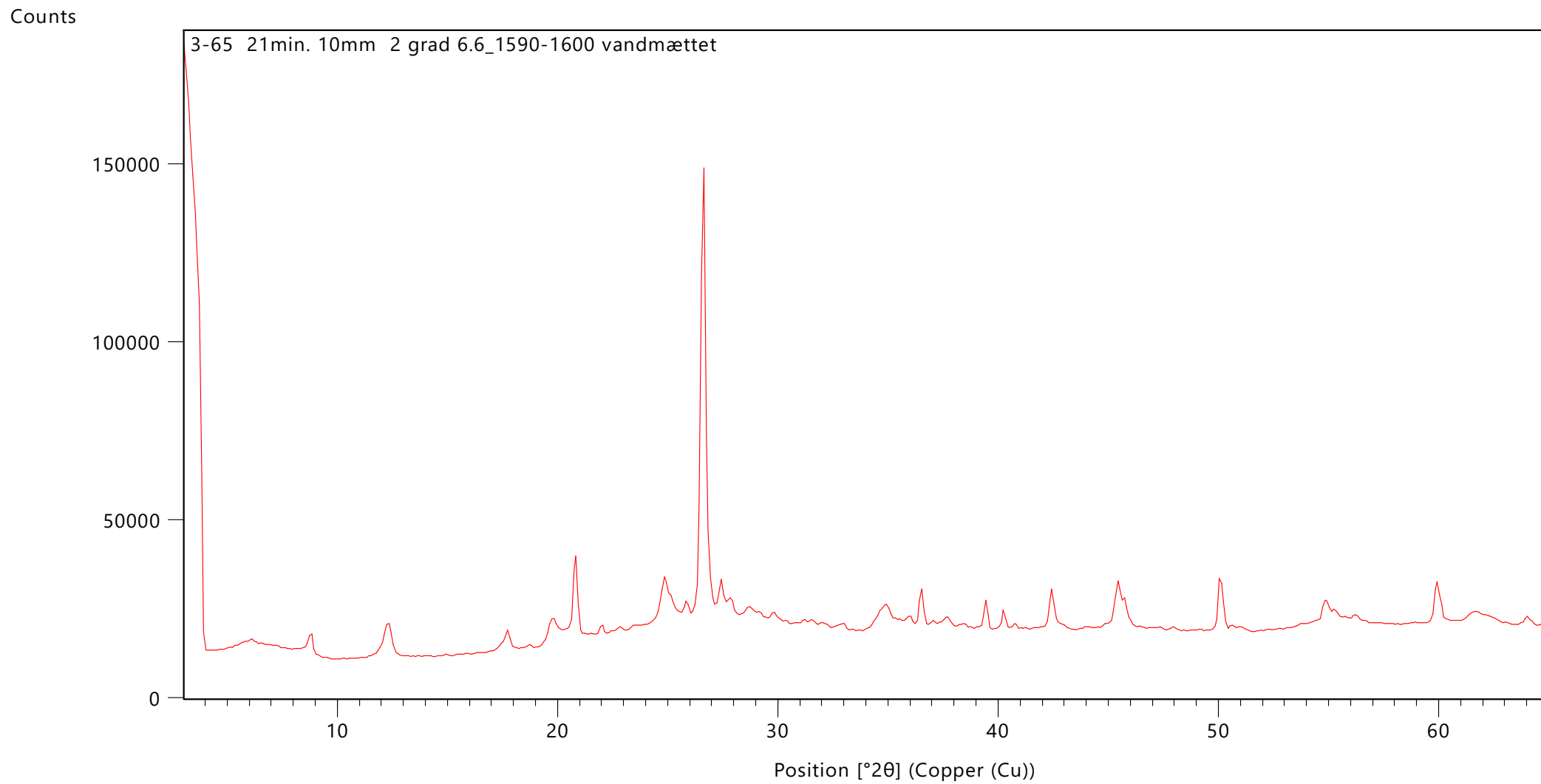
## APPENDIX C – XRD ANALYSIS

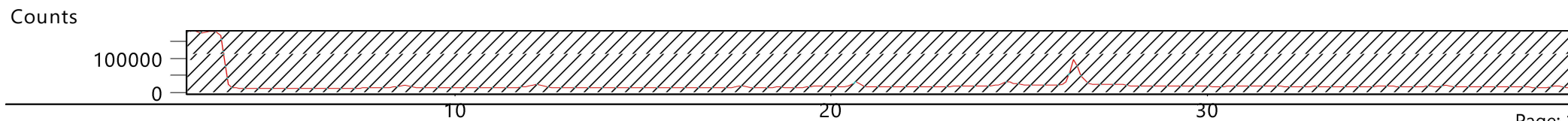
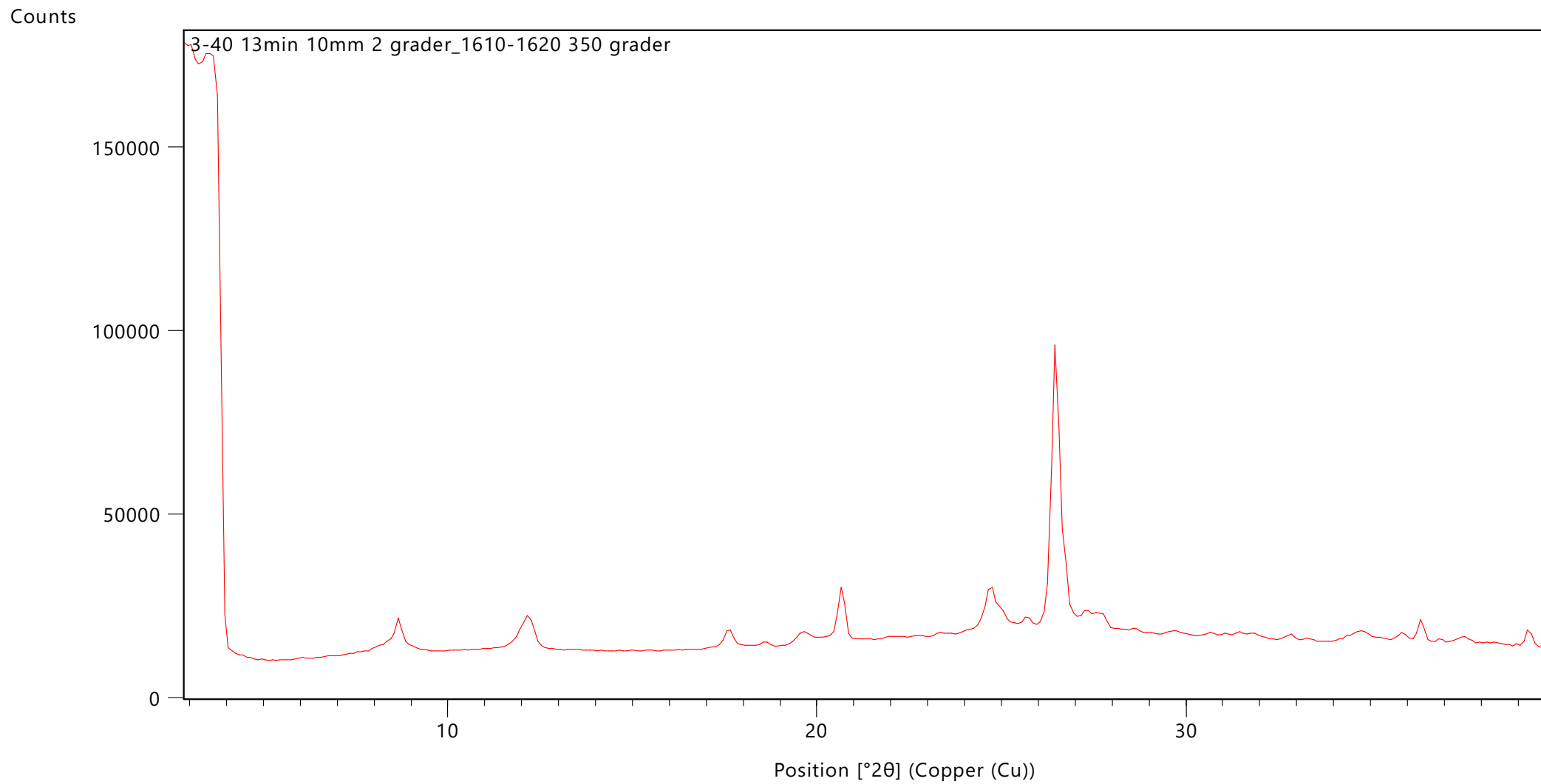


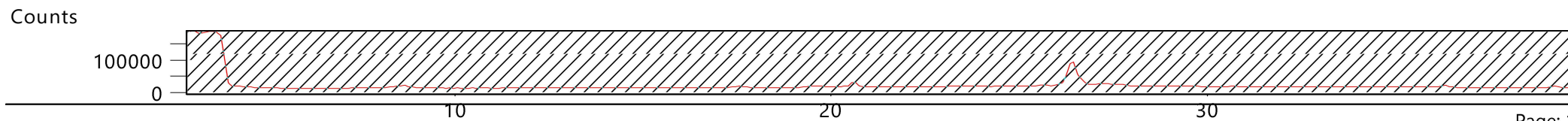
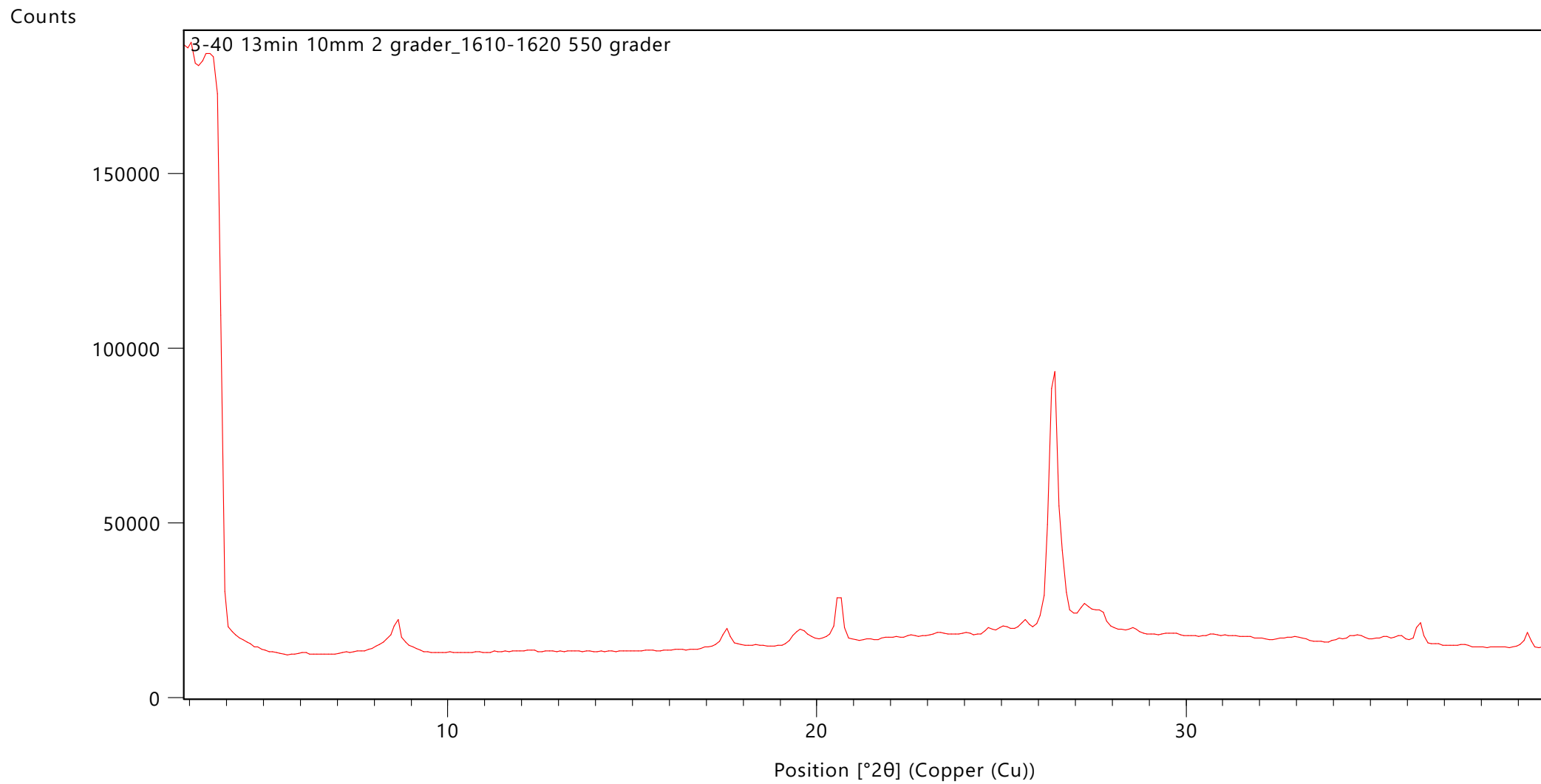


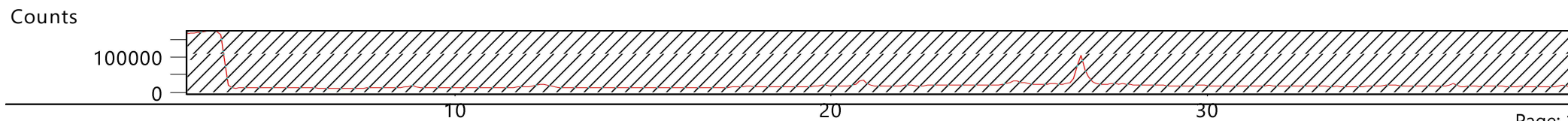
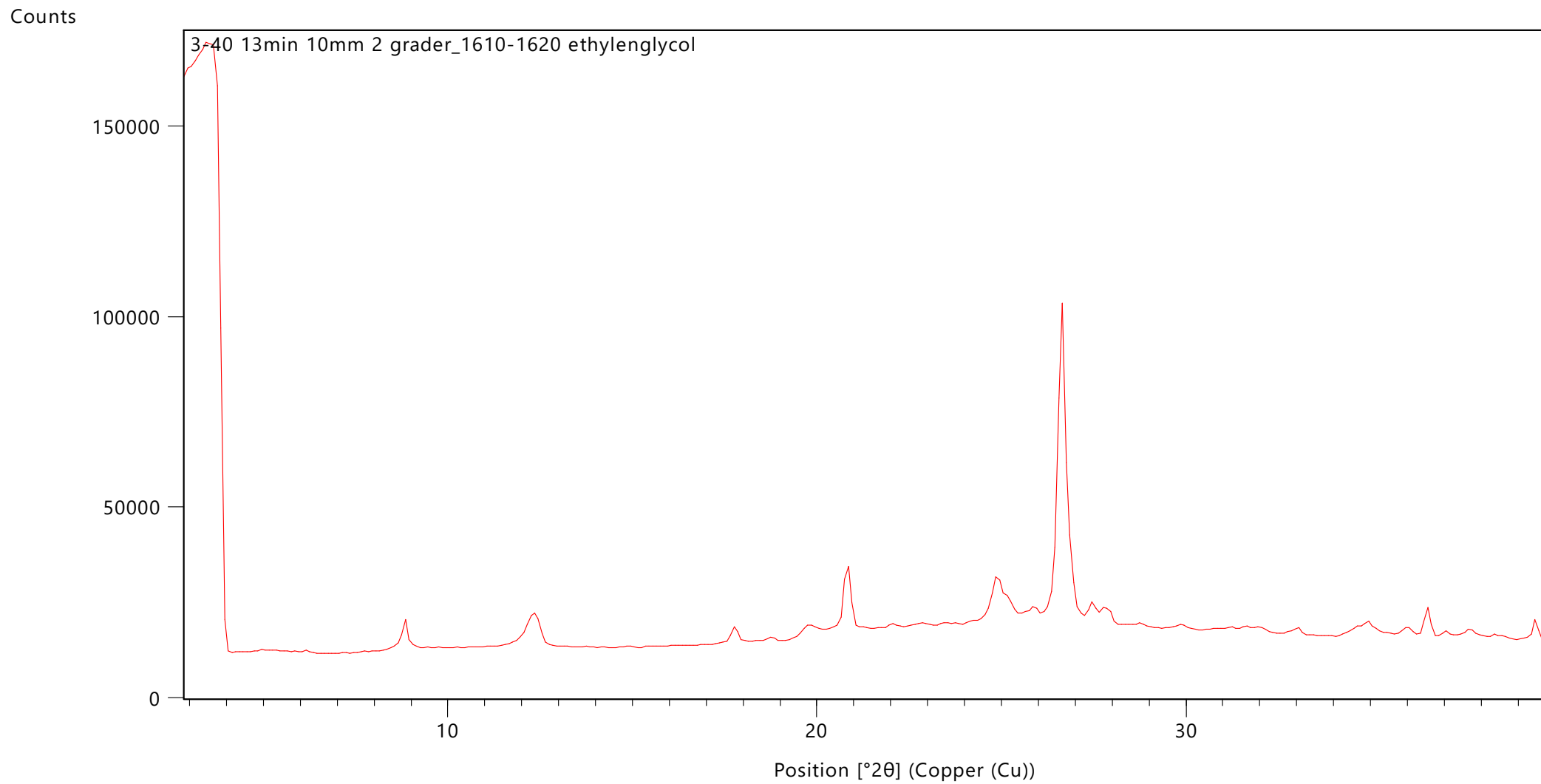


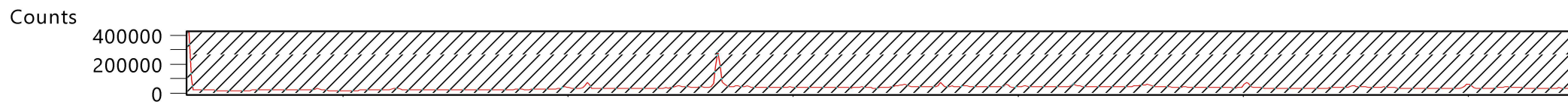
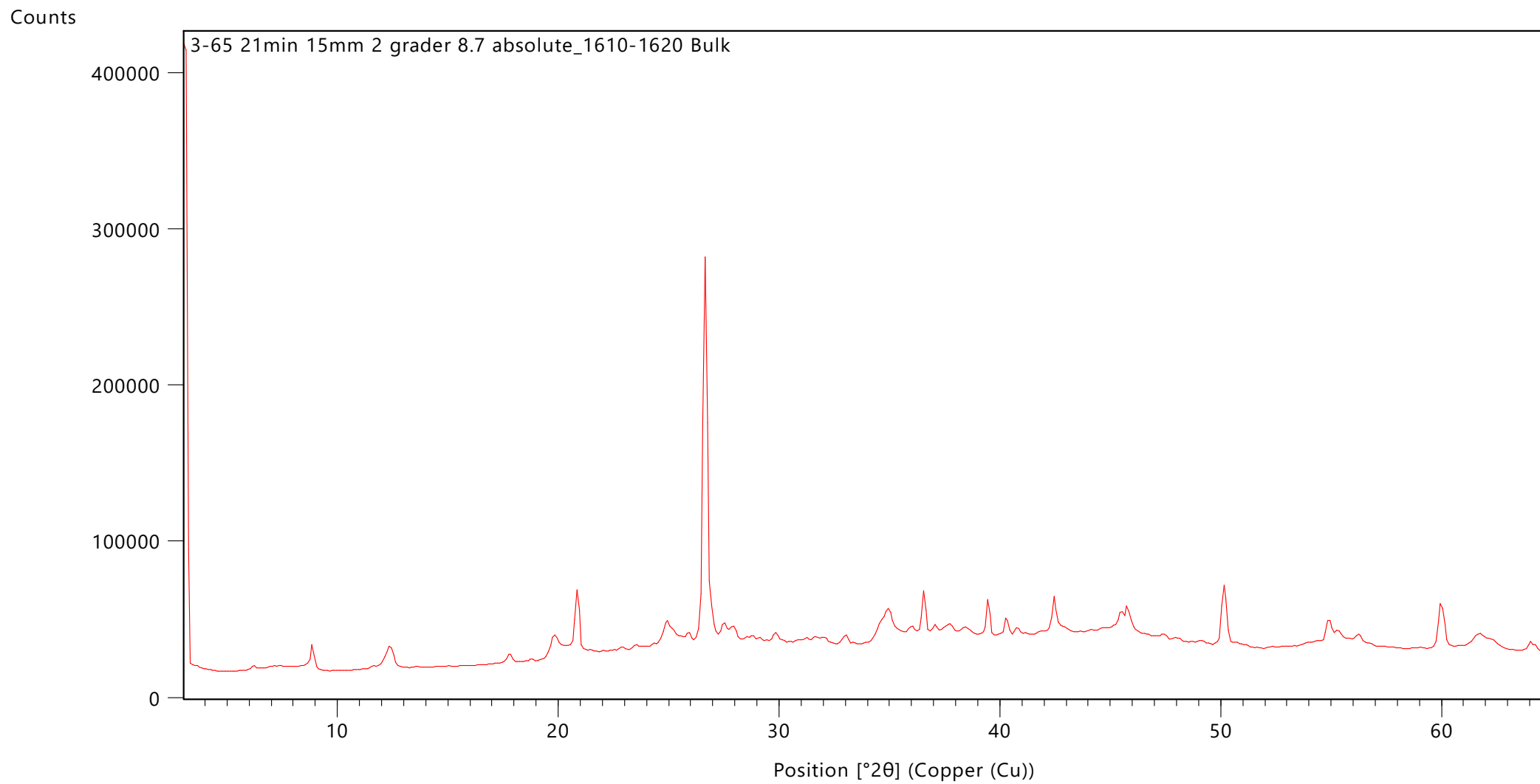


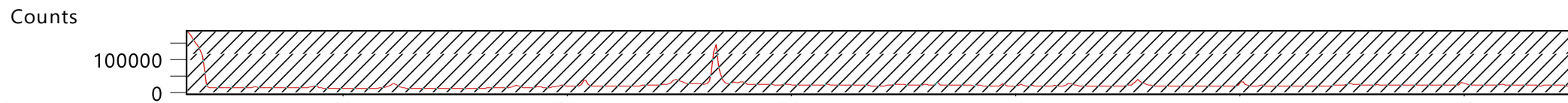
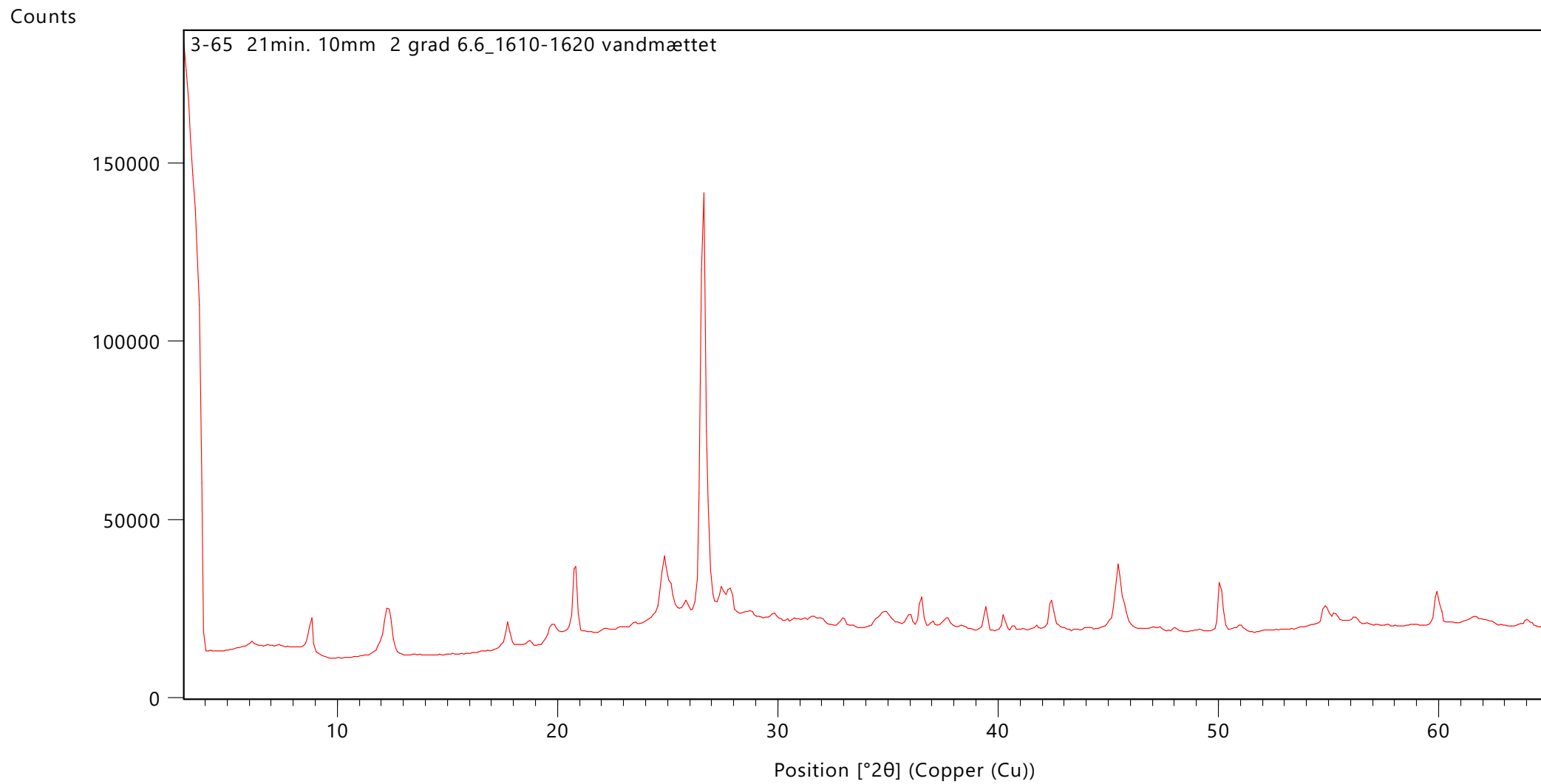


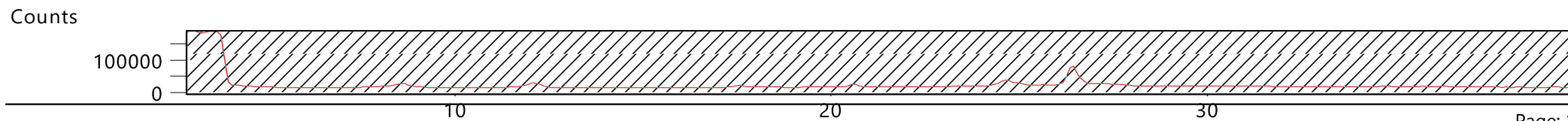
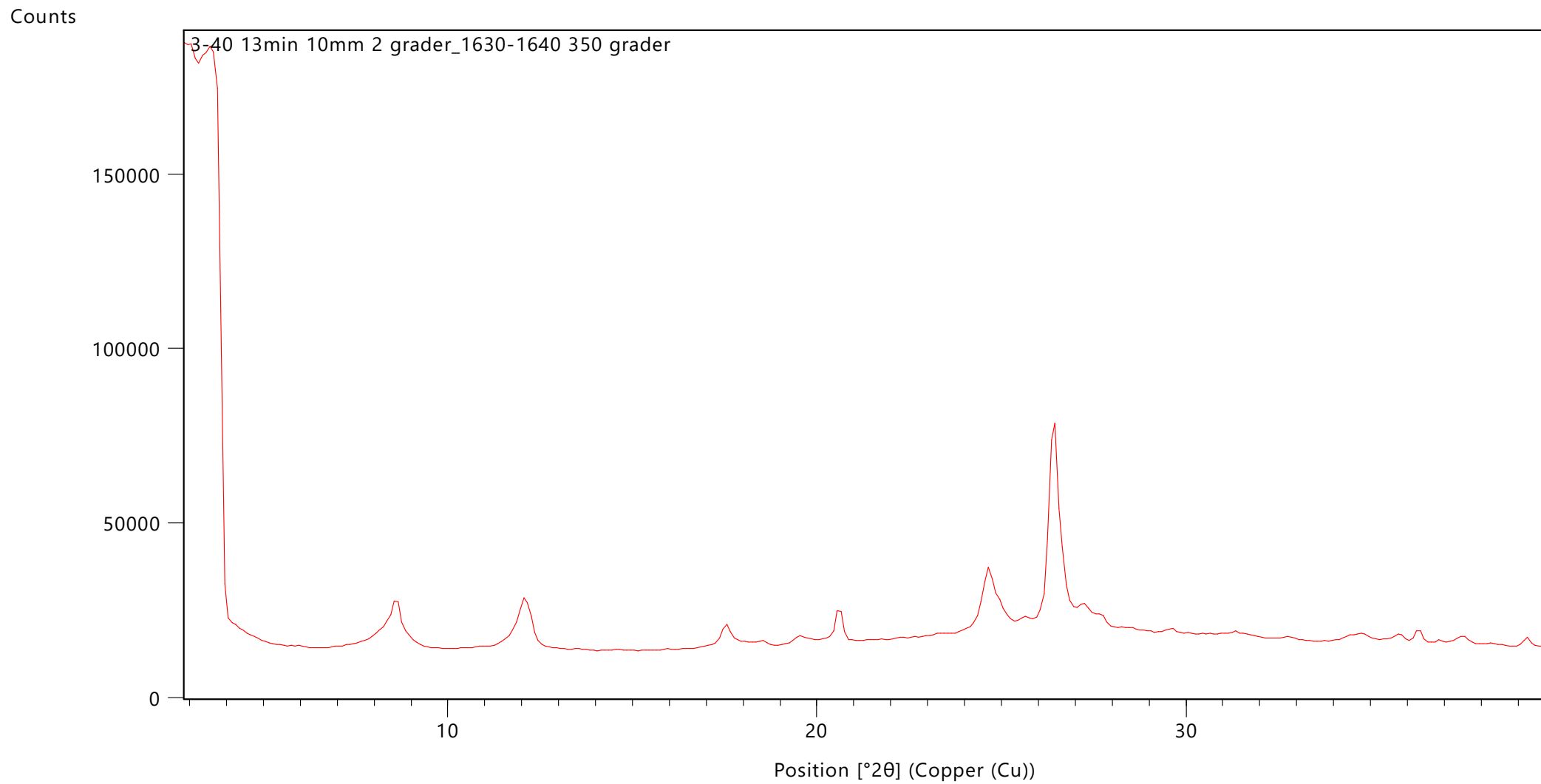


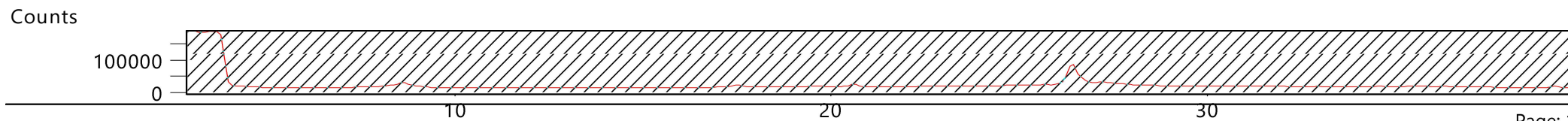
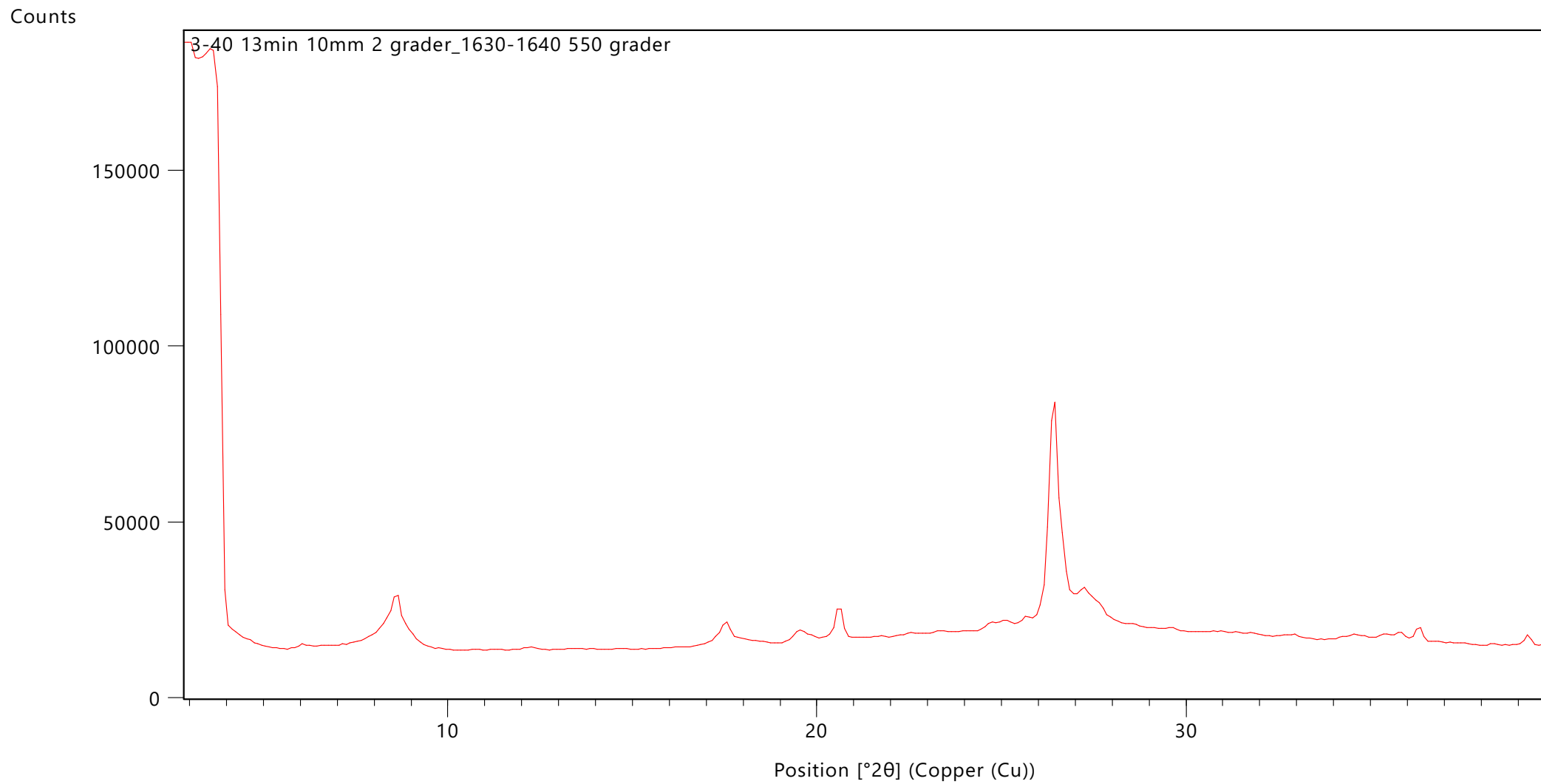


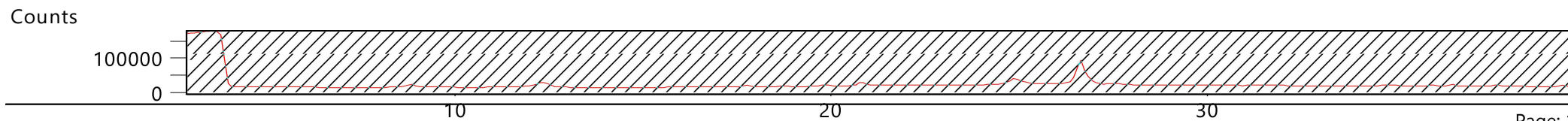
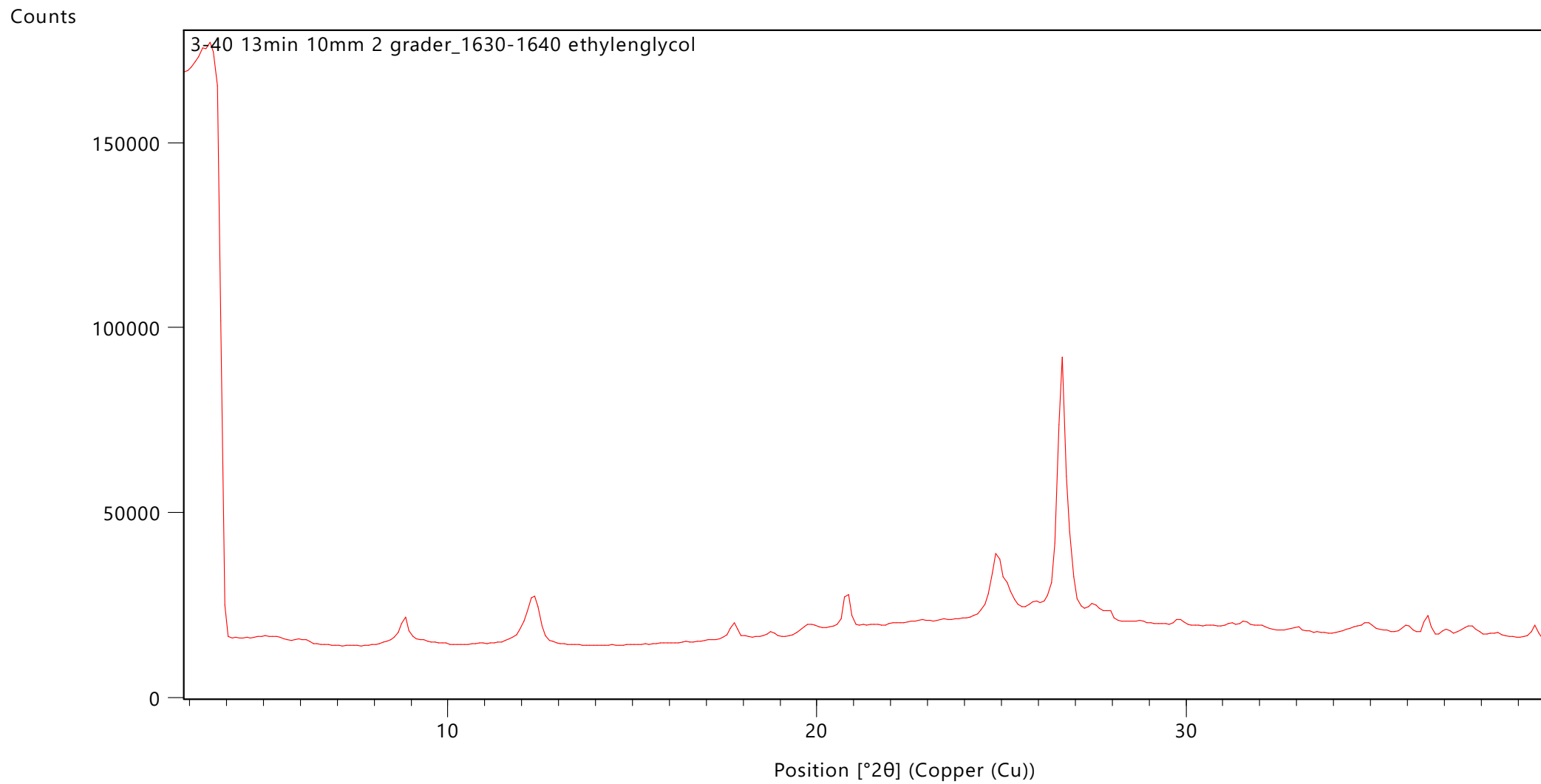


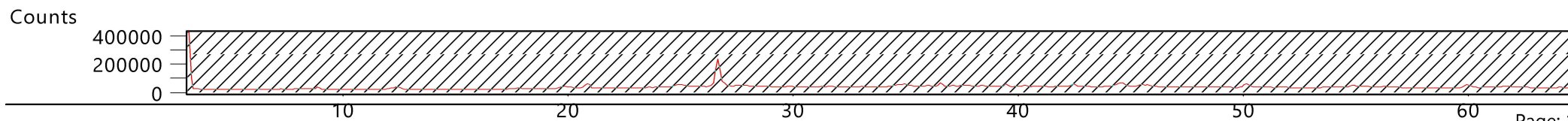
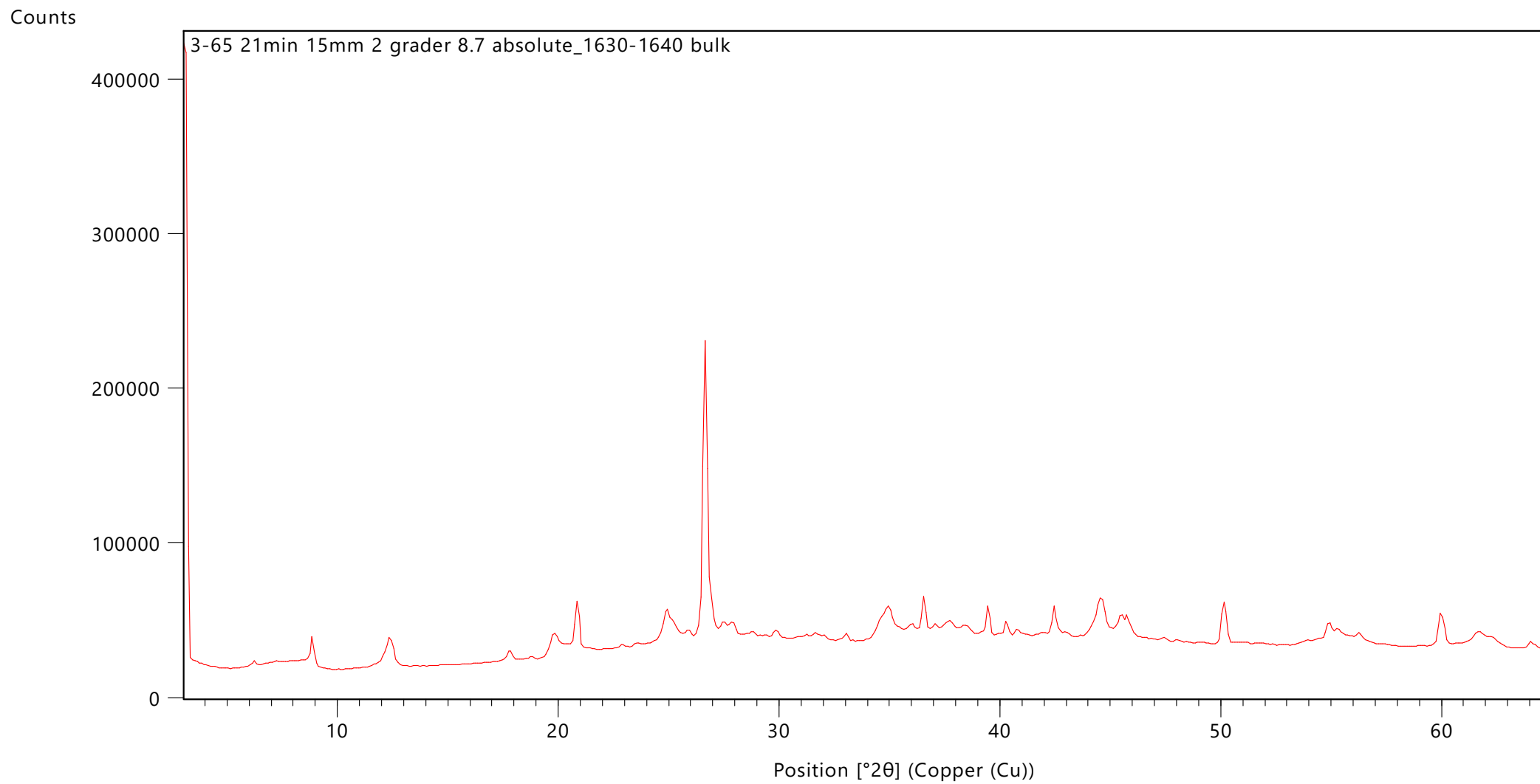


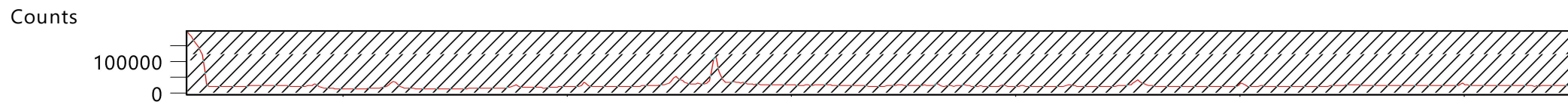
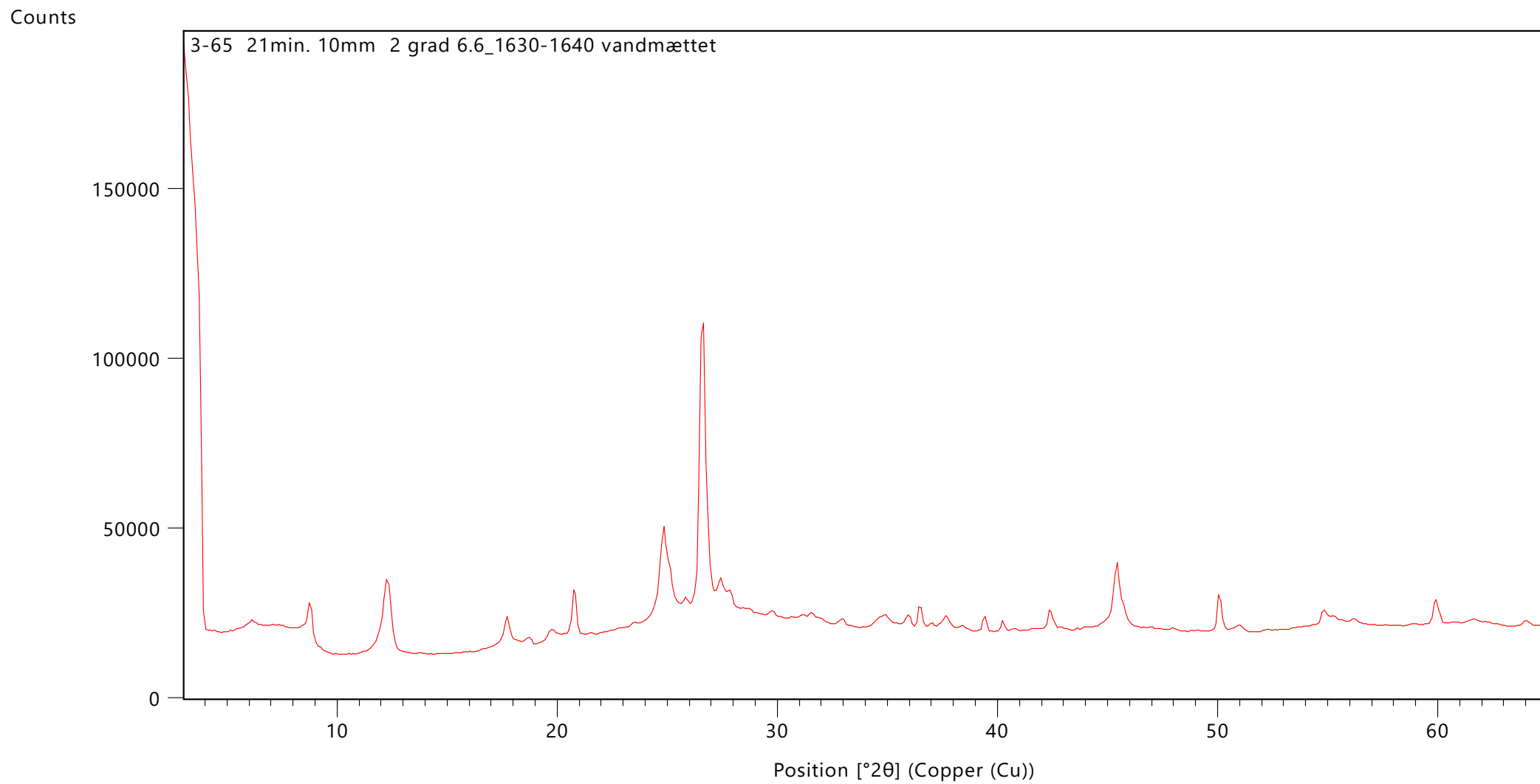


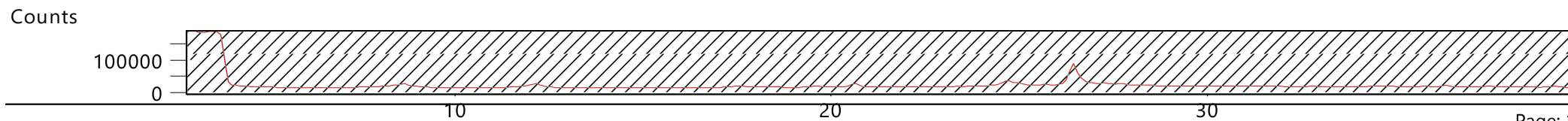
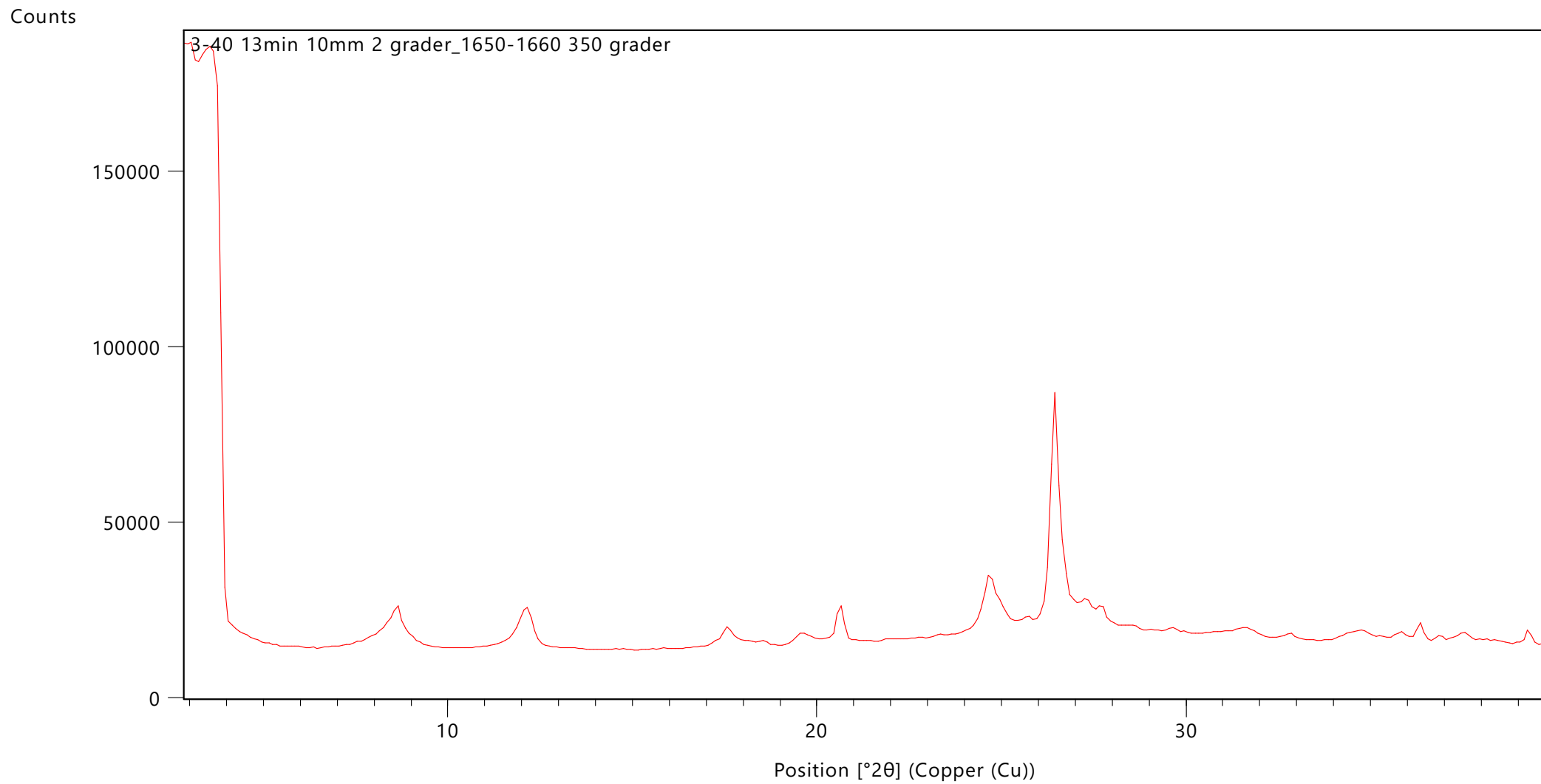


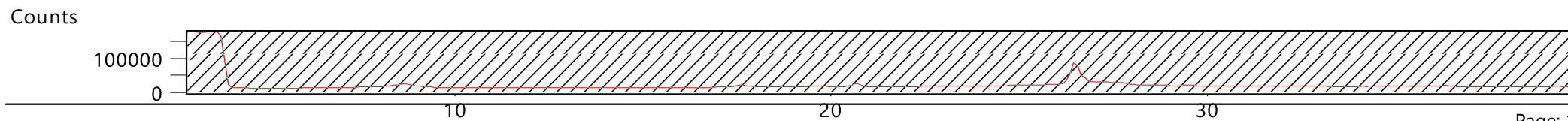
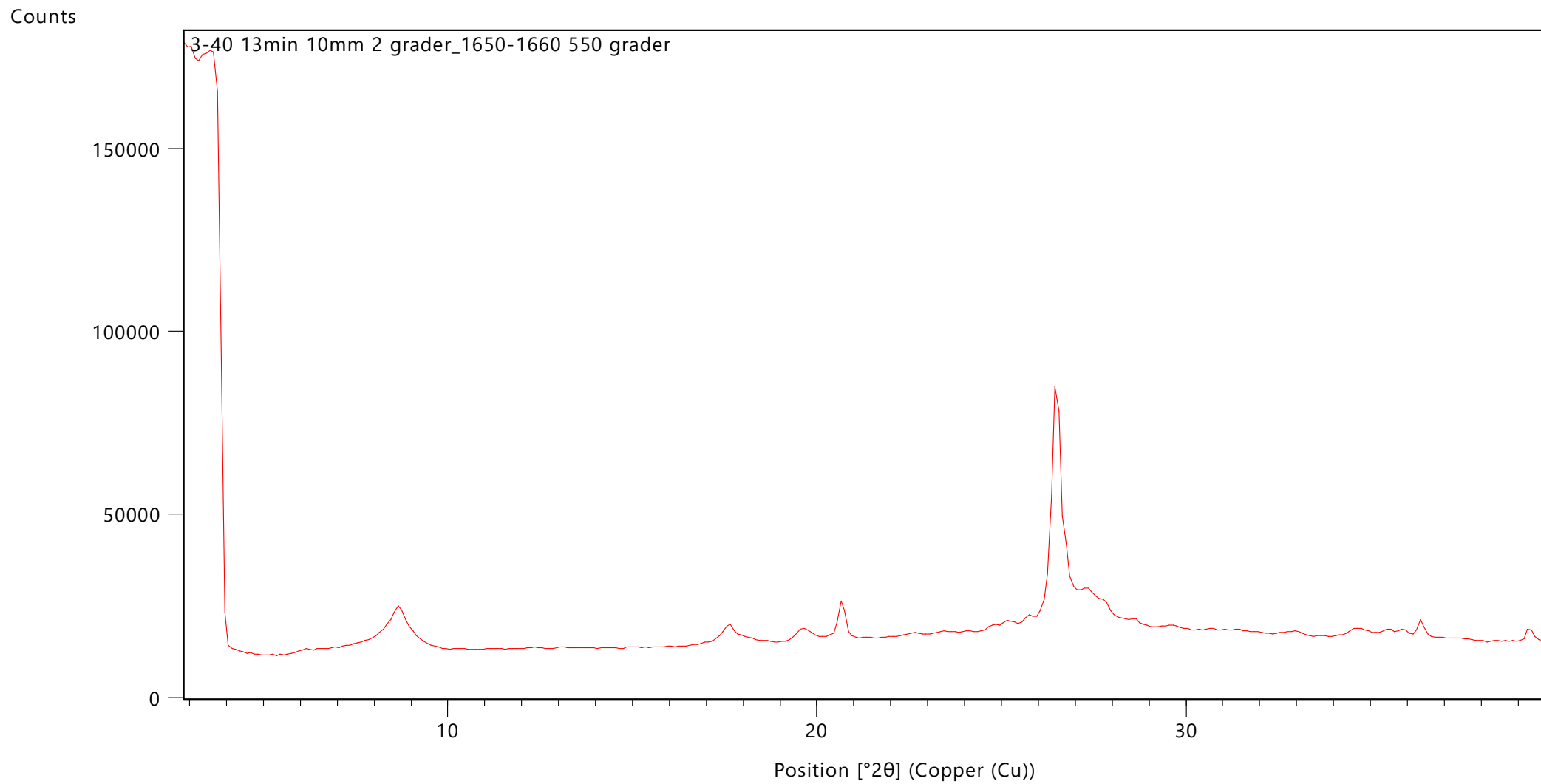


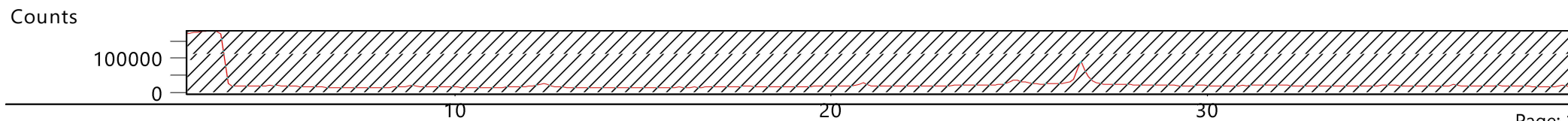
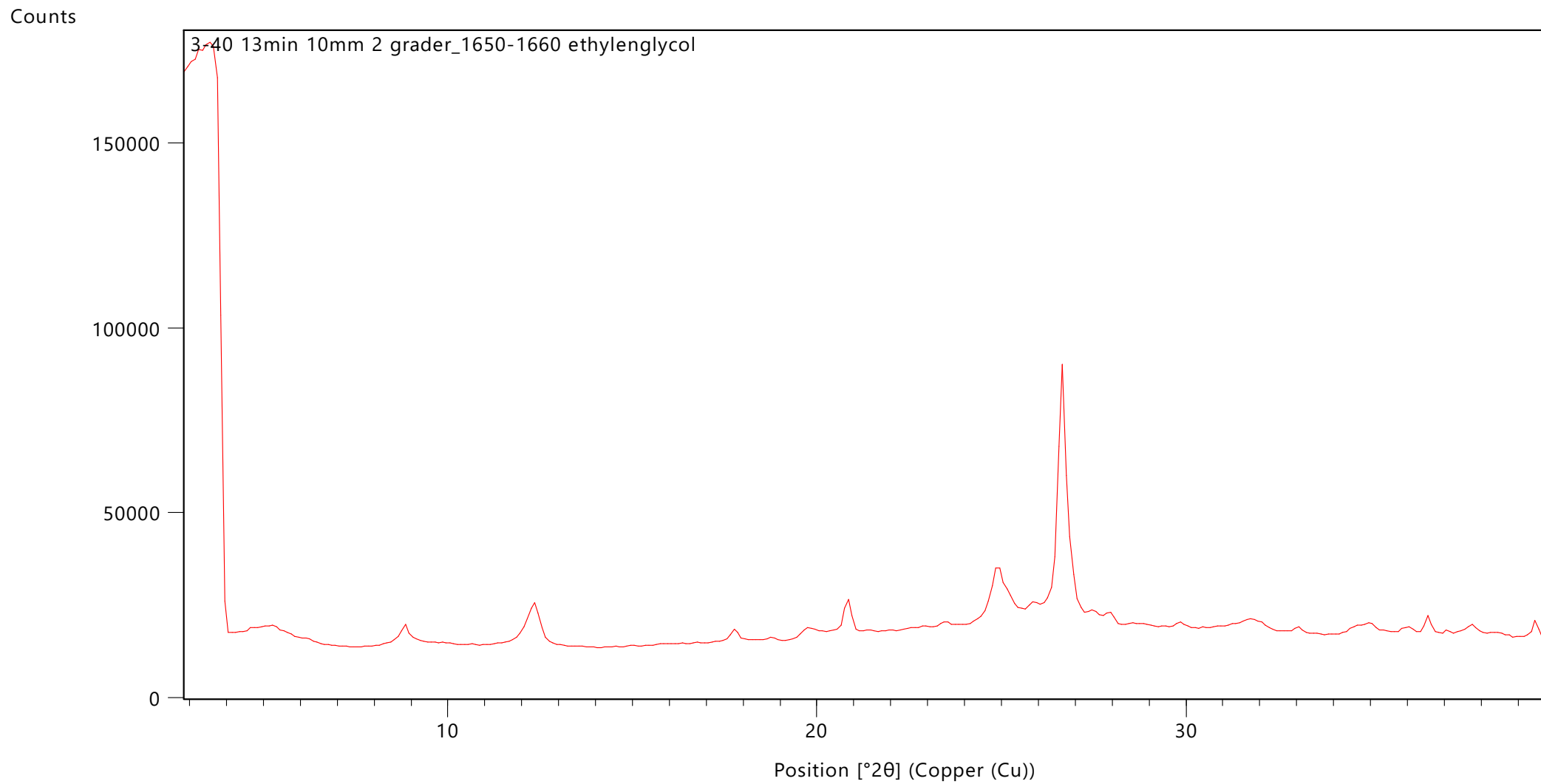


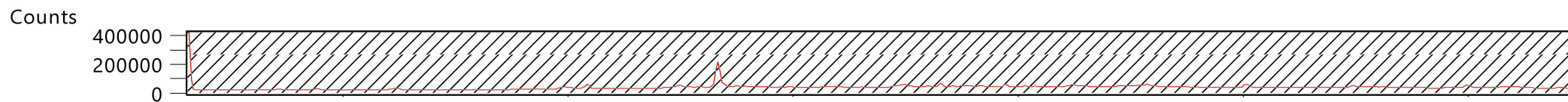
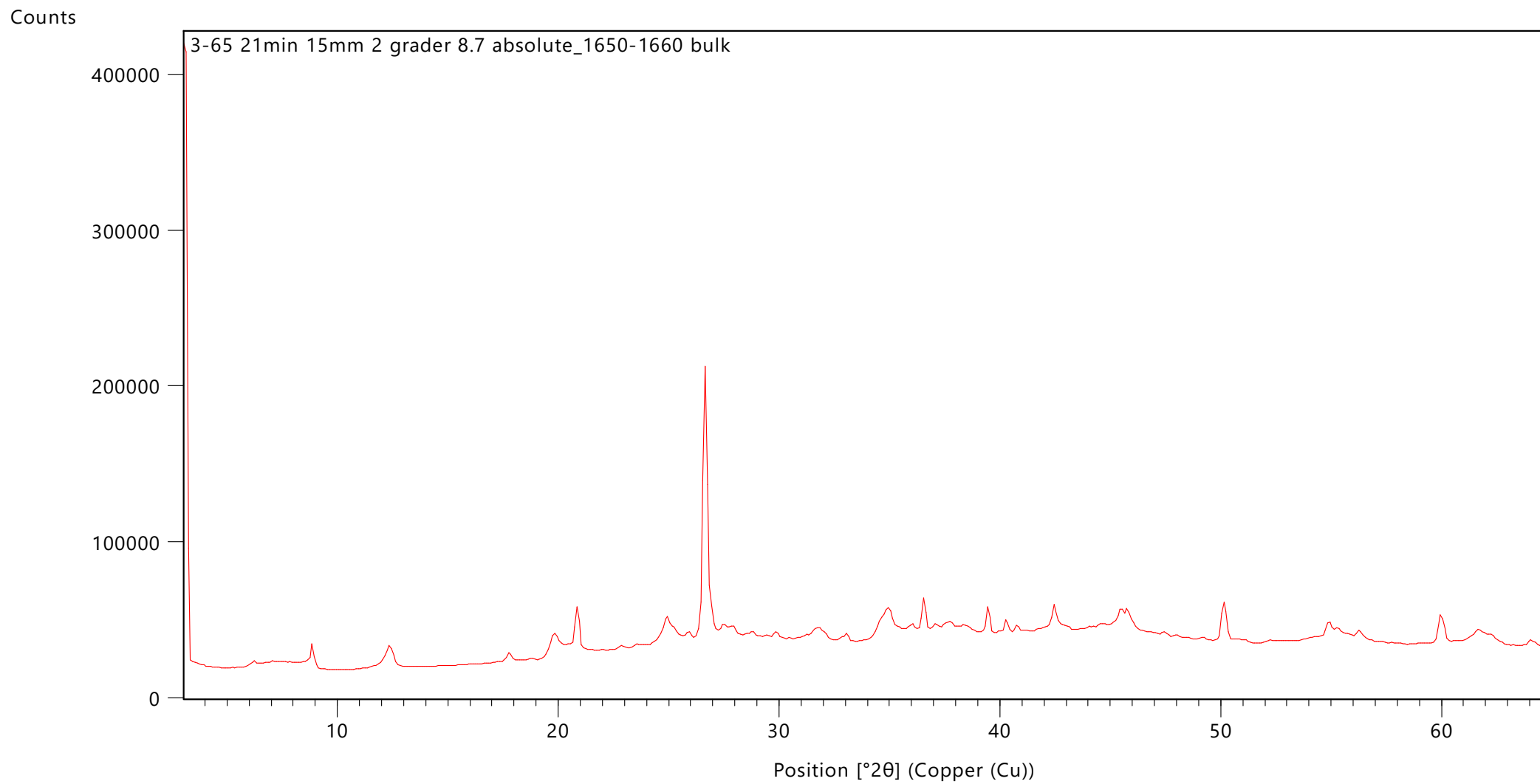


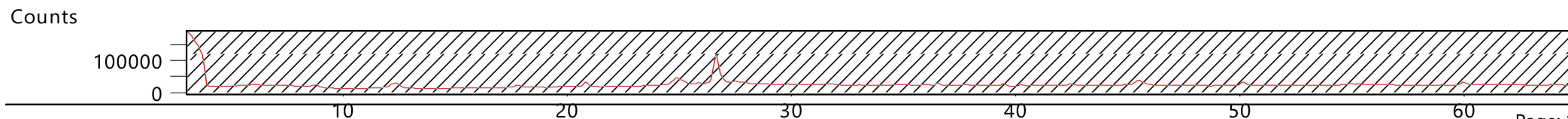
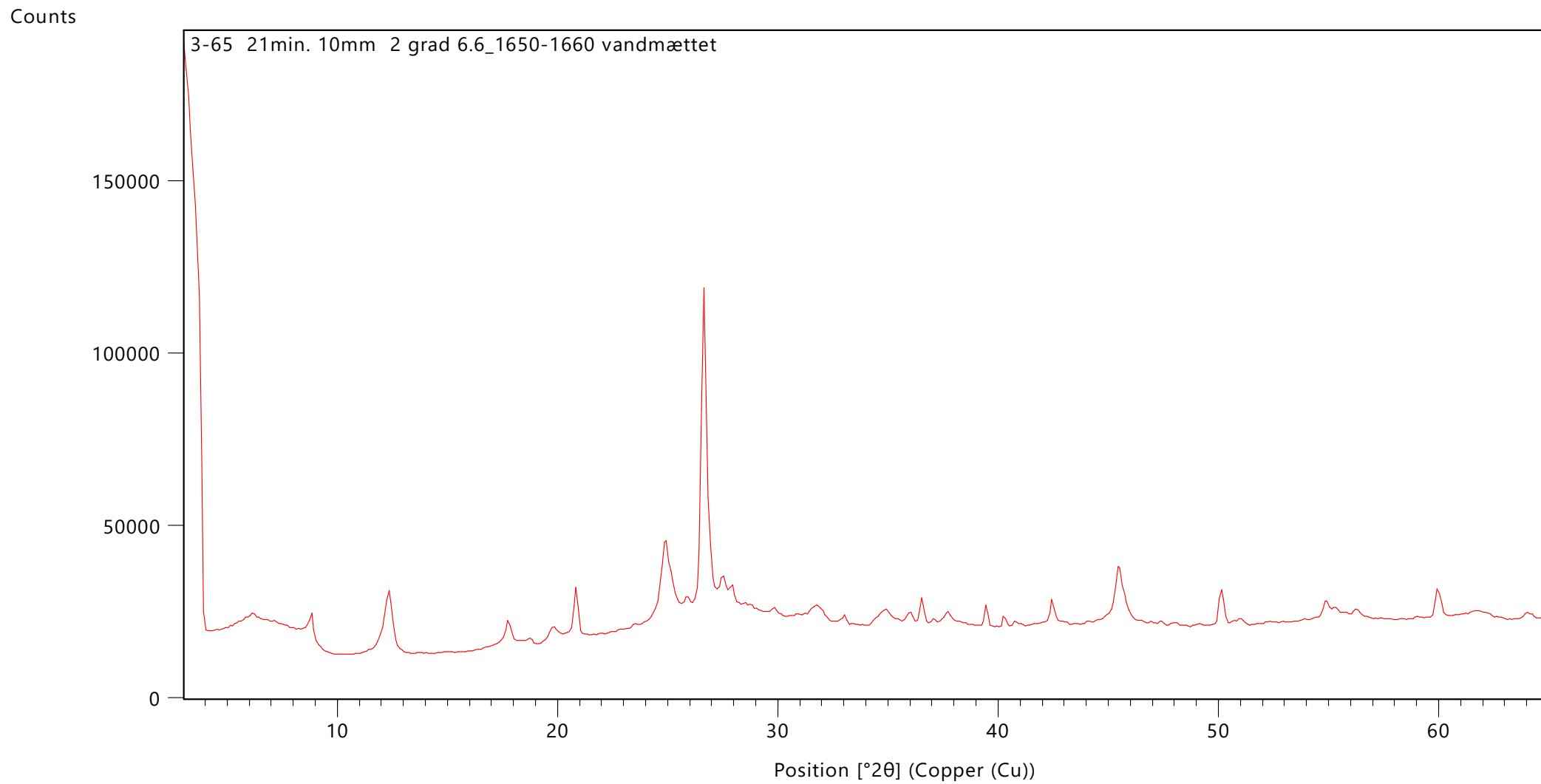


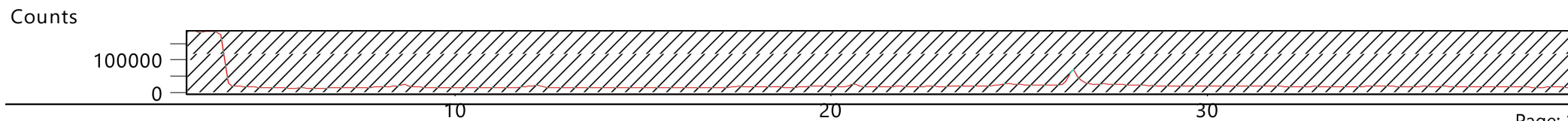
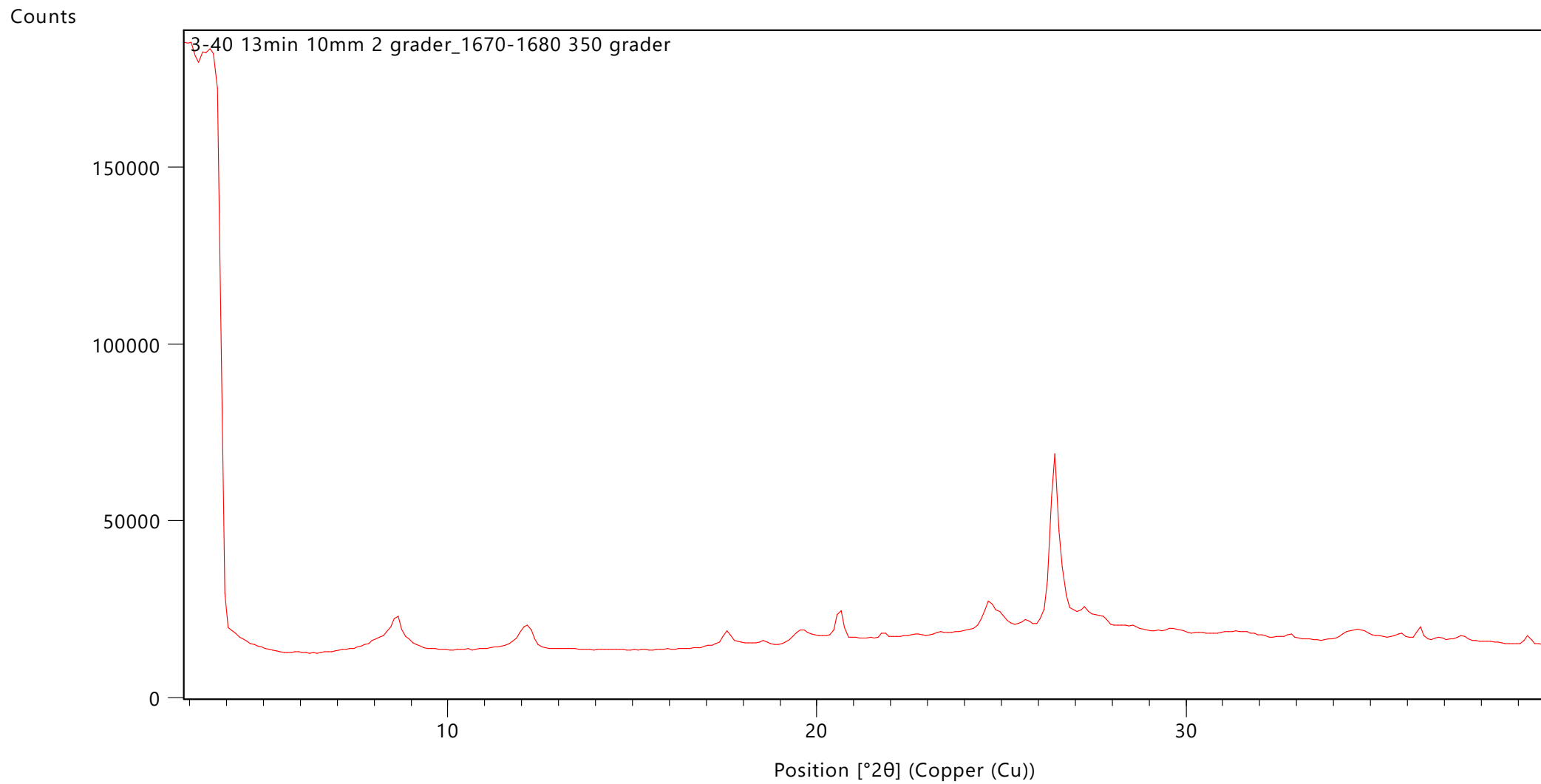


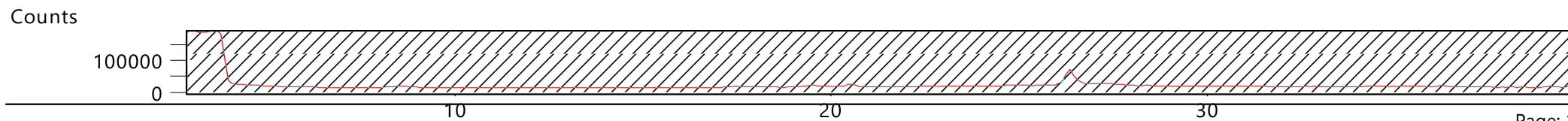
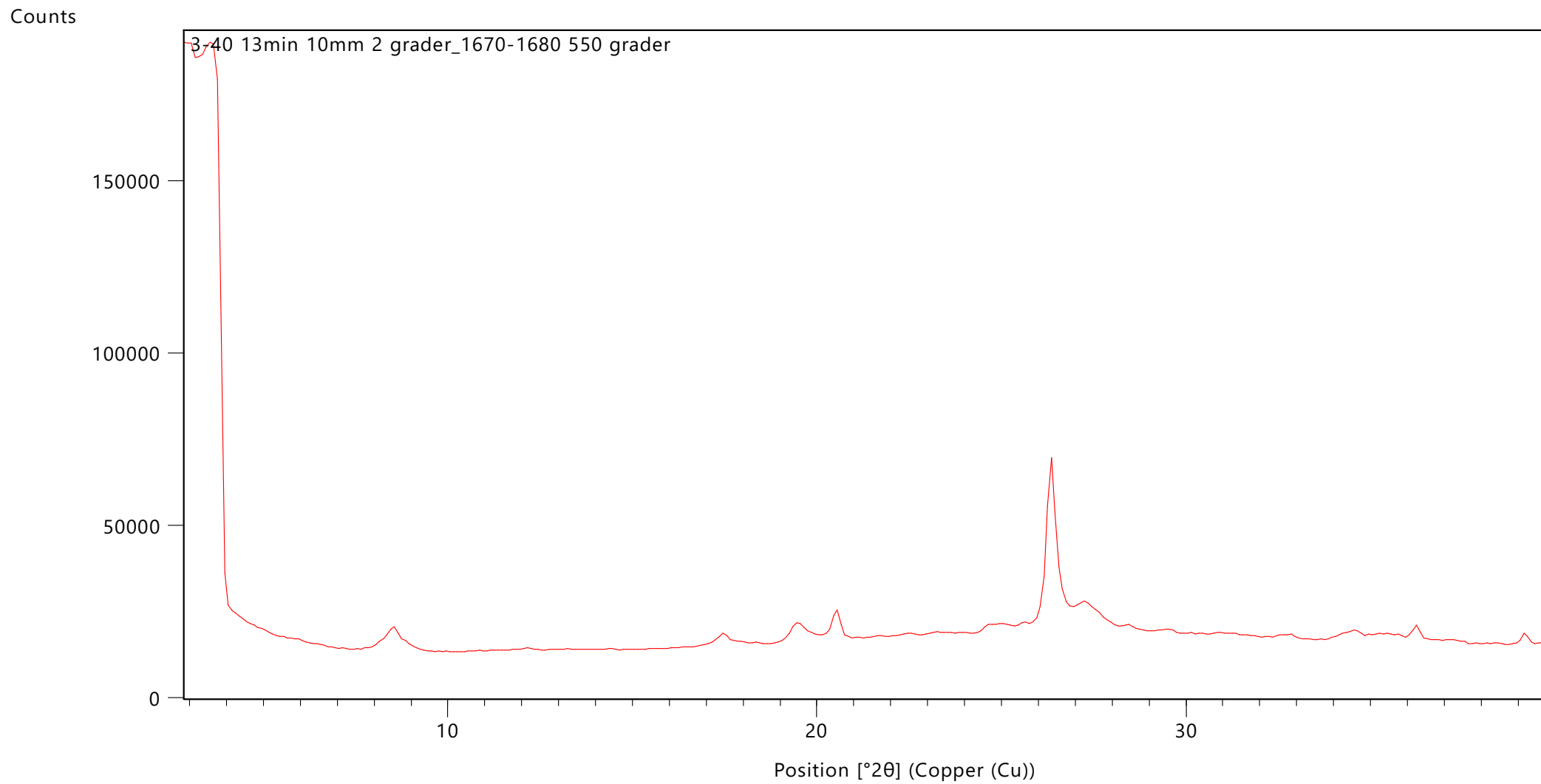


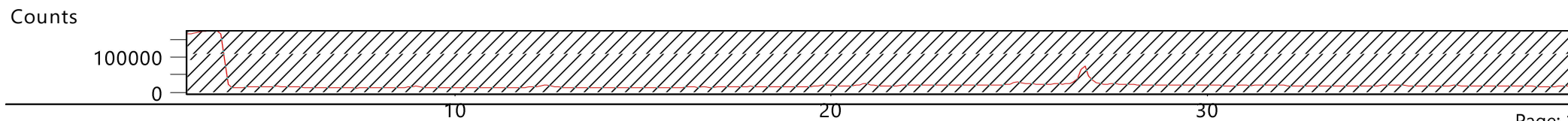
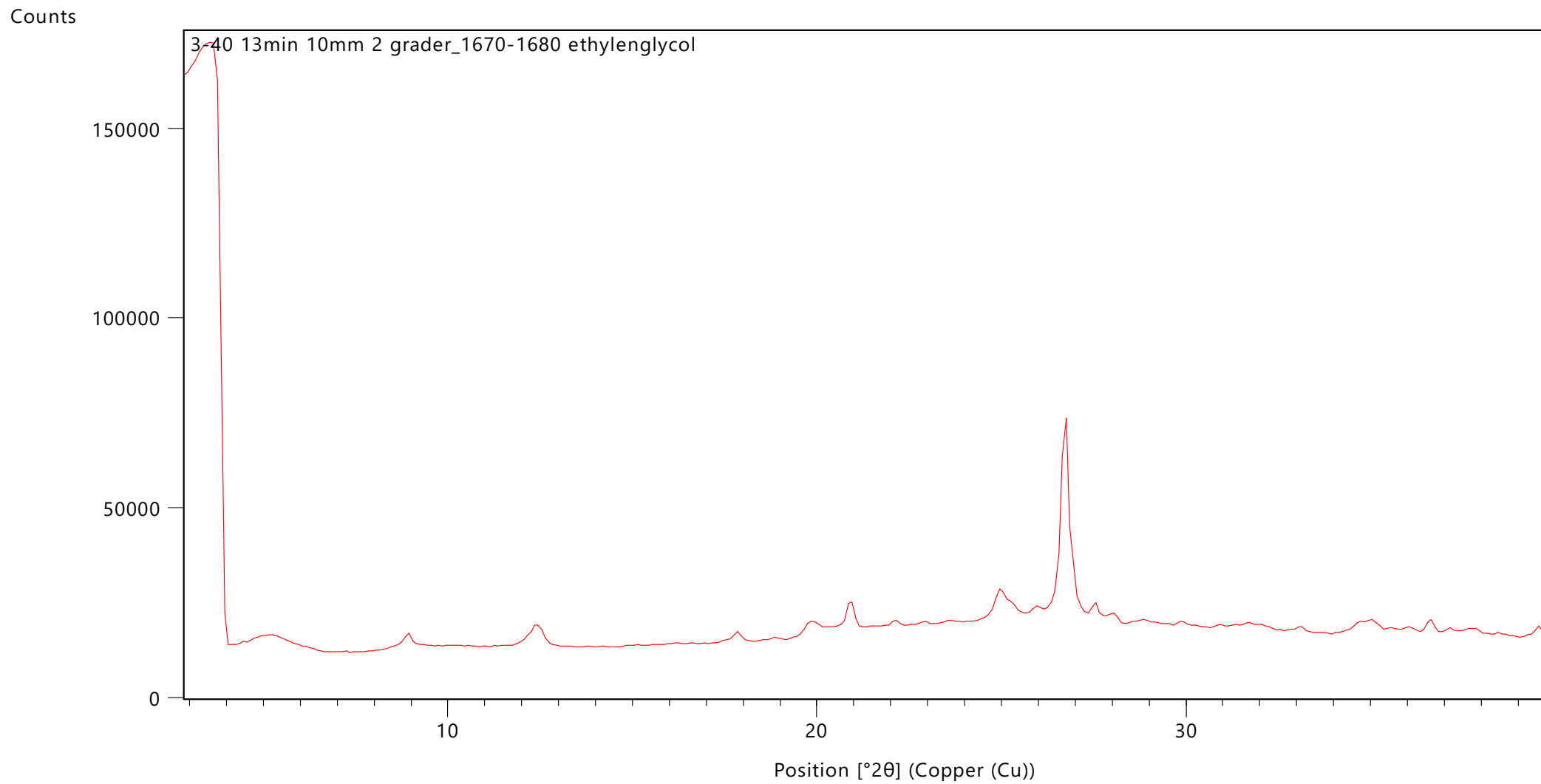


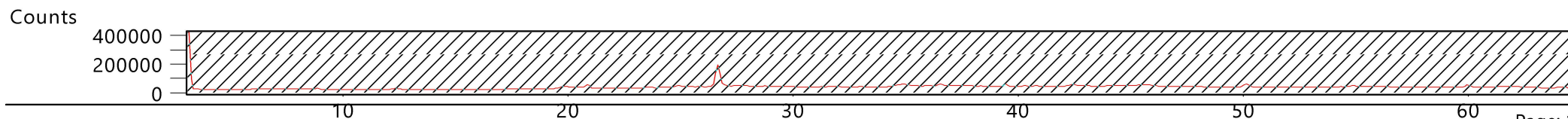
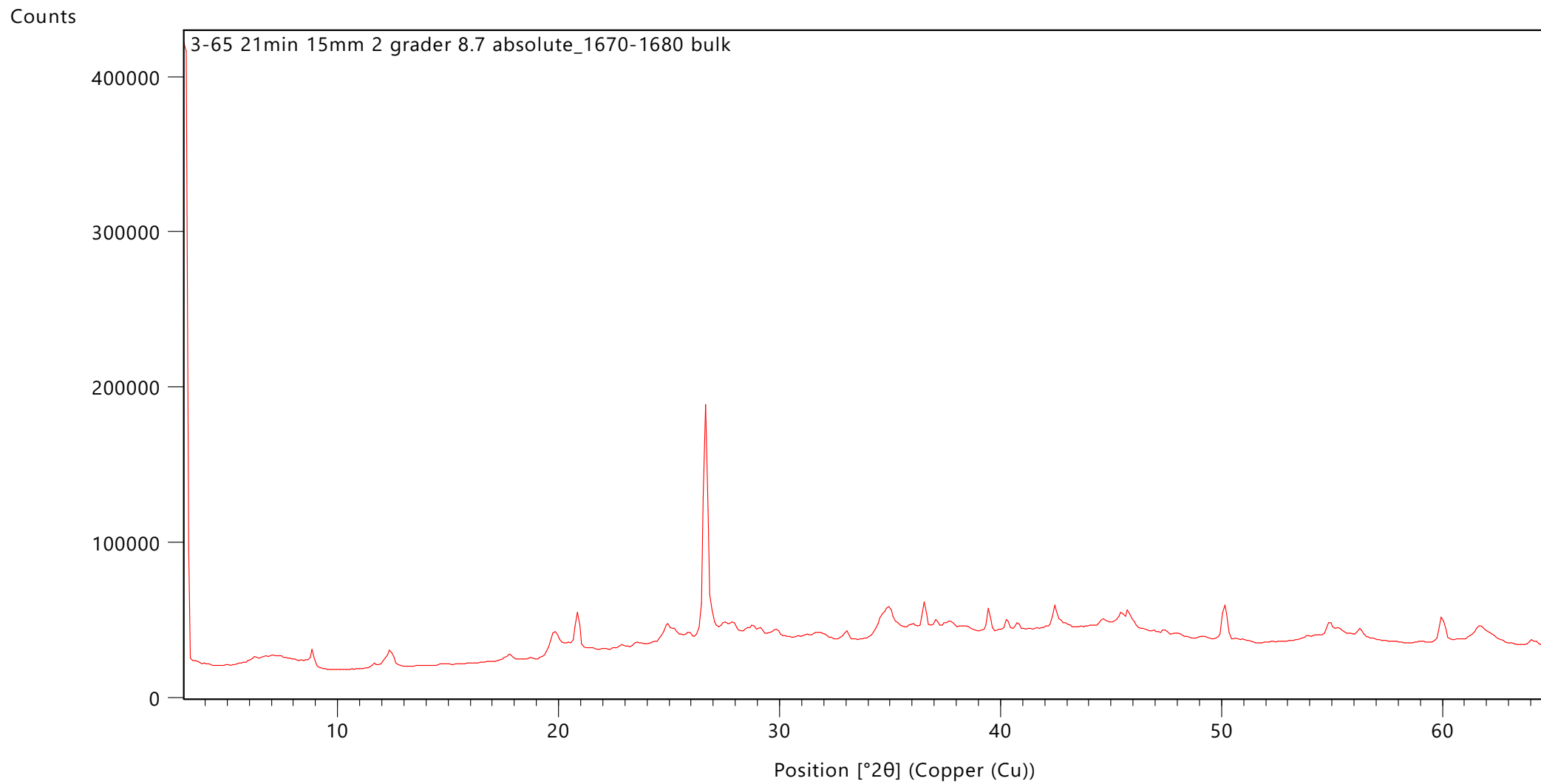


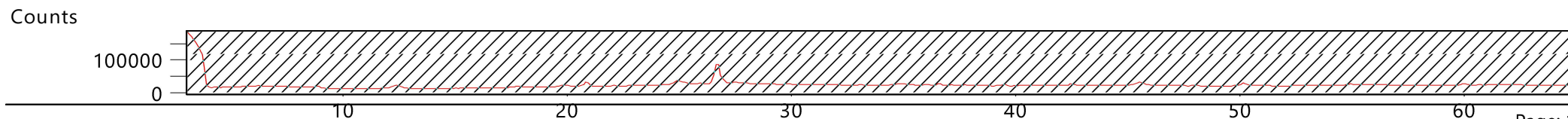
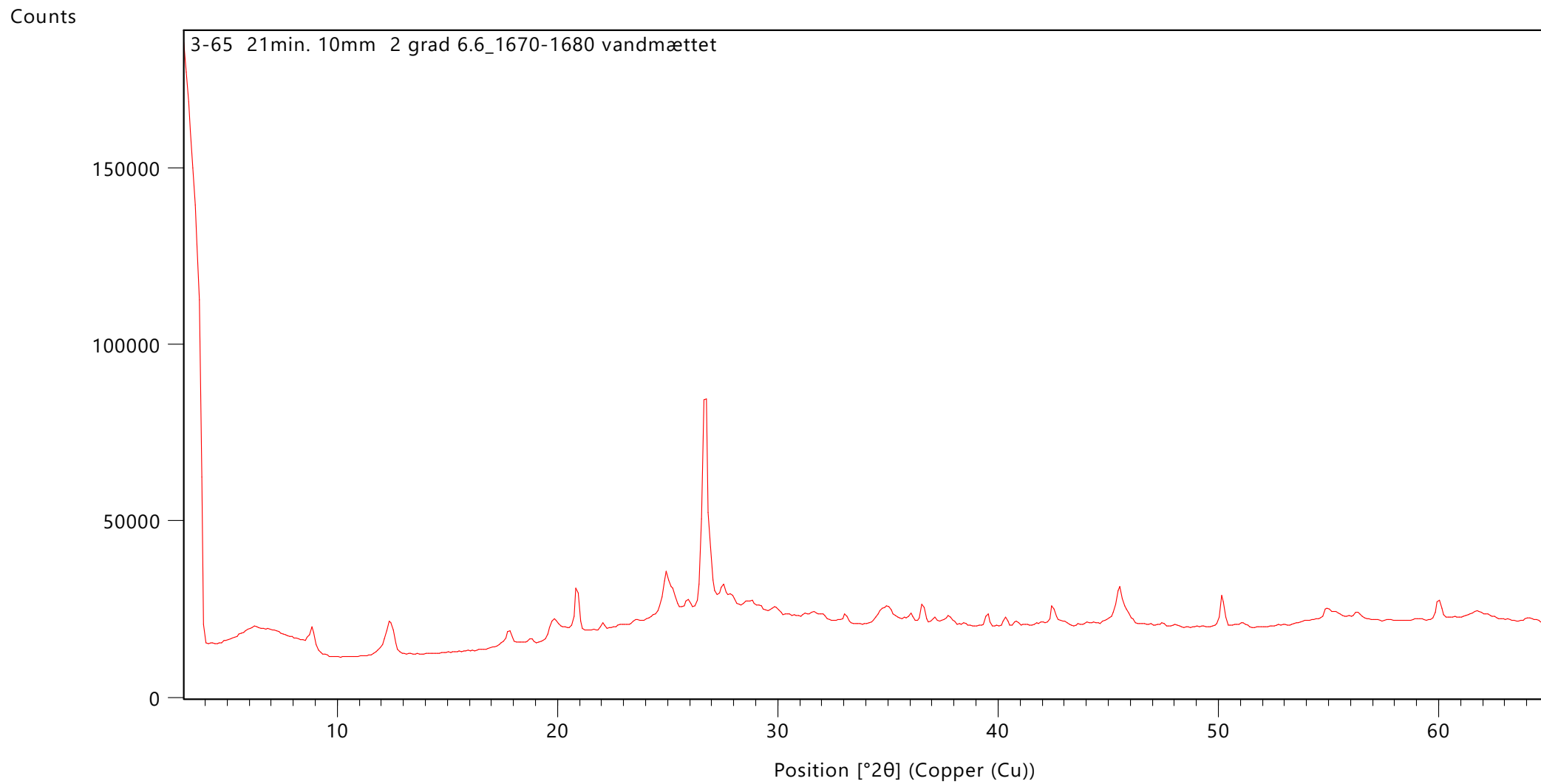


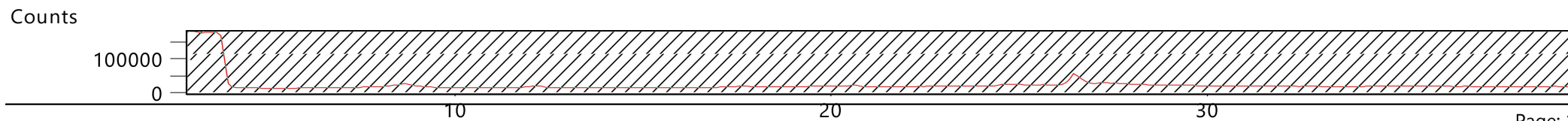
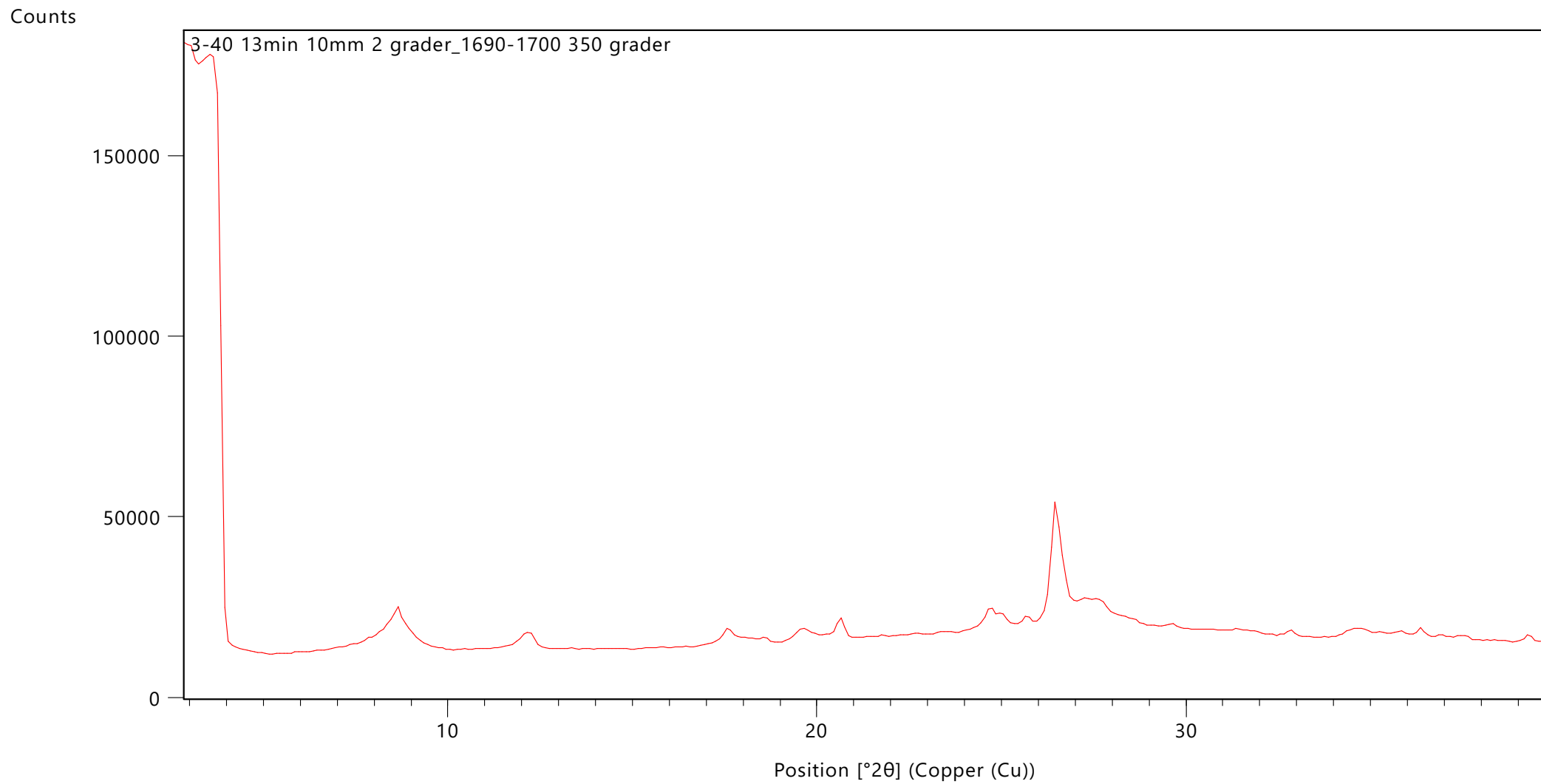


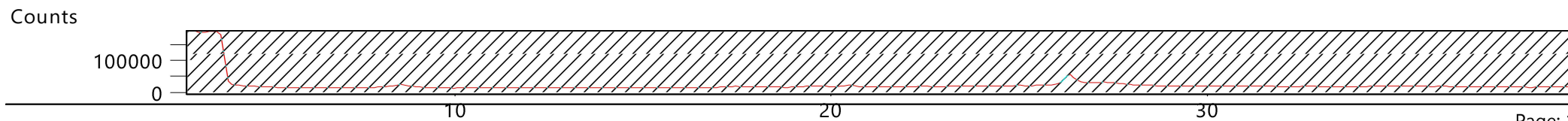
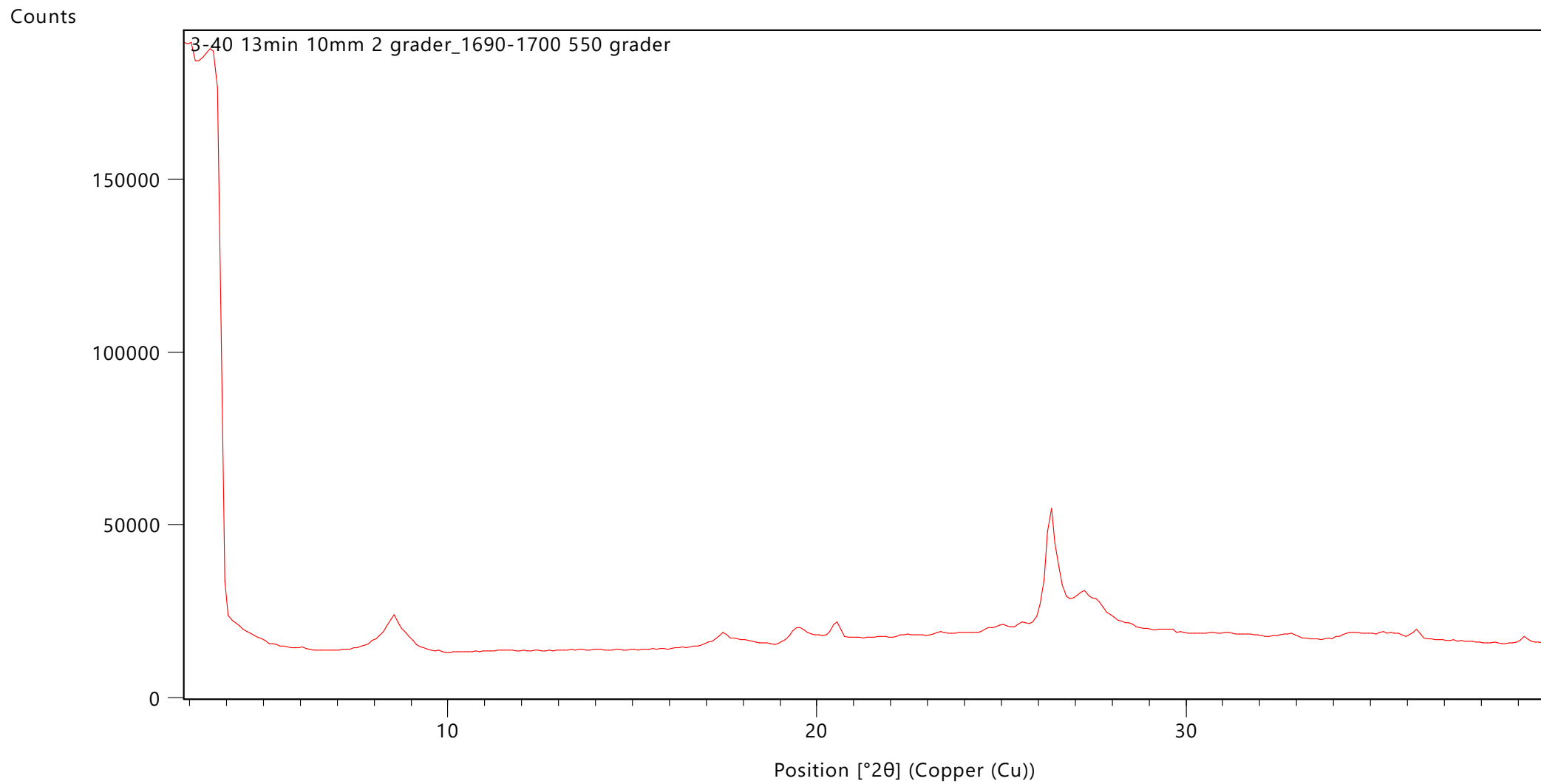


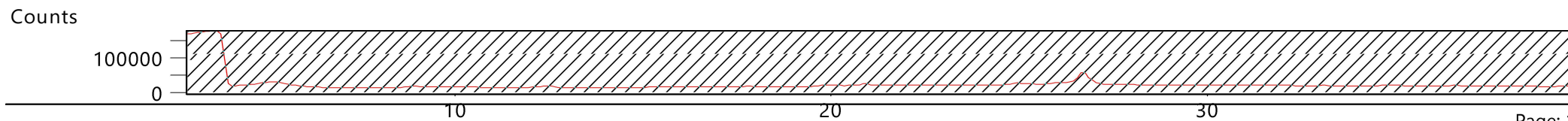
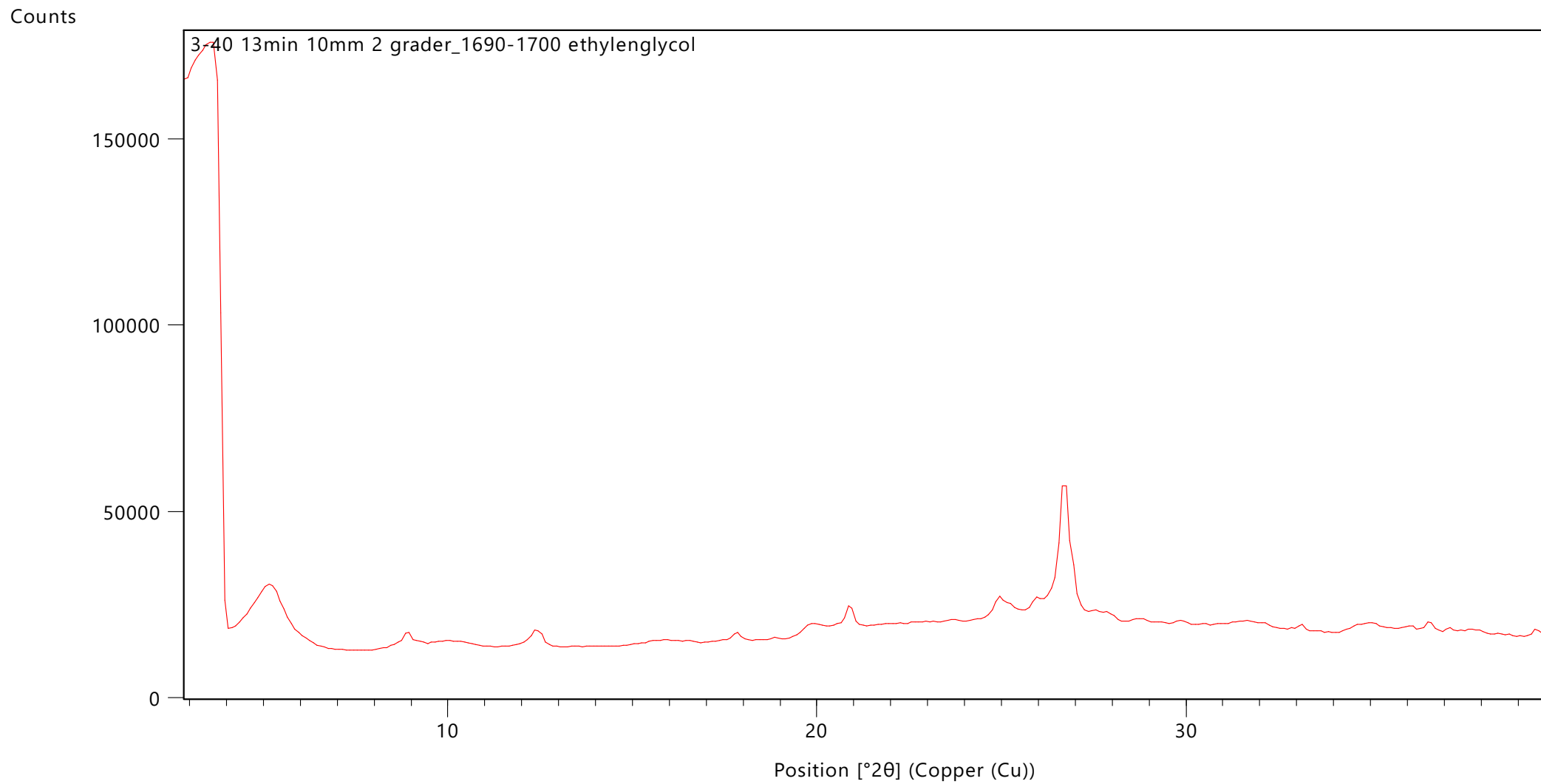


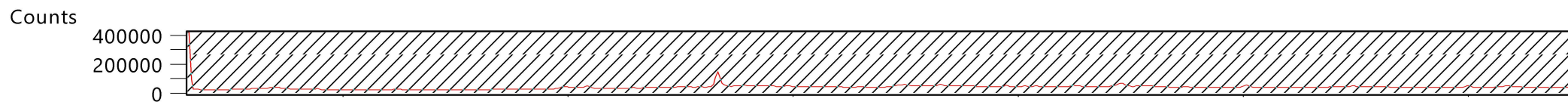
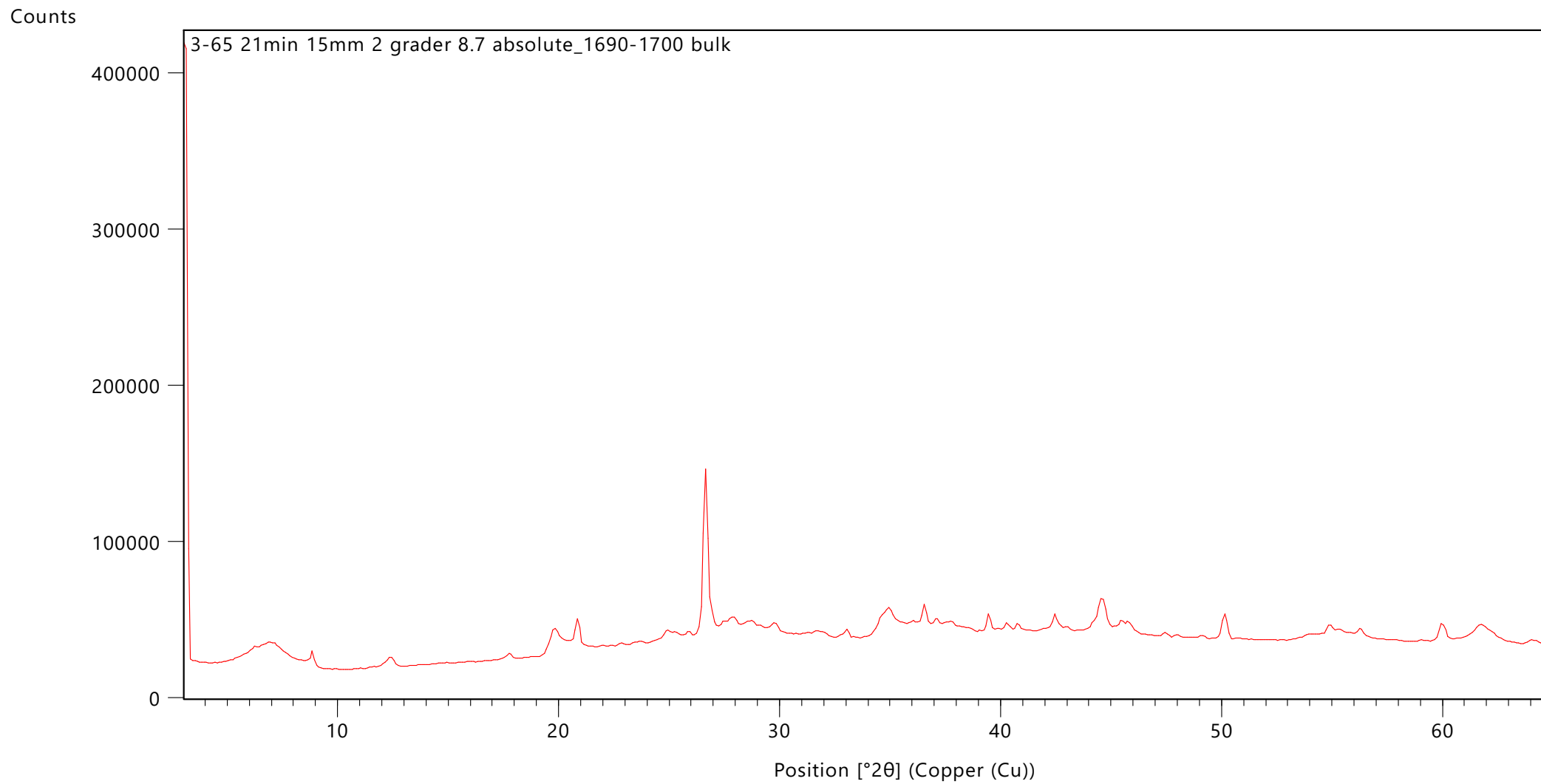


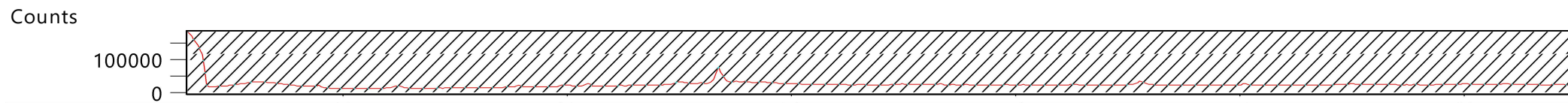
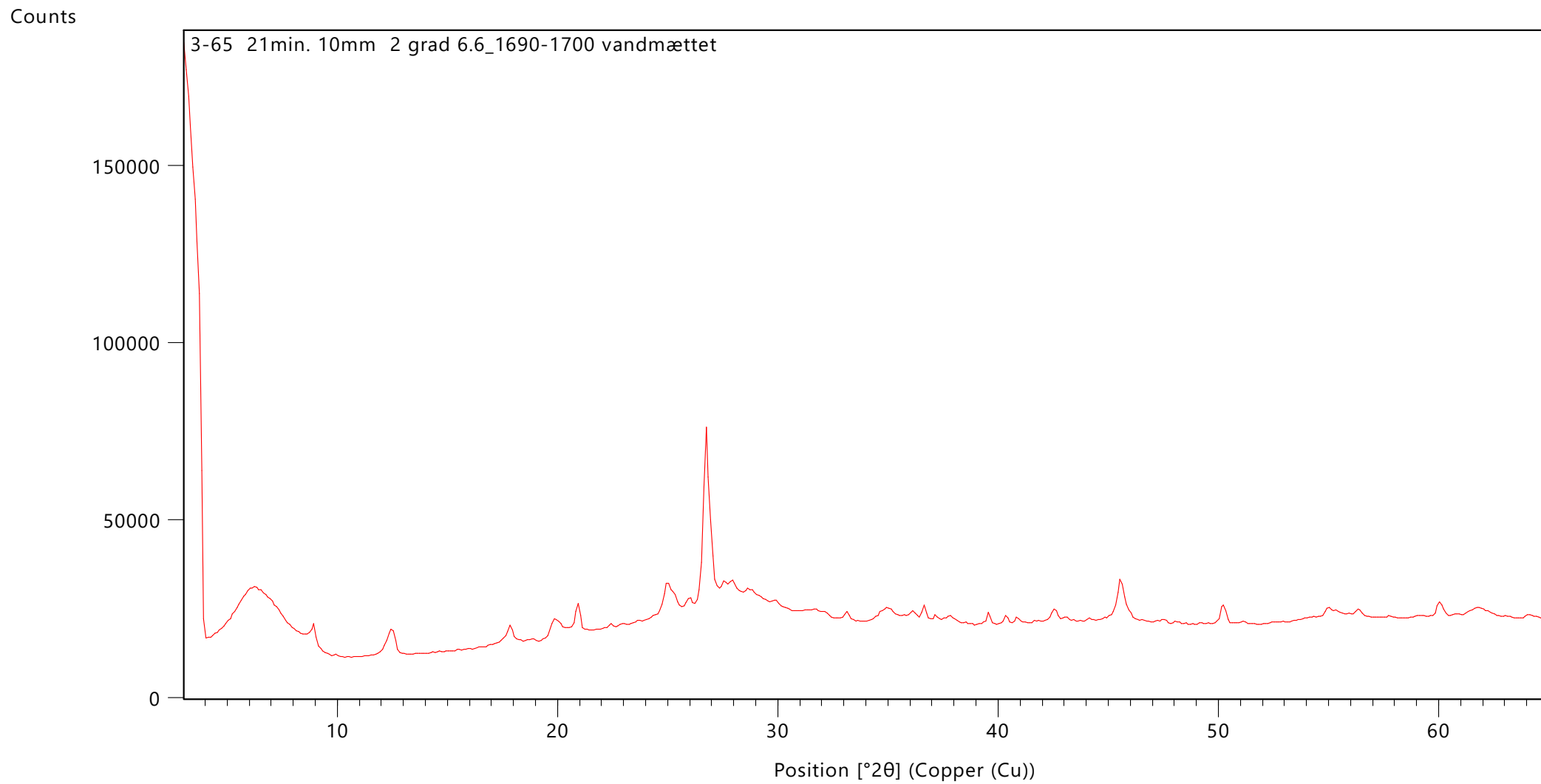


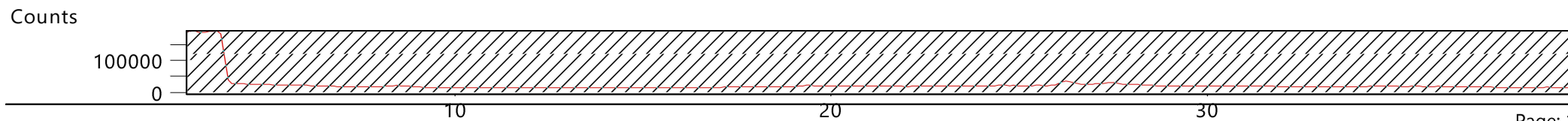
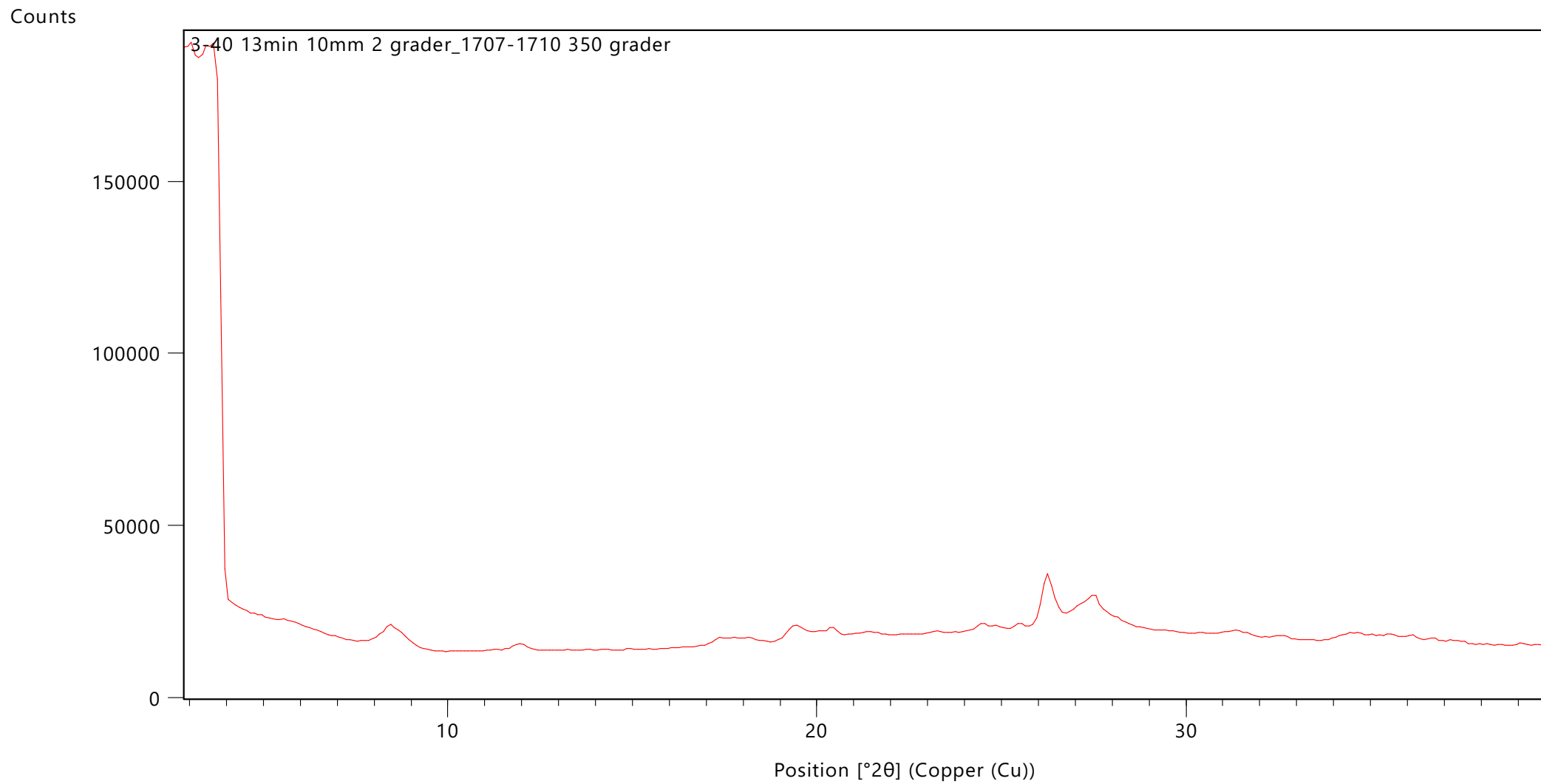


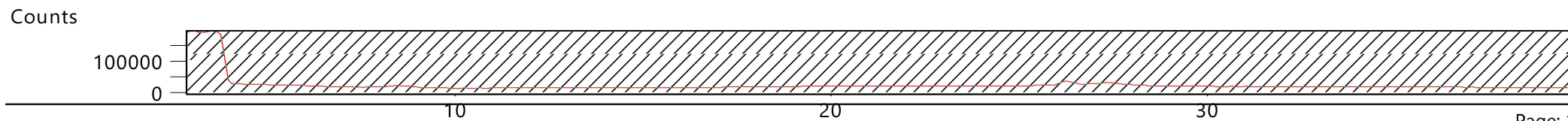
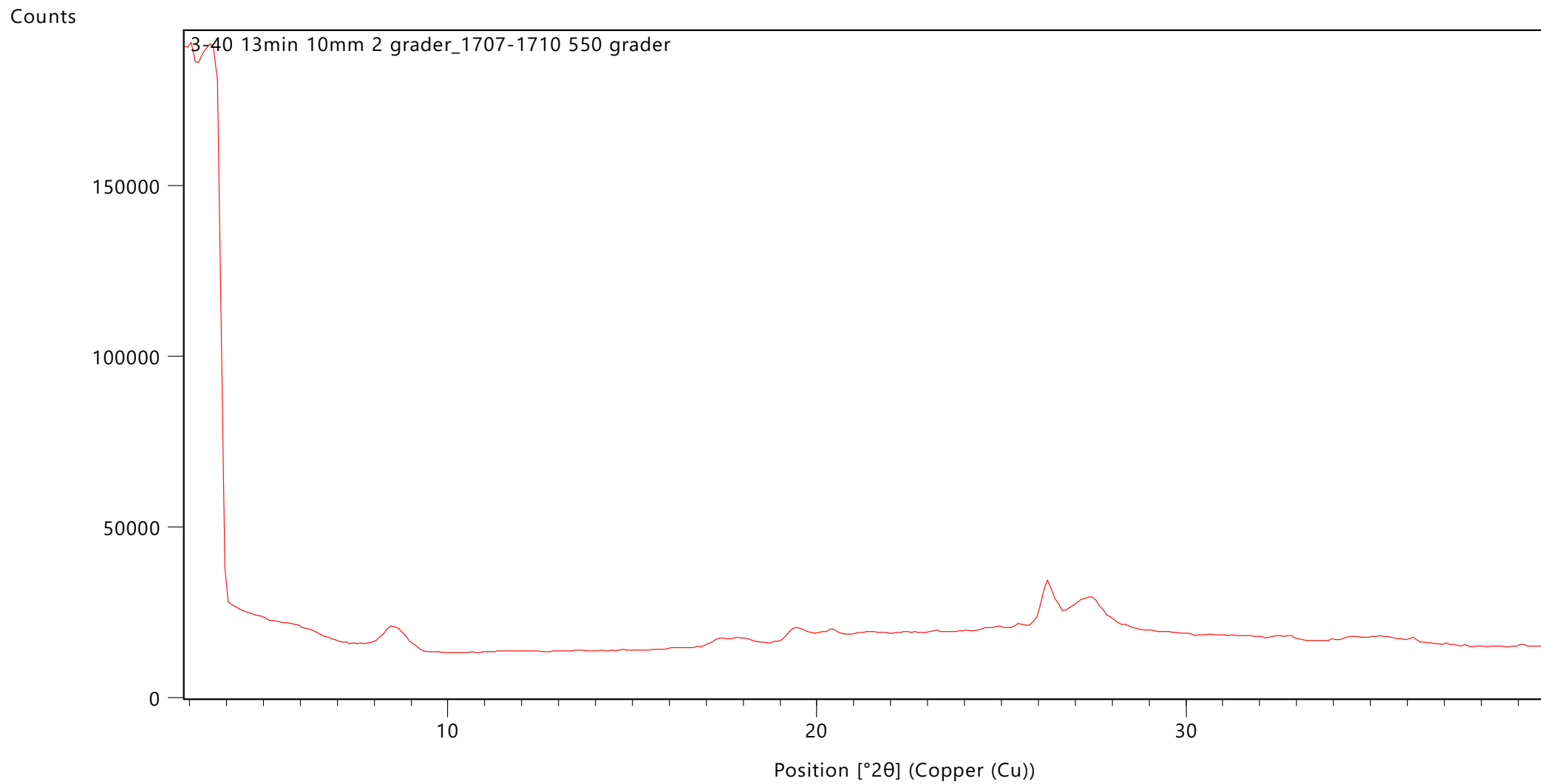


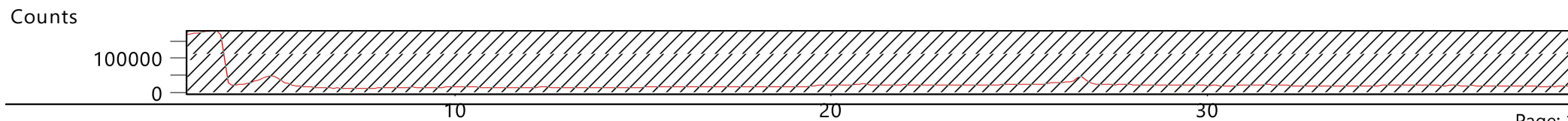
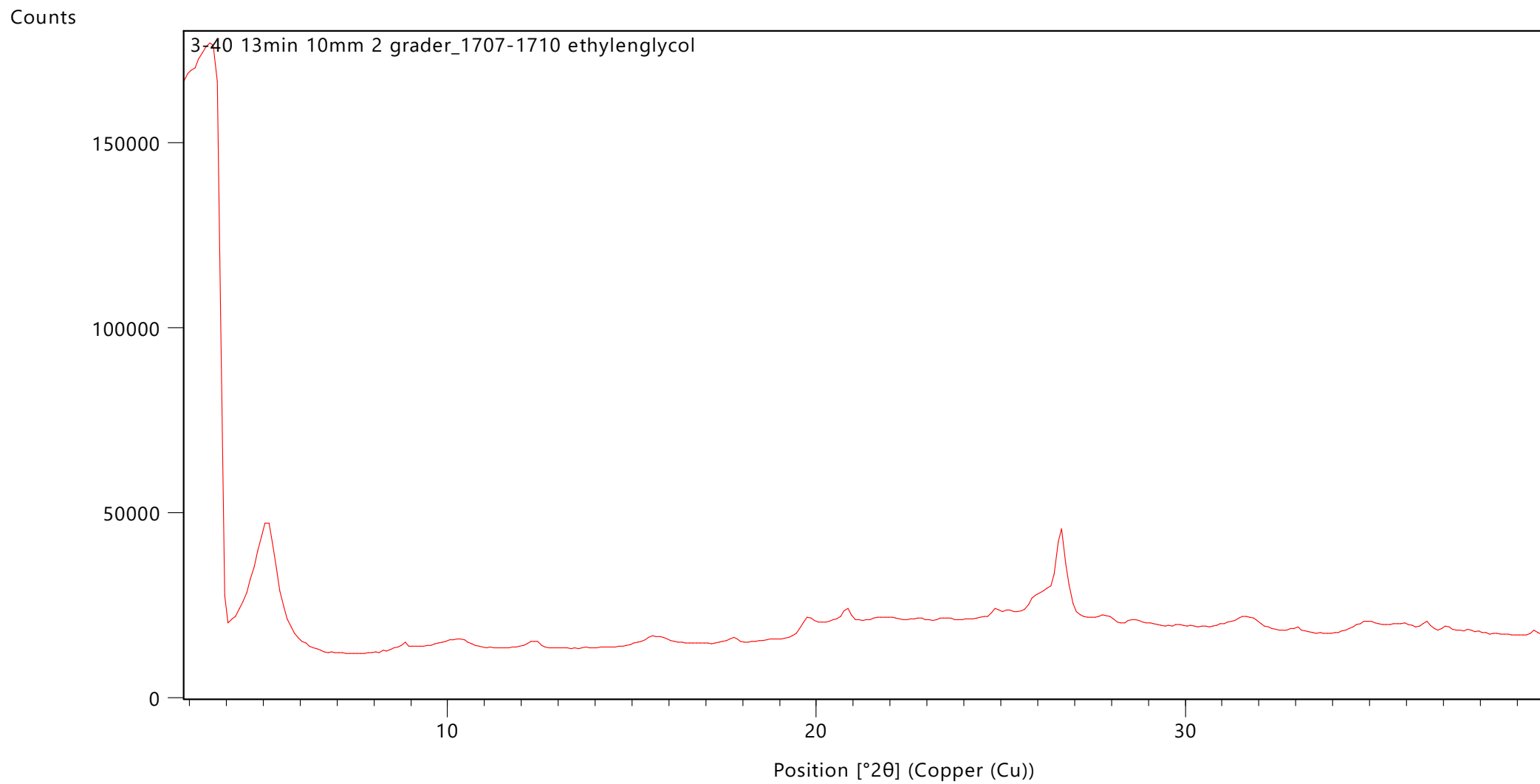


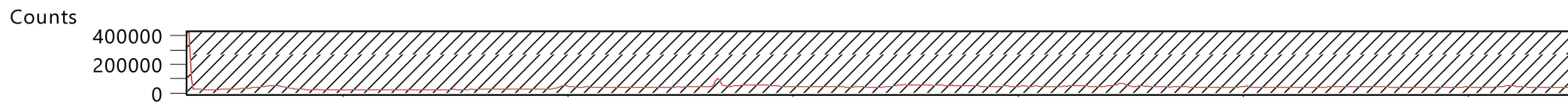
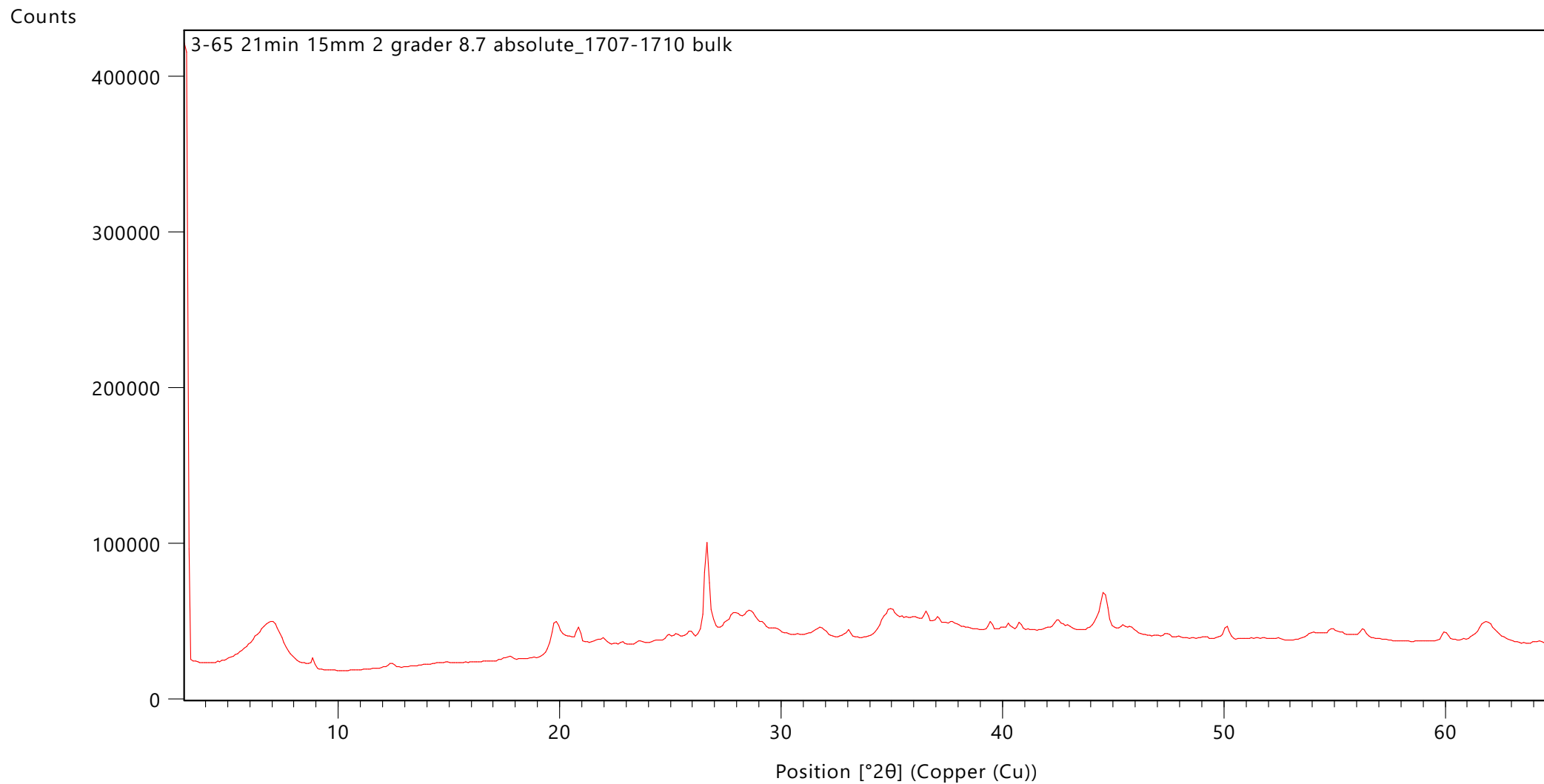


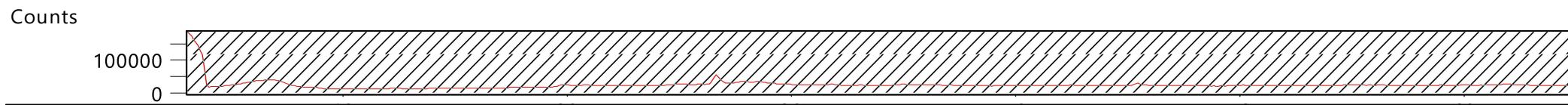
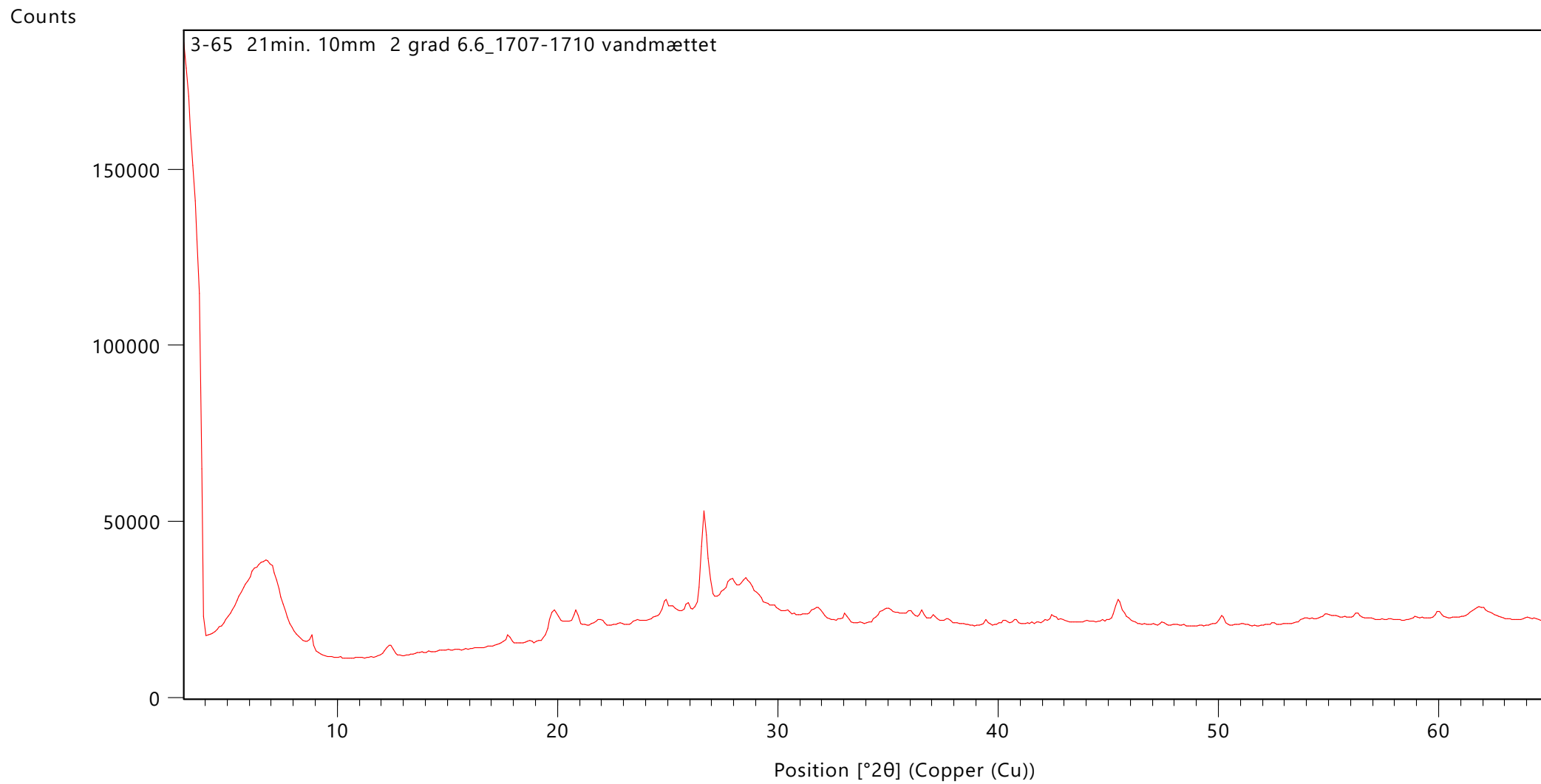


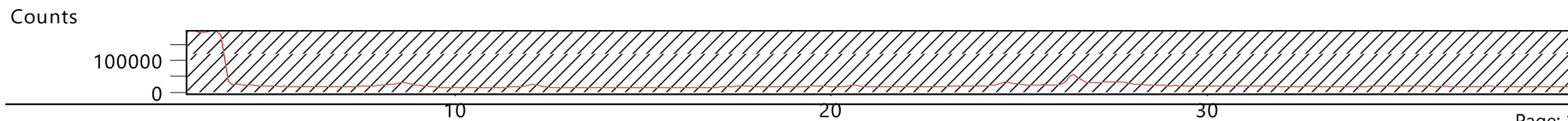
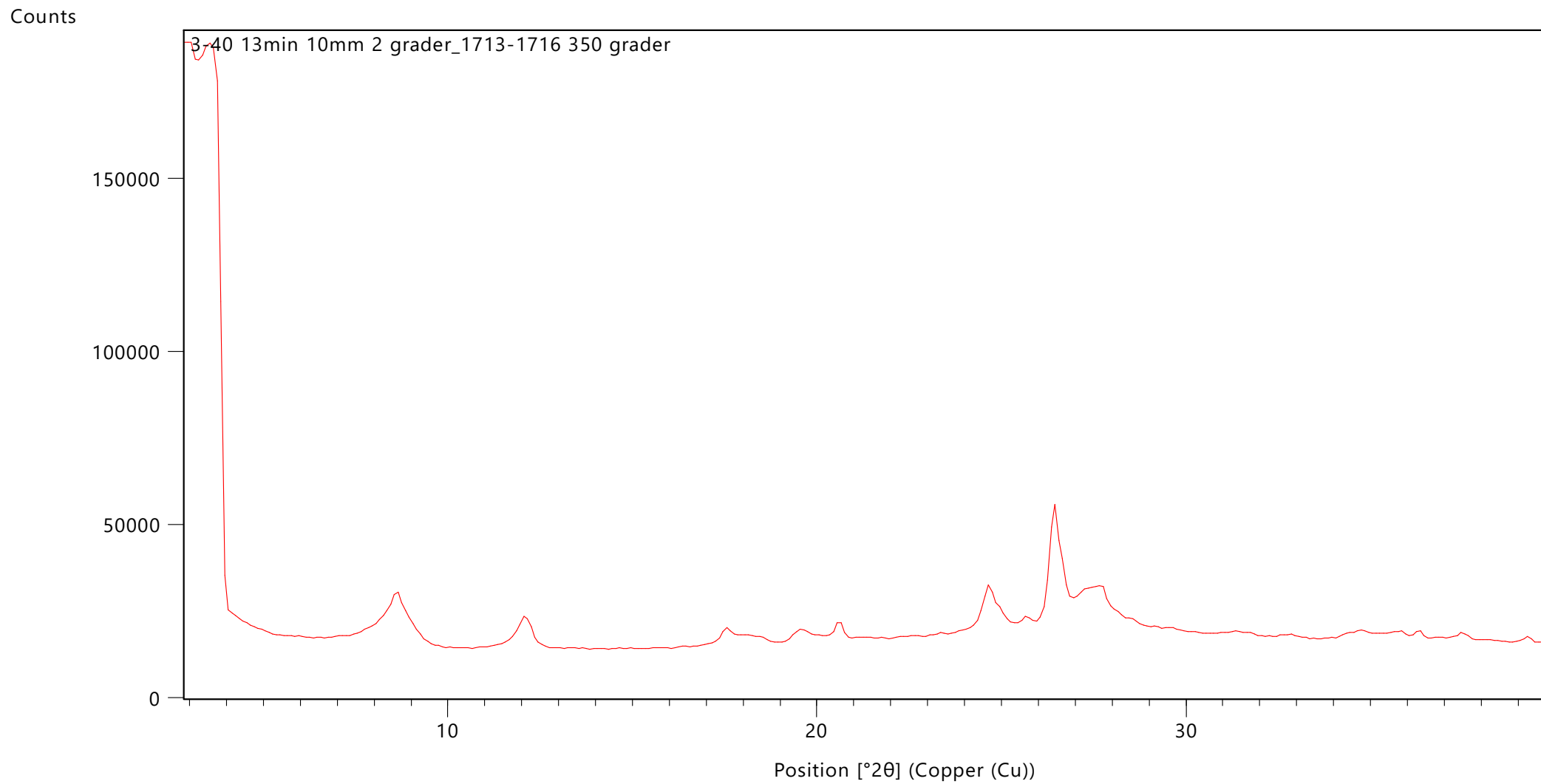


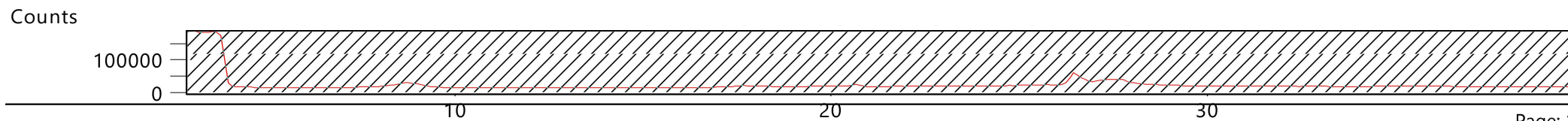
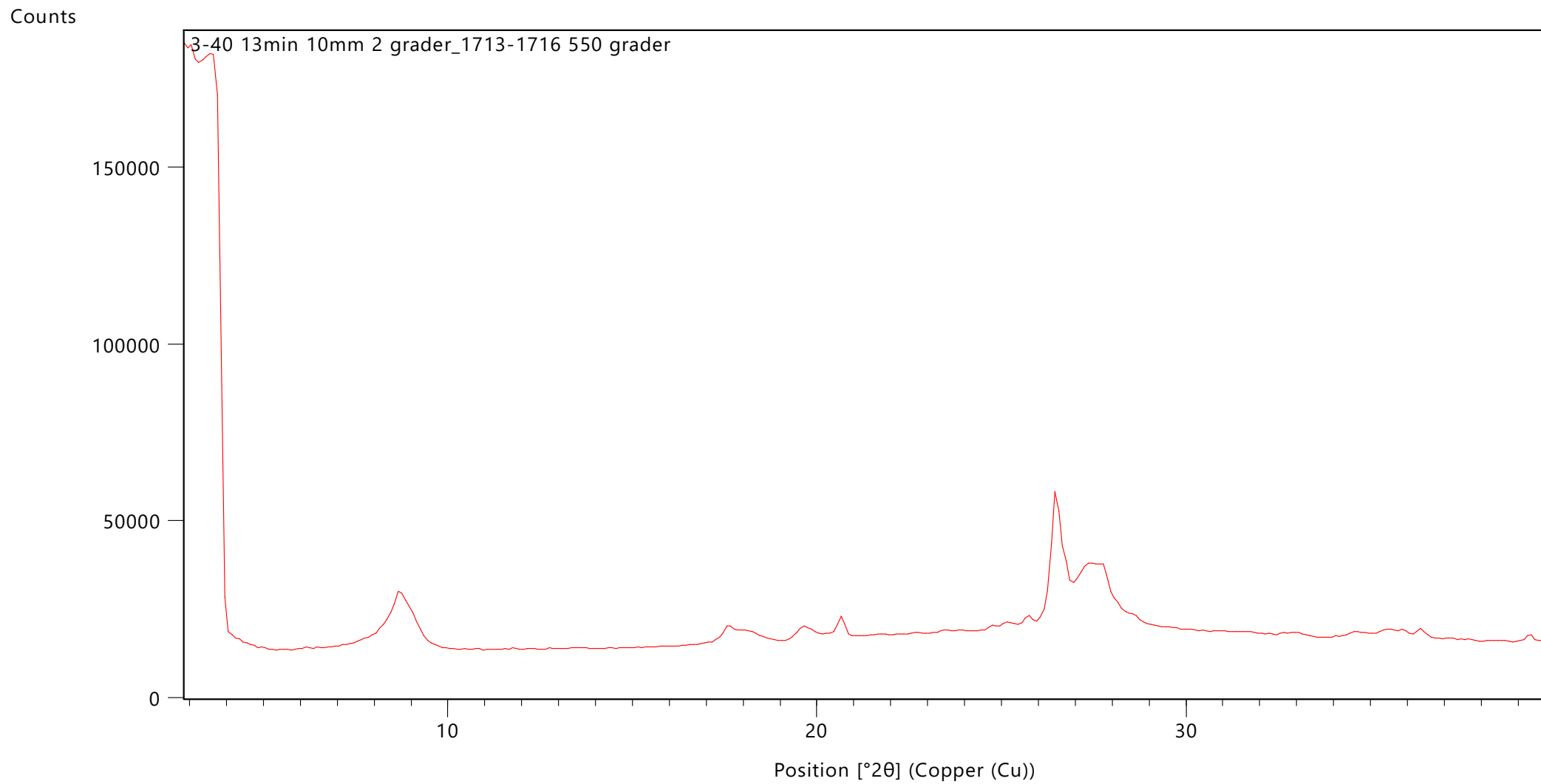


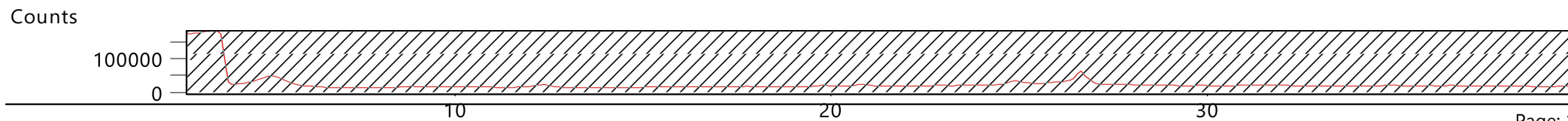
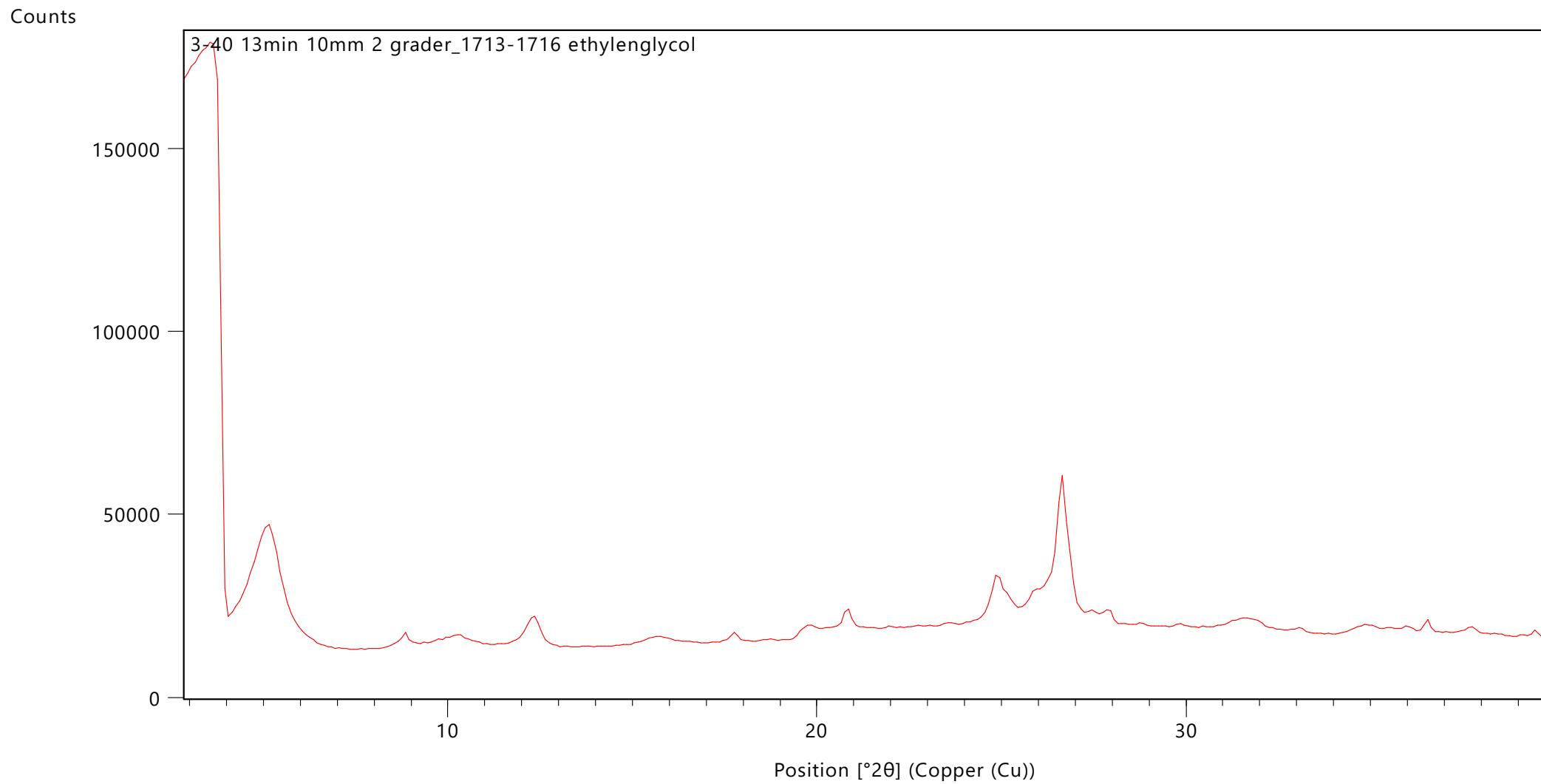


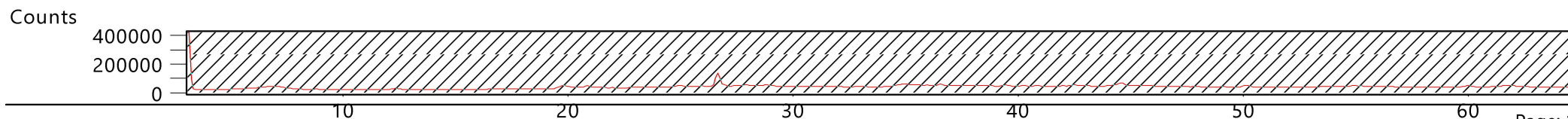
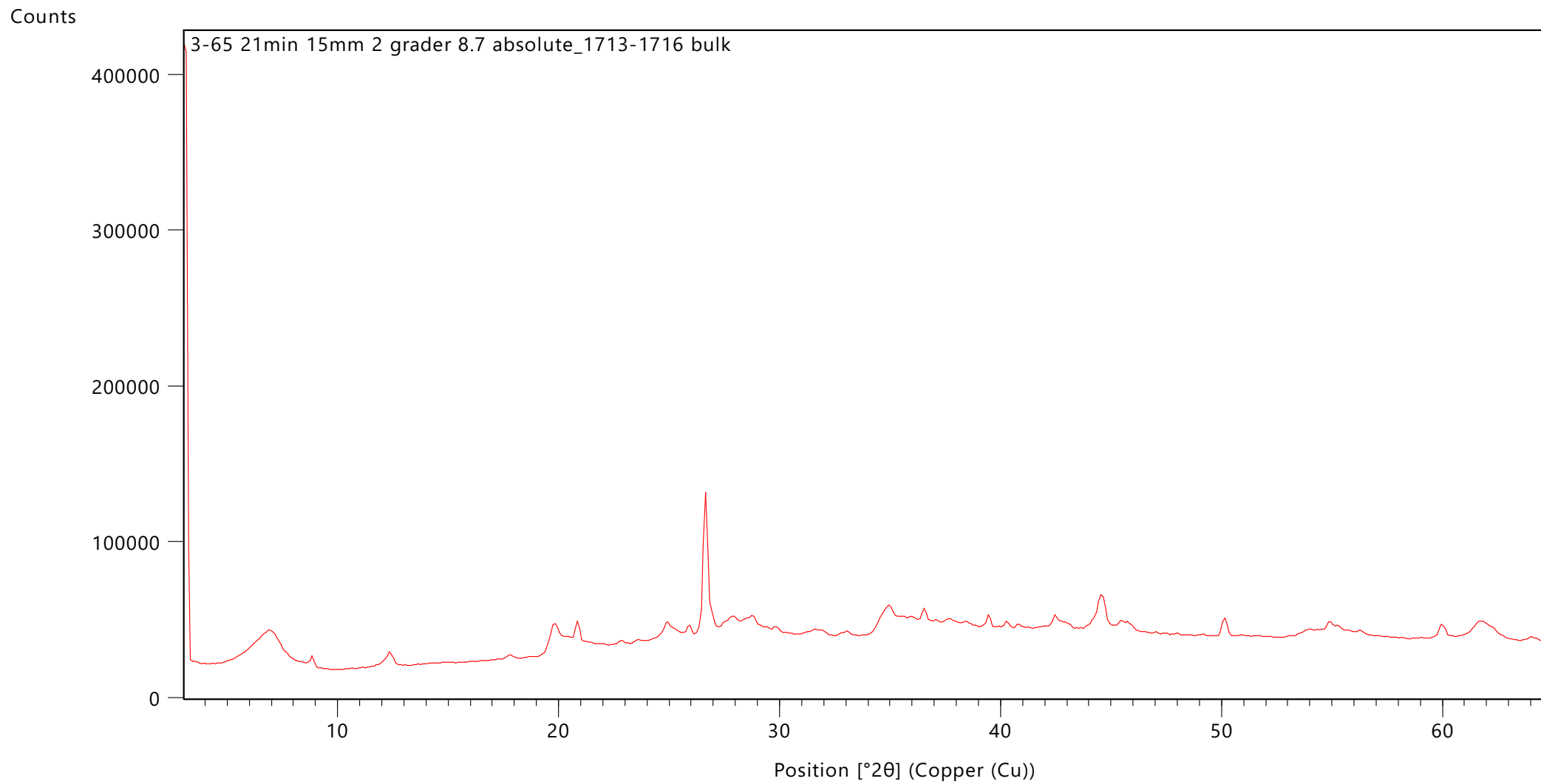


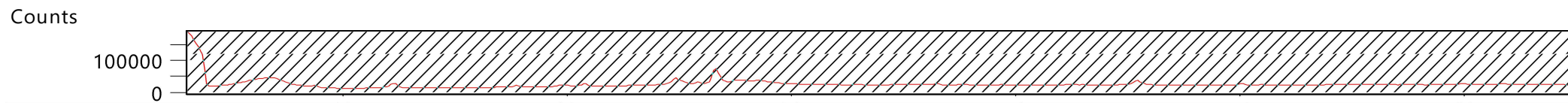
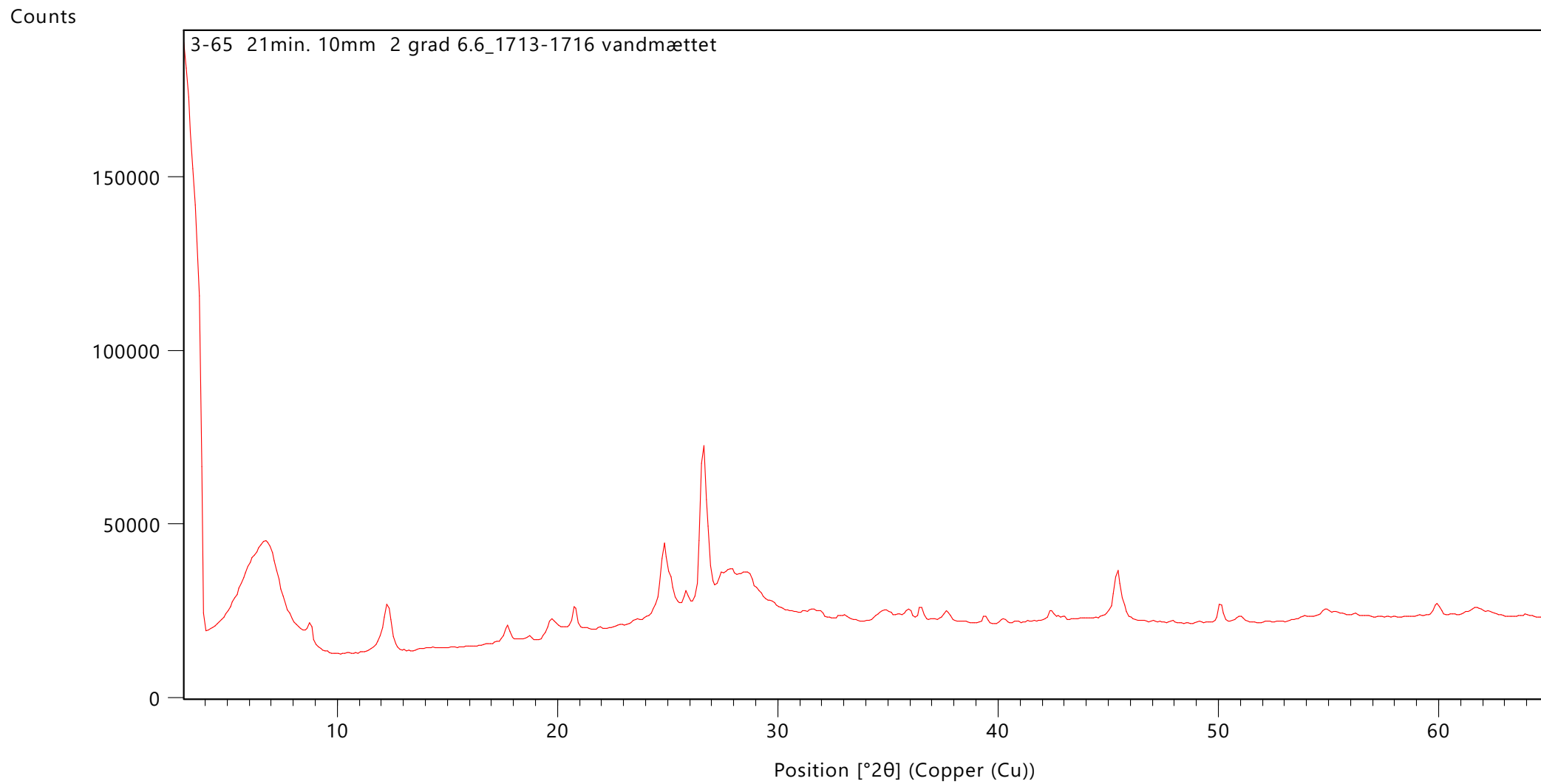


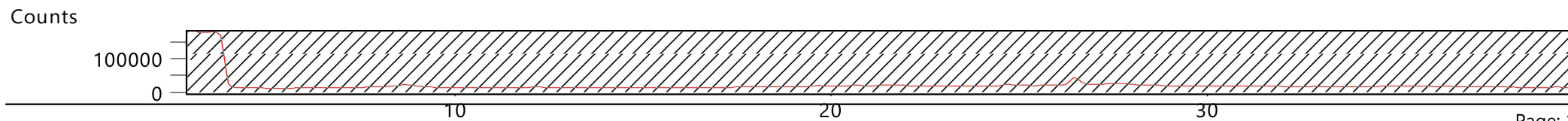
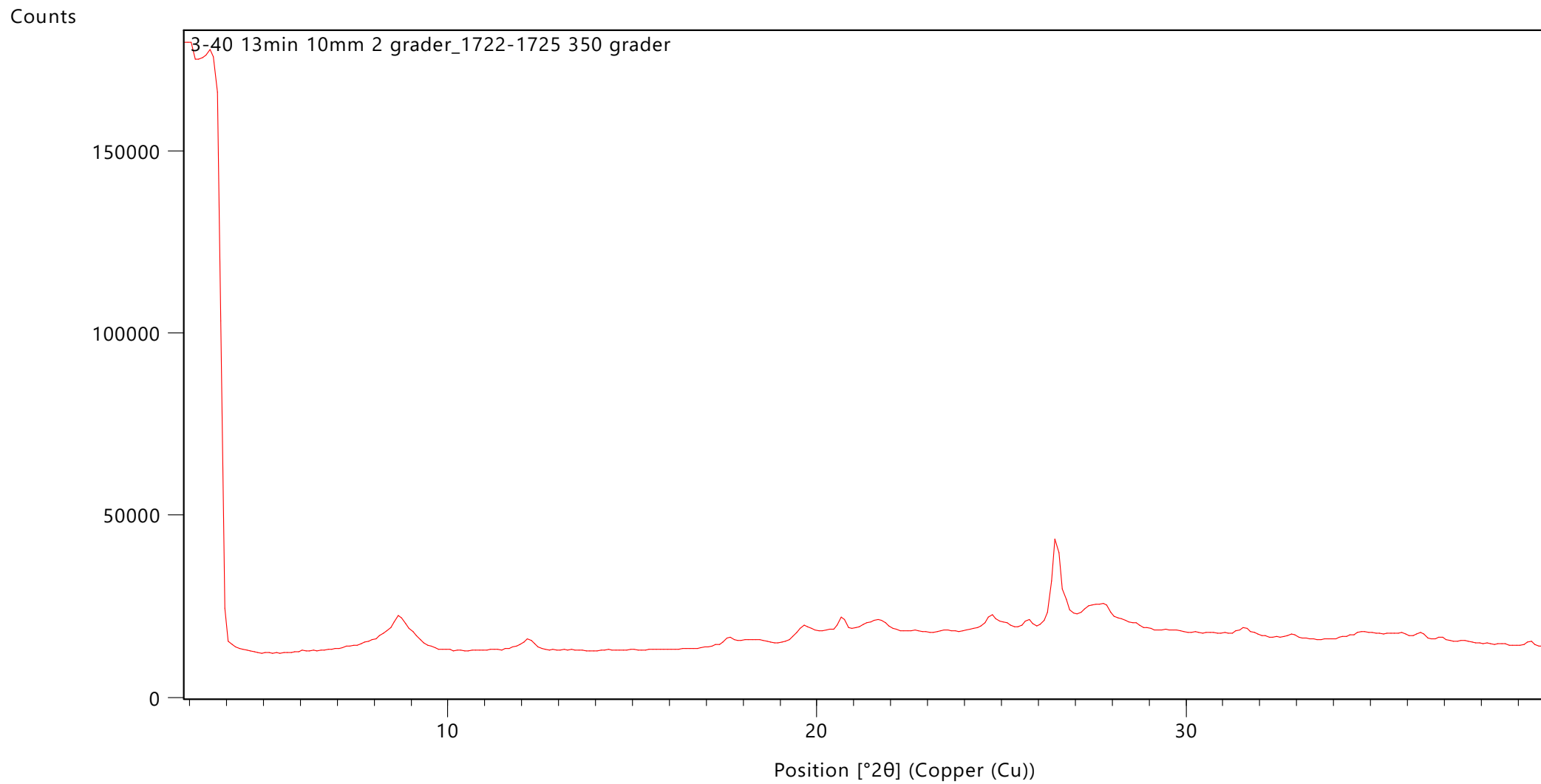


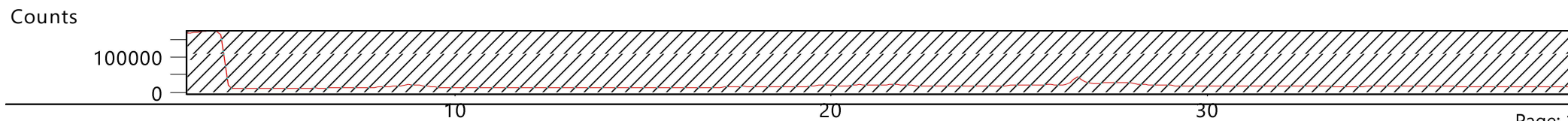
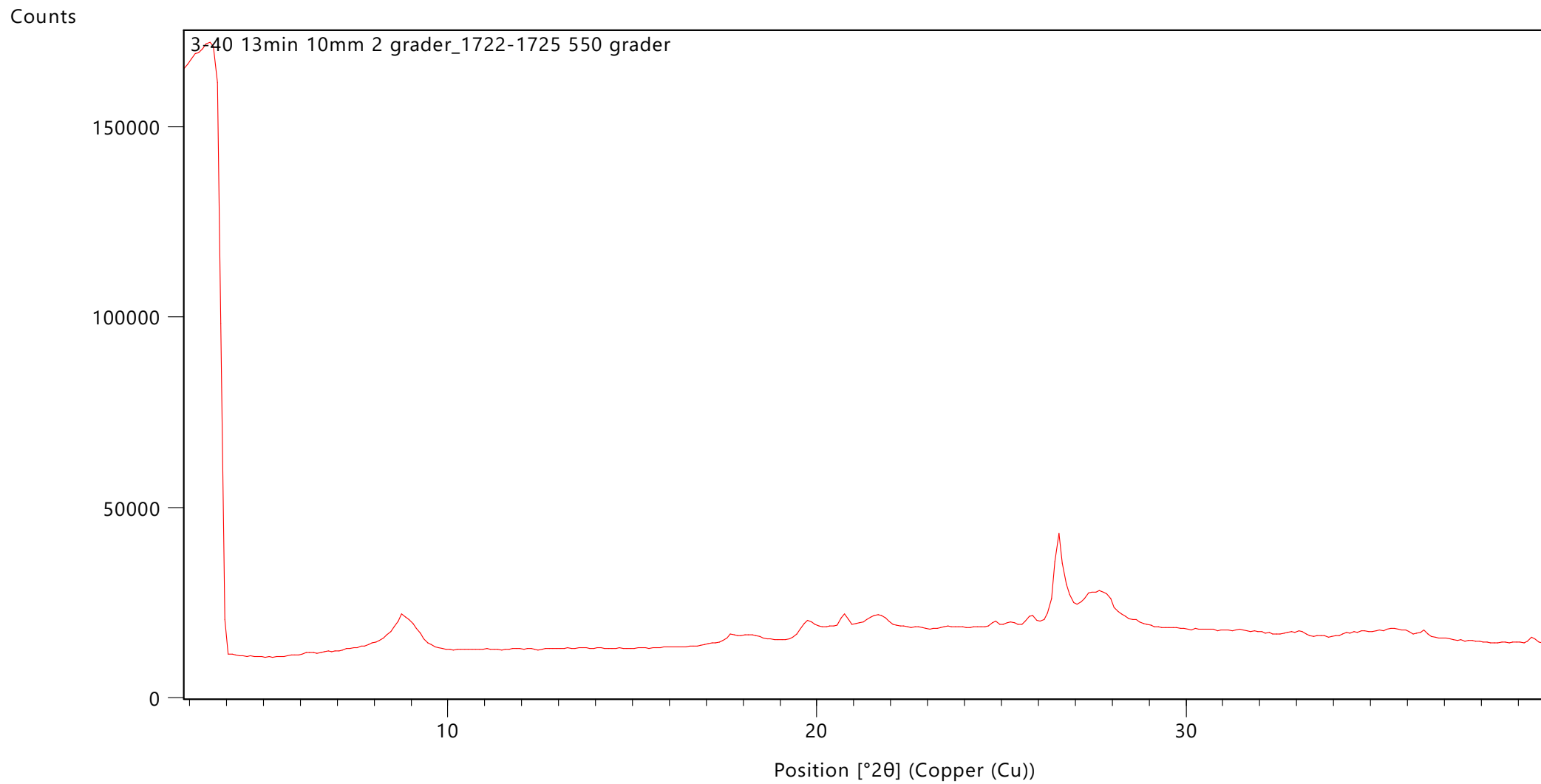


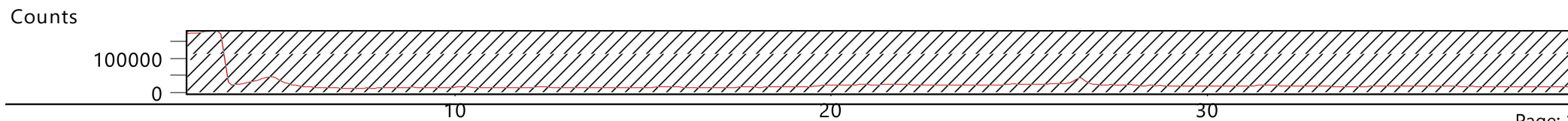
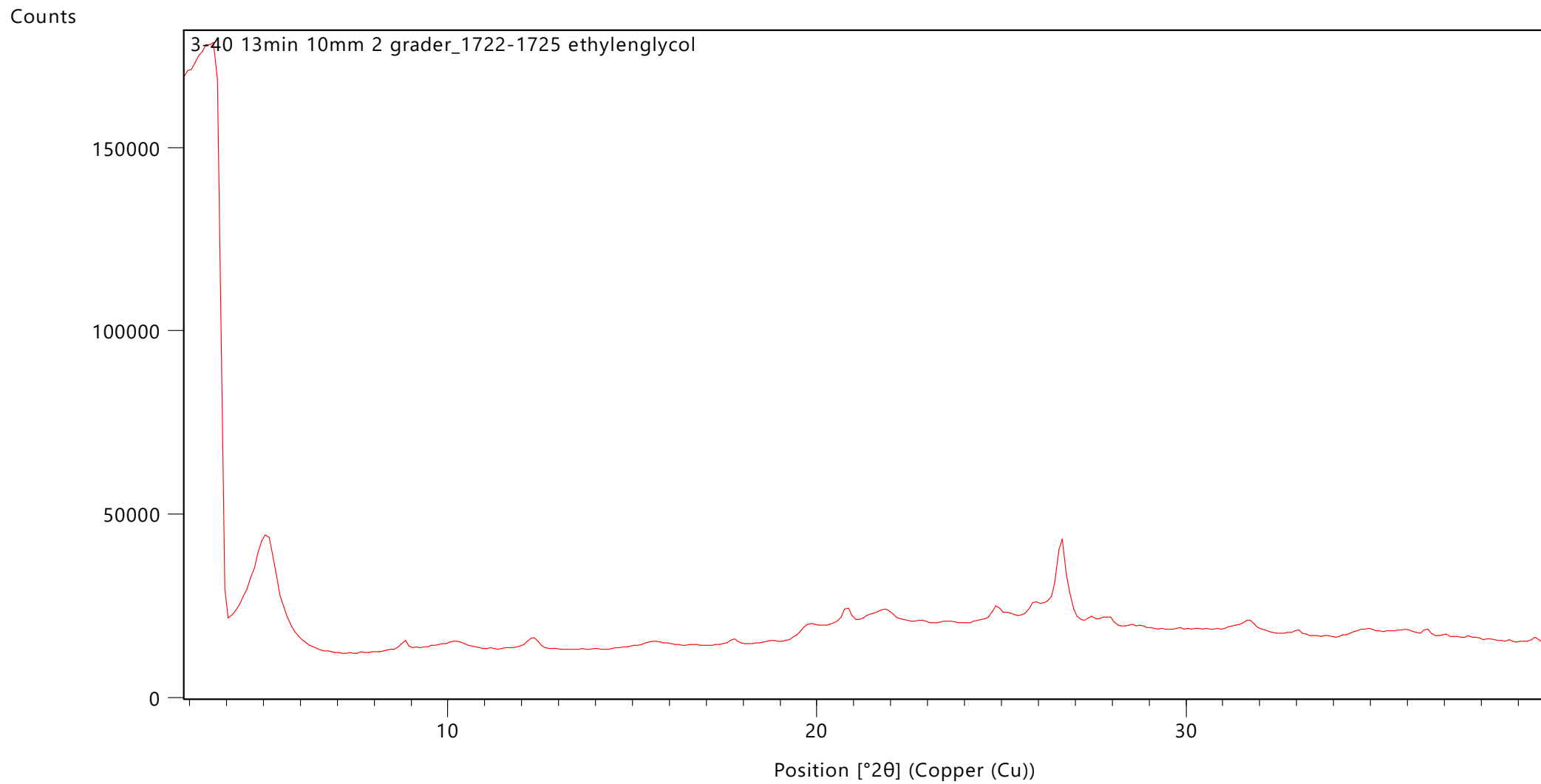


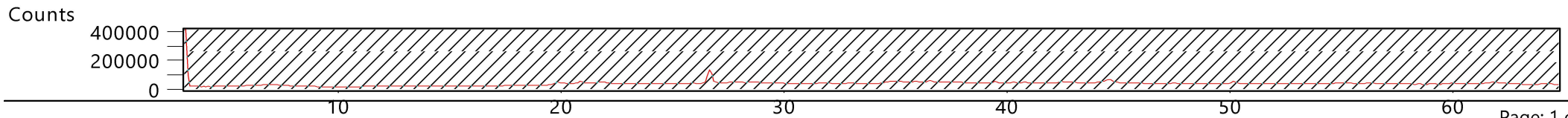
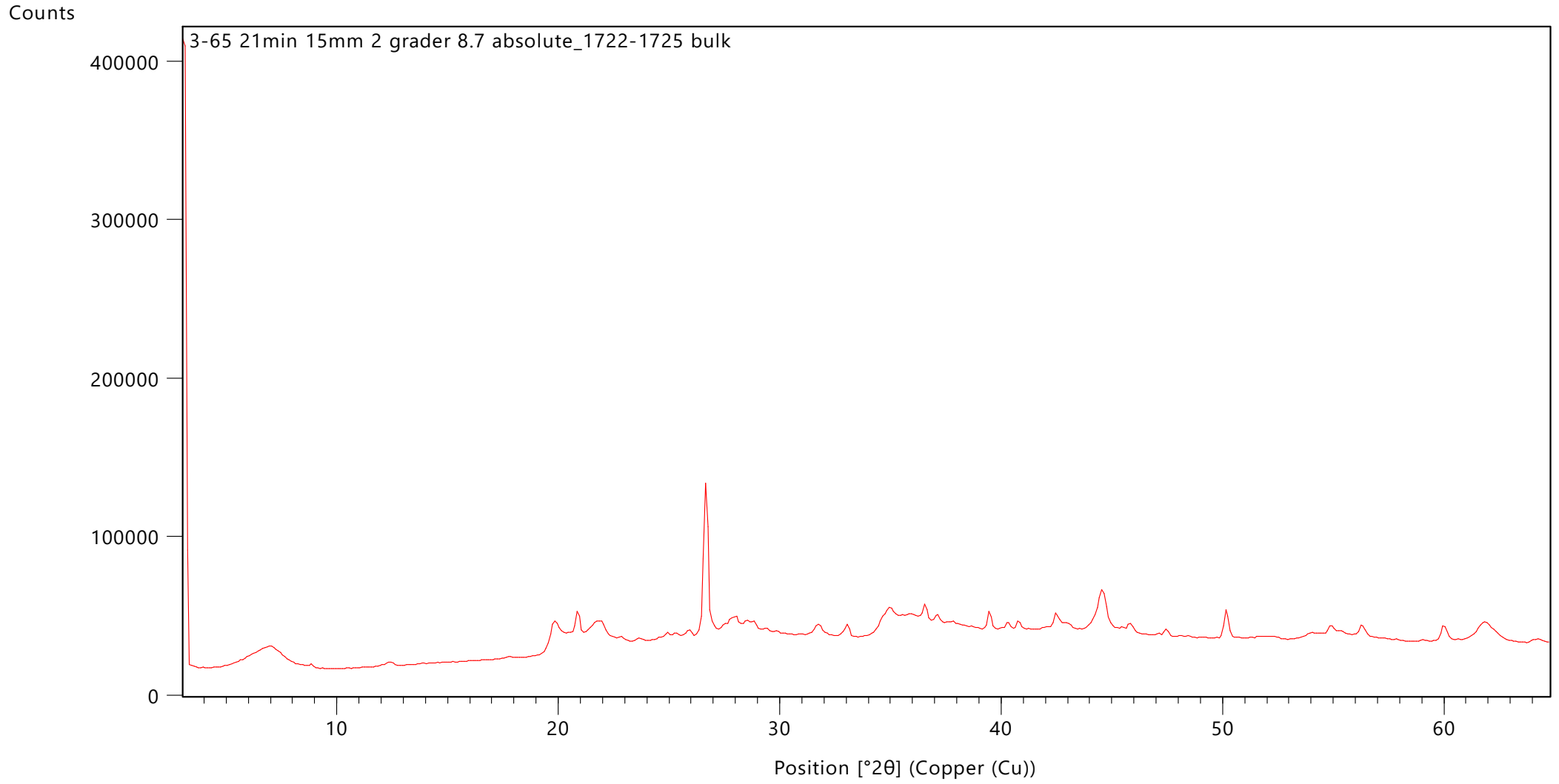


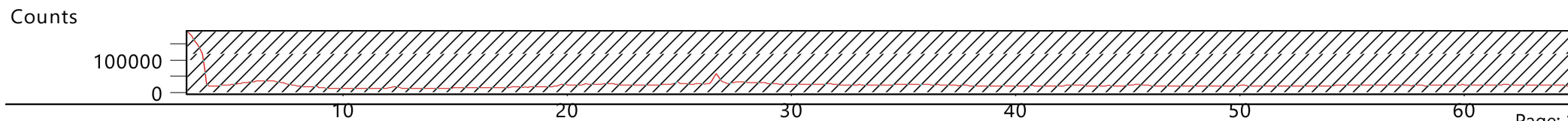
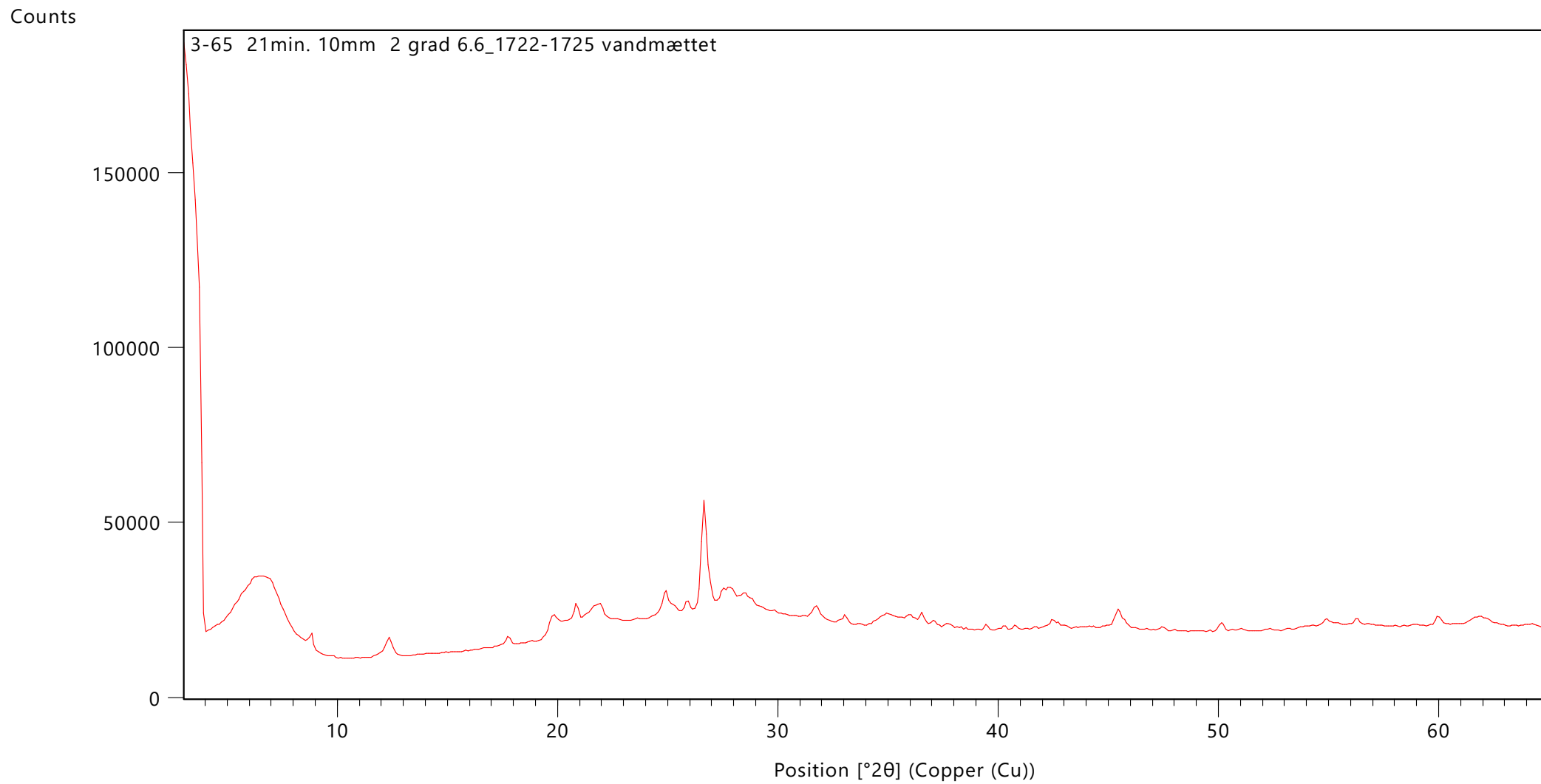


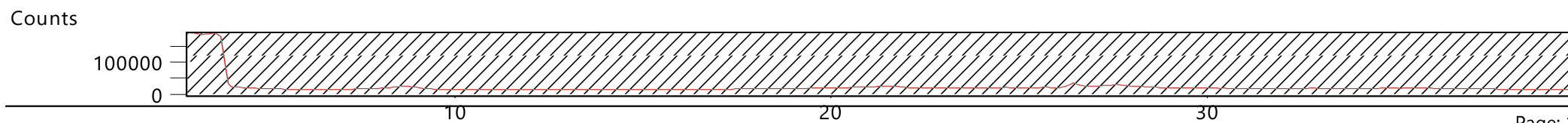
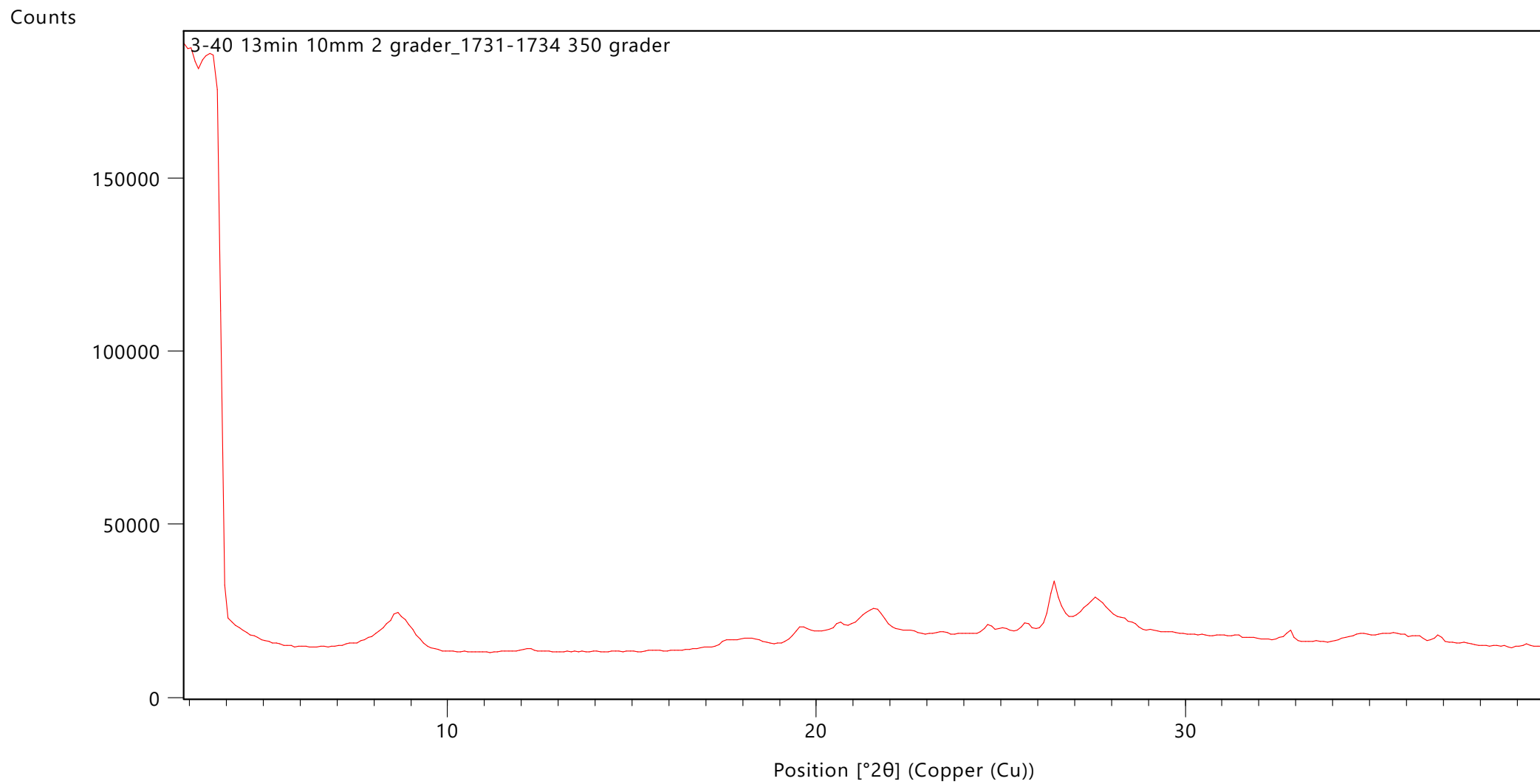


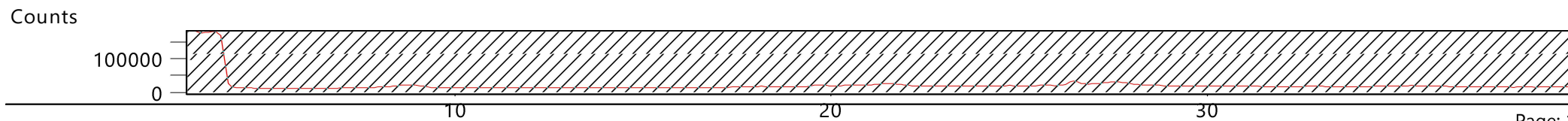
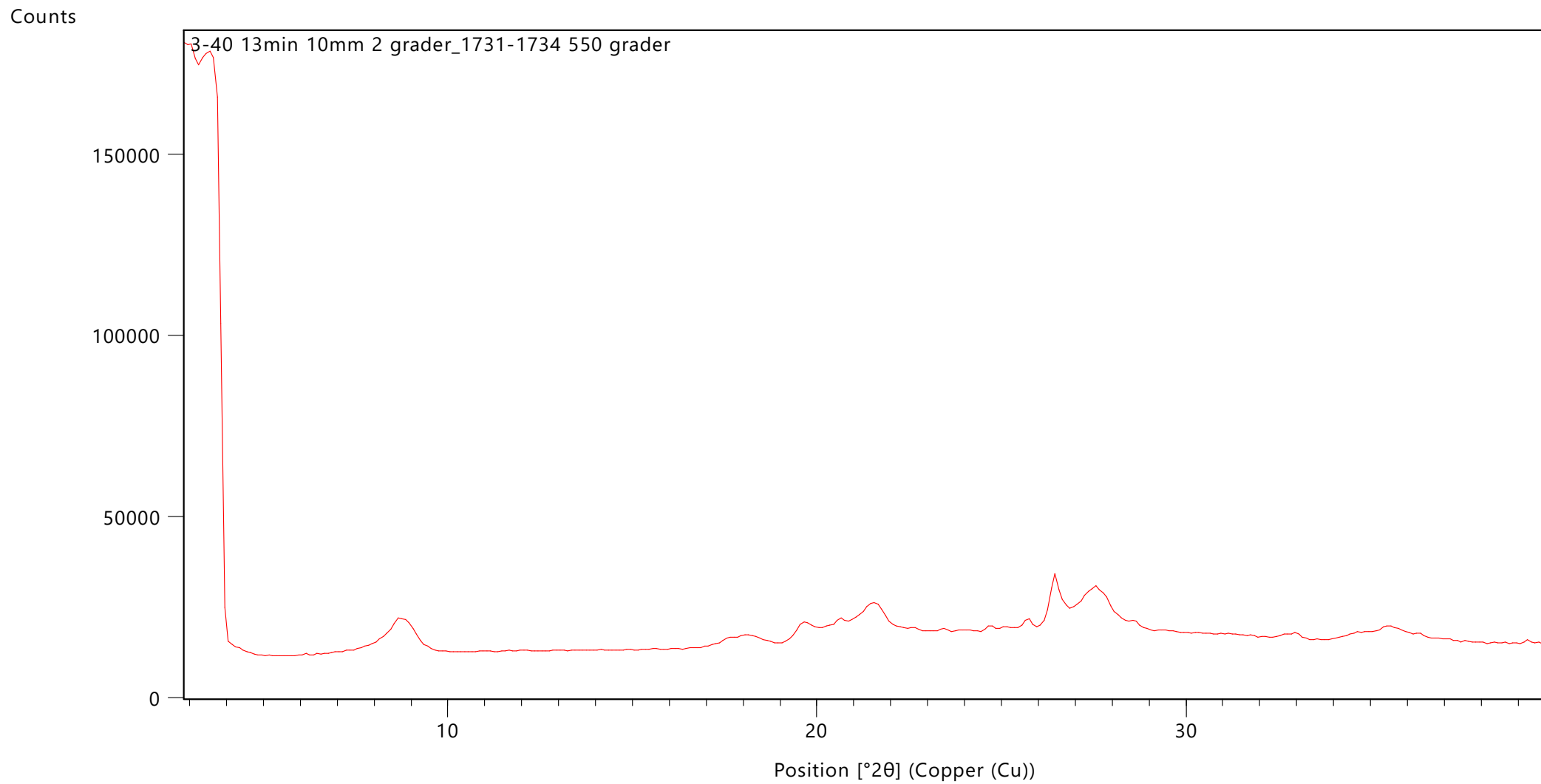


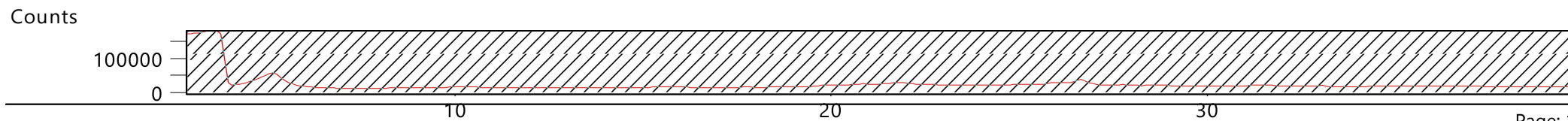
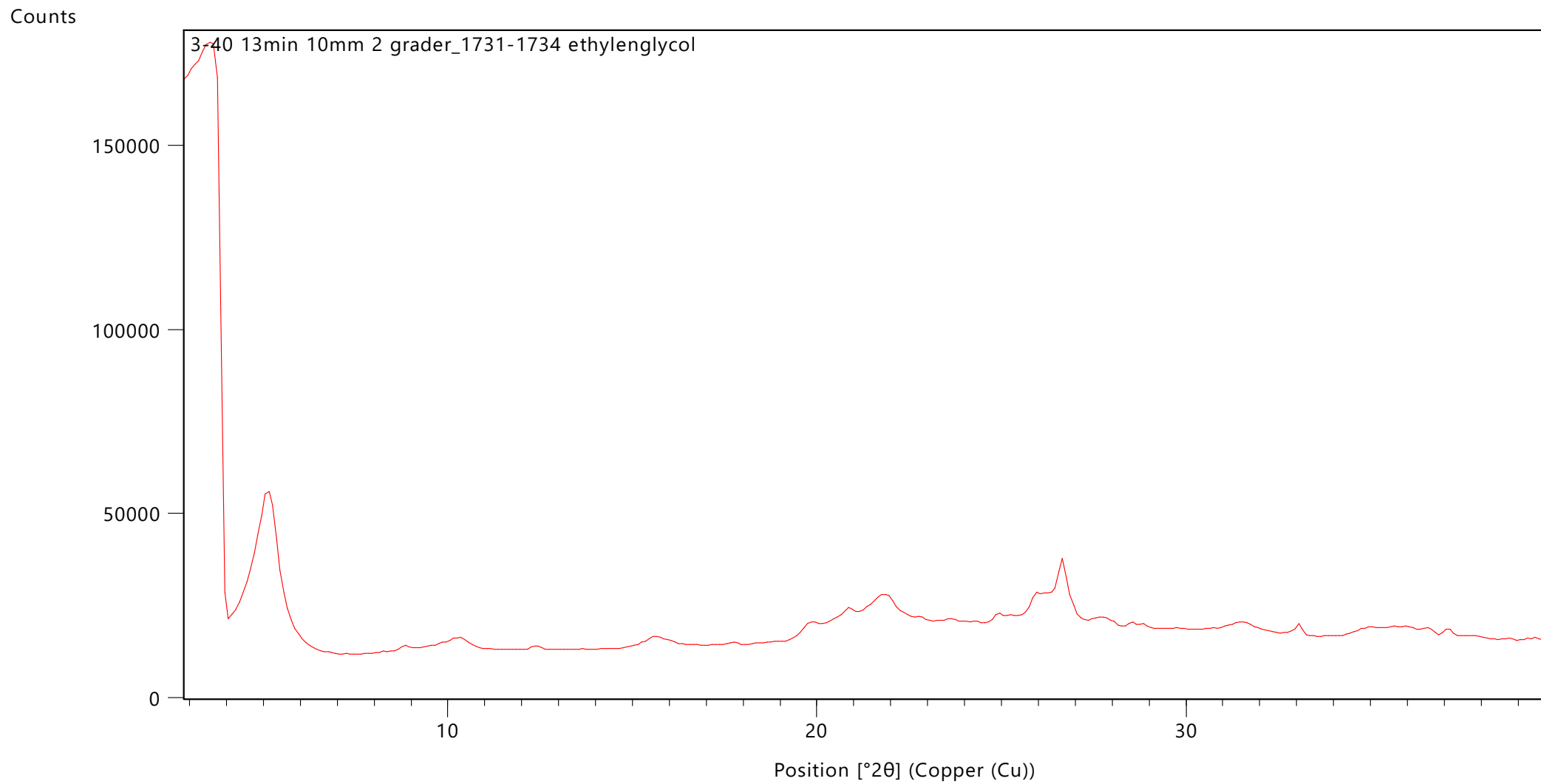


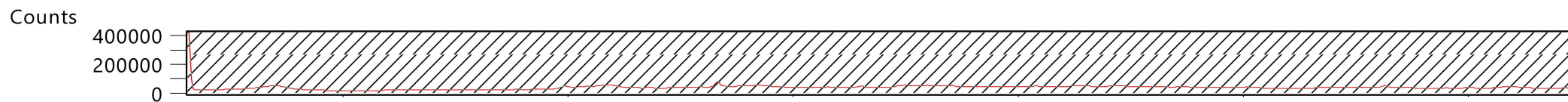
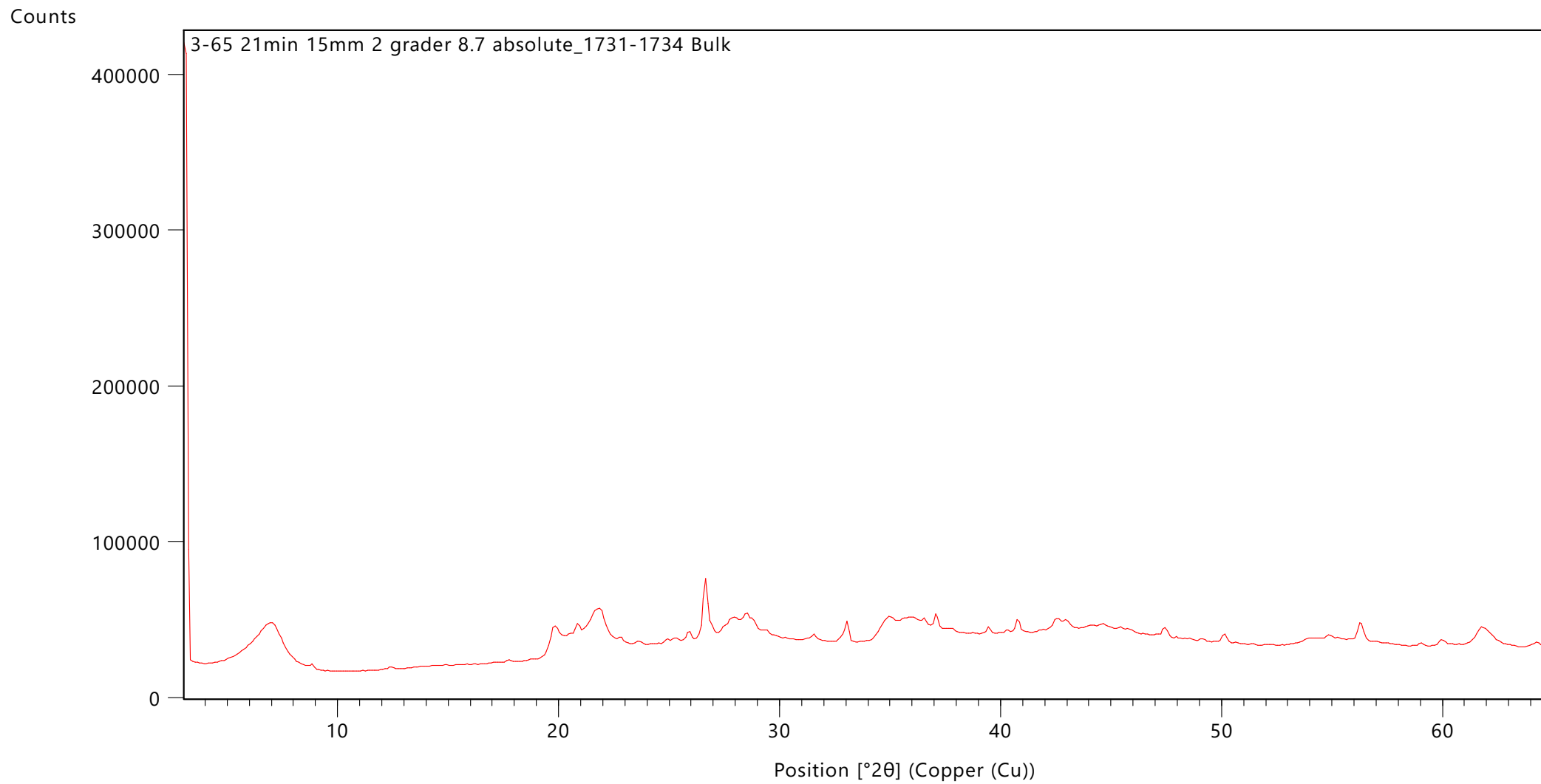


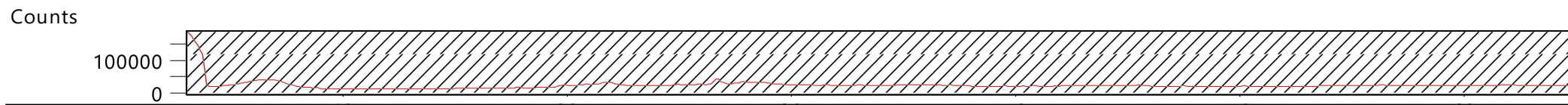
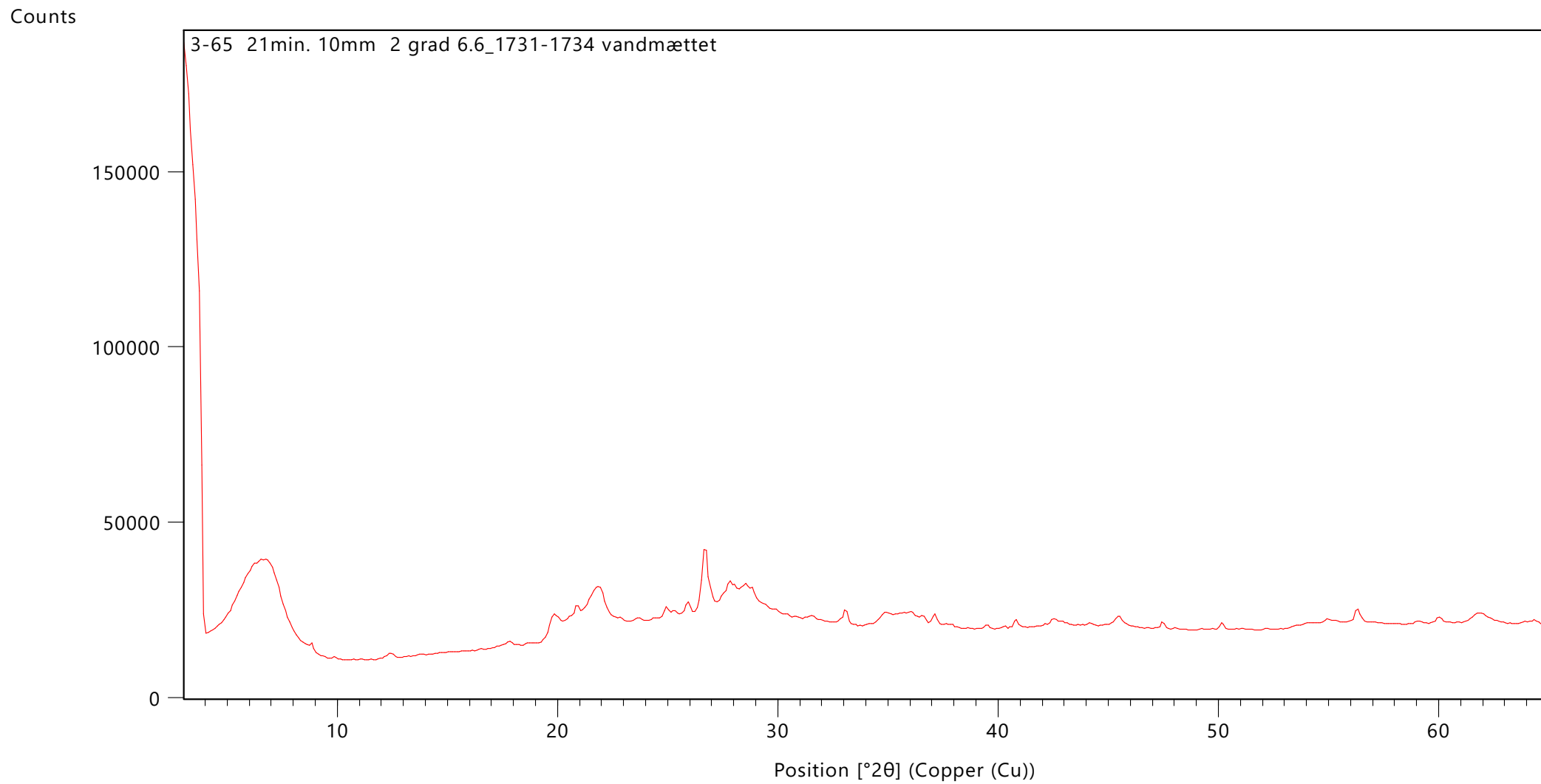


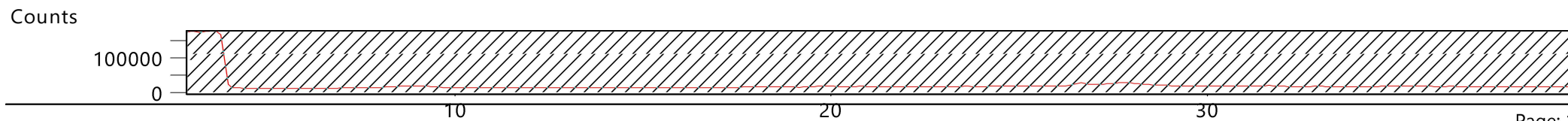
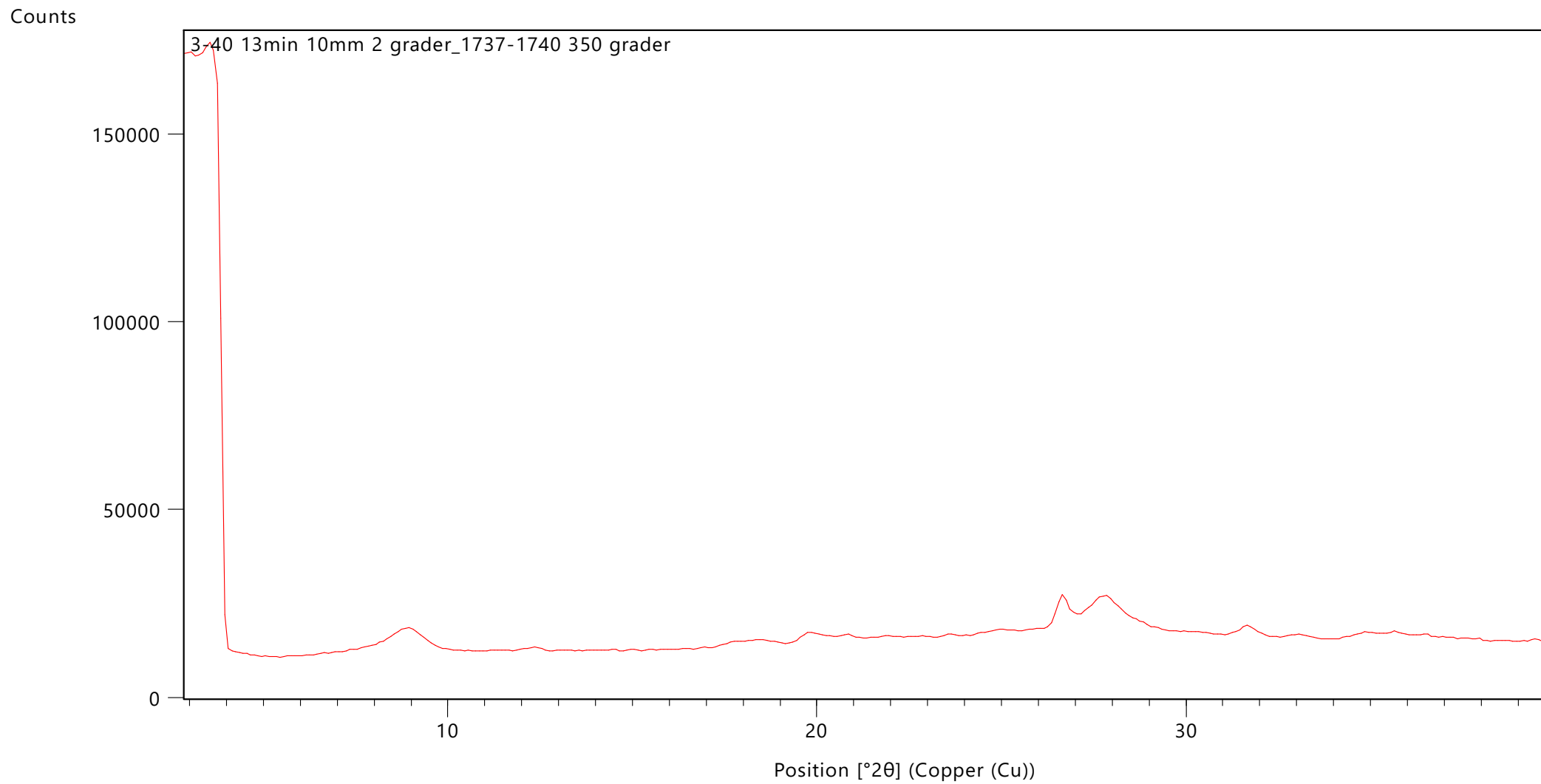


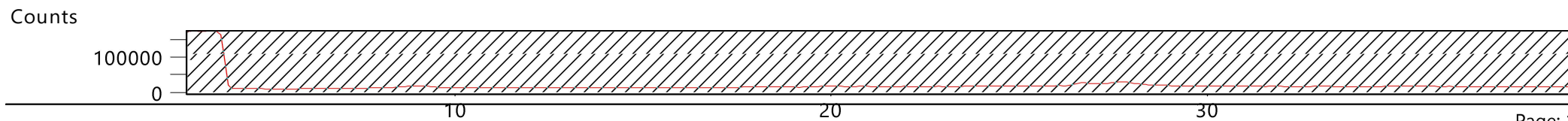
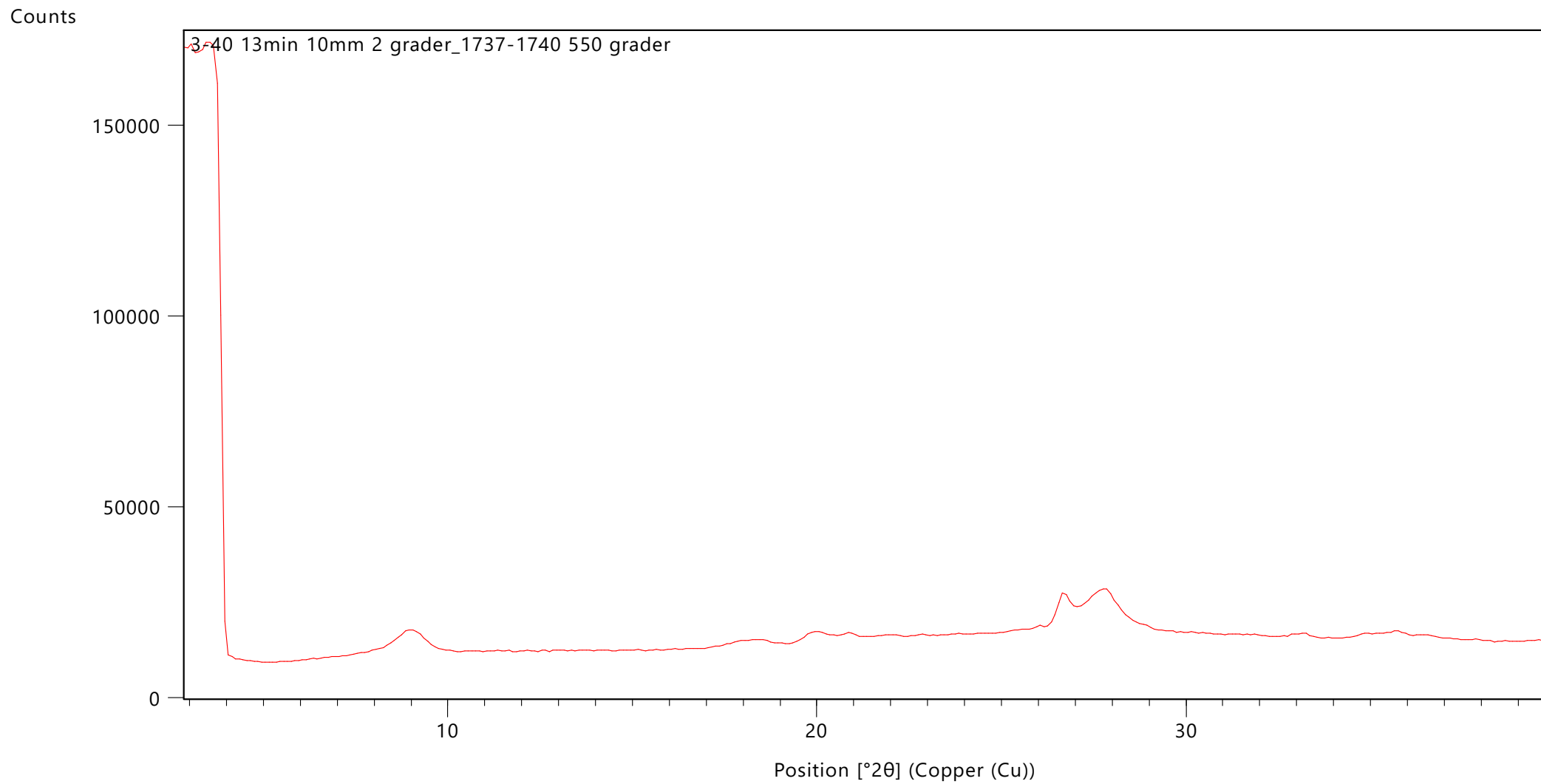


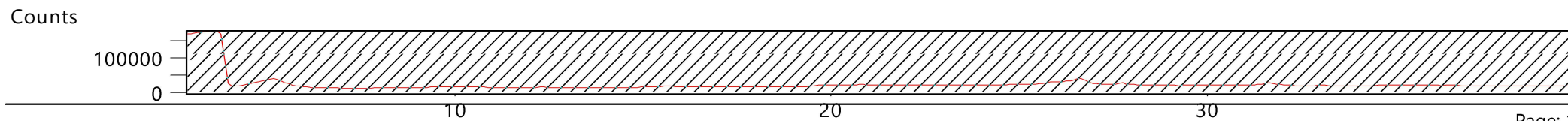
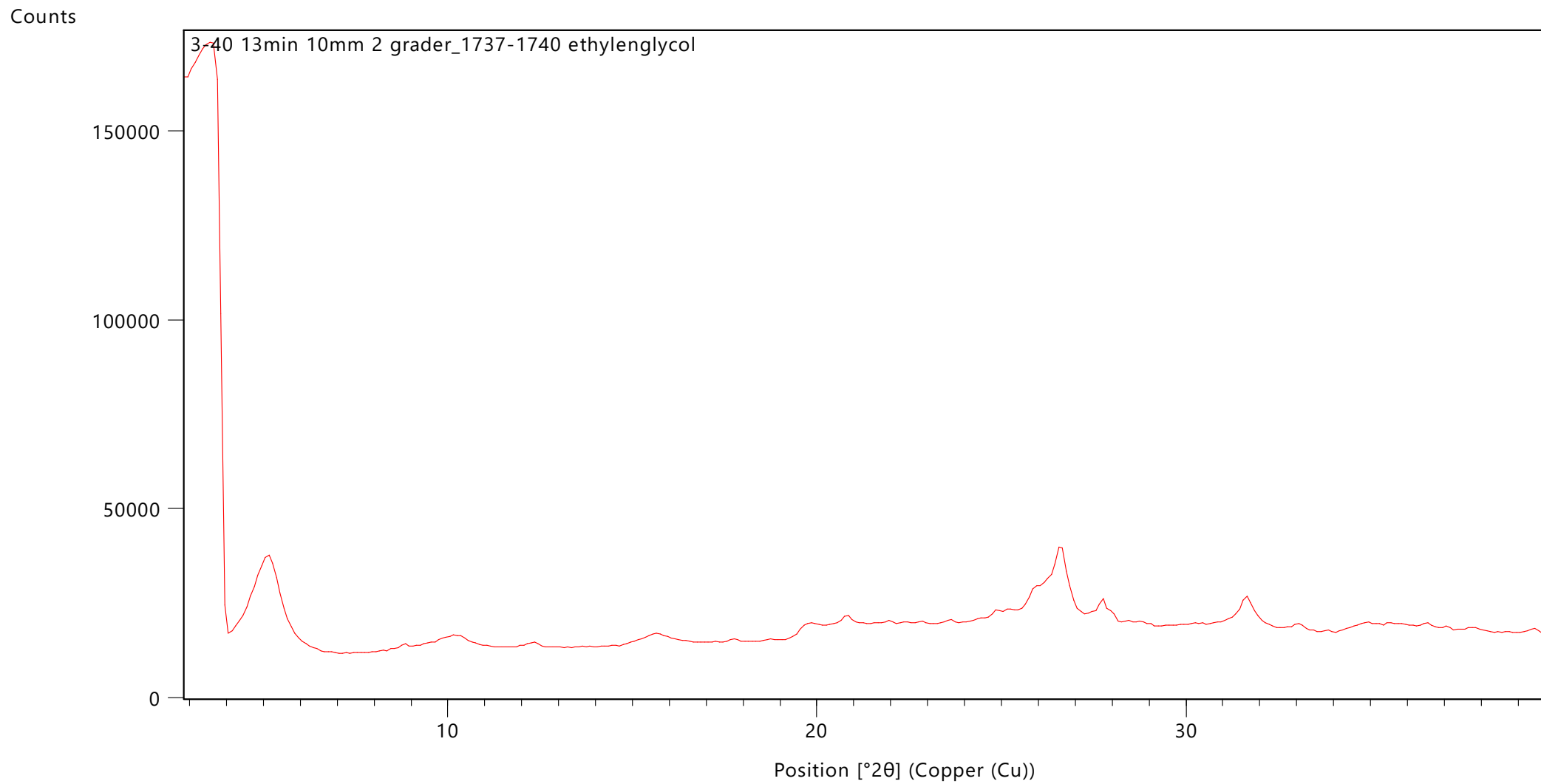


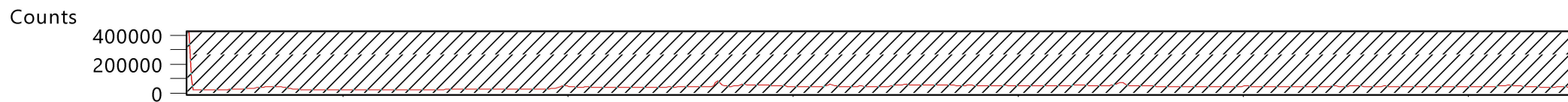
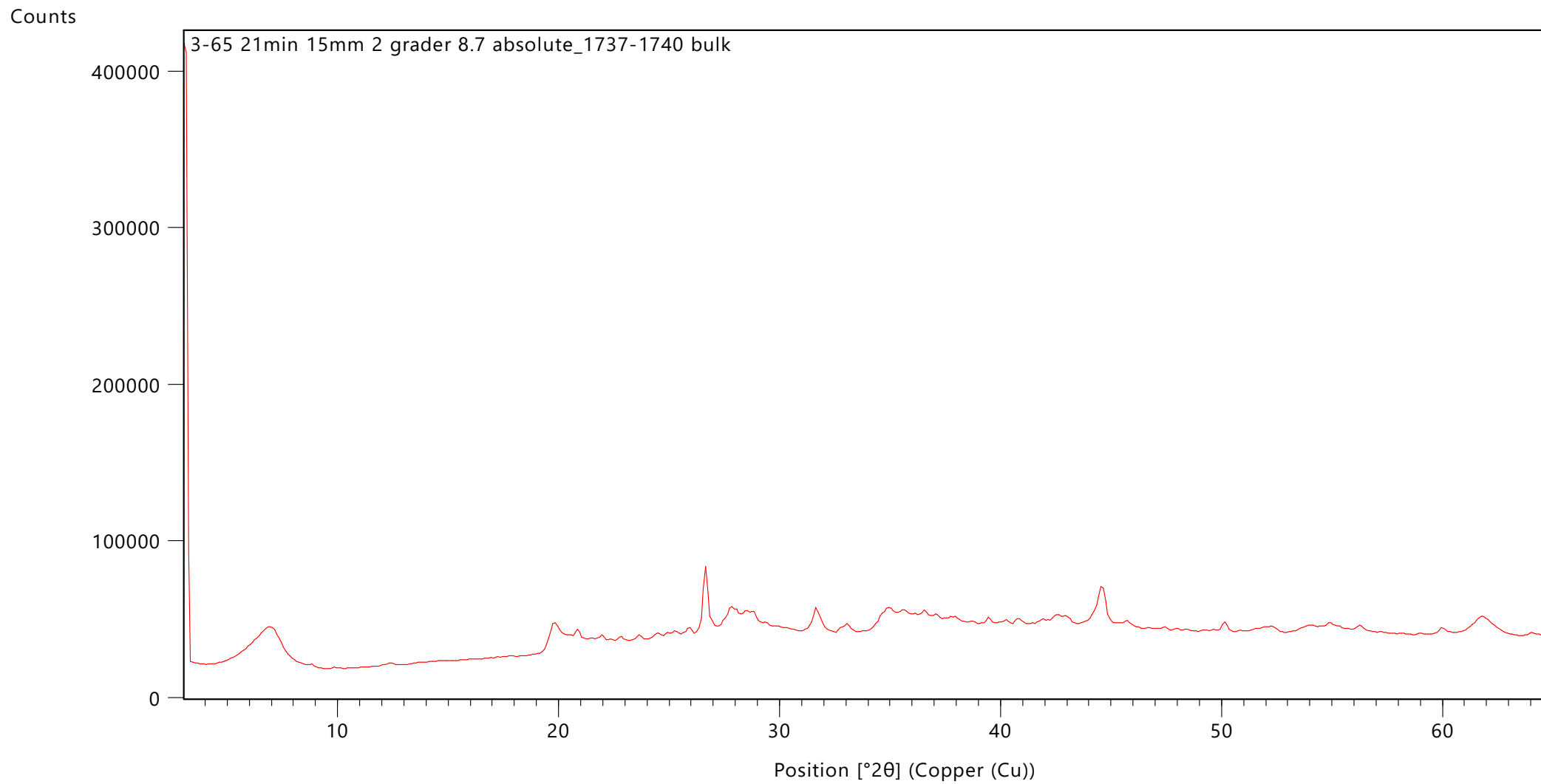


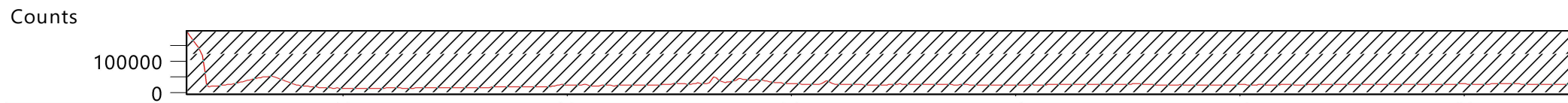
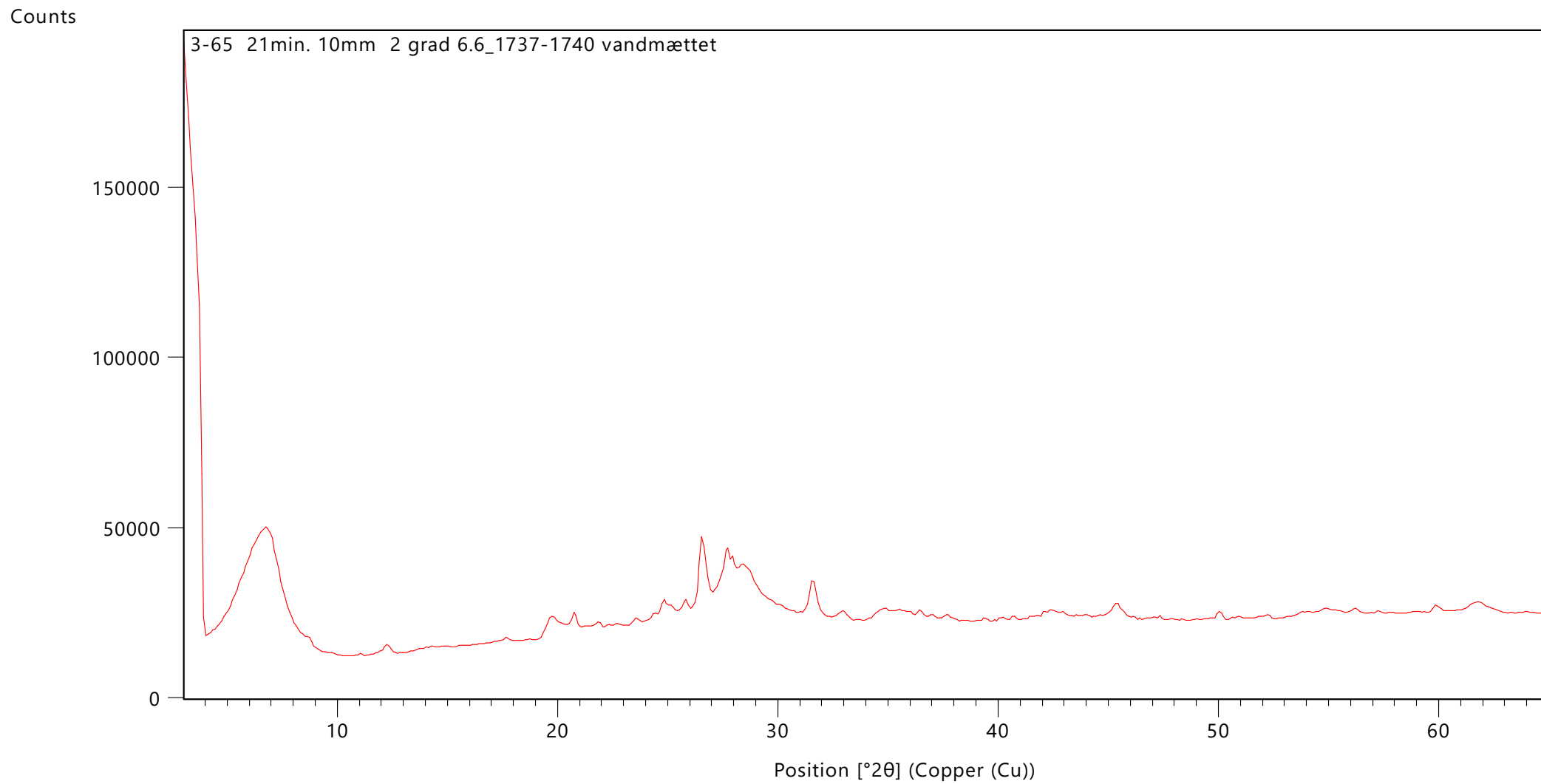


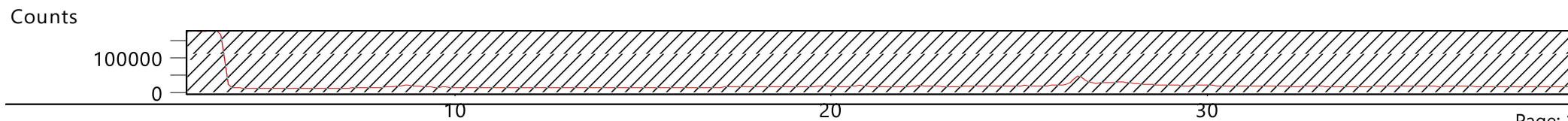
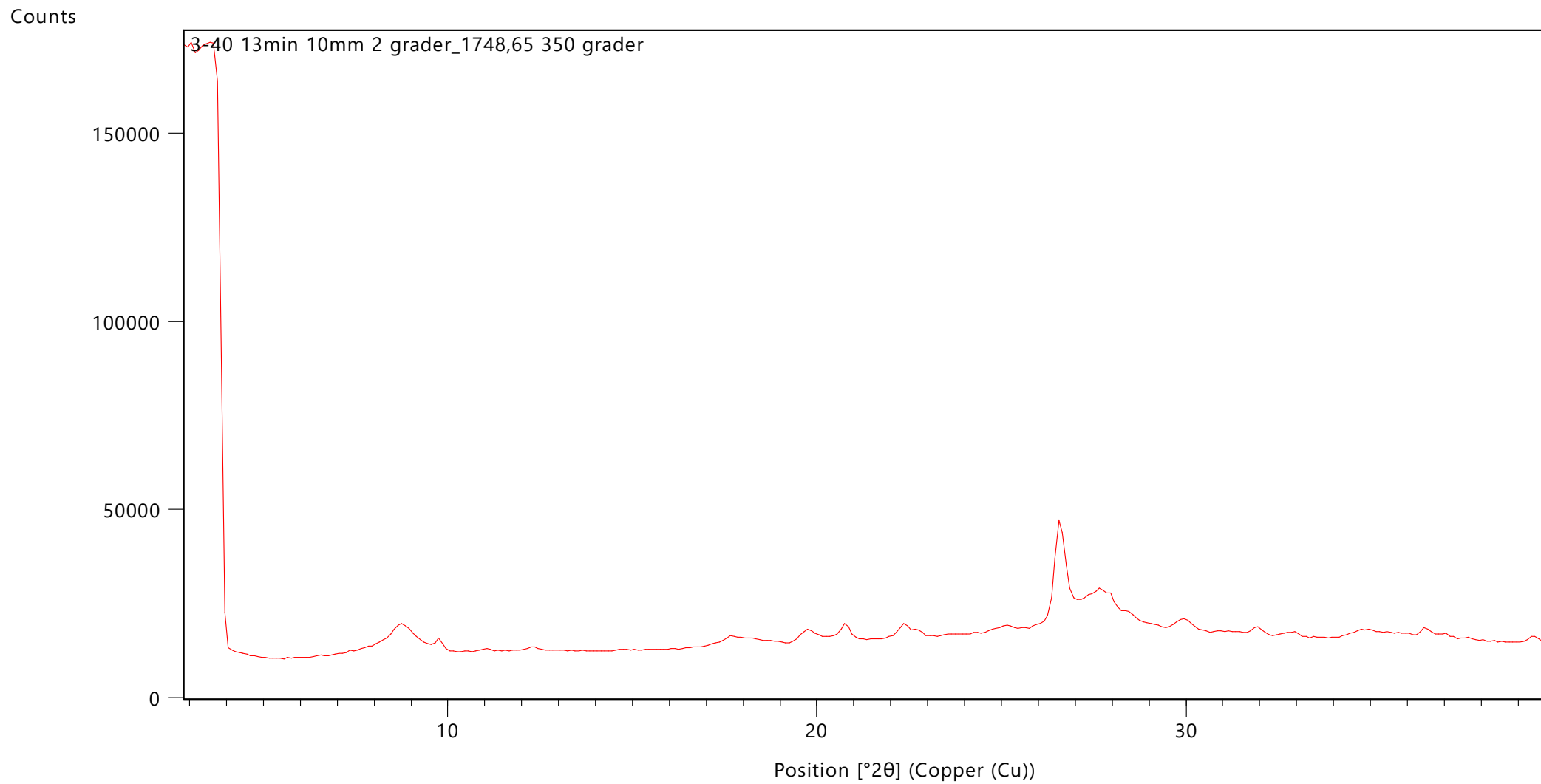


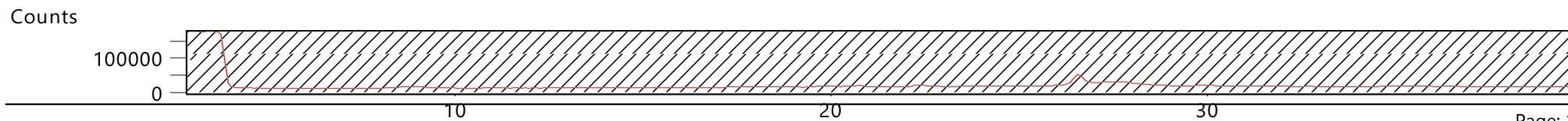
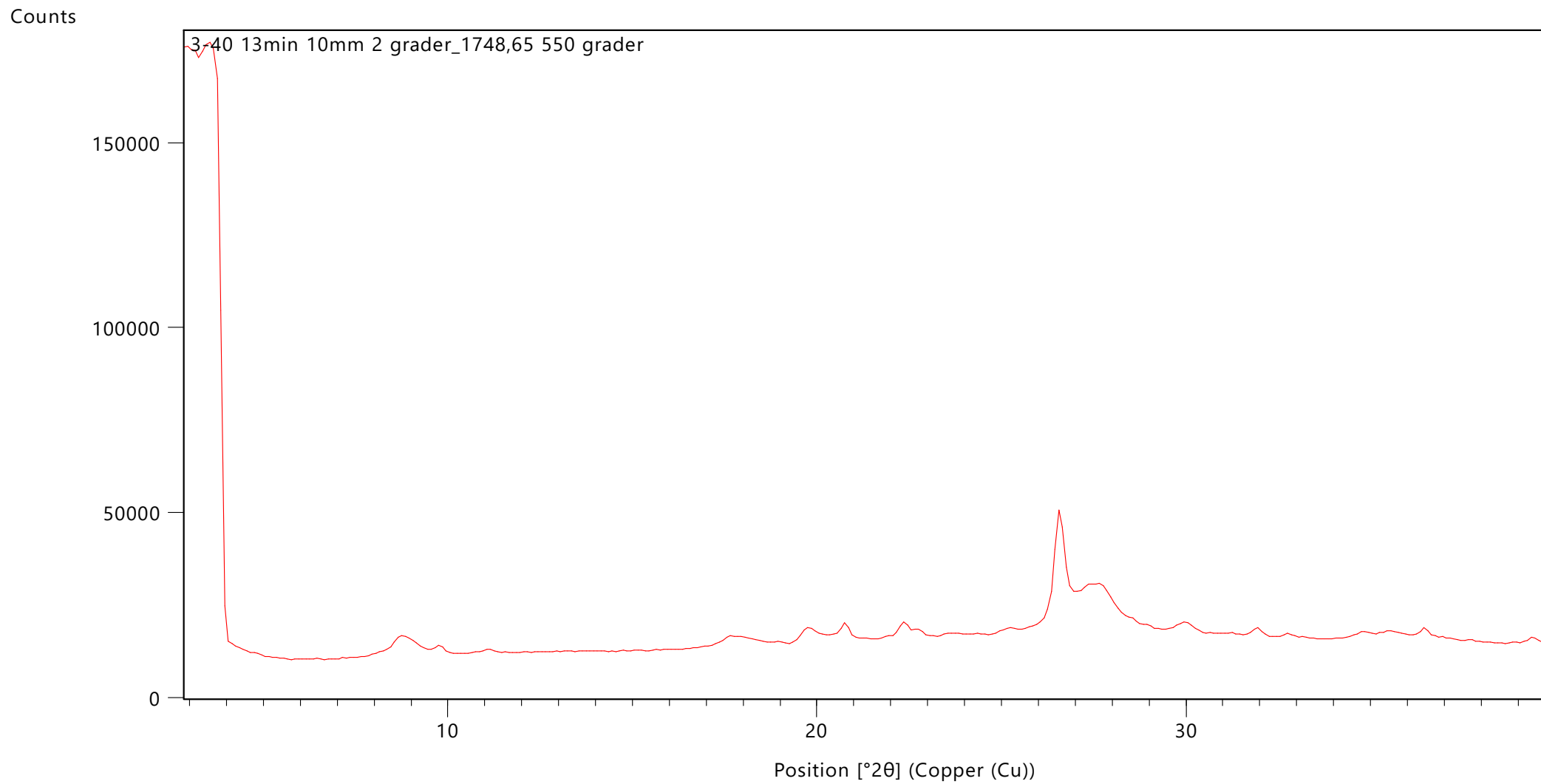


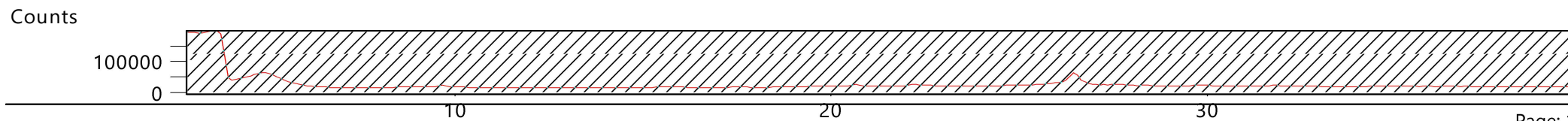
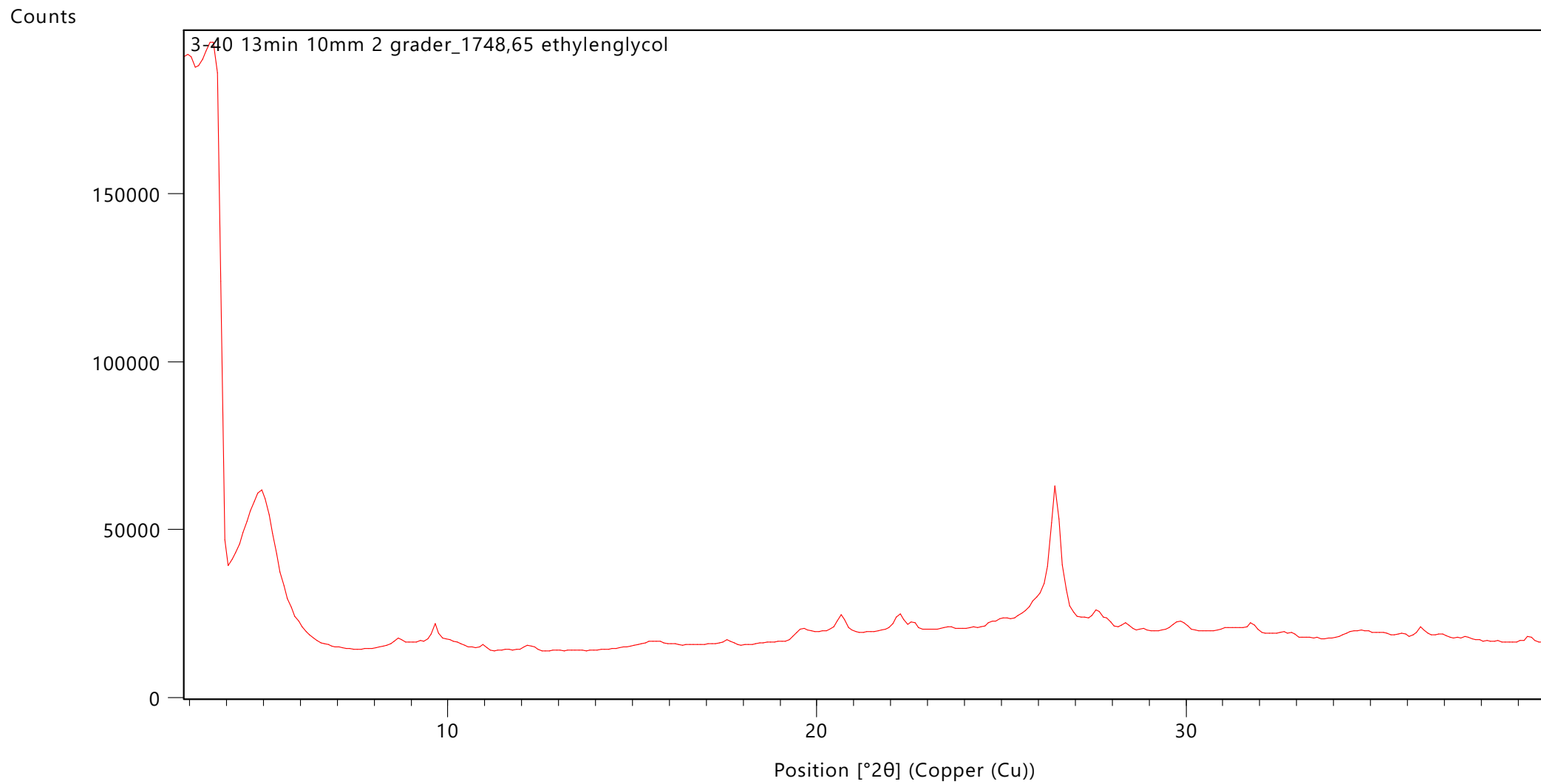


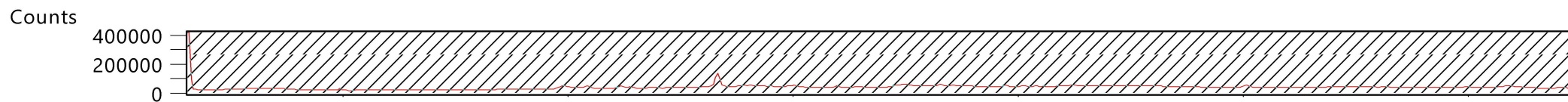
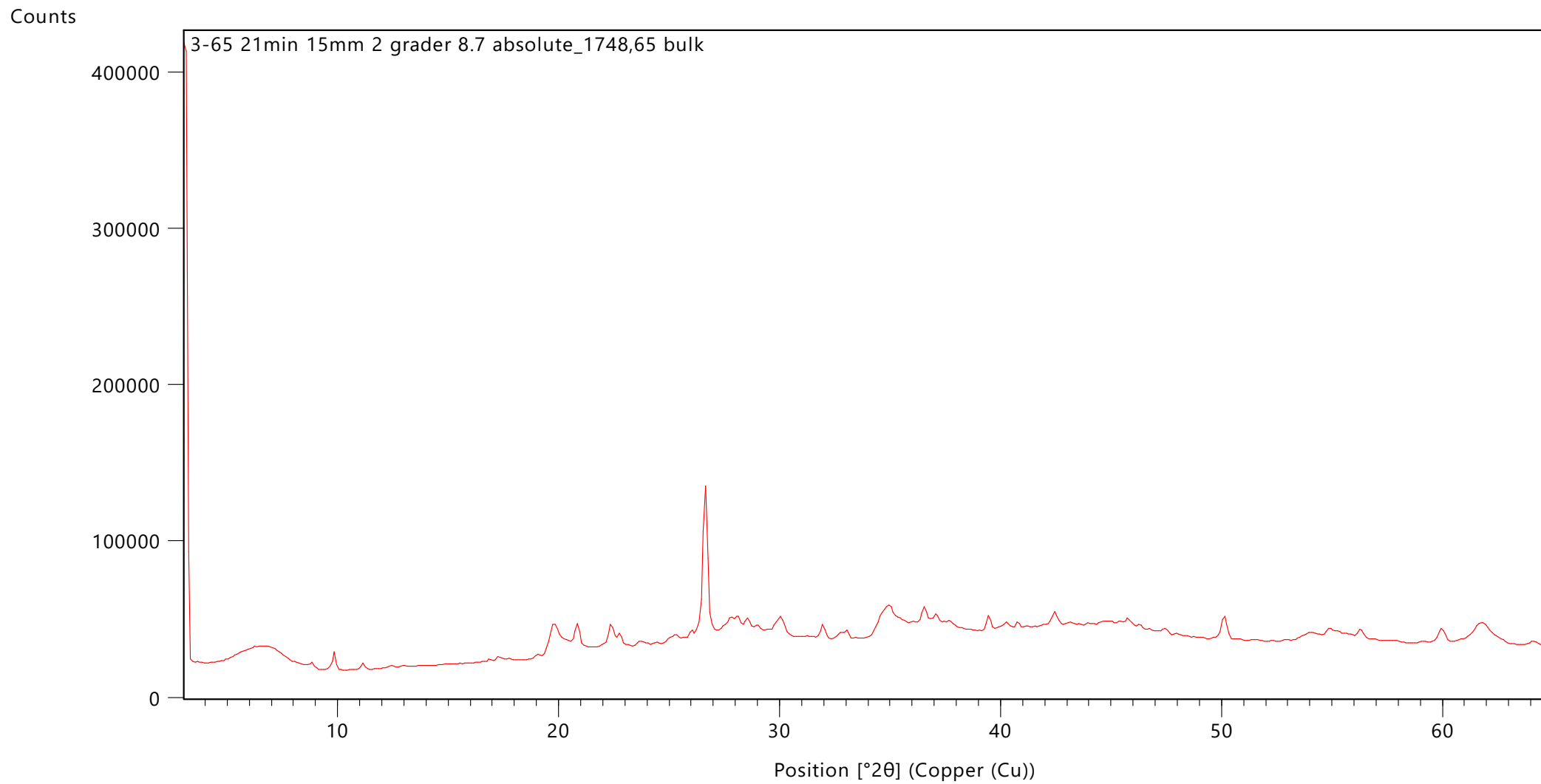


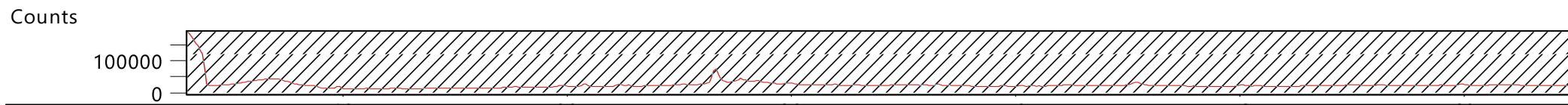
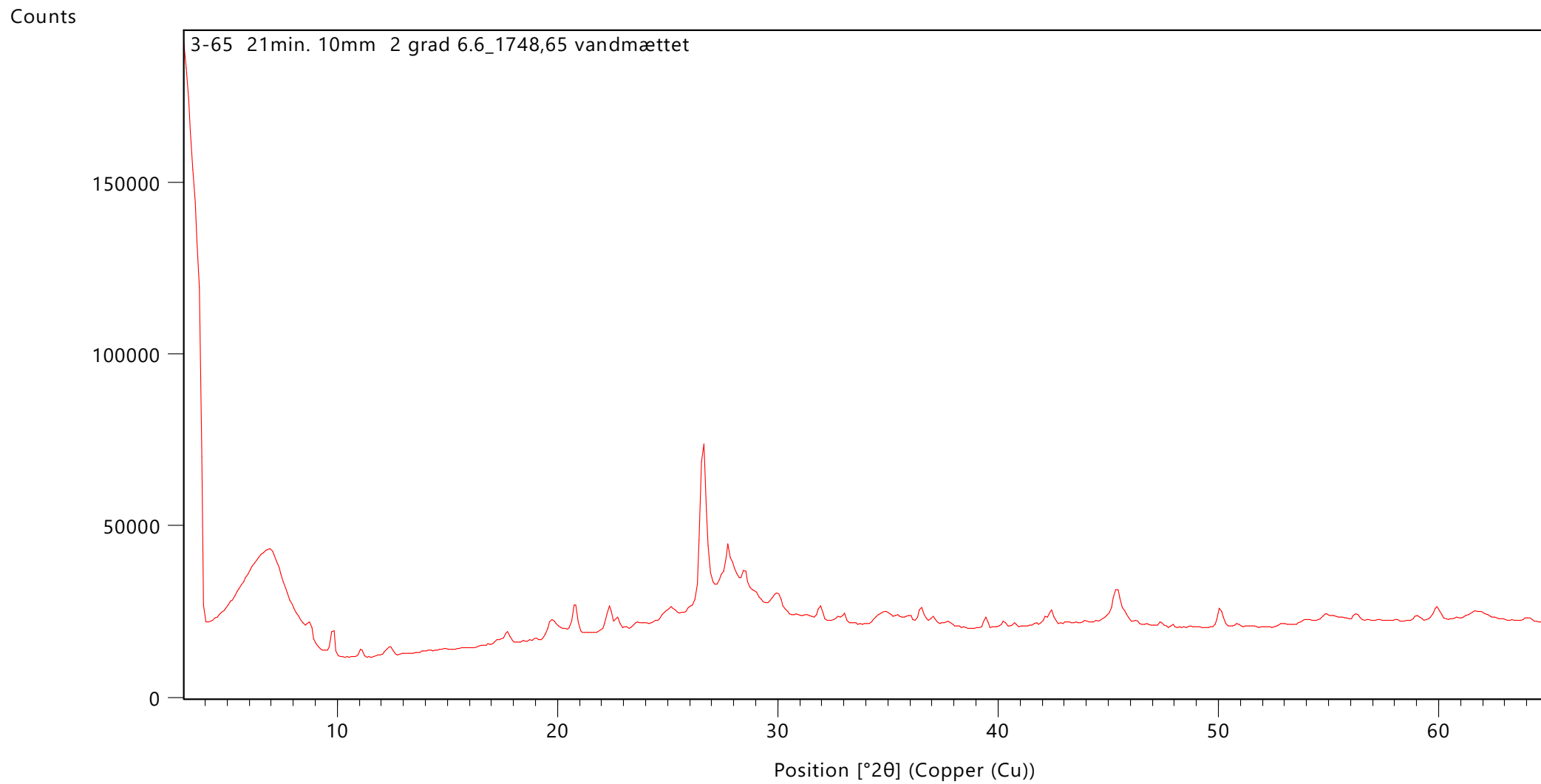


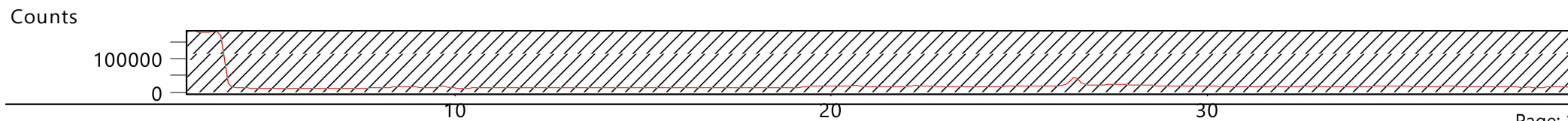
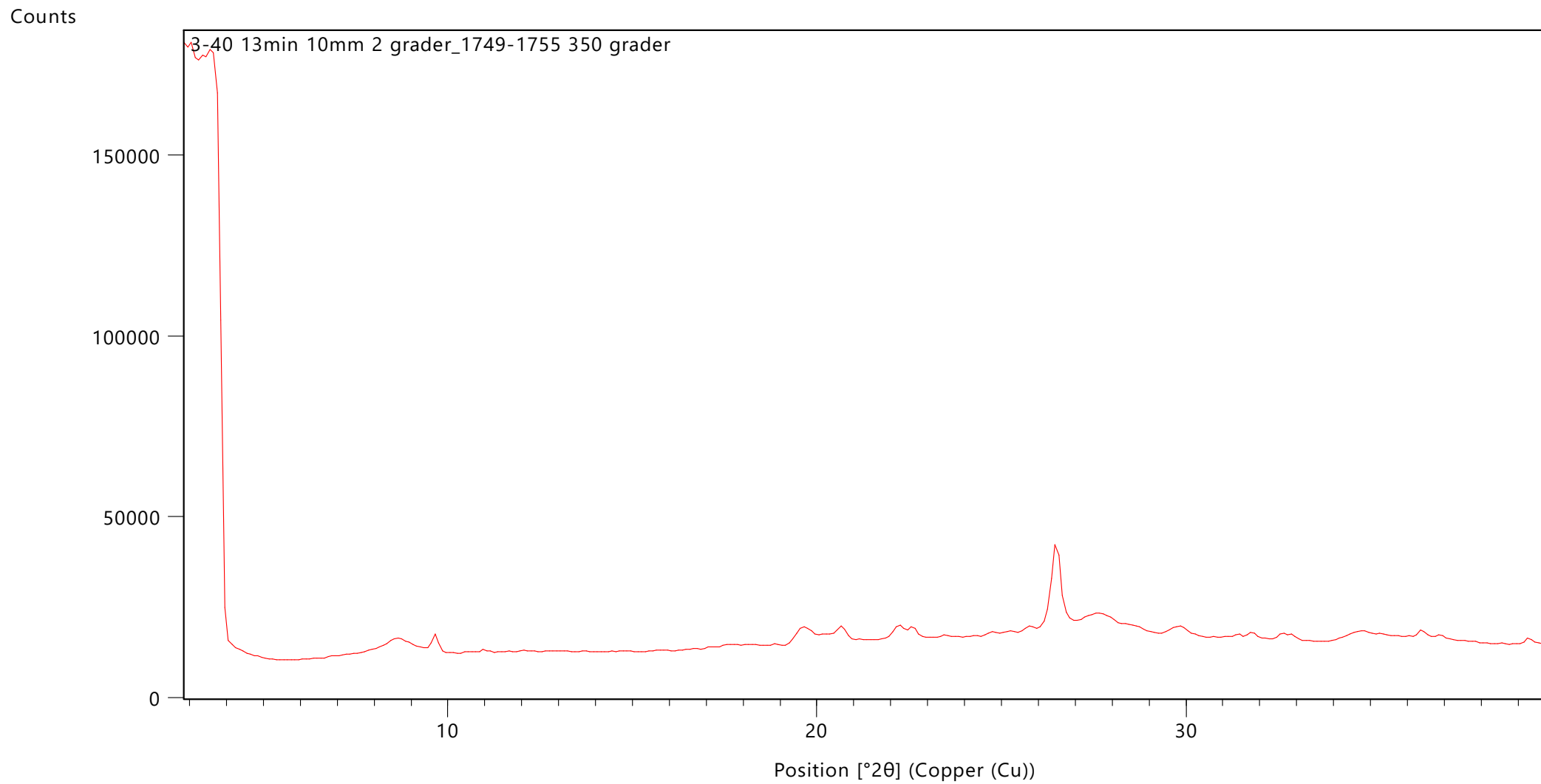


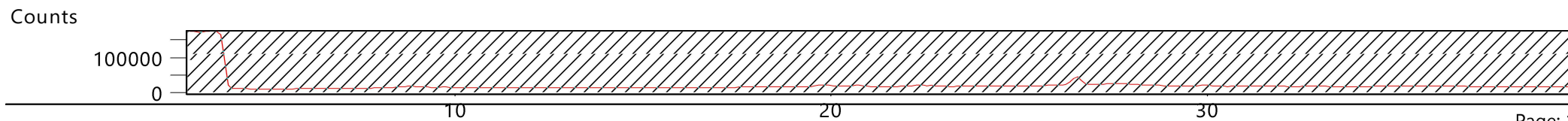
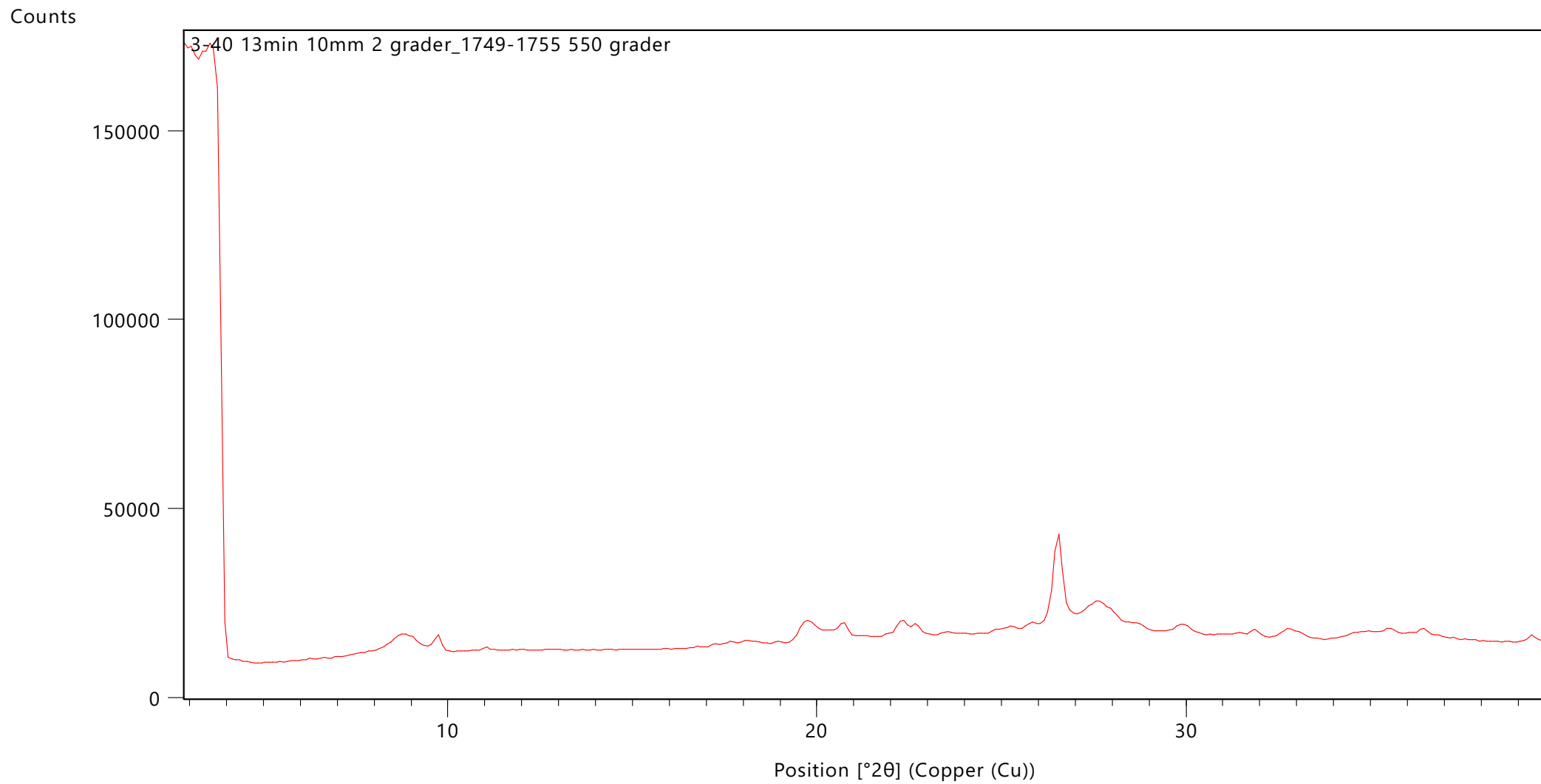


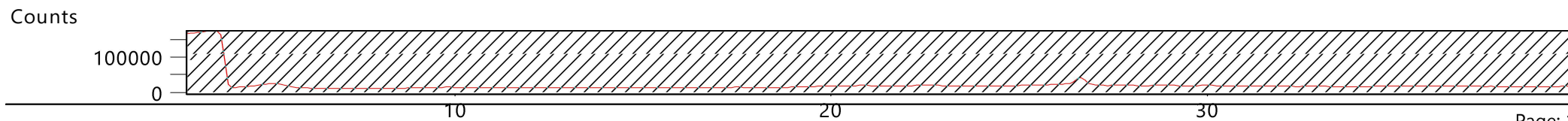
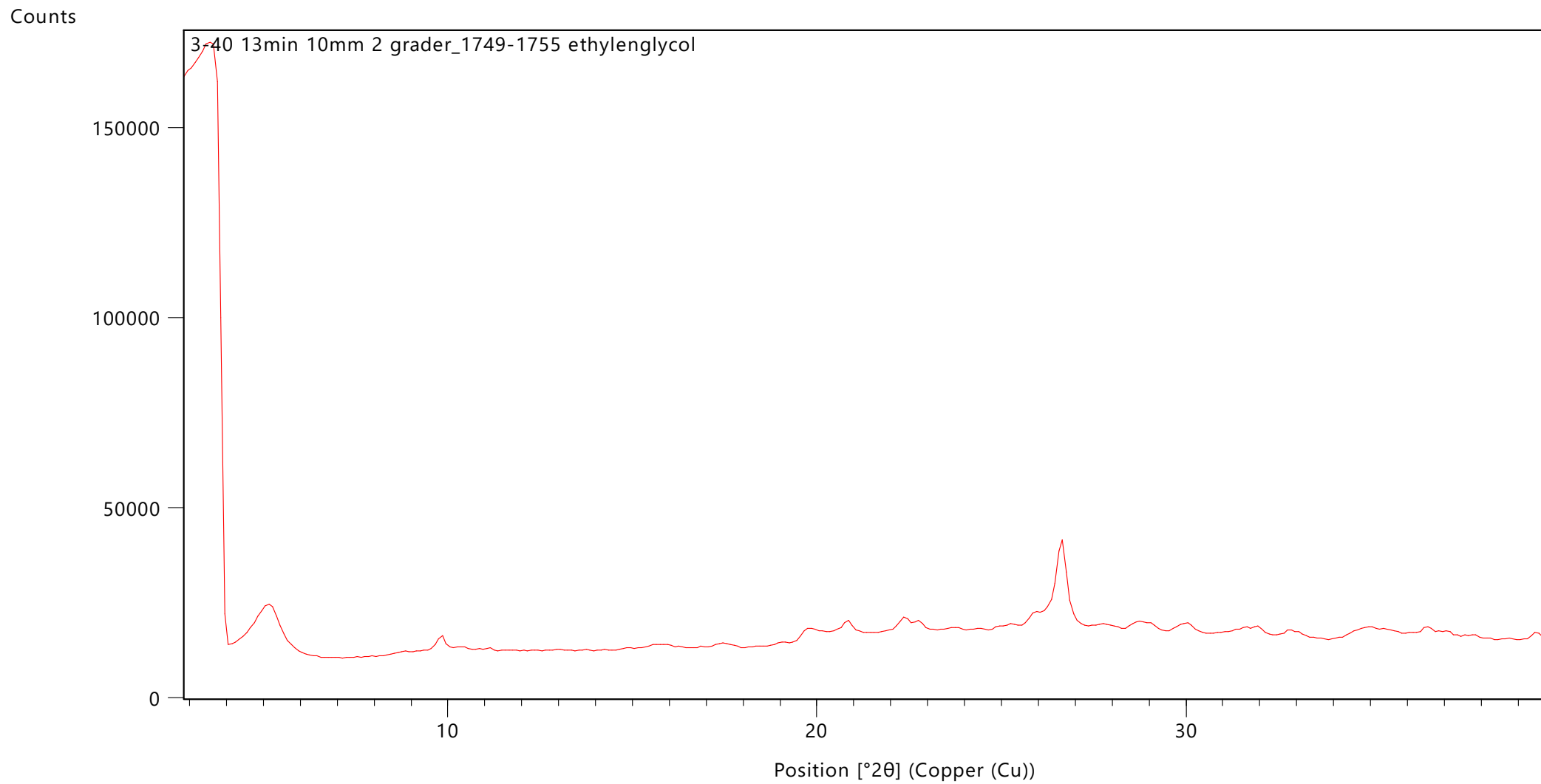


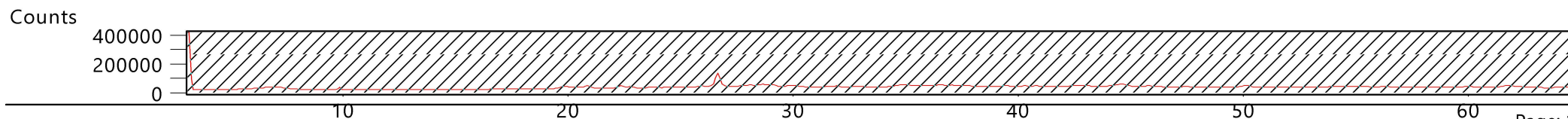
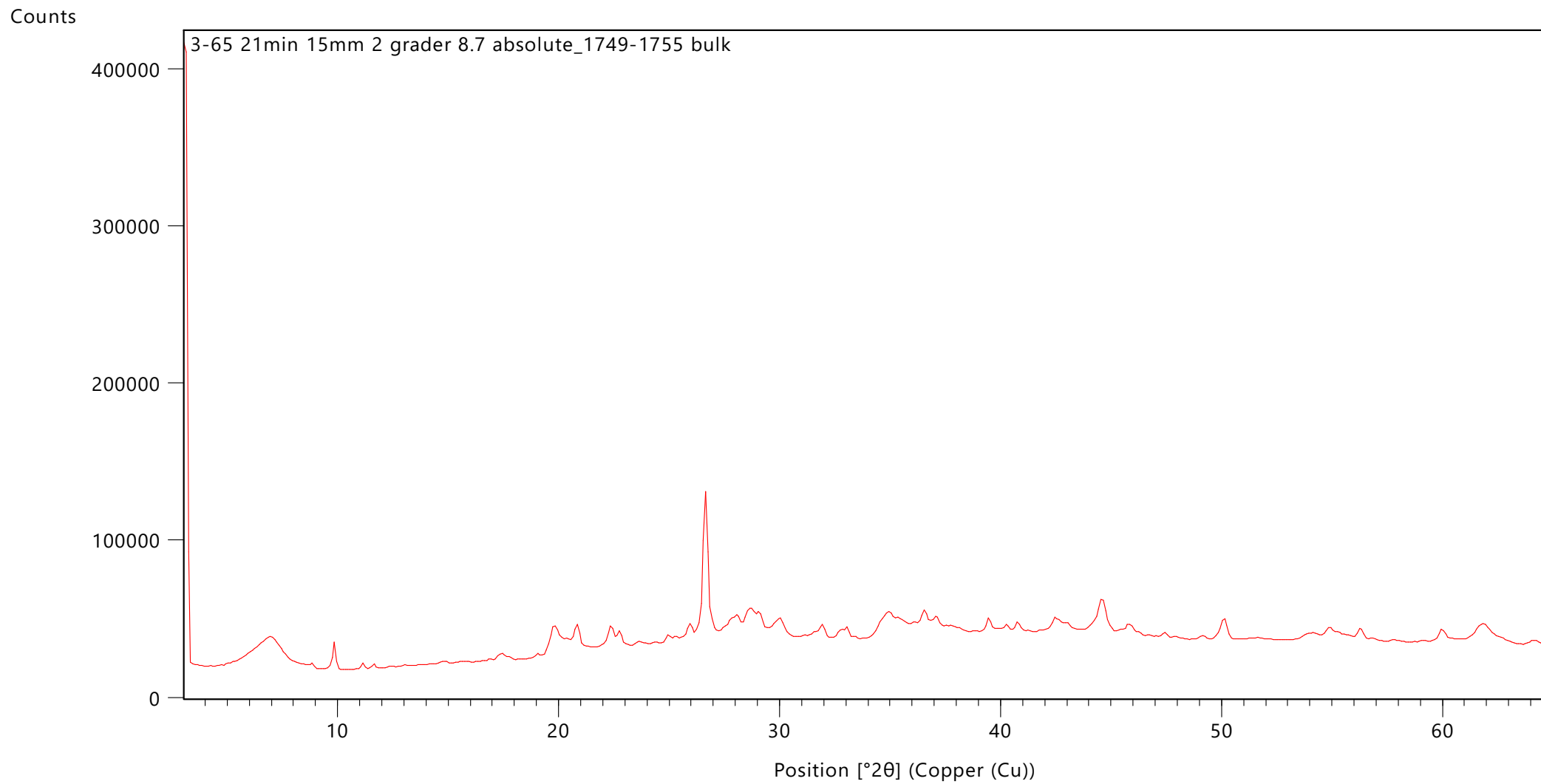


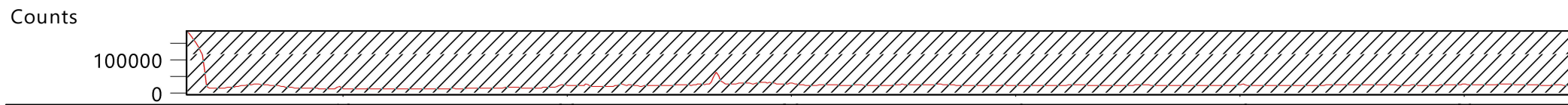
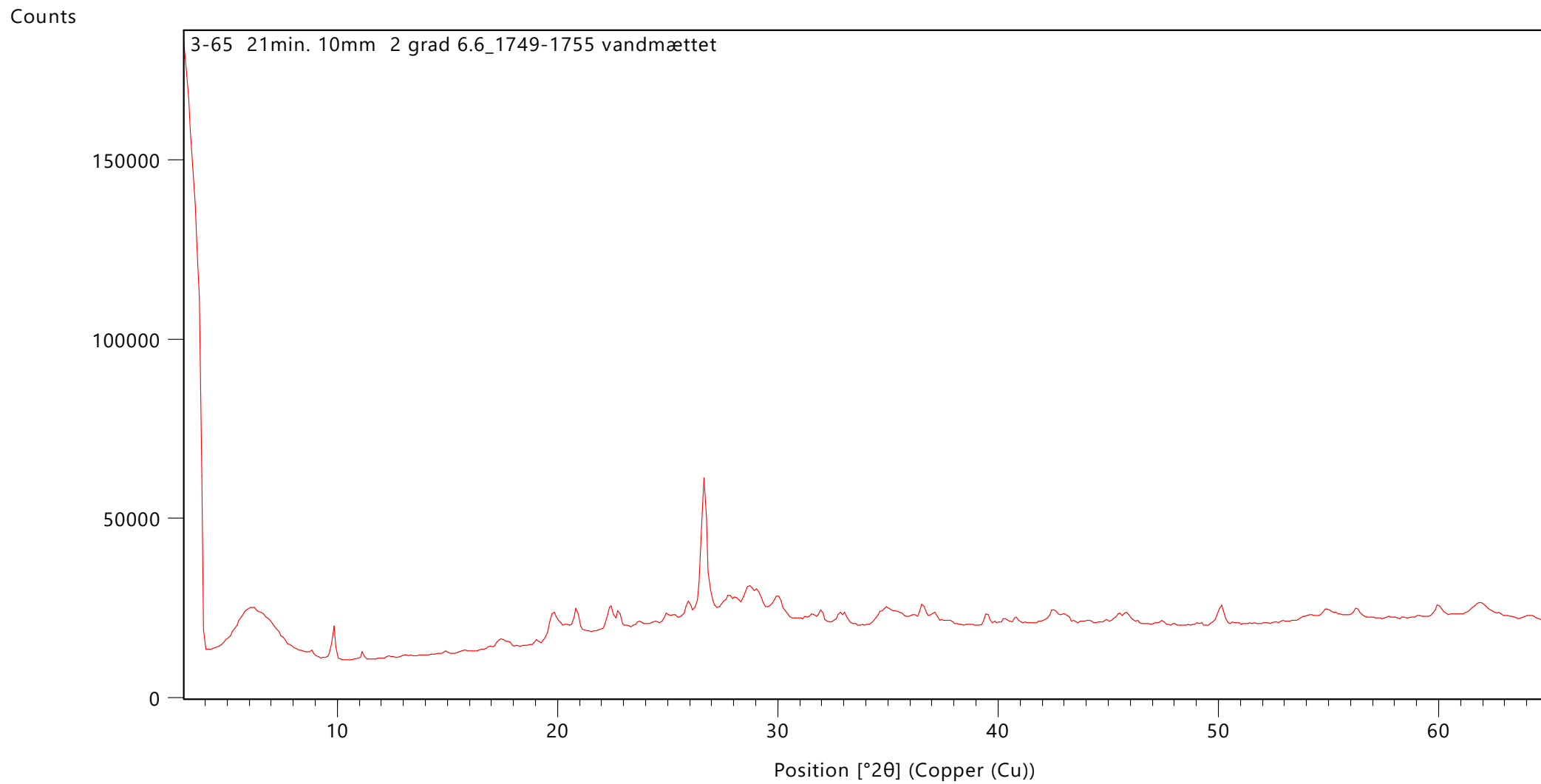


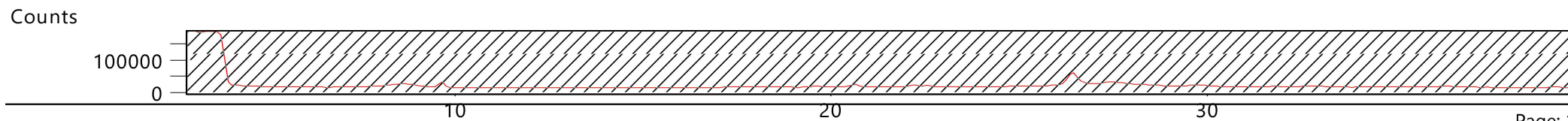
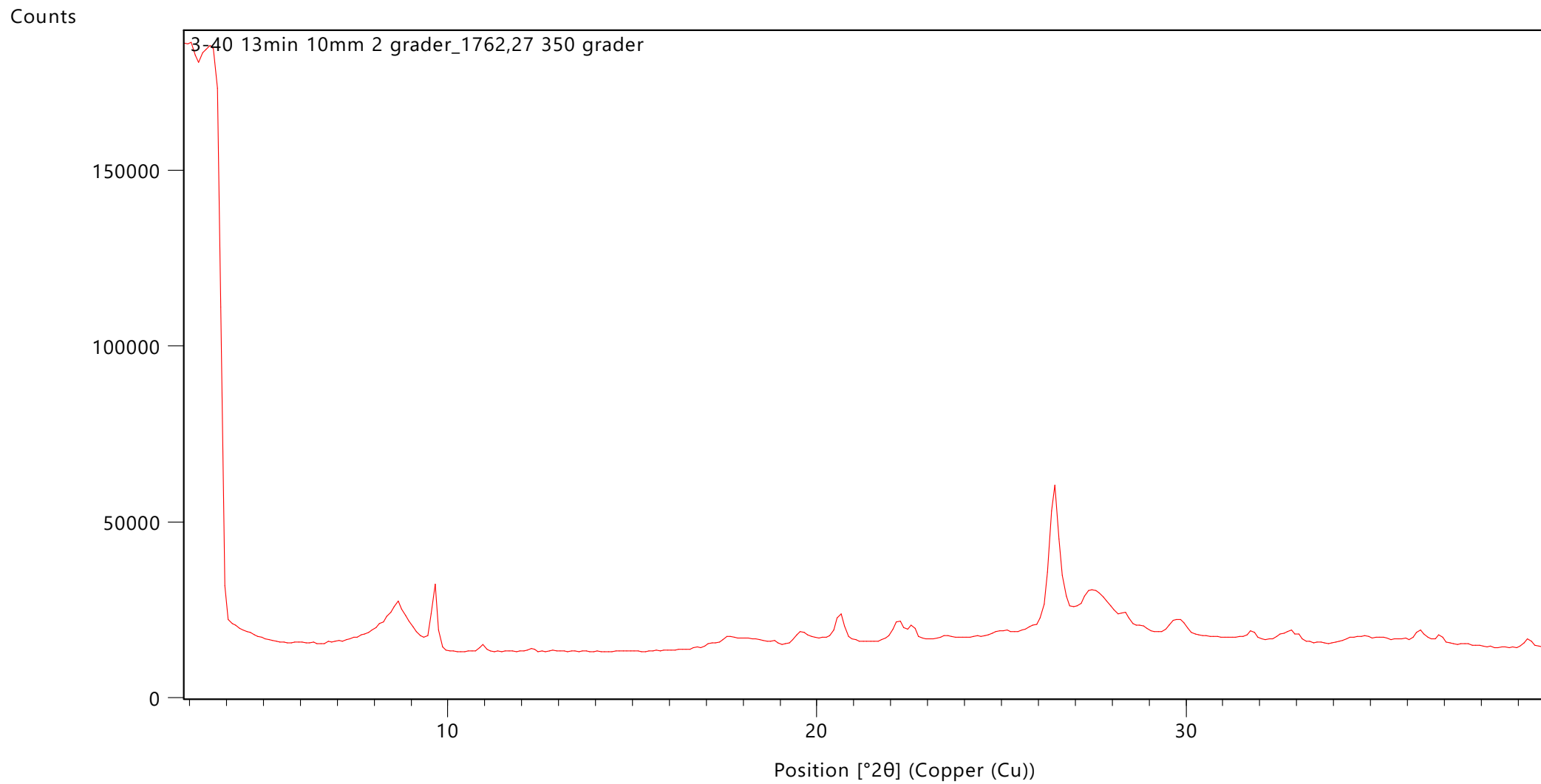


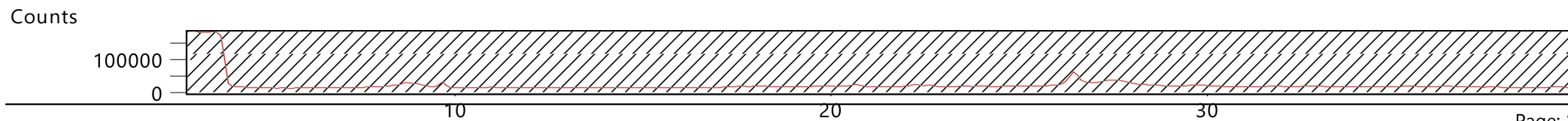
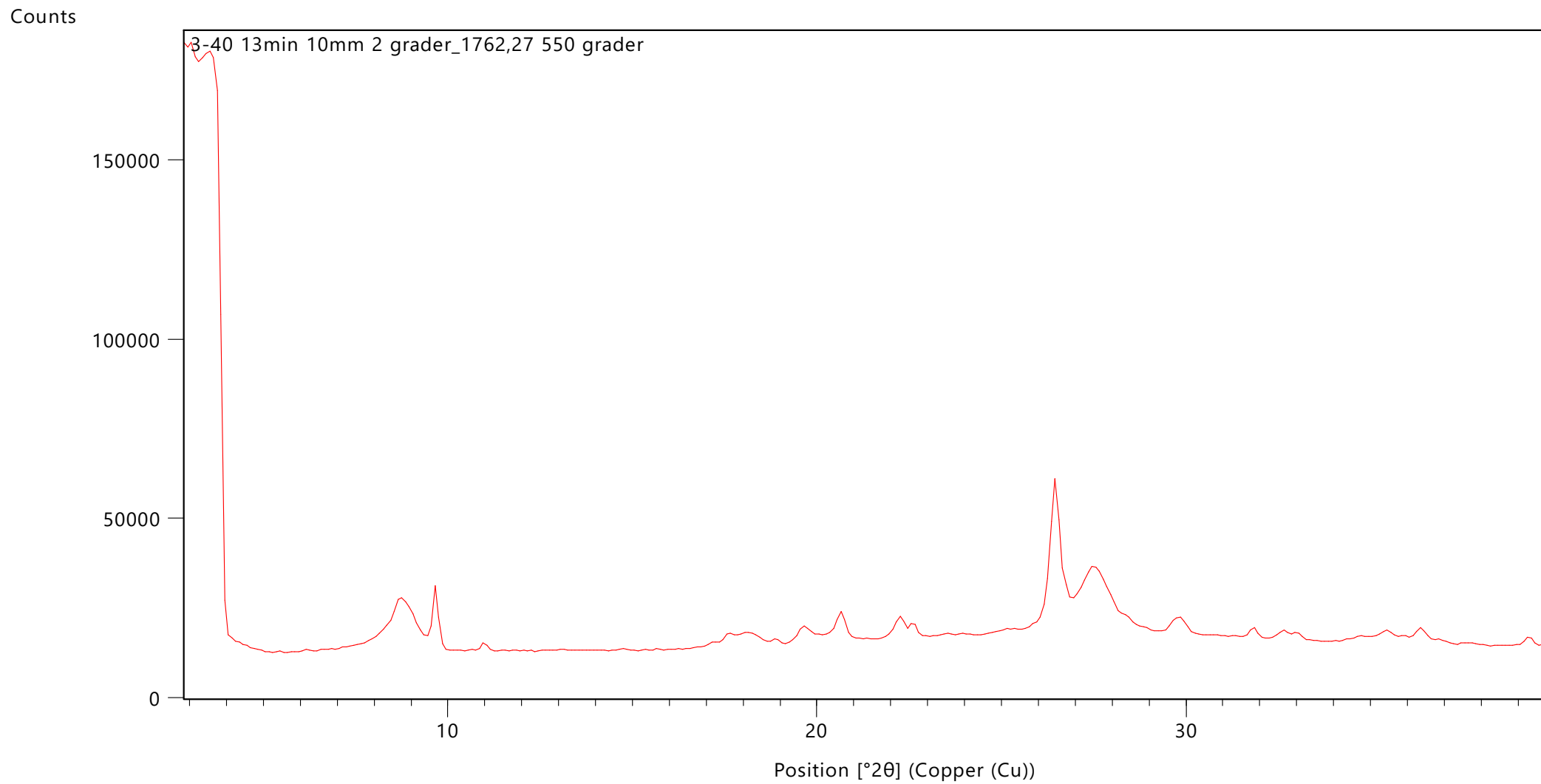


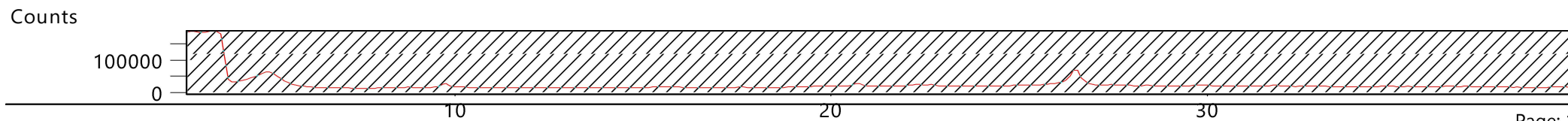
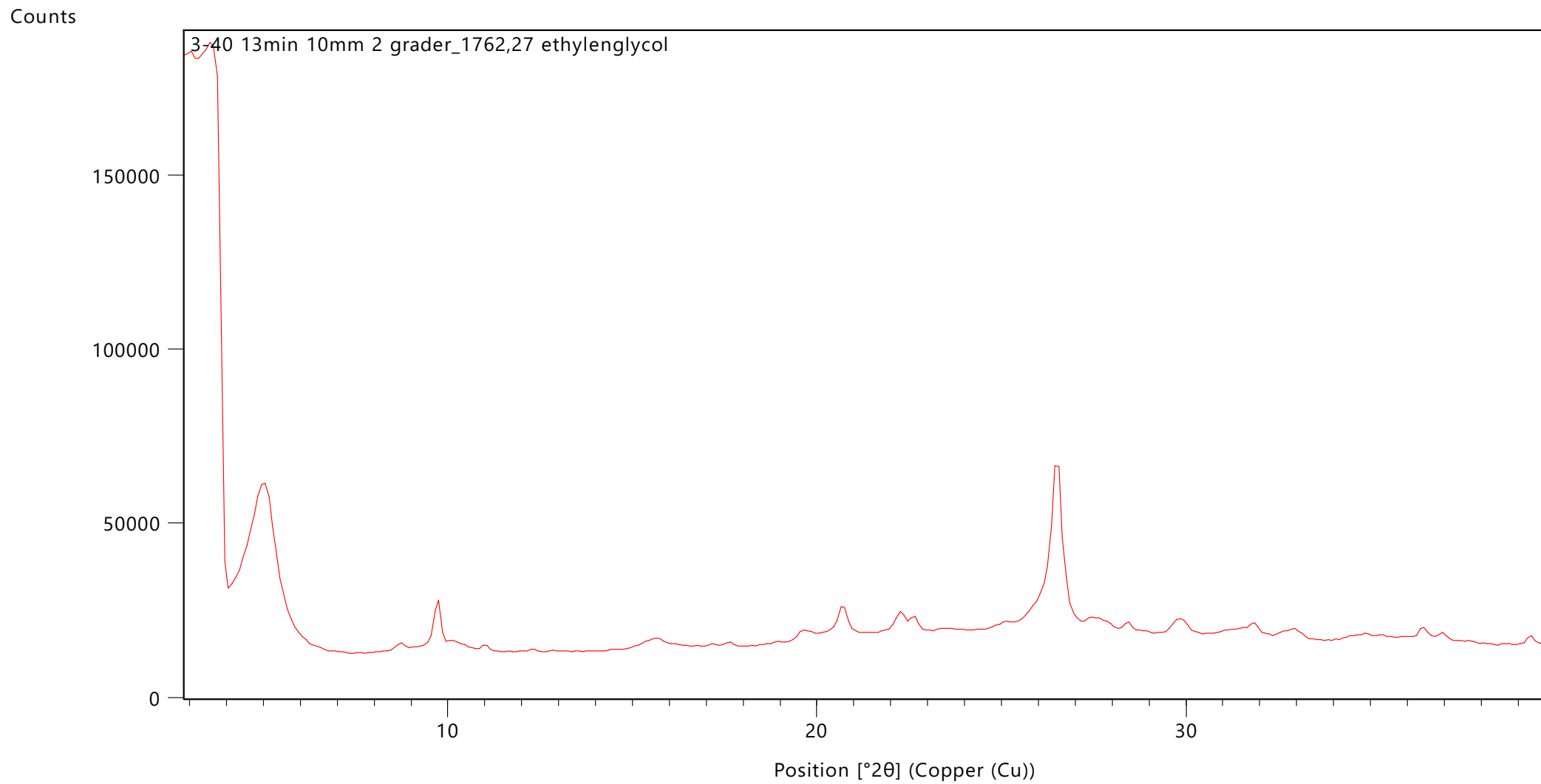


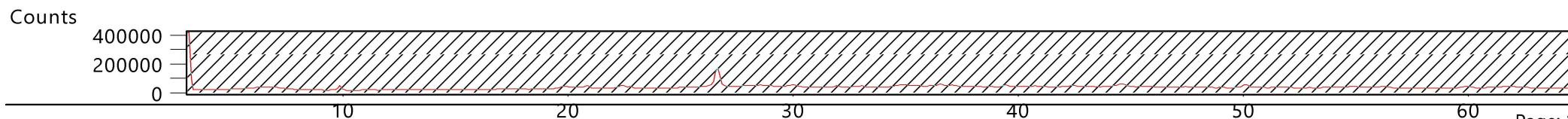
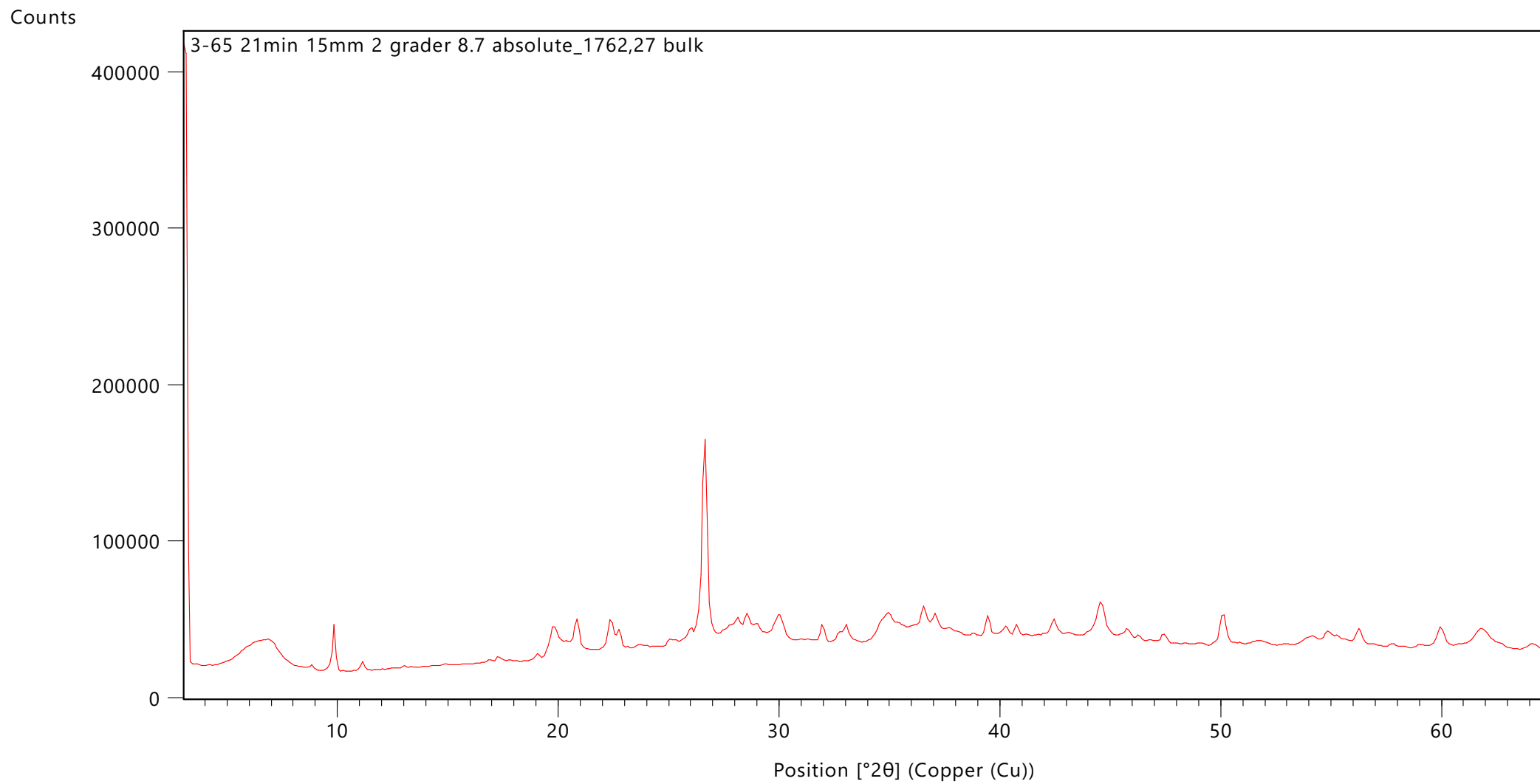


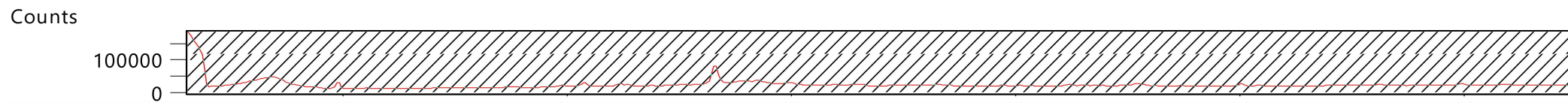
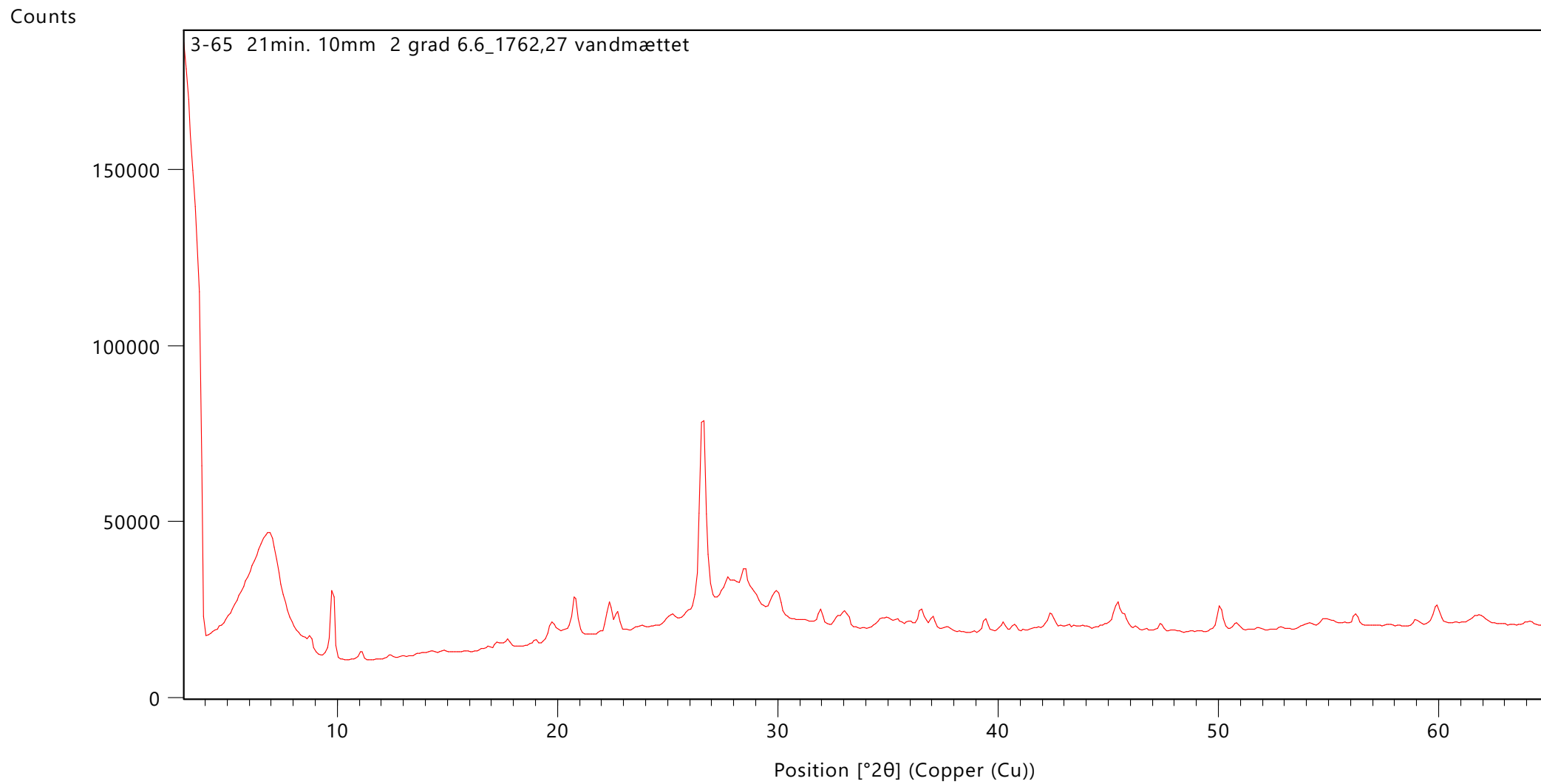


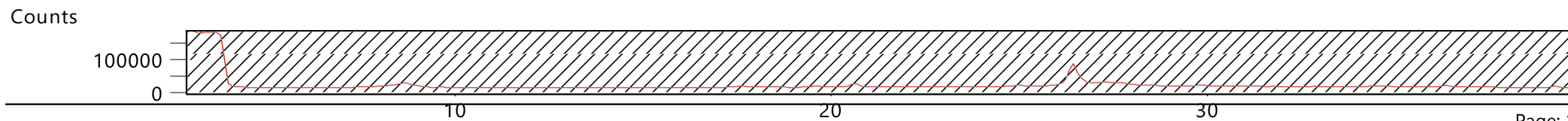
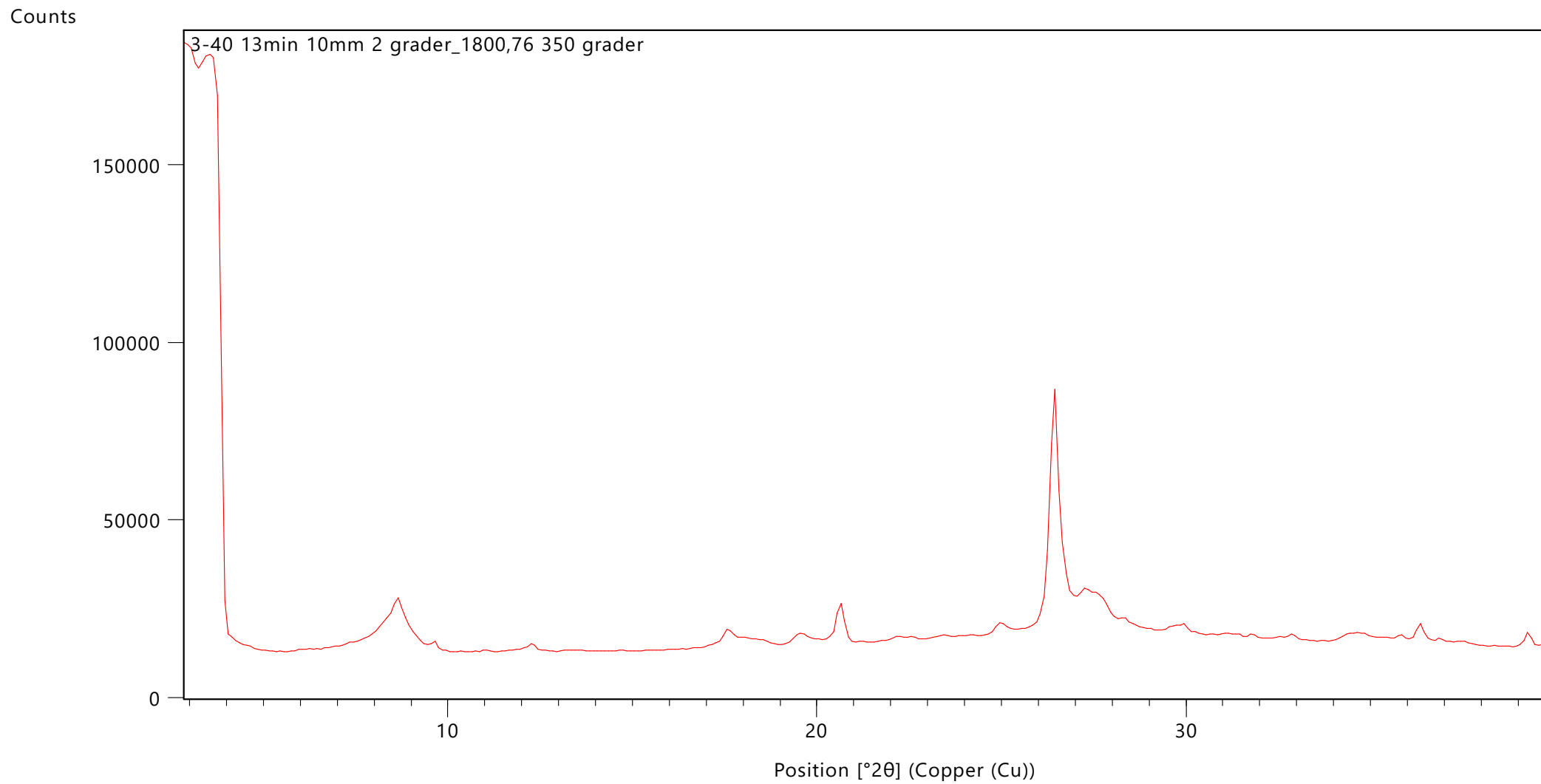


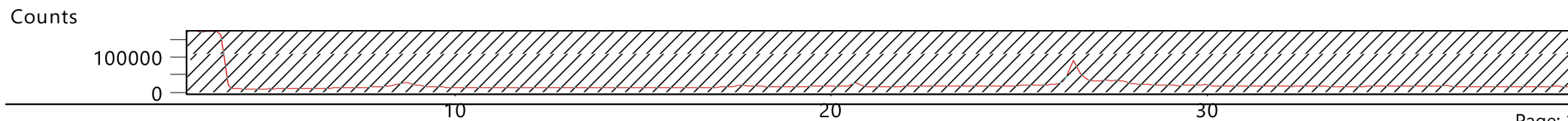
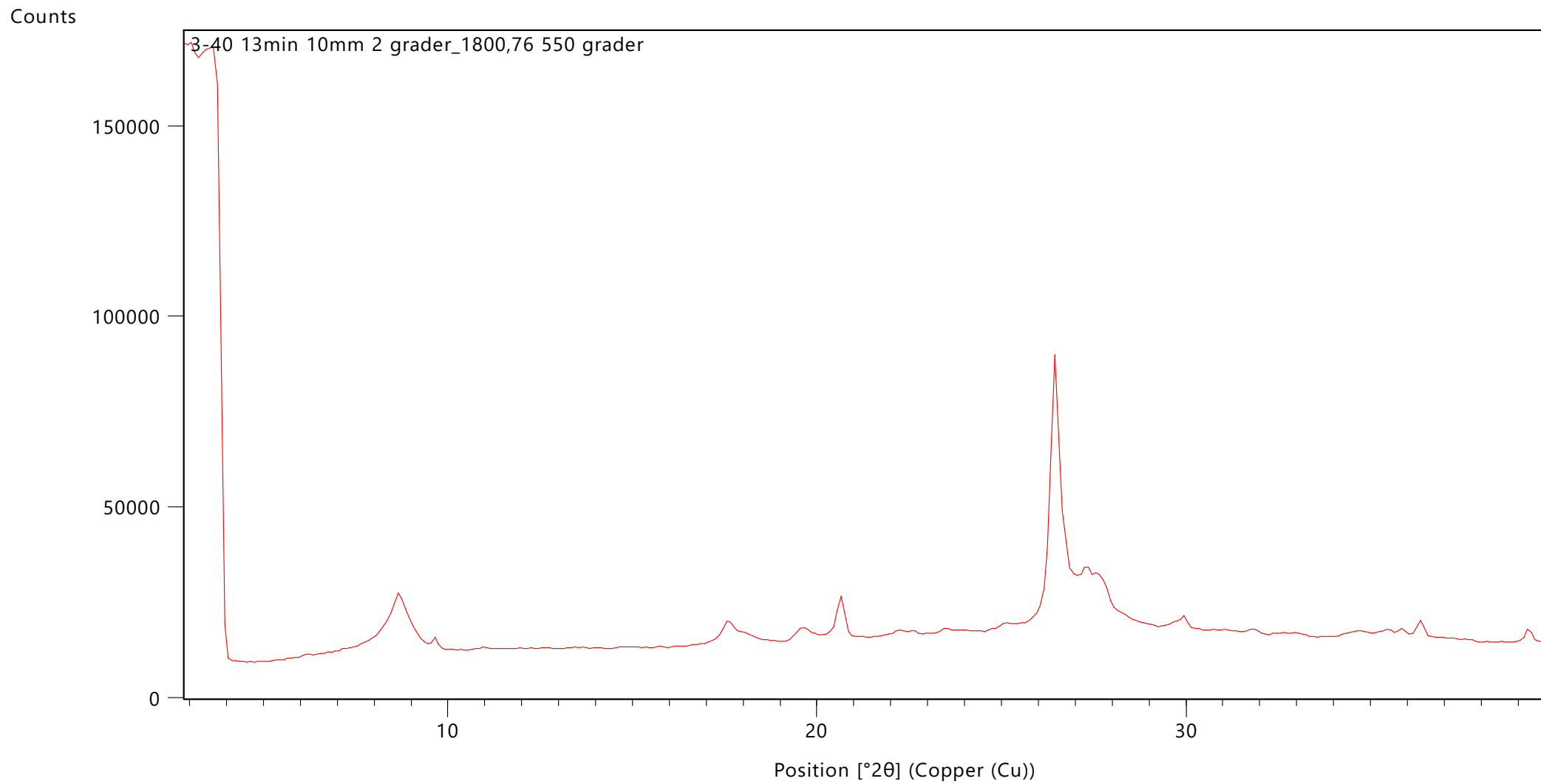


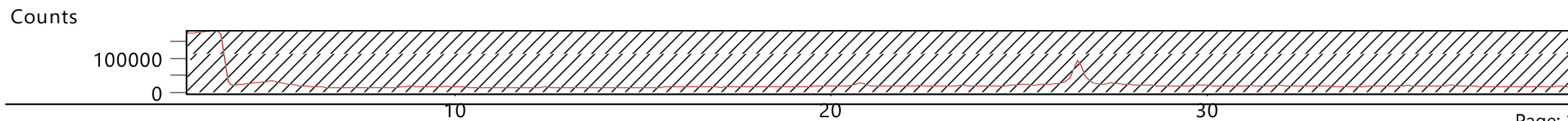
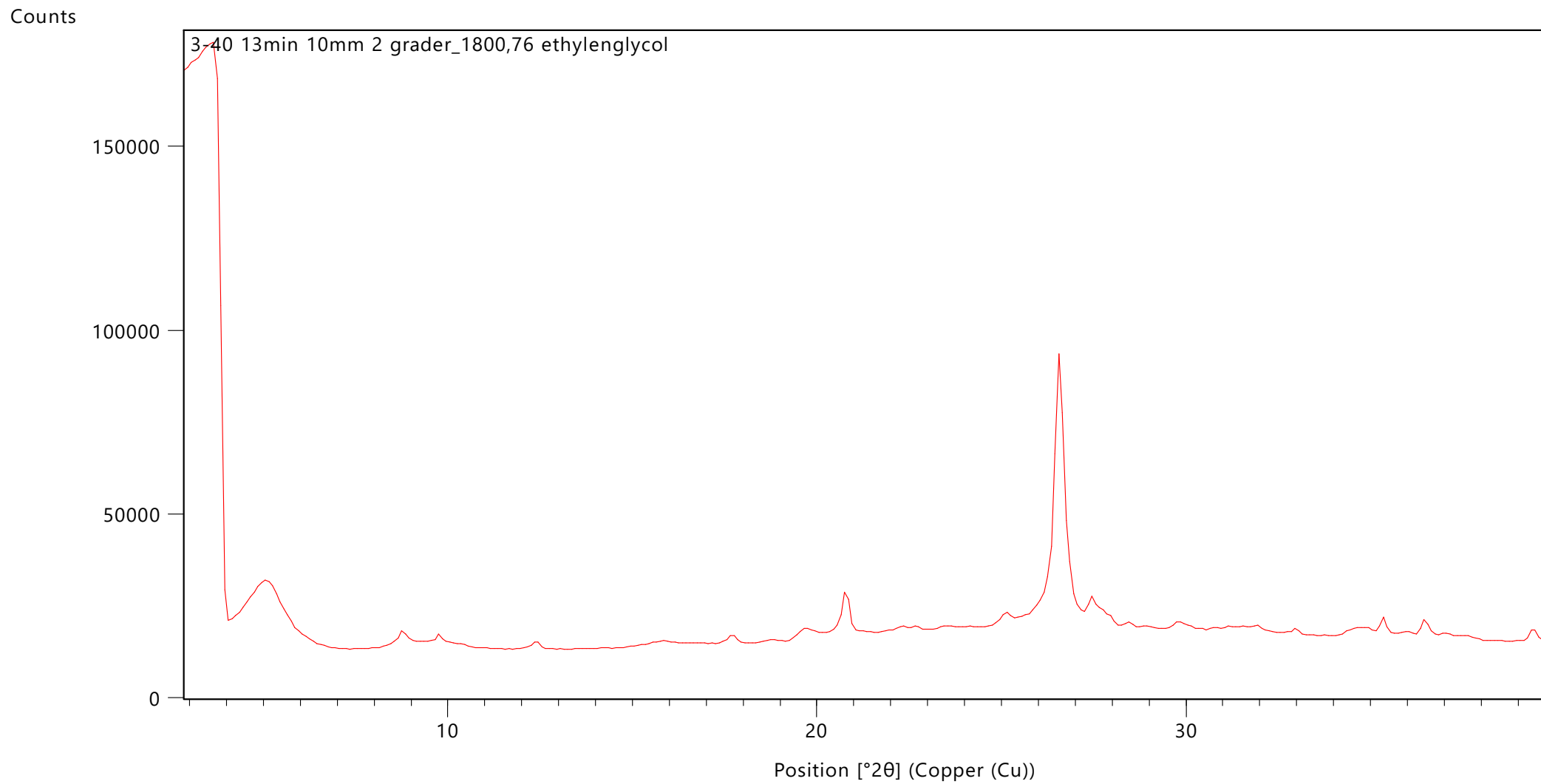


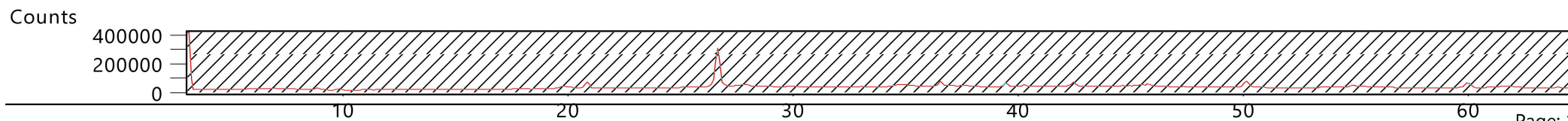
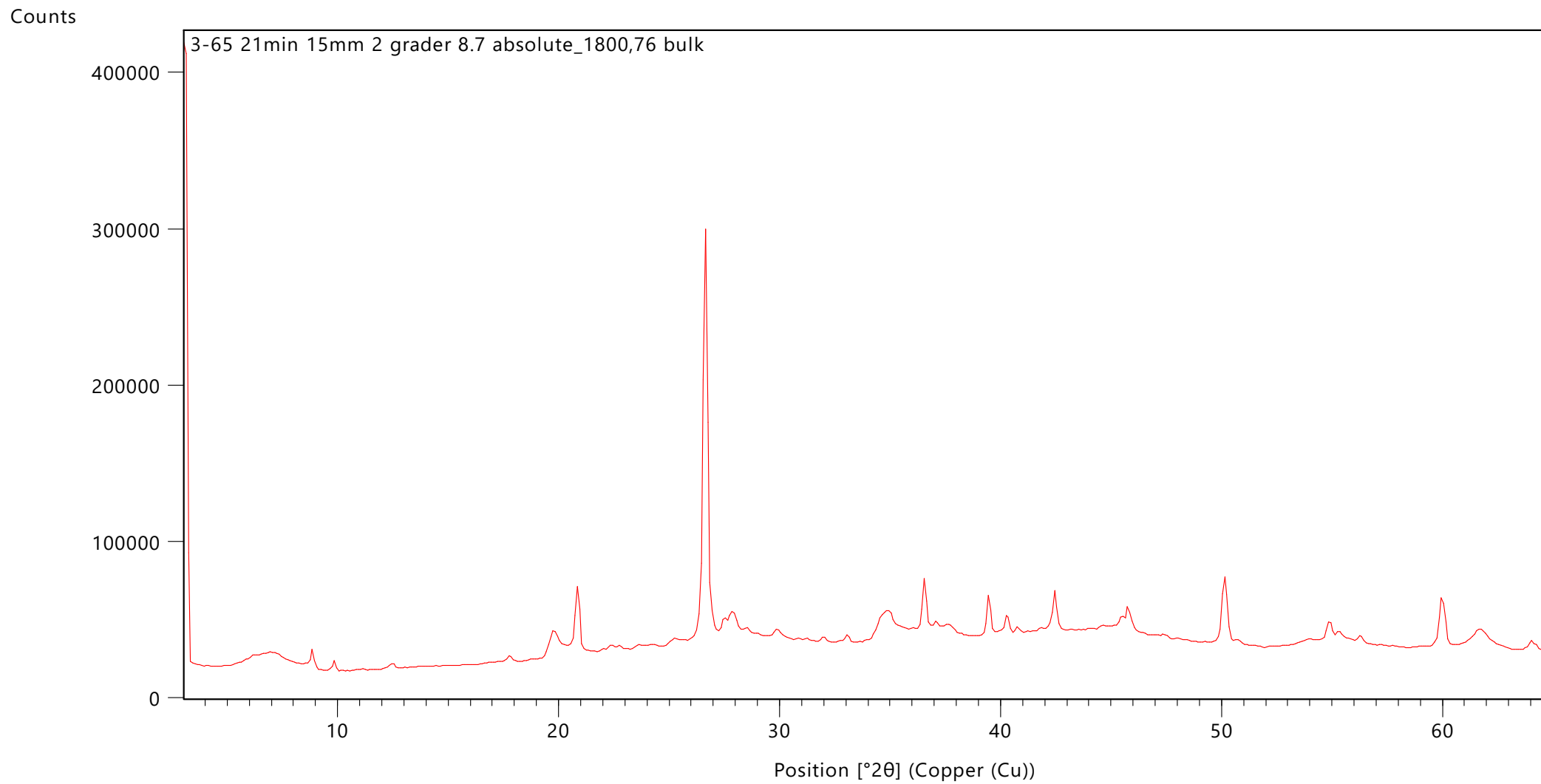


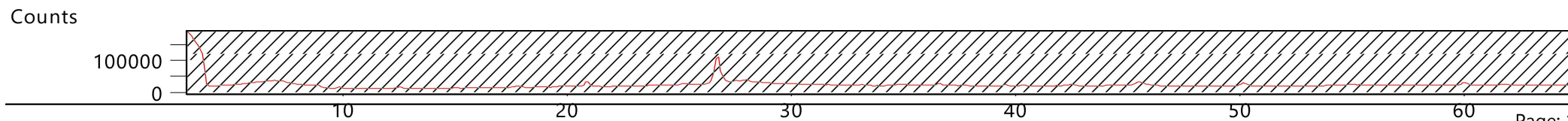
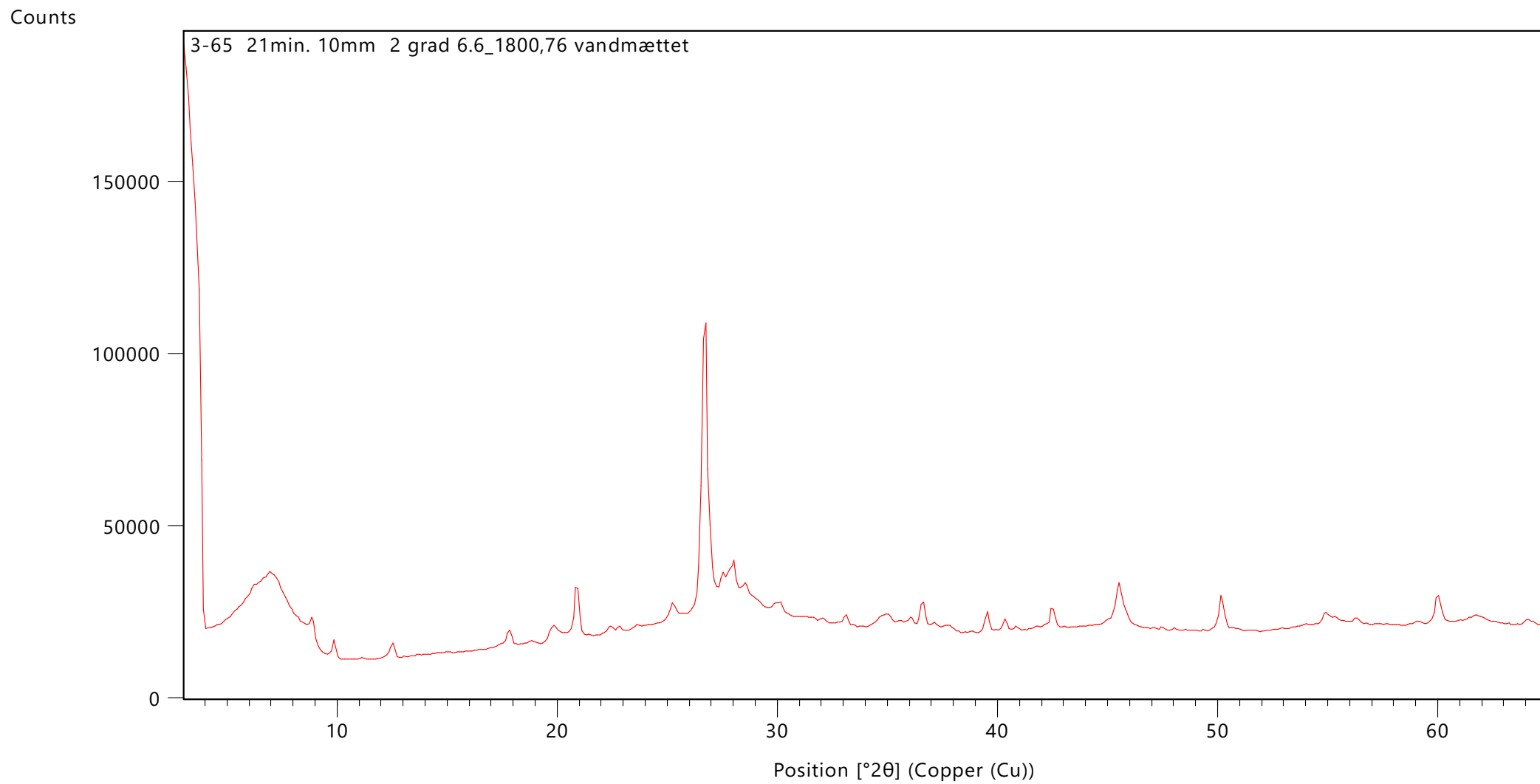


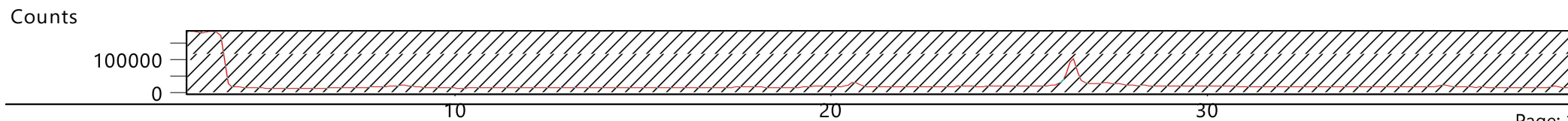
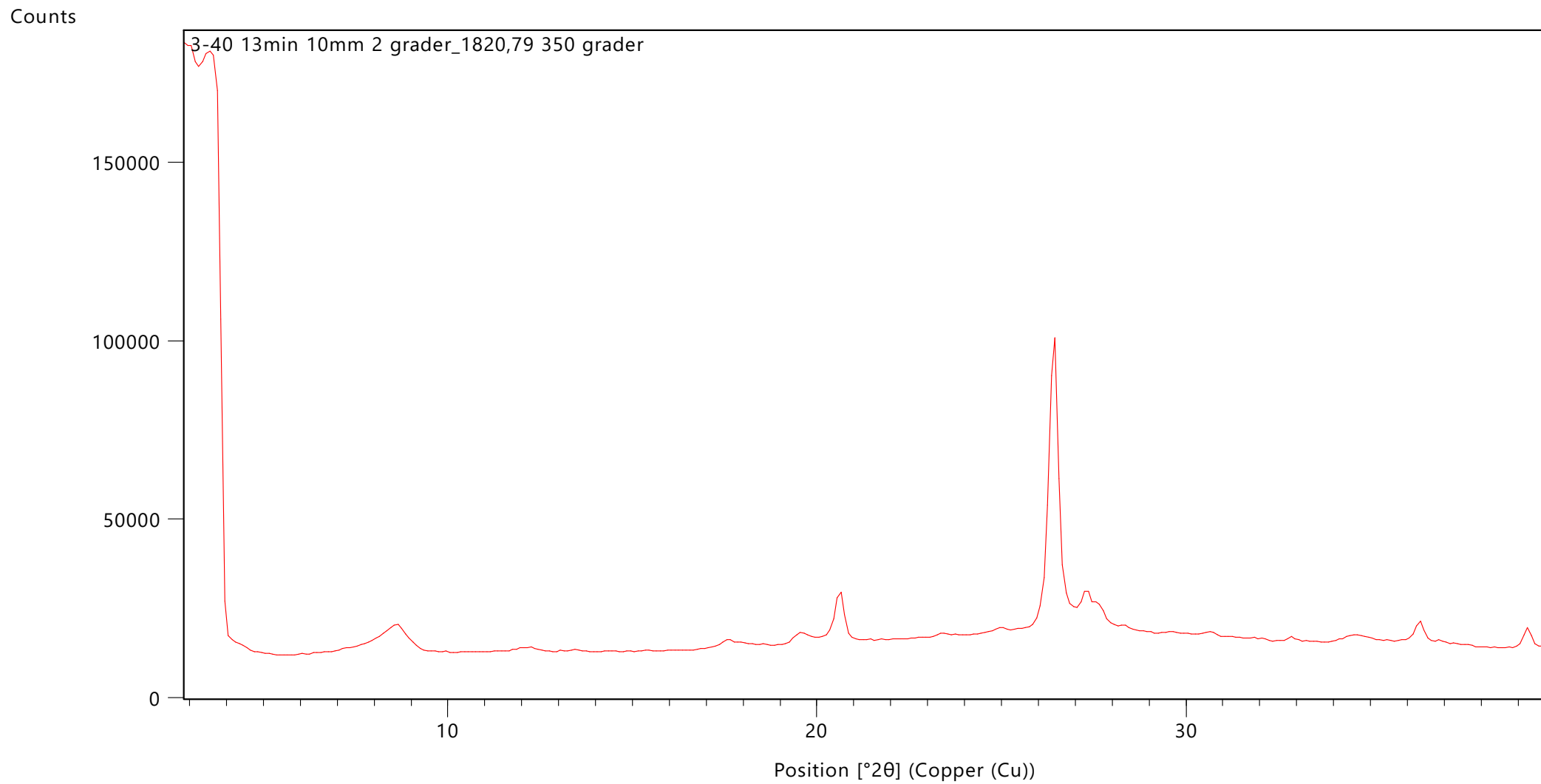


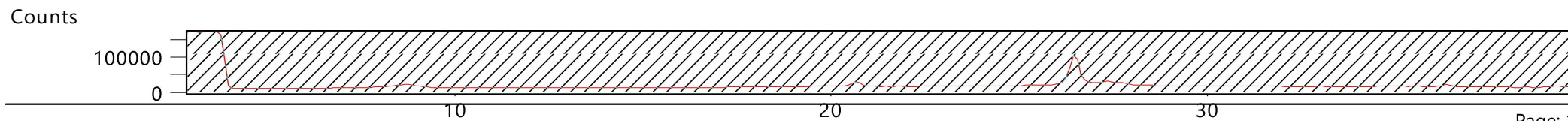
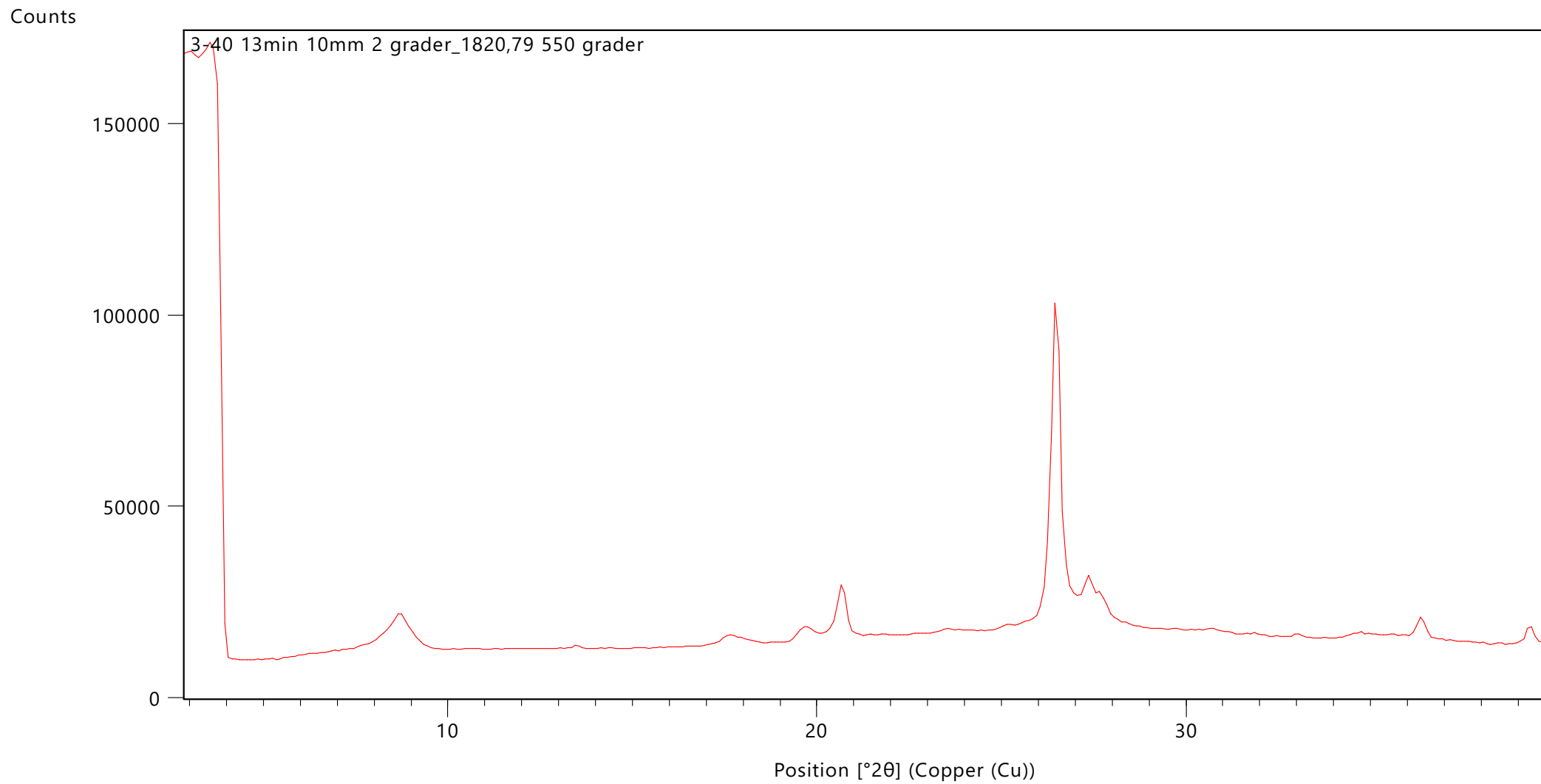


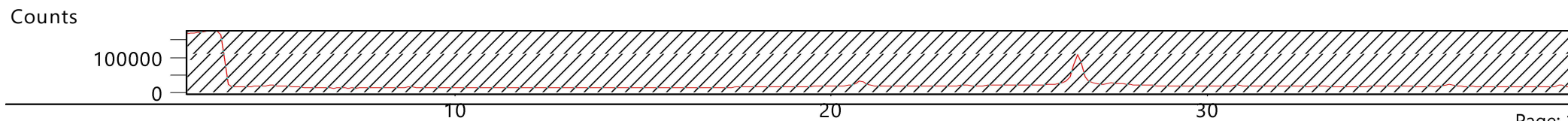
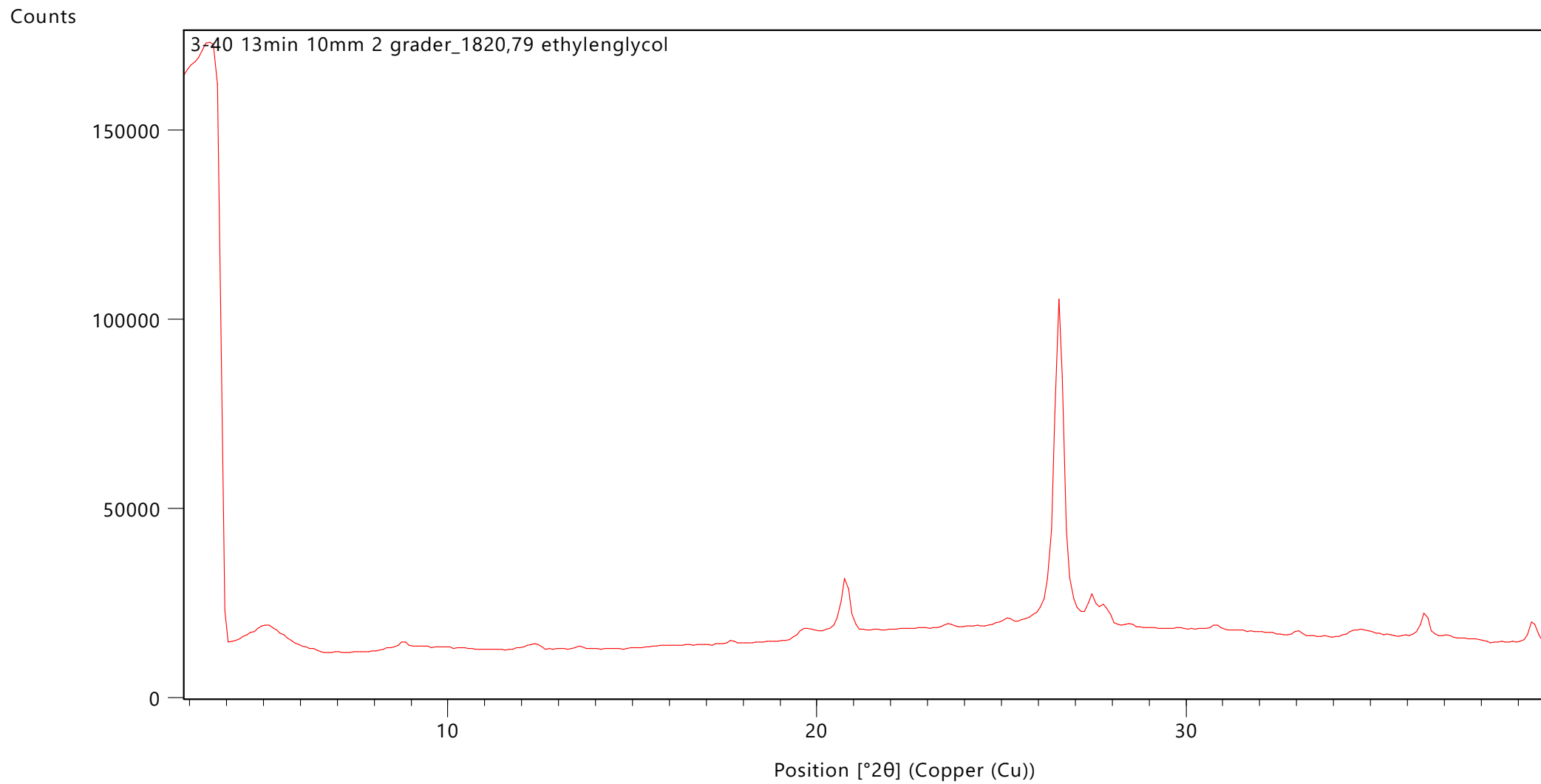


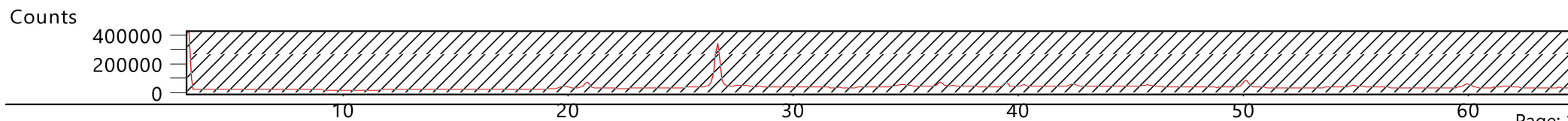
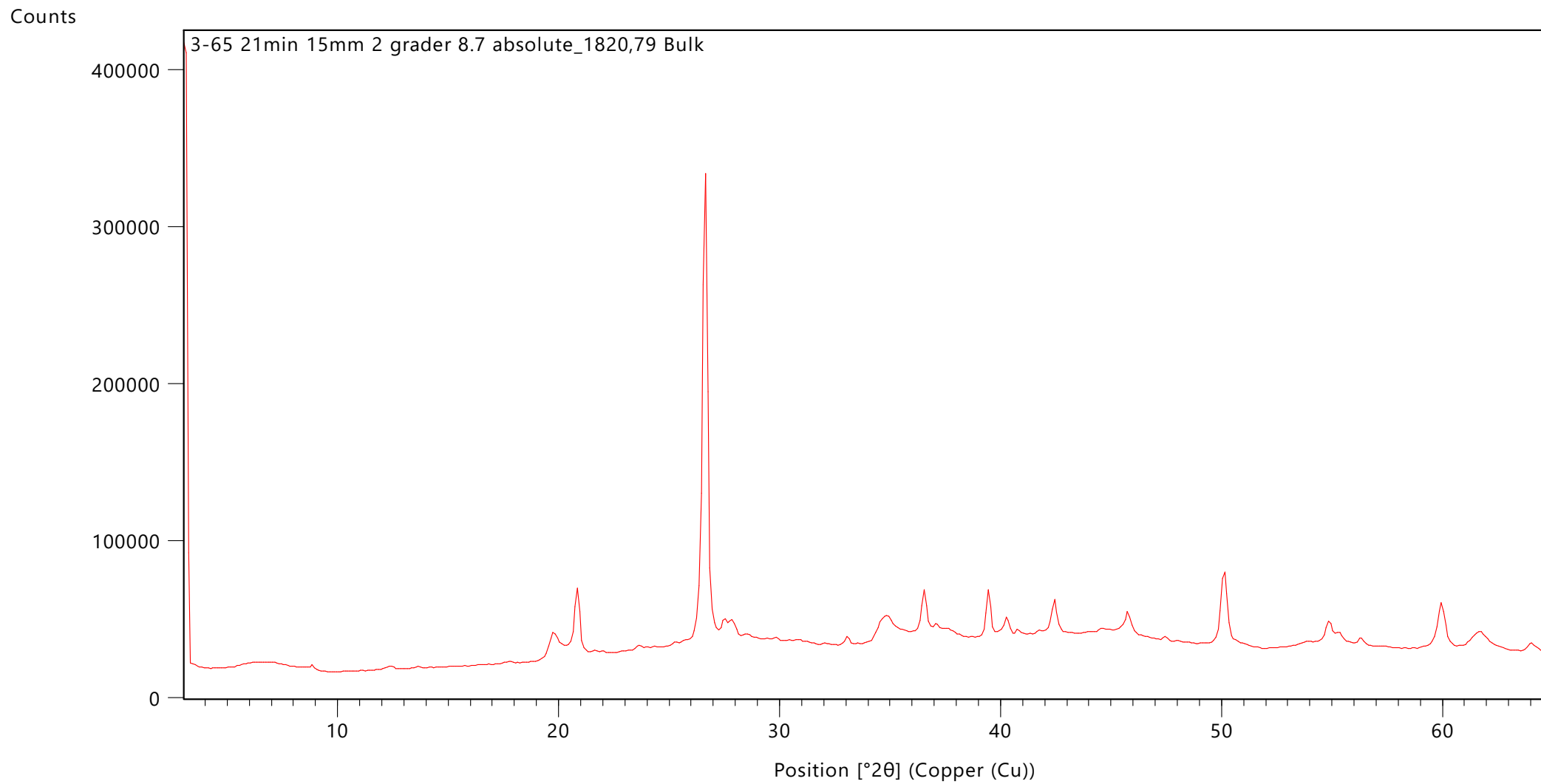


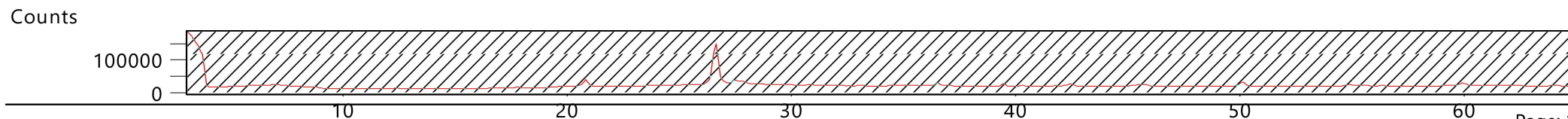
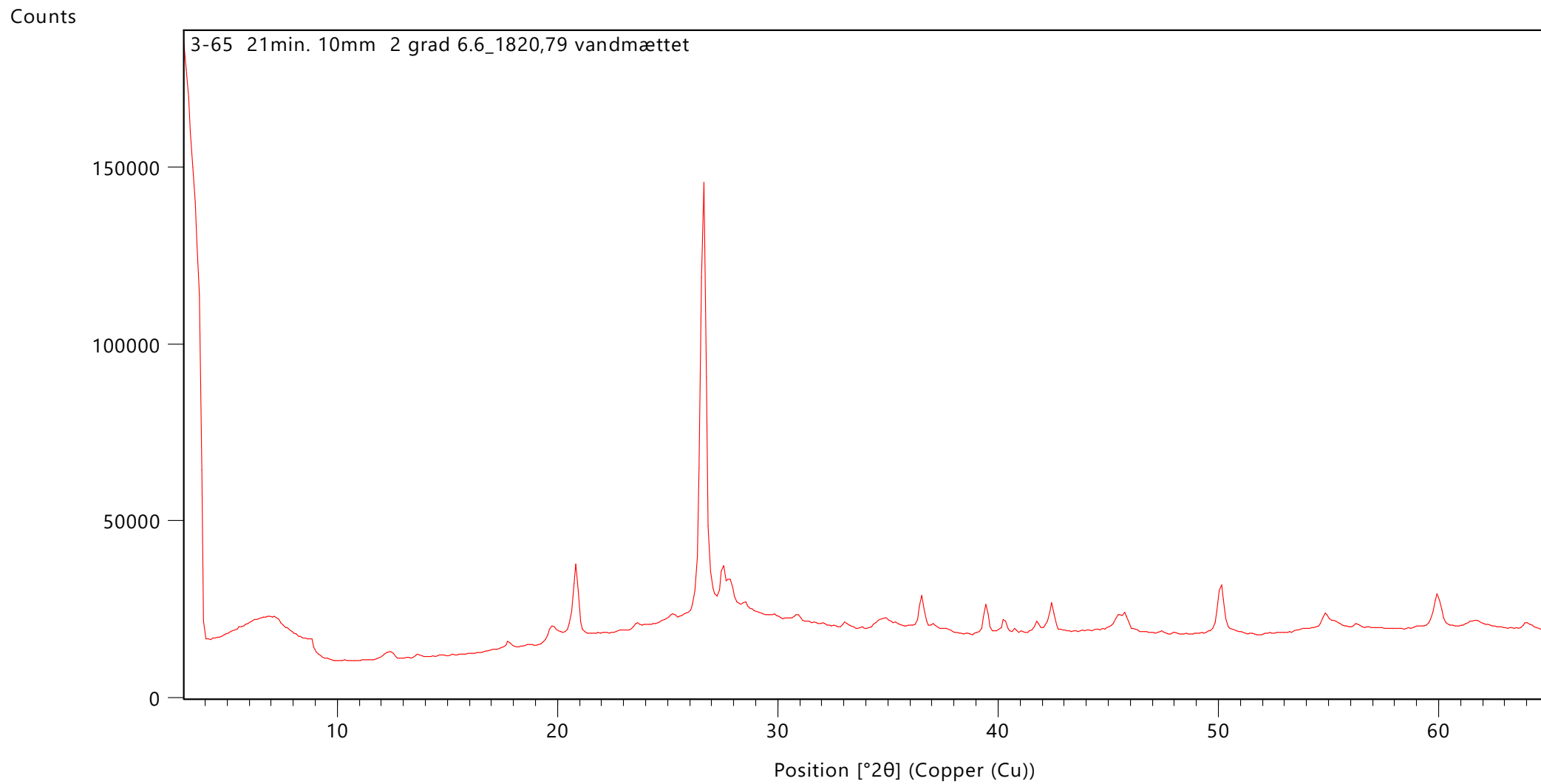


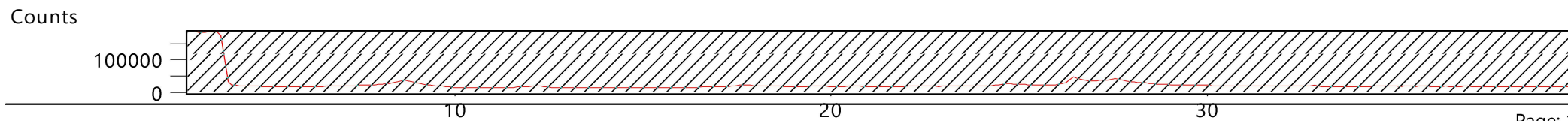
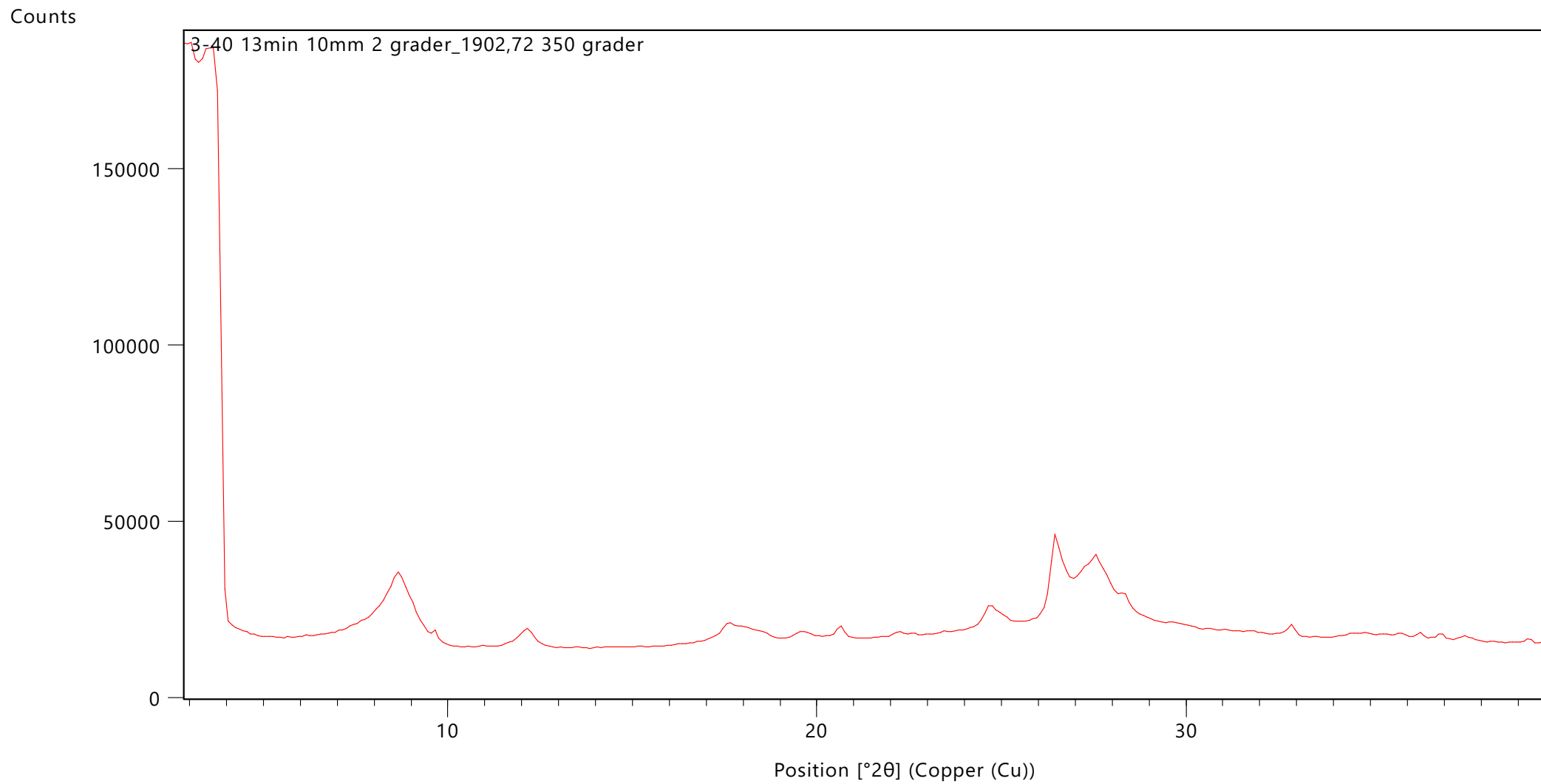


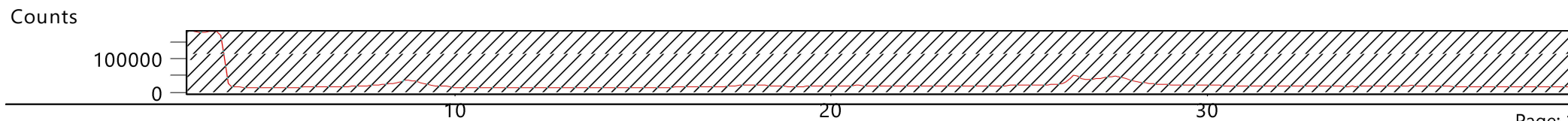
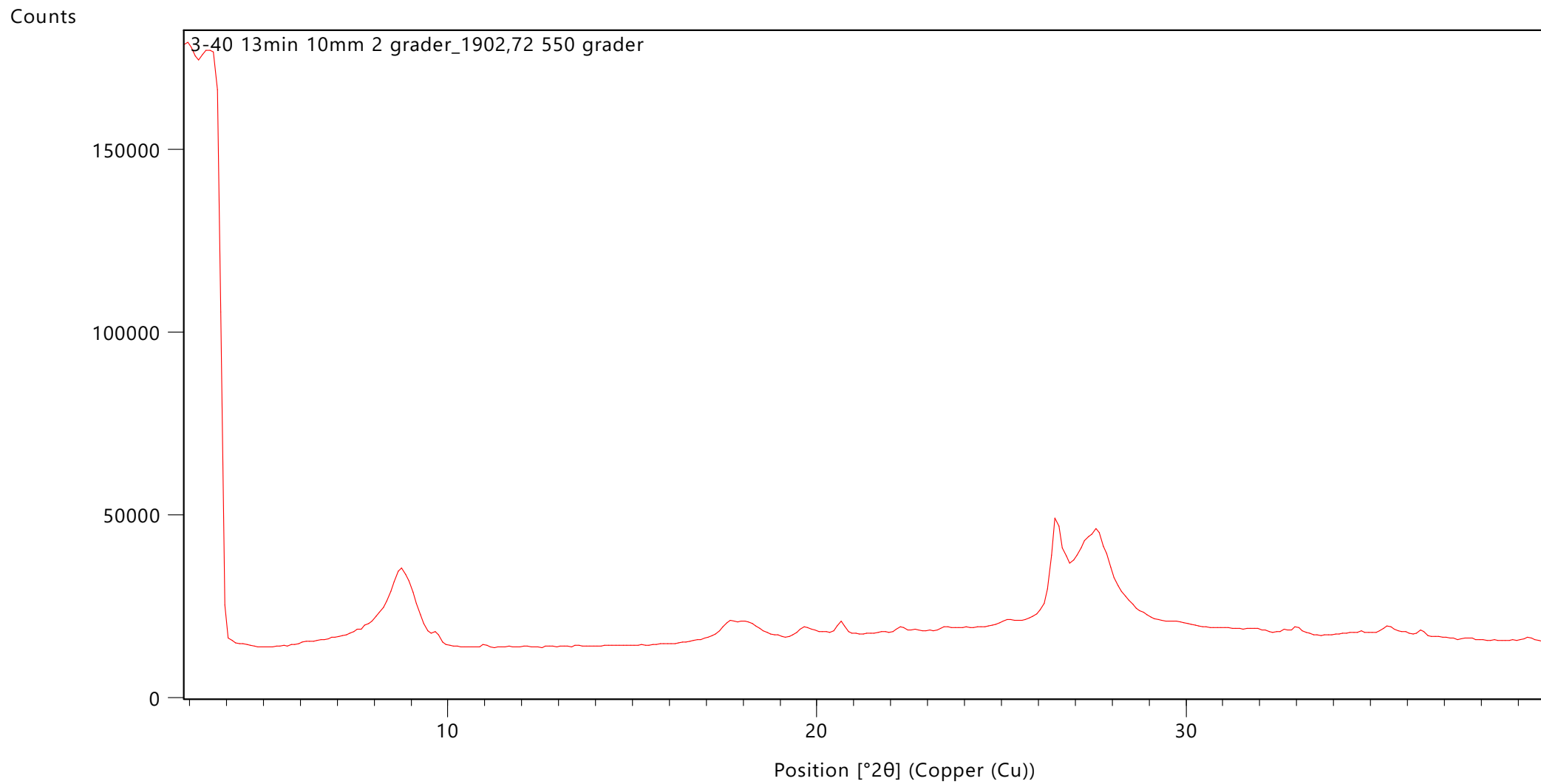


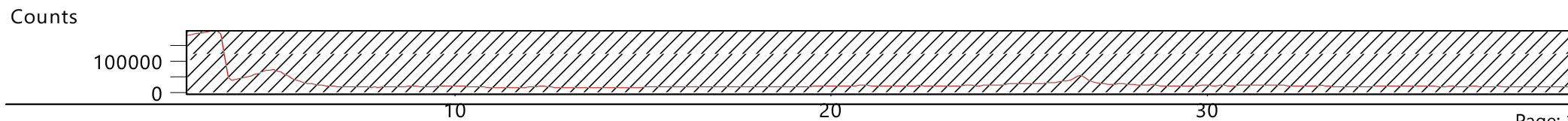
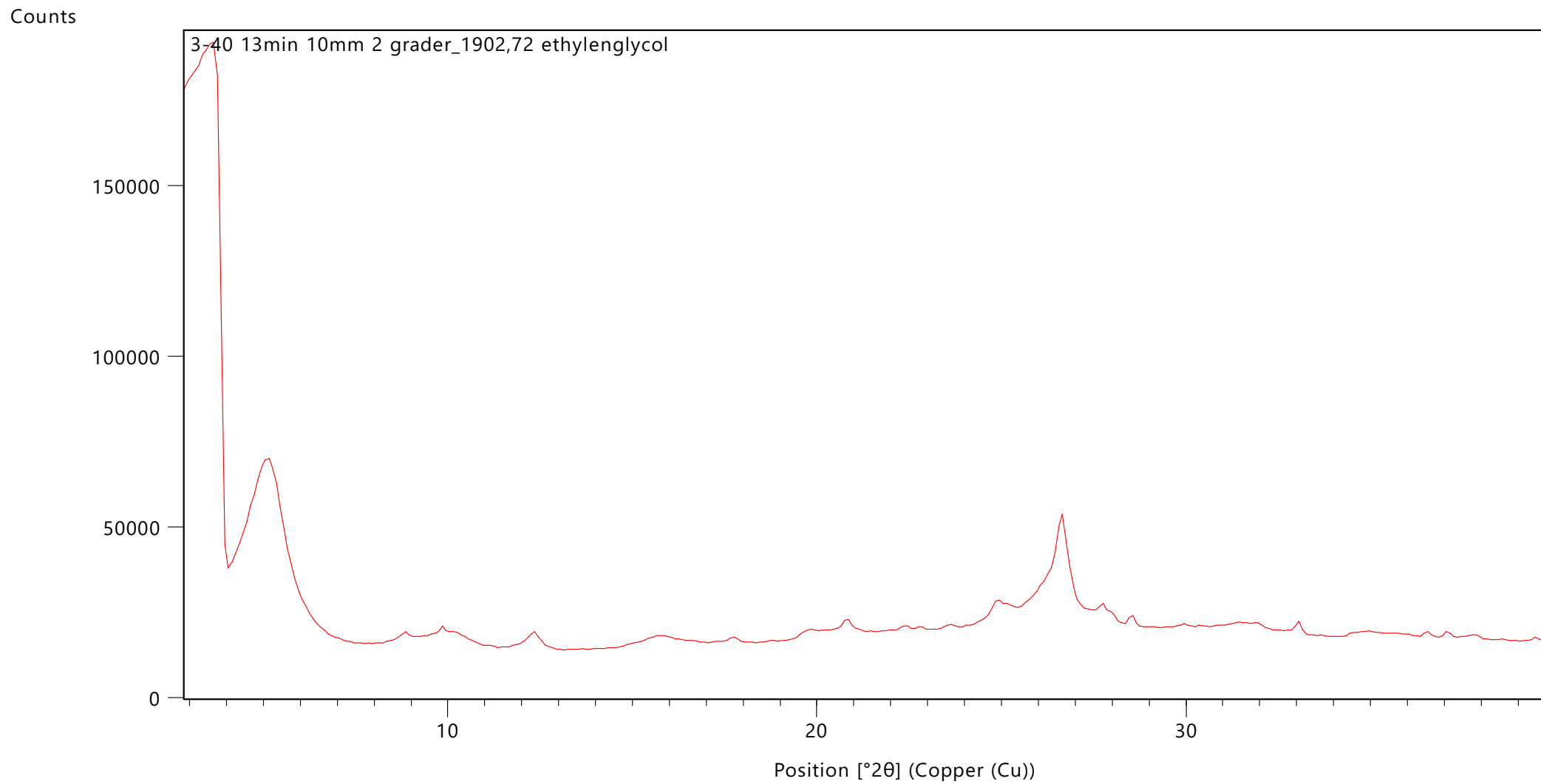


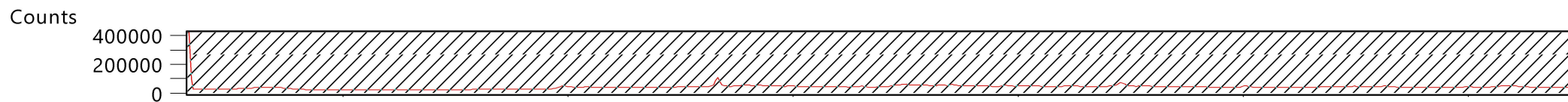
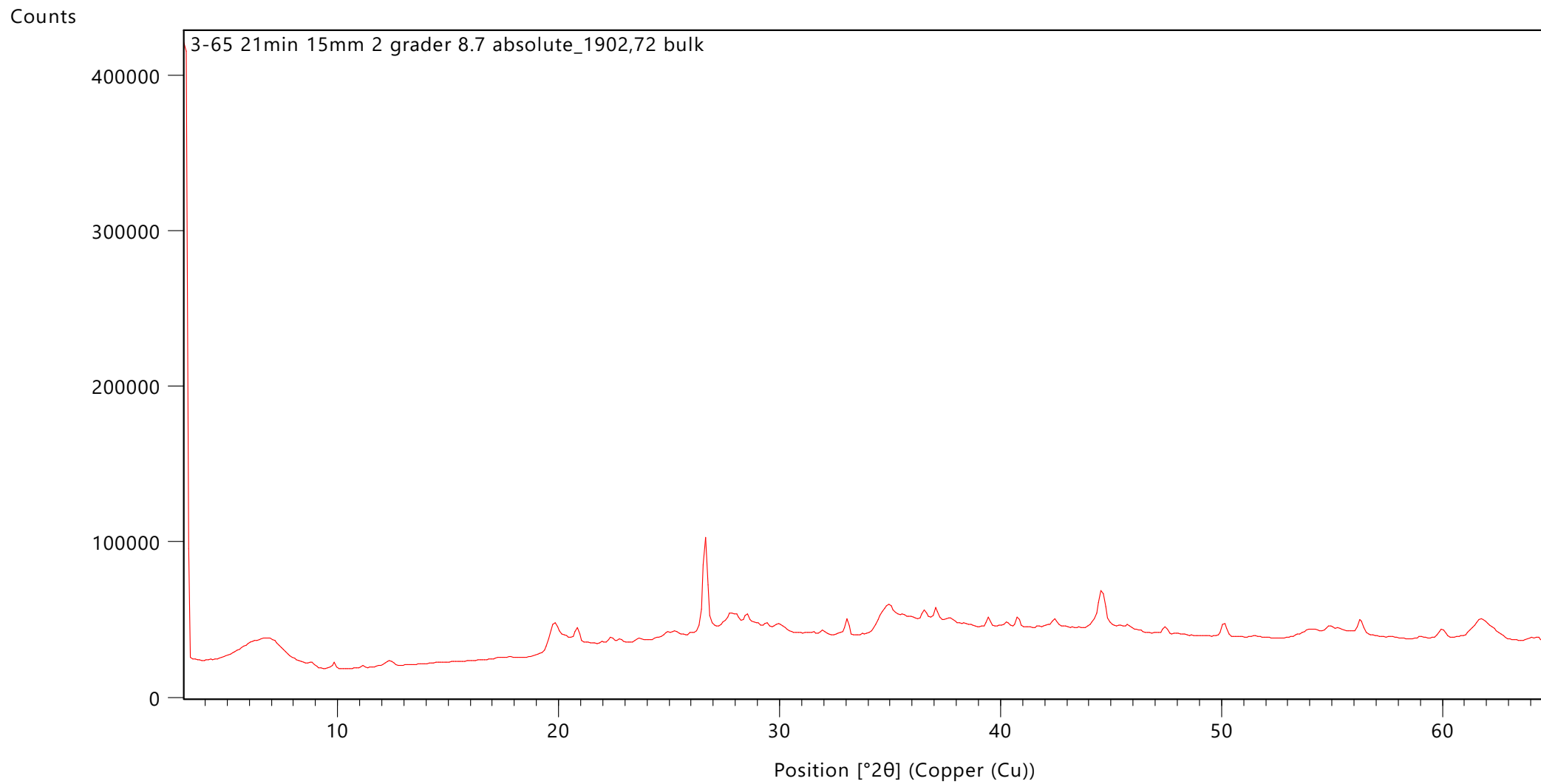


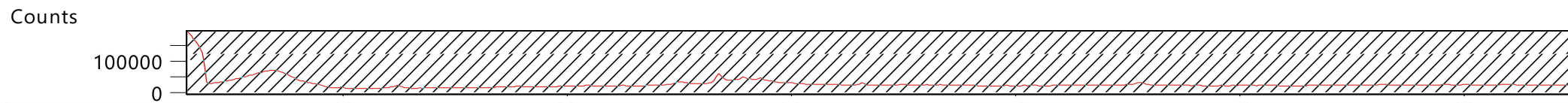
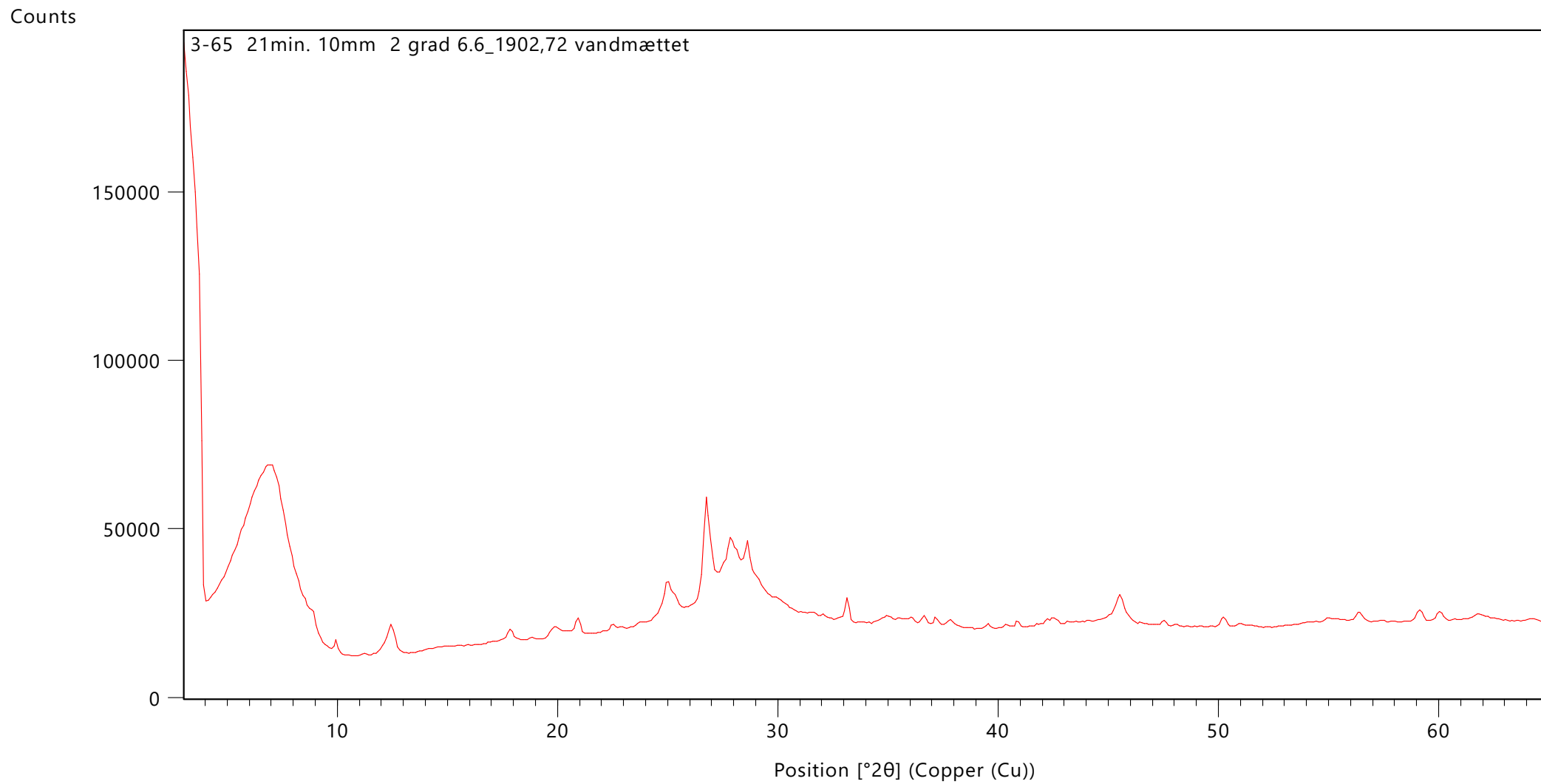


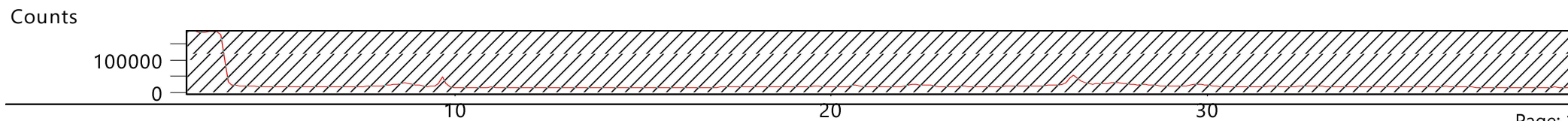
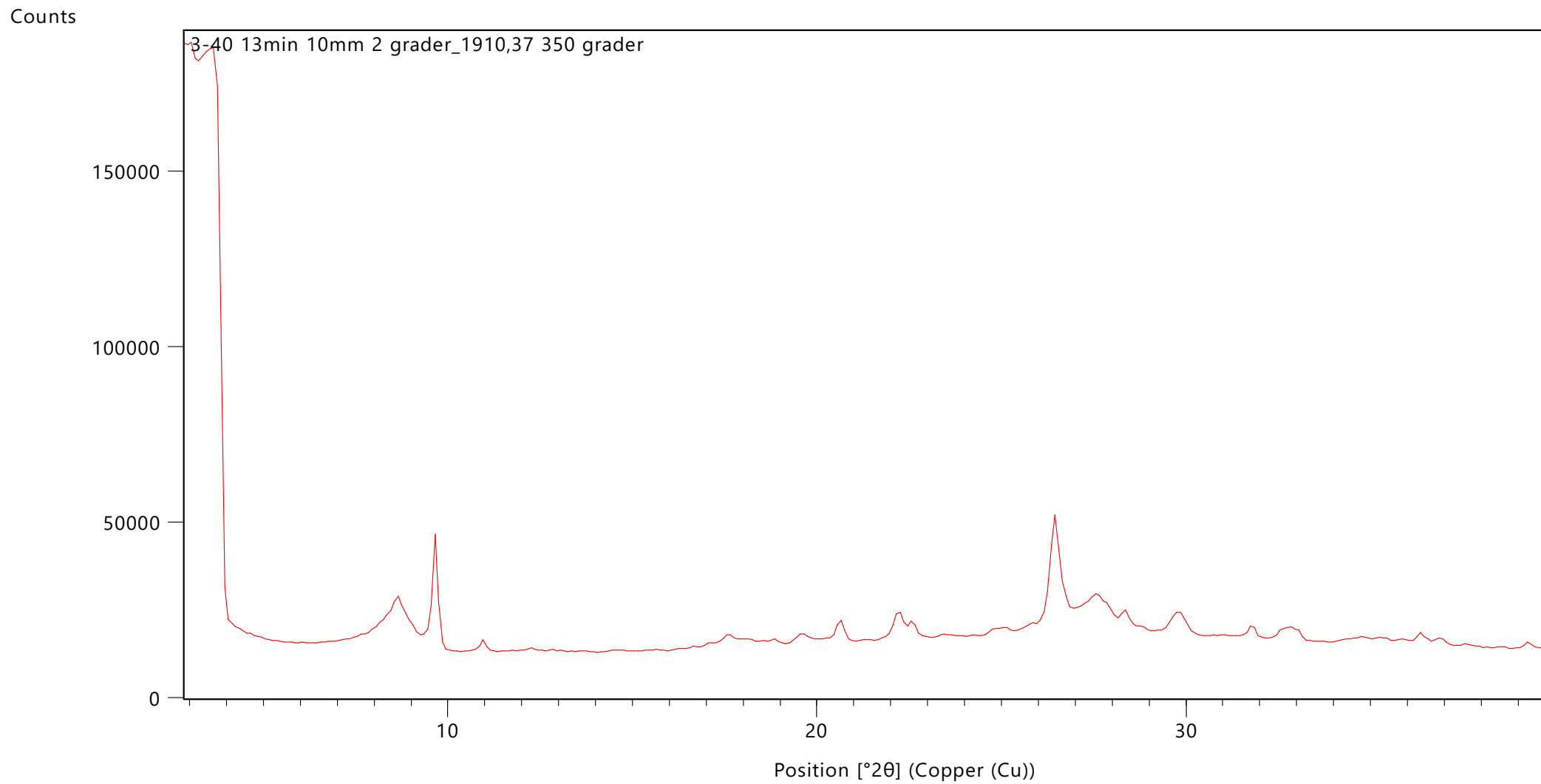


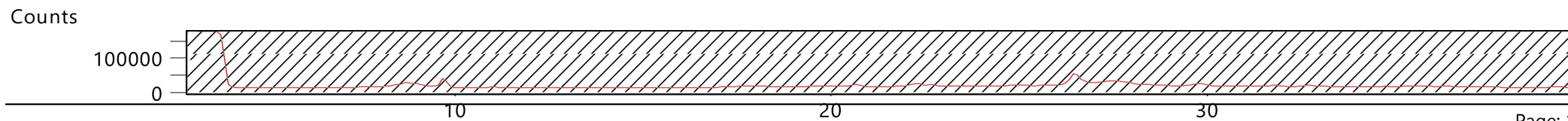
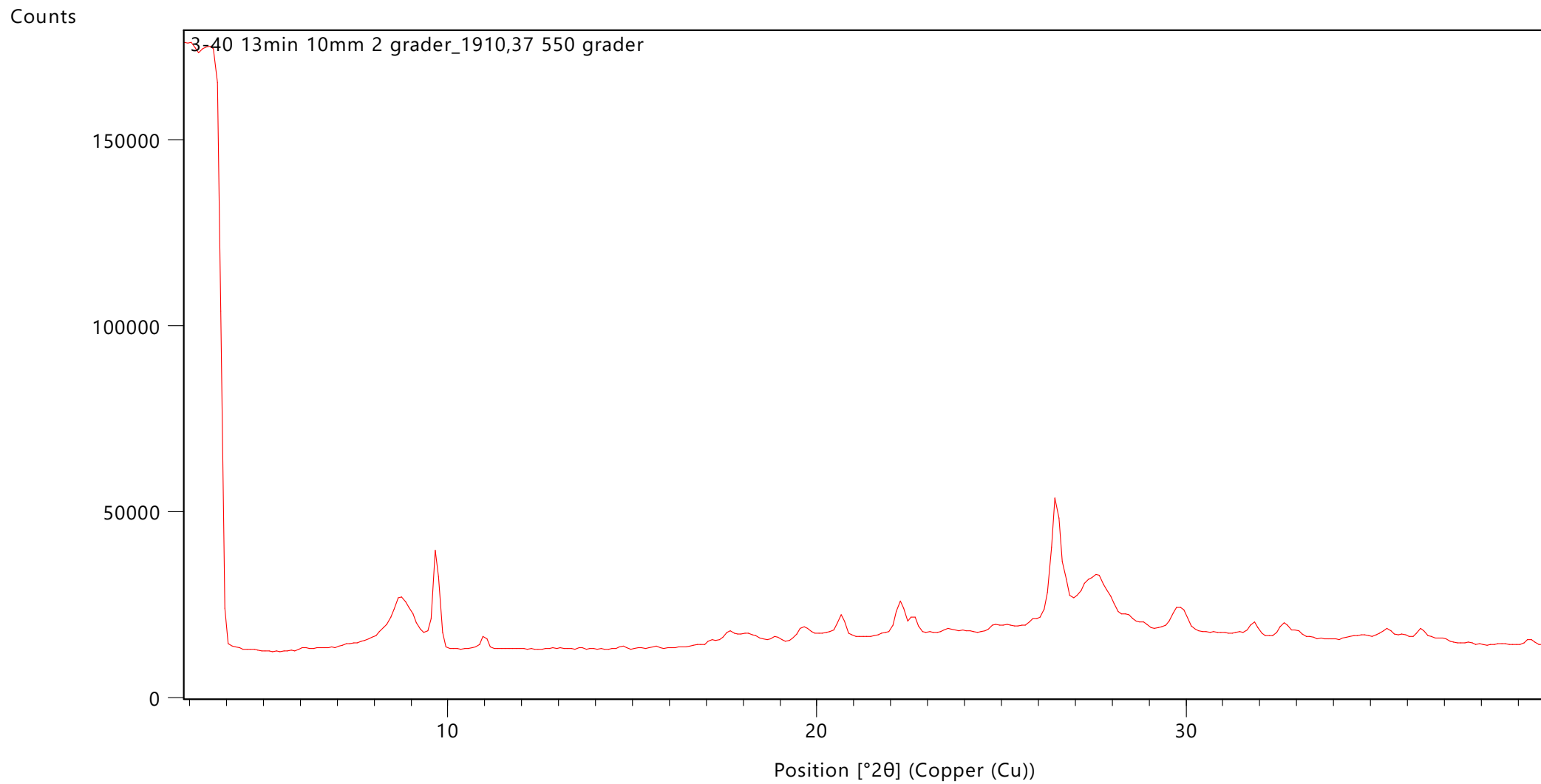


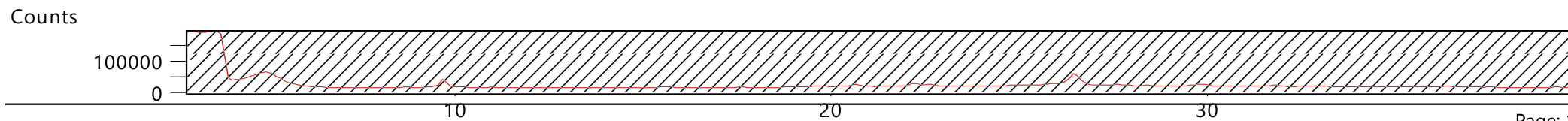
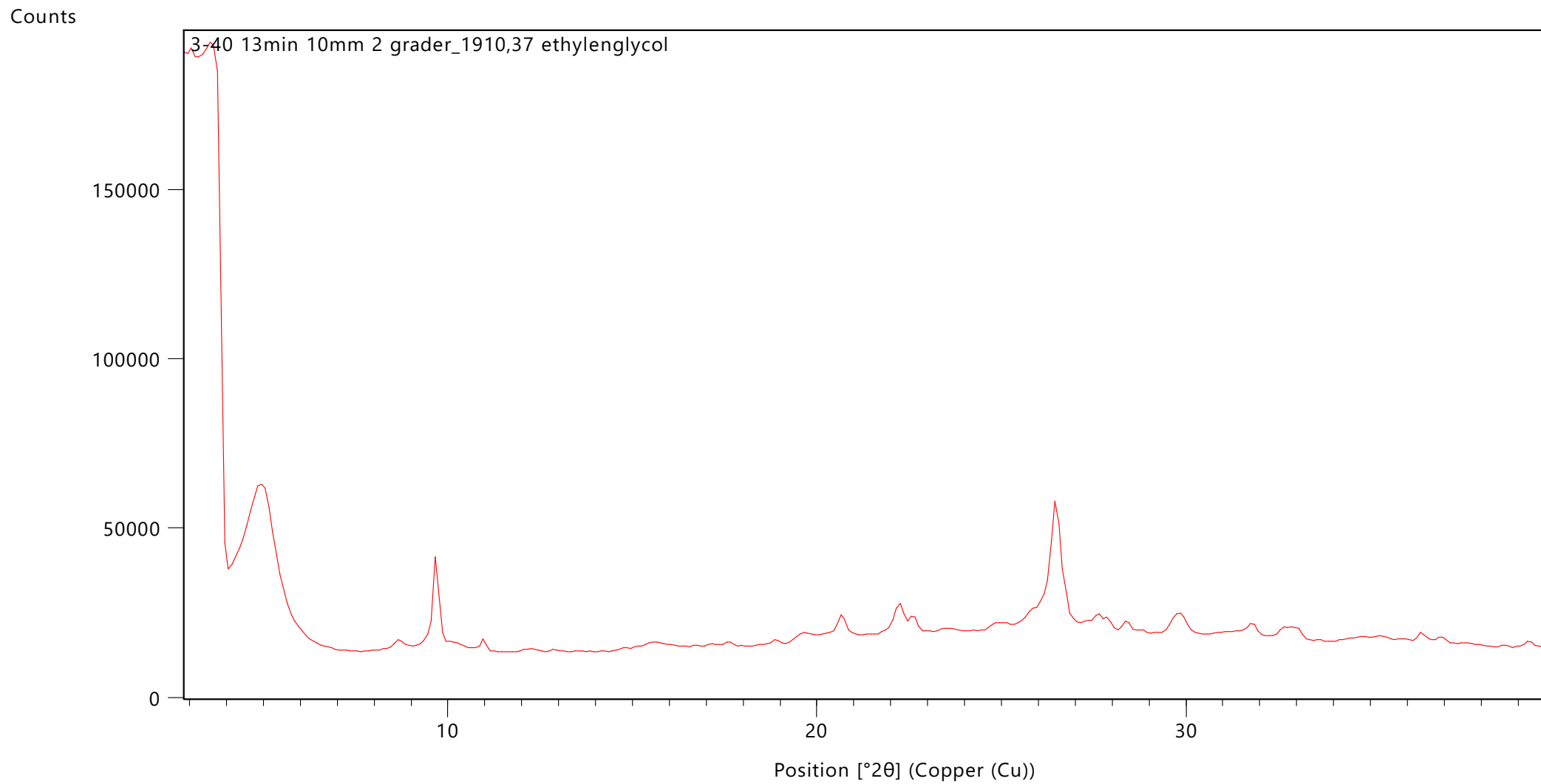


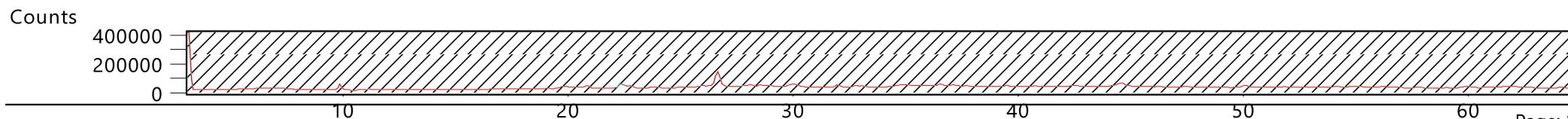
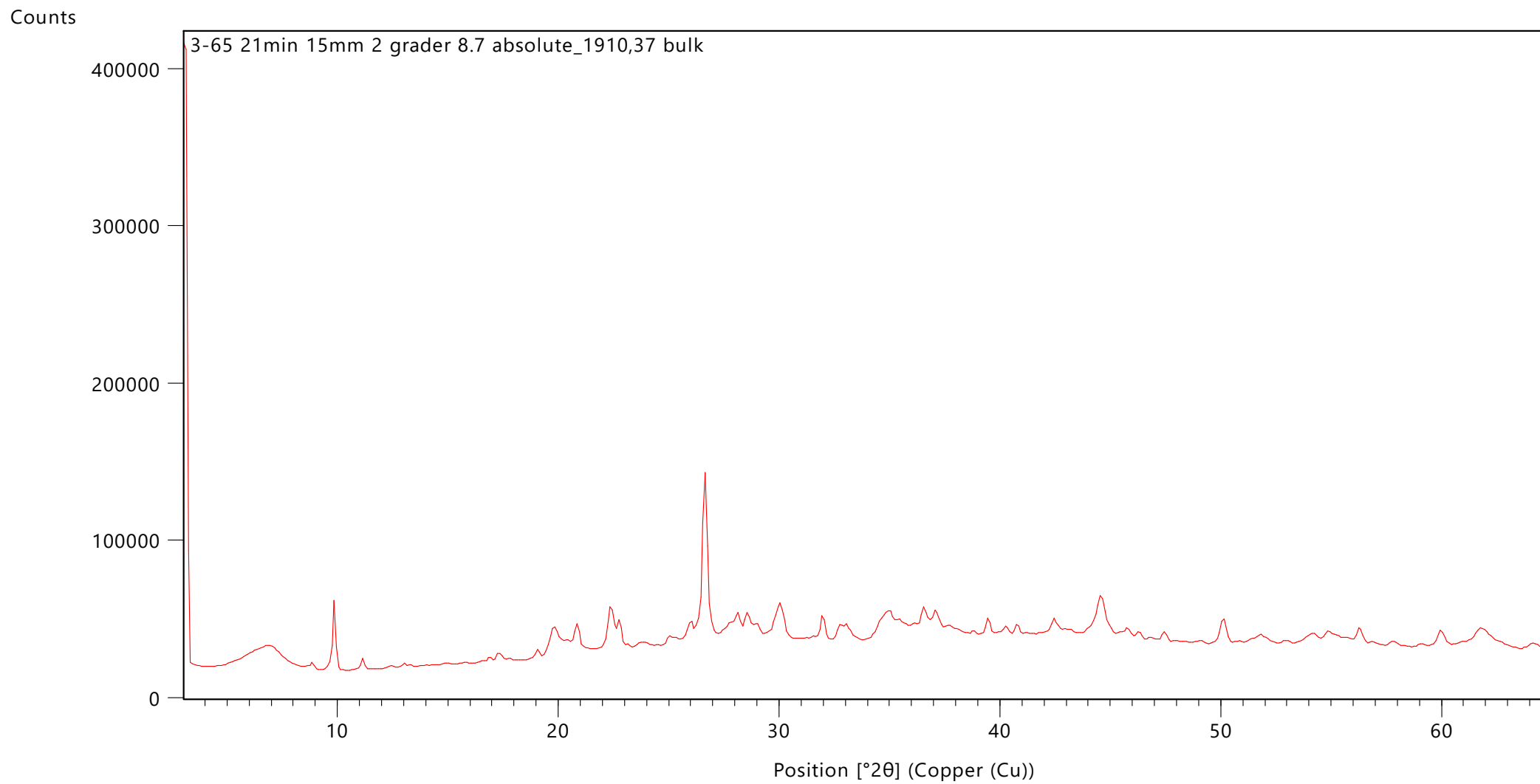


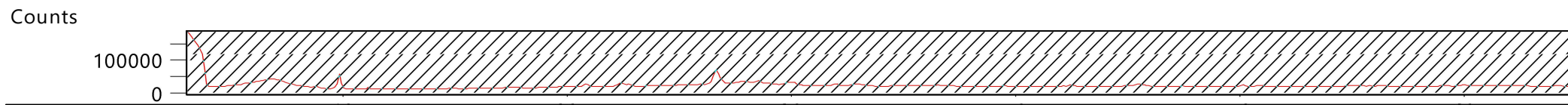
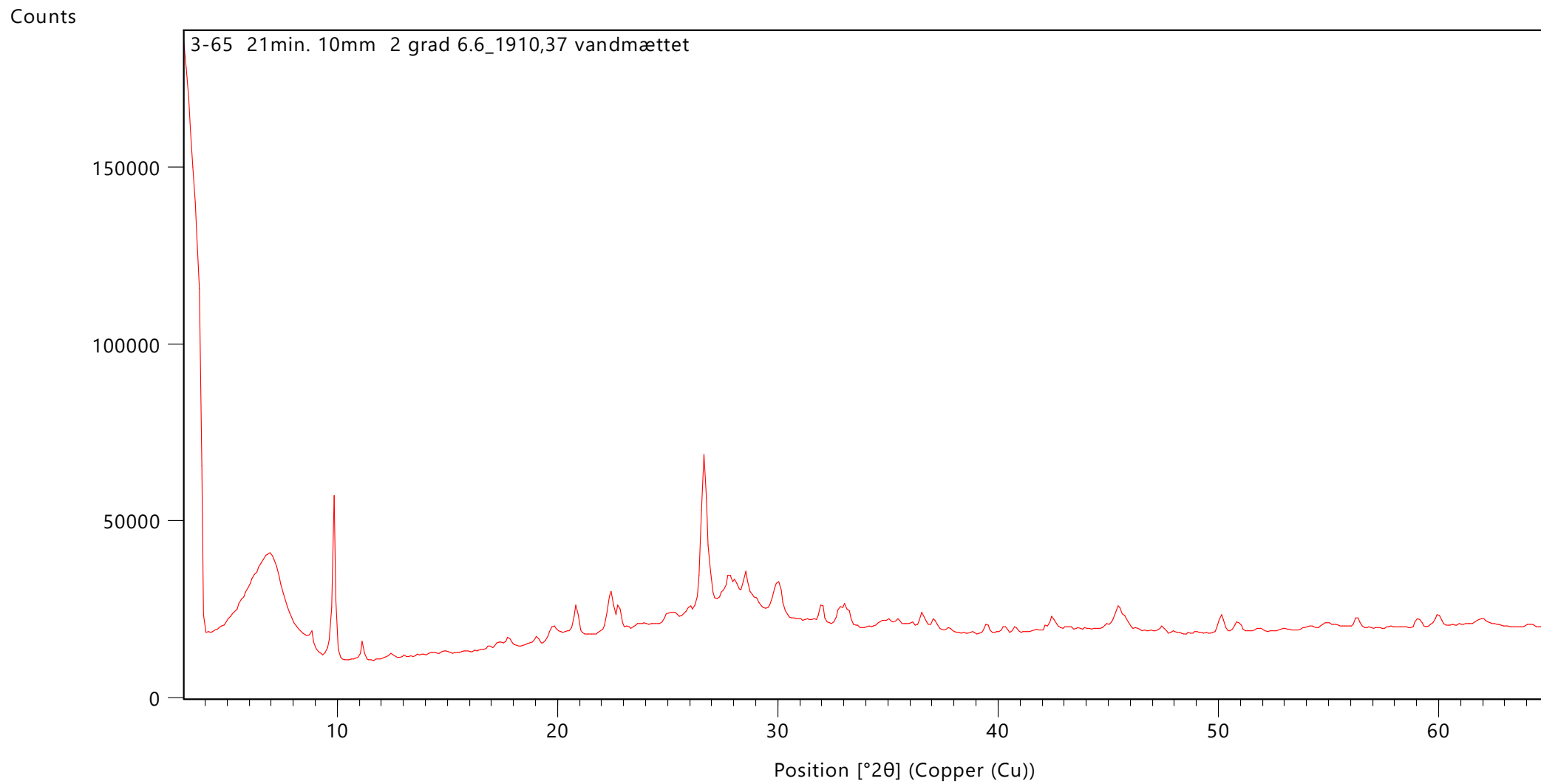


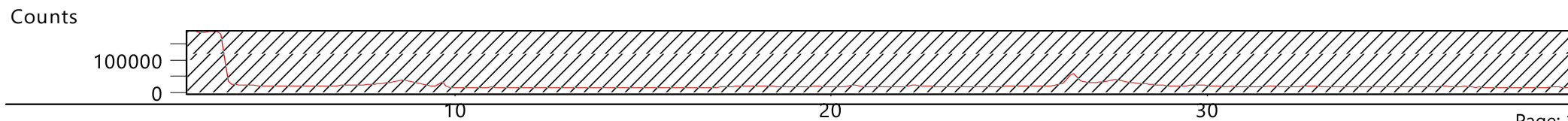
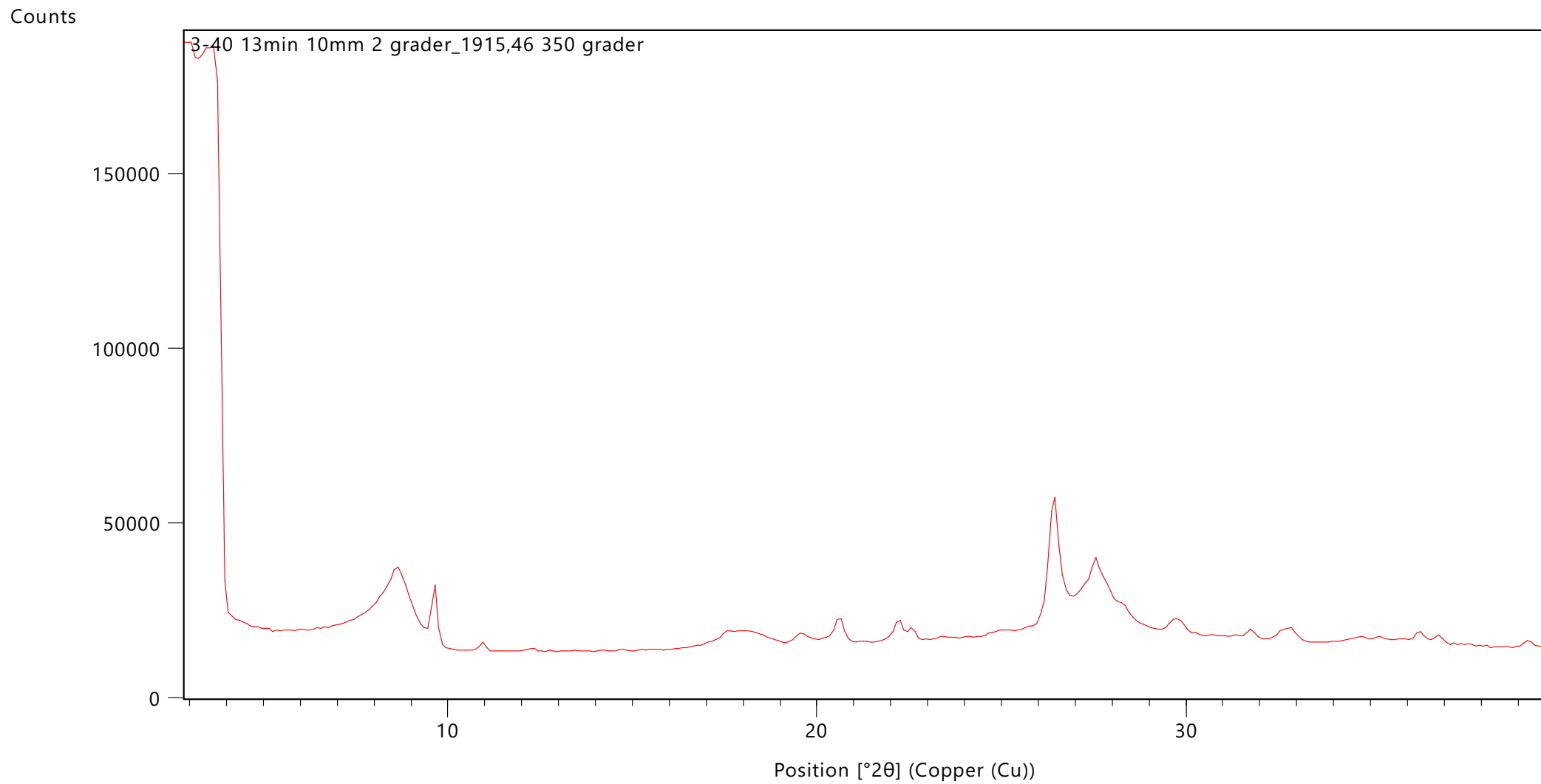


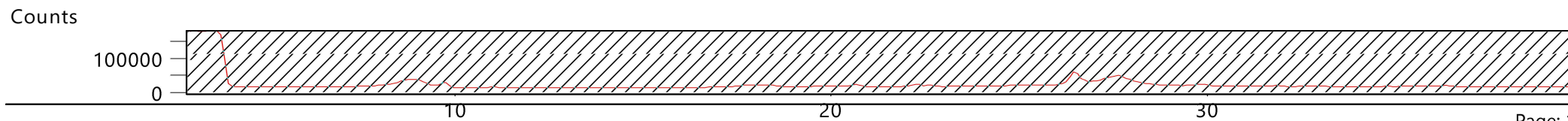
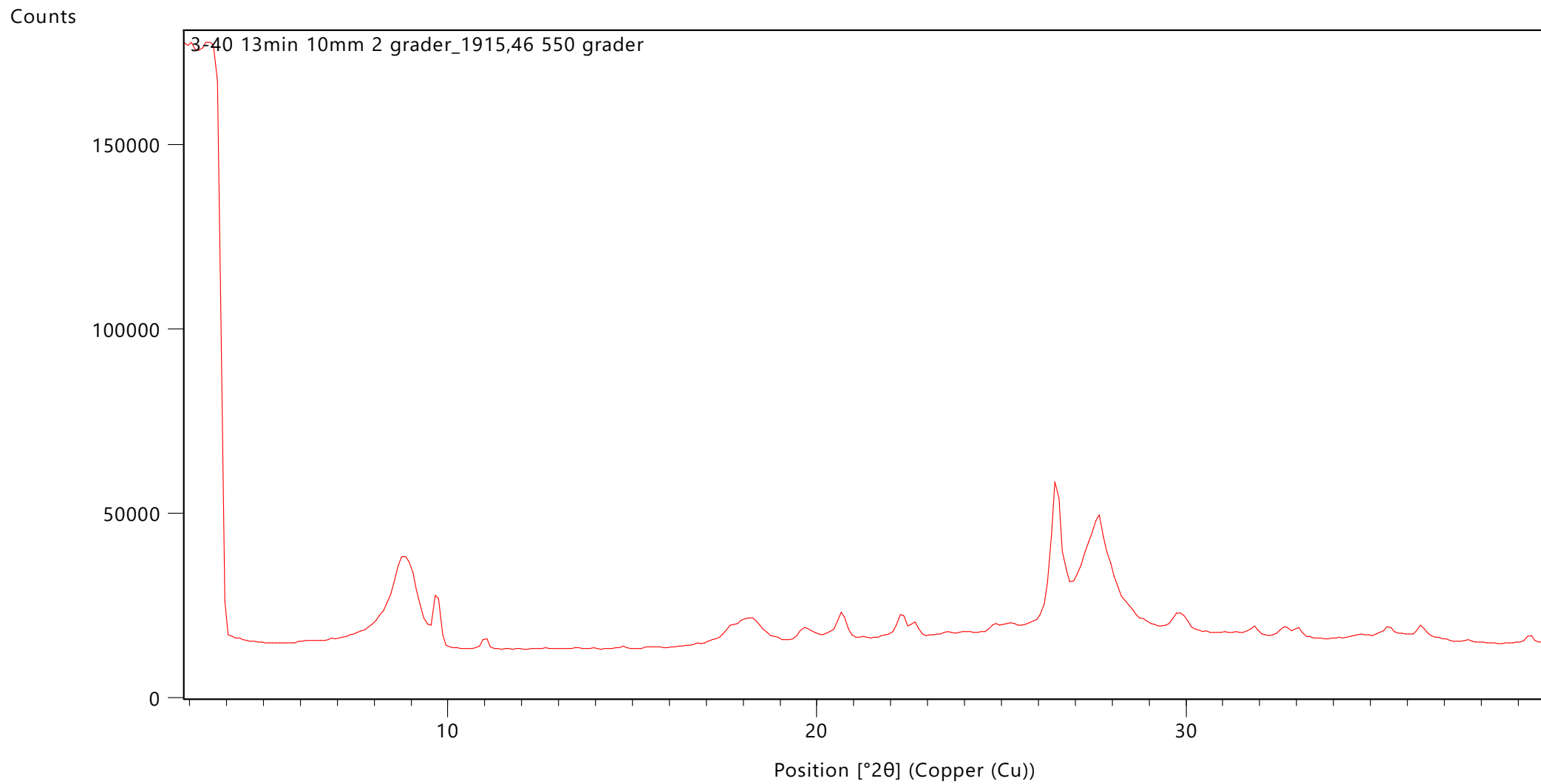


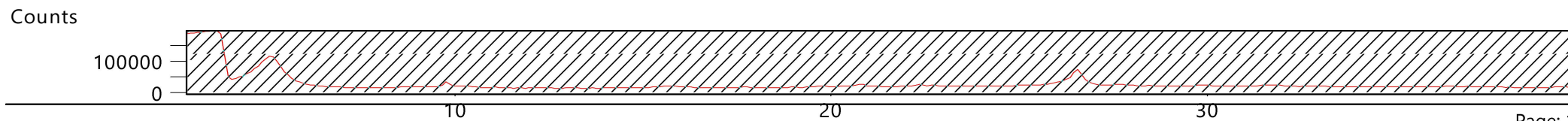
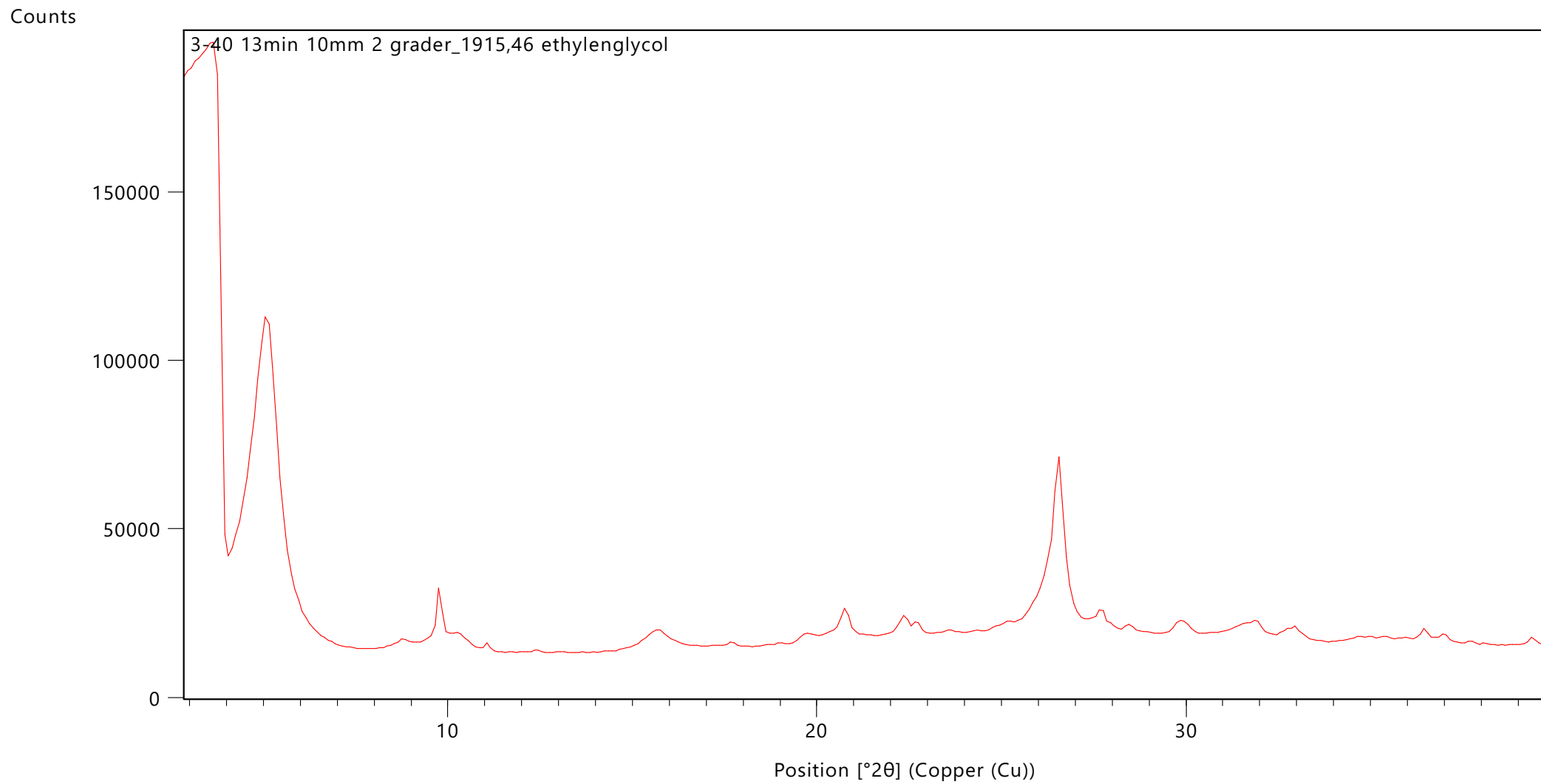


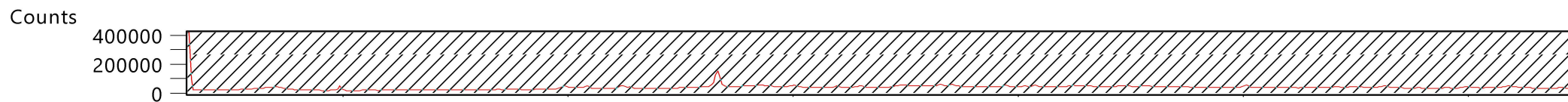
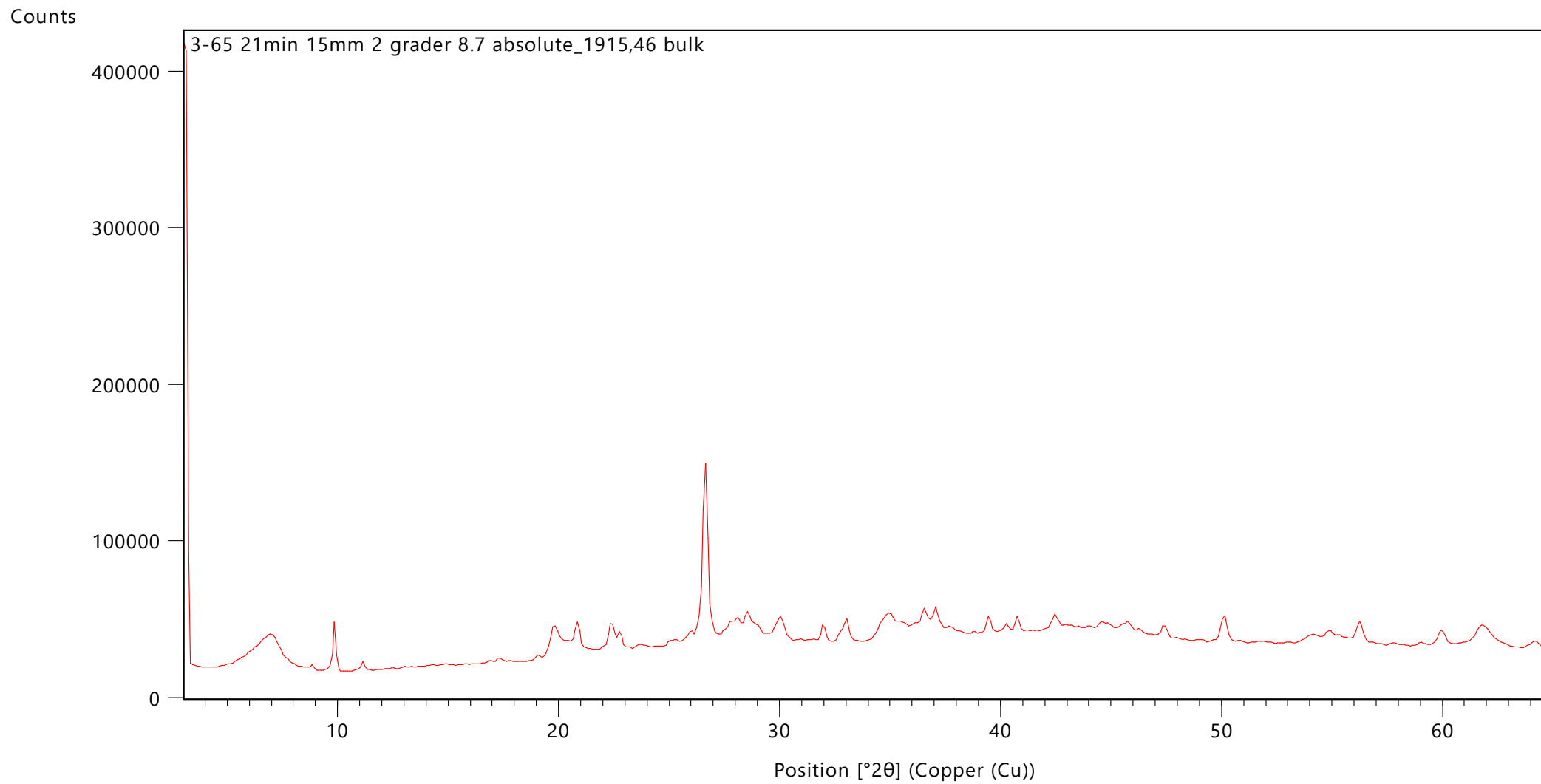


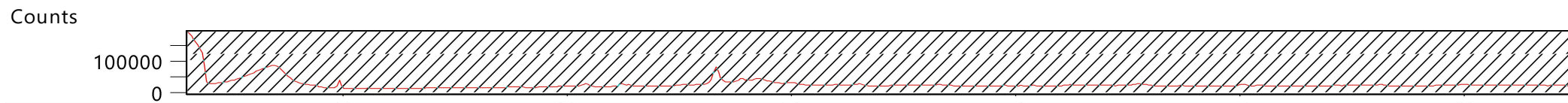
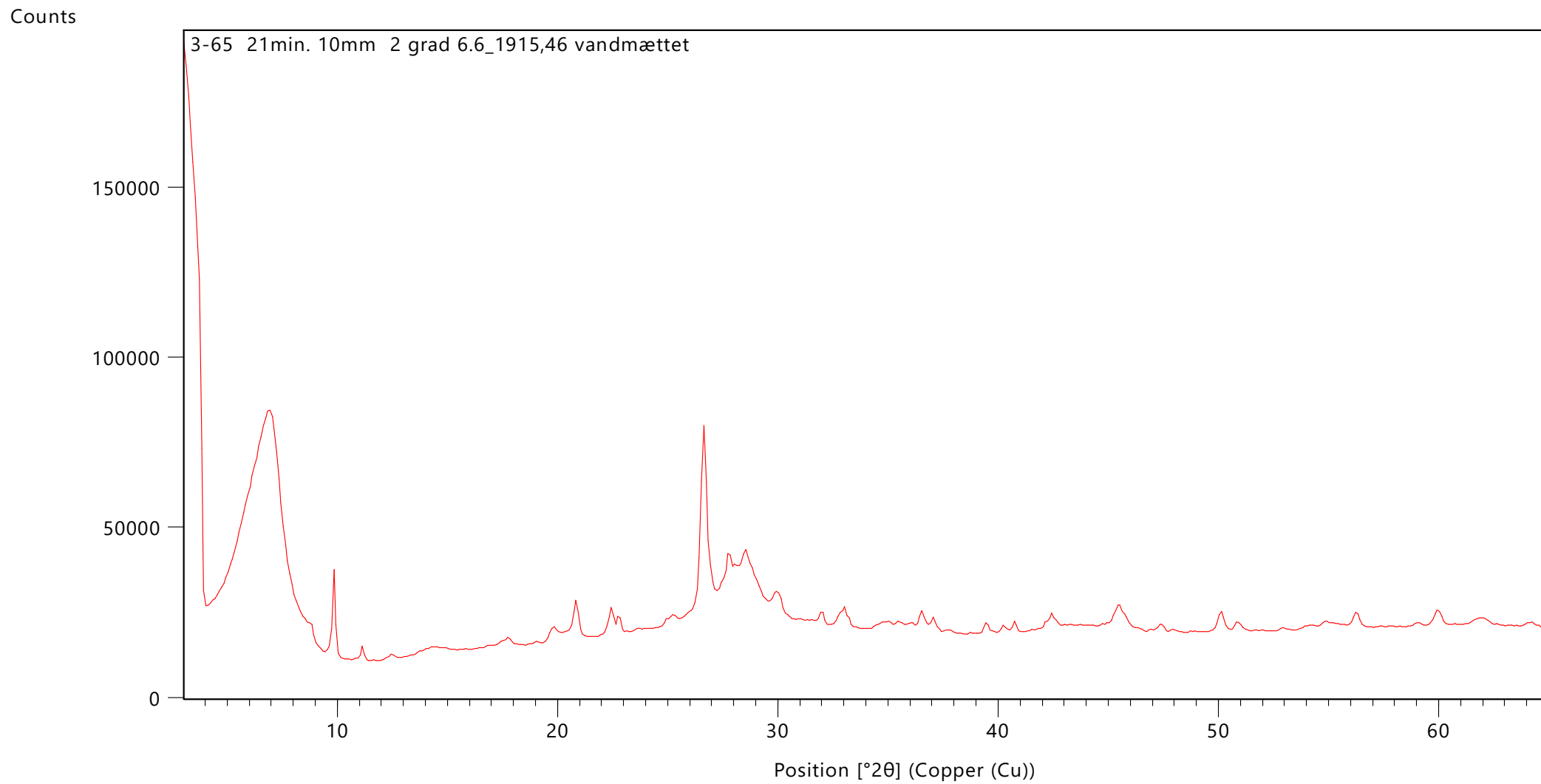


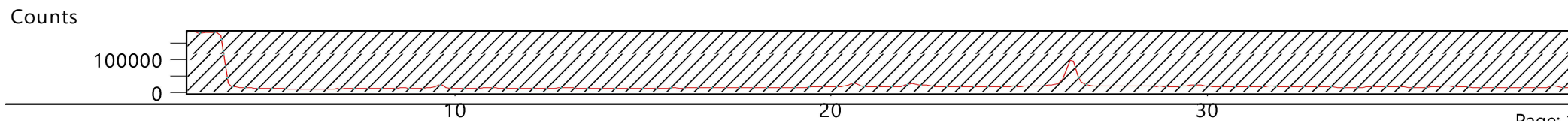
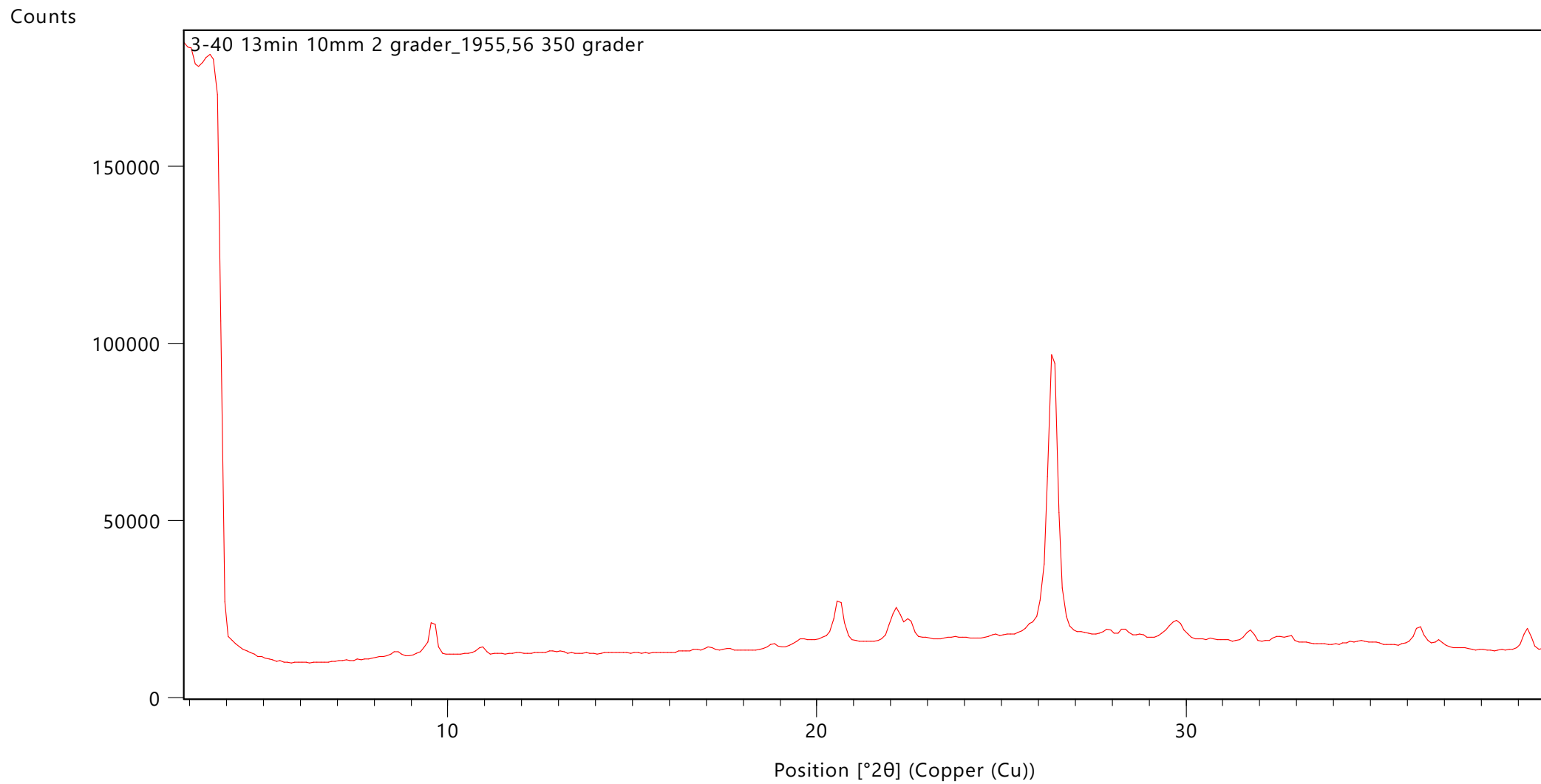


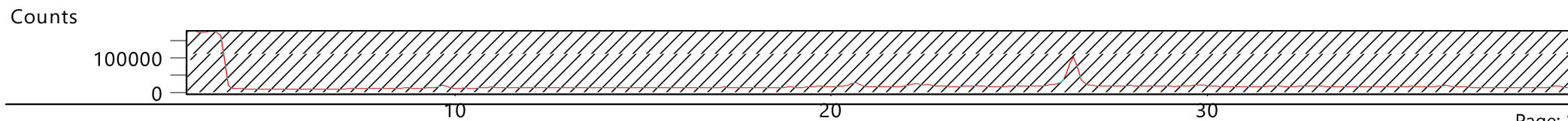
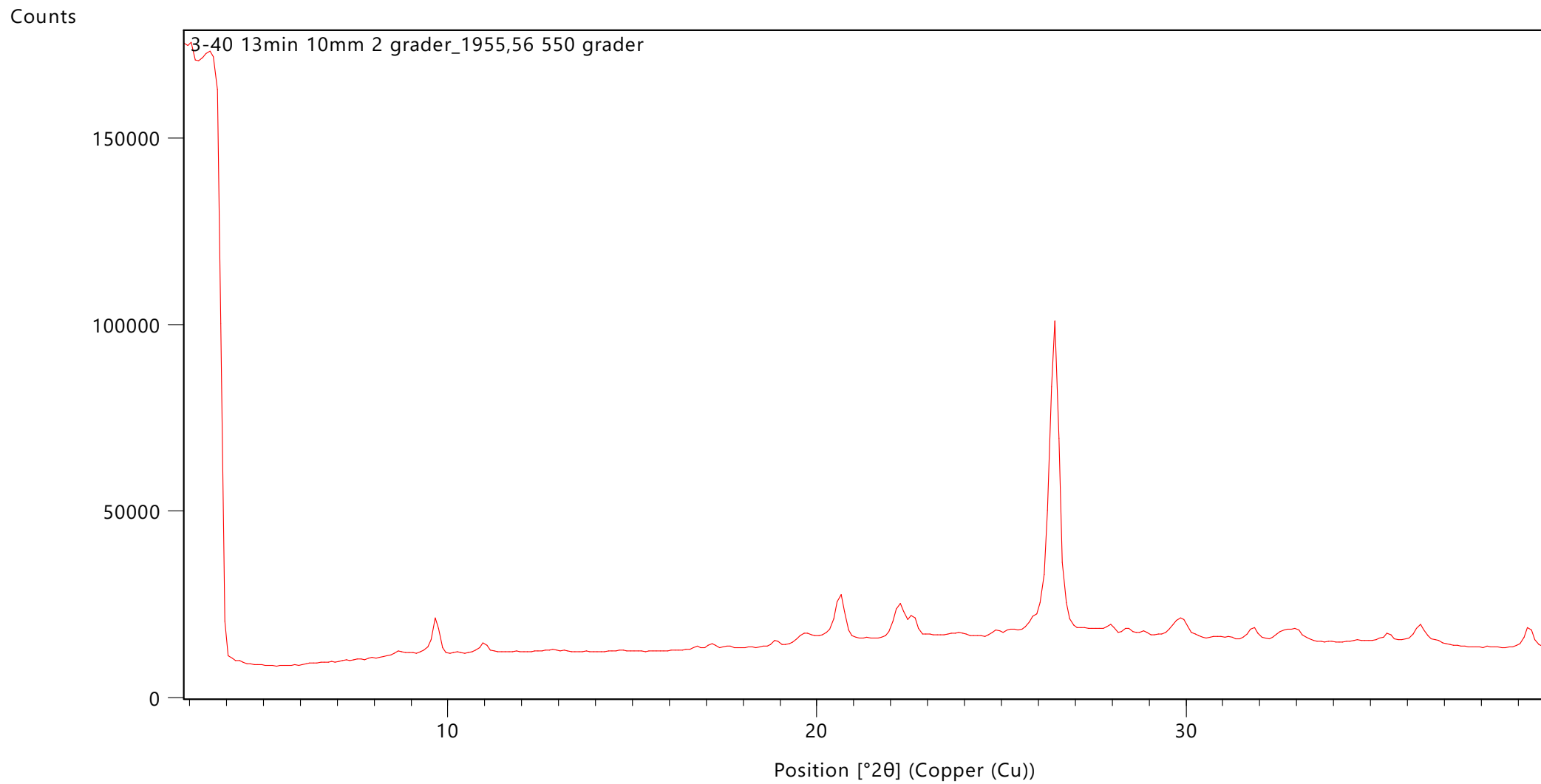


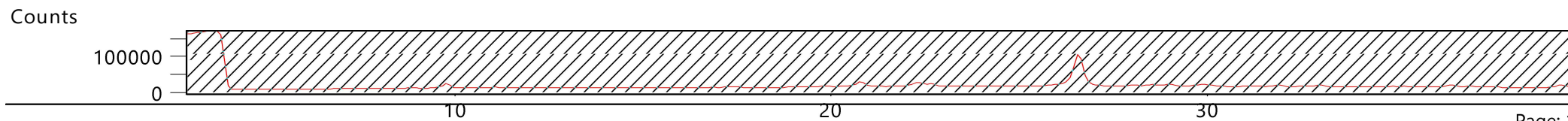
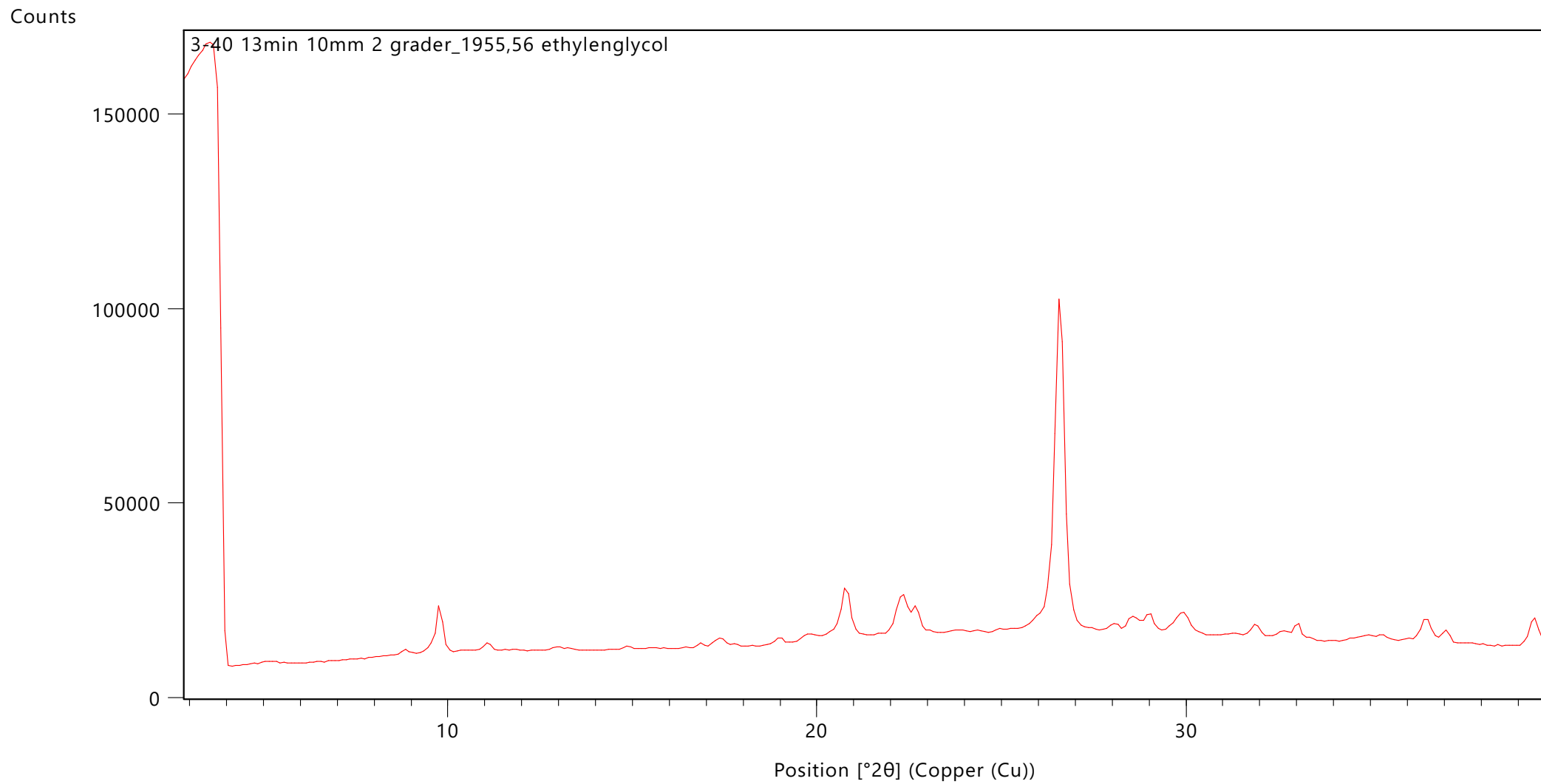


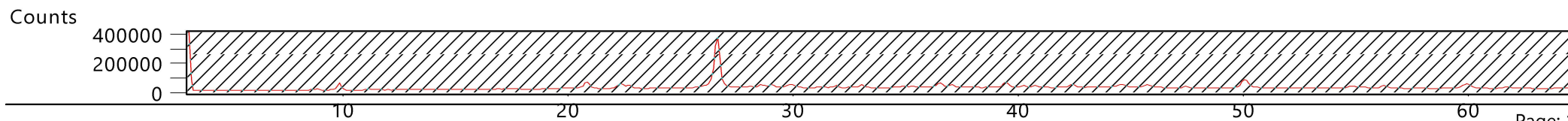
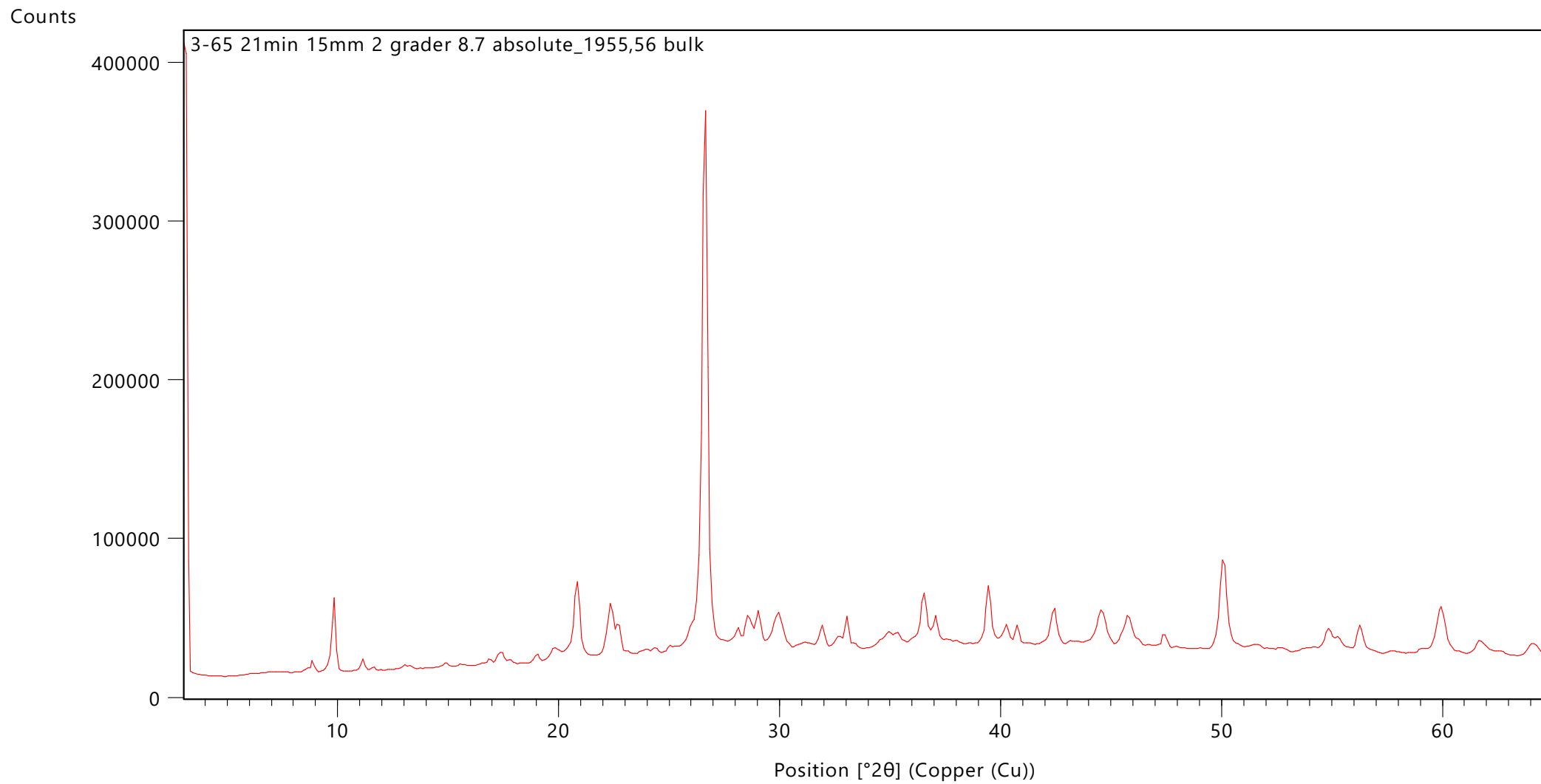


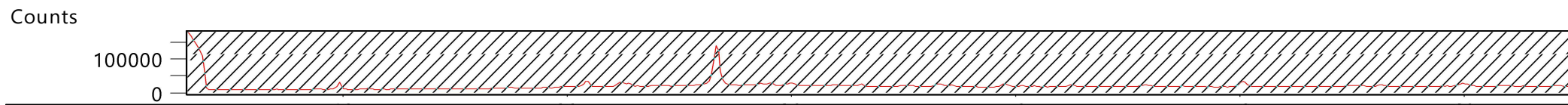
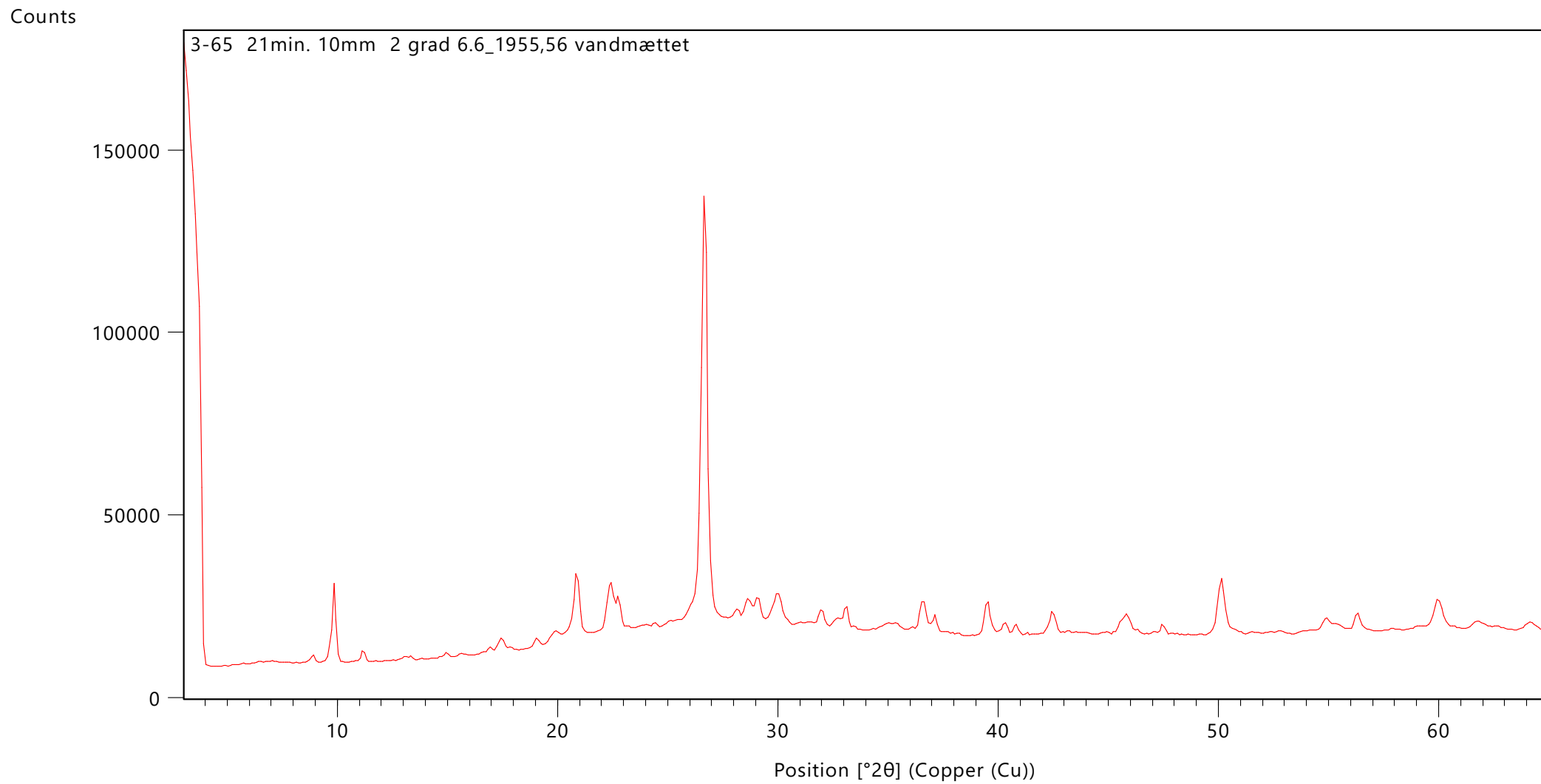












## **APPENDIX D – RESULTS IN EXECL SHEET**

(only digital as Excel – chart)